“The metabolic implication of linear ubiquitination during obesity-induced inflammation”

I n a u g u r a l D i s s e r t a t i o n

zur

Erlangung des Doktorgrades

Dr. nat. med.

der Medizinischen Fakultät

und

der Mathematisch-Naturwissenschaftlichen Fakultät

der Universität zu Köln

vorgelegt von

Ximena Hildebrandt

aus Hurlingham, Buenos Aires, Argentina

2026

Betreuer/in:	Prof. Dr Nieves Peltzer
Referent/in:	Prof. Dr. Silvia von Karsted
	Prof. Dr. Jens Brüning

Datum der mündlichen Prüfung: 08.01.2026

Acknowledgements

I have a lot of people to thank for this journey; most likely, I will still forget some. With the liberty of being unfair in choosing the order, I would first start with the person who trained me during the past five years to become a scientist. Thank you, Nieves, for your unconditional support throughout this crazy life path that we call science. It has been a long run, filled with plenty of adventures and misfortunes, but what I would like to highlight most is how much I learned from it all. Thank you for the training in pronunciation, the countless abstract corrections, the emphasis on presentations, for giving me all the tools to grow, for sending me to amazing conferences, and for trusting me to represent the lab in every single one of them. But also, thank you for opening your home, sharing your family, the alfajores, cakes, glasses of wine, the spontaneous Sunday runs to get things done, and for always pushing to deliver our very best. Although, I am still undecided whether my new obsession with colors and line thickness is a blessing or a curse... Work hard, party harder.

I also want to acknowledge my labmates, who shared this project throughout the years and listened to all the presentations about linear ubiquitination. To Onay, Lucas, Yuan, and Hyoubi, who not only listened to my complaints about life in science but also helped, contributed, and developed this project alongside my PhD journey: thank you for your help and support, for scoring mice on weekends, for the mate and gossip moments, for the beers and CECAD parties. I want to make a special remark on Agata, the amazing CECAD animal technician who supported our projects all these years. Thank you for your commitment to animal welfare, for caring for the experiments as if they were your own, and for always having that spark of complicity every day in the animal house.

I extend my thanks to the Annibaldi lab (Ale, Kristel, Carlos, Matea, Kristhy, Denis and Ina) and the Liccardi lab (Giammy, Kostas, Julia, Debora, Christina and Hassan), who shared the first years of being a small group, shared reagents, protocols, journal clubs, and lab meetings, asked the hardest questions, and contributed to my scientific growth.

On a special note, I want to thank Eva and Henning Walczak, Eva for being so warm and giving me my first birthday present when I started in the lab, always with a smile and a “Hi Xime how are you?” every morning. To Henning for all the generosity through these years, for sharing his labspace and many resources but also opening new avenues for us to grow in Cologne. I also want to say thank you to Diego, Giammy, and Santi, who during the hard times of the pandemic, with all the restrictions at CECAD, supported me when I started as a technician, shared long hours, helped me to establish techniques, and greeted me every day

with a smile and a “good morning.” Thank you for not letting me feel alone in 2020. And especially to Giammy, who, once the restrictions were softer, was always generously inviting beers, playing music on the rooftop, and taking fabulous pictures for Instagram. Those moments helped us to feel “normal” in a context where we were all isolated, alone, and far from home. I will never forget those little gestures. Also for all the party hard in the Schaafenstraße strasse and other corners of the city and every refreshing fashionista detail through the years.

I also want to thank Silvia for the guidance in these years as thesis advisor, you have always been the sharpest in questions but also a role model on how to be a woman on science, always raising your voice and never afraid to speak, also to Isil, for all the carnival parties, SFB retreat, glasses of wine and Karaoke sessions, thank you for your tenderness, sense of humour and lightness, was a pleasure to share with you all those moments, but remember you still own me the Gin and Tonics in your balcony.

I also want to thank Phillipp for his sorrowful sense of humor, for caring about my mental health status for no reason, and for always seeing some beauty and opportunities in the most difficult parts of science, but also for the chillness of "don’t worry, it will work out in the end." Thank you daaaarling.

Now I will take the liberty to switch languages.

También quiero agradecer a mis amigos. Tengo la suerte de tener muchos, y de que estén presentes en mi vida. A Lauri, mi marida, por compartir siempre mis momentos locos, por querer estar conmigo mientras limpiábamos, arreglábamos cosas, o simplemente manejando solo para pasar la mayor cantidad de minutos a mi lado cada vez que estaba en Argentina. A Lau, por todos esos momentos de crisis académica, quejándose de la realidad pero recordándome que había luz al final del túnel. A Barbi, por todas esas actualizaciones por audio que me hacían sentir cerca. A mi Chocho Carena, siempre esperando con mates y esmalte de uñas, para tomar birritas hasta cualquier hora, compartiendo un año entero de novedades en 6 horas, siempre saltando a mis brazos para un abrazo. A Agos, mi heroína, la eterna turista siempre en un destino fascinante, gracias por alojarme tantas veces en Barcelona, por venir a Colonia en días lluviosos solo para estar con nosotros, y por todos los hermosos momentos que compartimos a lo largo de los años. A Seba, esa hermosa alma, por la música, los dibujos, la dulzura y la sensibilidad. A Luchito, por cada risa, cada baile, y cada momento sincero. A Lau por cada conversación sobre política con la que

nunca estamos de acuerdo, pero al final sí… por los asados, el vino y los habanos, las anécdotas y el fútbol.

A mis amigas, a mis mujeres fuertes, locas, migrantes y estresadas, mi aquelarre de Colonia. A Fofi, por todas las fotos, los tips, los viajes, las comidas, y los consejos duros pero necesarios. A Sofi, por todos tus reconocimientos, bajadas de línea, opiniones fuertes con una sonrisa increíble, y por esas llamadas random de una hora solo para ver cómo estoy y sí respiro. A Mina, por la libertad, los bailes, las risas imparables, la complicidad y el fuego interno. A Flor, por disfrutar cada momento con intensidad, por cada crema para el rulos, cada consejo de skin care, cada botella de vino, postre o pizza, y sobre todo por tu intensidad y sentido del humor. A Yas, por todos los detalles amorosos, las tarjetas, los regalitos, cada abrazo, cada sticker, el glitter, el canto, las imitaciones, las voces, la amorosidad y cada “¡Dale Marcelaaa!” por whatsapp. A todas por el empuje y el “dale Xime ya estas”. Las amo.

A Mirna, mi amiga científica. Esa loca que piensa que todo es posible y va y lo consigue sin pedir disculpas. Gracias por todas las charlas hasta la 1 de la mañana, las videollamadas durante la pandemia, cada consejo, cada crisis, cada visita y momento compartido en la aventura alemana.

A mi amiga Nati, la cordobesa original (con perdón de las otras dos, es solo cronológico), le quiero agradecer especialmente por dos momentos. Un retiro espiritual con mujeres increíbles para conectarse con la vida en 2022, y mi última visita a tu casa. Siempre sos torbellino de emociones y reflexiones en cada encuentro. Gracias por este último empuje, el último aire que necesitaba para entregar este manuscrito. Gracias por conectarme con lo importante, por filosofar, por abrirte de par en par, por confiar y atreverte a más, pero sobre todo recordarme que la vida es hoy.

Alla nostra famiglia adottiva, Maria, Sabino ed Ema. A Ema, grazie per averci aperto la tua casa, per averci trattato come fratello e sorella fin dal primo mese, per tutte le focacce, le briscole, le vacanze con i tuoi genitori. Le parole non basteranno mai per esprimere quanto siamo stati fortunati ad incontrarti in questo viaggio. A Maria, per ogni abbraccio che non ami dare, per ogni parmigiana portata a pranzo il lunedì, per tutte le volte che ti sei preoccupata di come stavamo, per ogni gesto da vera mamma. A Sabi, per tutte le ricerche su Google, per tutte le battute, le complicità in ogni lingua, per tutti i balli, i formaggi e i prosciutti condivisi negli anni e per tutte le briscole e i momenti felici. Ci mancherai tantissimo.

E a tutta la comunità italiana che ci ha accolto, Leo, Valen, Domenico, Giussy, Ana, Marcelo, Sabrina, Rosario, Francesco. Per ogni grigliata, ogni bicchiere di vino (specialmente Leo, “el Potro”, un diavolo che non lascia mai il bicchiere vuoto). Per ogni canzone al karaoke (soprattutto Valen con “Rolling in the Deep”). Grazie per il senso di comunità, ci avete fatto sentire a casa ogni volta. Grazie per i pranzi, i compleanni, i matrimoni, per aver condiviso la vita con così tanta passione e amore. Grazie a tutti.

También quiero agradecer a mi tía Adri, por cada mensaje, cada foto, cada cuenta regresiva y cada gesto dulce que me hizo sentir conectada con Argentina, y por siempre querer que vuelva a casa. A mis abuelos, Felipe, Coca, Ricardo y Alicia. En sus bases y enseñanzas se encuentran partes profundas de mi crecimiento personal, de mi amor por el estudio y de mi constancia con el trabajo. Gracias por acompañarme aunque algunos de ustedes ya no estén en este plano. Este logro, si lo podemos llamar así, también es de ustedes y de todo lo que sacrificaron a lo largo de sus vidas para que sus hijos y nietos tuvieran educación universitaria.

Quiero también tomarme un momento para agradecer a mi Universidad madre, la Universidad Nacional de Quilmes, y a todo el sistema científico y educativo de la República Argentina. La educación es un derecho pero también una responsabilidad, y espero algún día devolver aunque sea una parte de todo lo que mis profesores me han dado a lo largo de mi formación inicial. ¡Aguante la Universidad Pública! Dentro de esto también me toca reconocer a tres profesoras de mi secundaria, Fer, Rome y Patri, quienes transmitieron su amor por la ciencia, especialmente la biología. Pero una mención especial a Rome, quien no solo me inspiró a estudiar ciencia, sino que también se aseguró de que me inscribiera a biotecnología, subiéndome a su auto a toda velocidad un viernes. Profesores así marcan tu vida, y espero algún día poder hacer lo mismo con mis futuros alumnos.

Coming back to English, I want to thank my students, especially Julian, Liane, Sara, and Joelle. In the darkest moments you all reminded me how exciting and beautiful science can be, and made me realize that the knowledge and wisdom I acquired during hard lessons on this journey are actually worth it. Seeing you learn and grow next to the projects will always be one of the most precious memories of my PhD. I hope you learned how to be critical with your own data, set proper controls, trust your results, gain confidence in your capacities, and value the importance of ethics in doing science. Techniques can be improved, mistakes are part of the process, but being responsible for the data you generate and defend is the most important contribution. Thank you for making me feel that the lessons I learned can be passed on to the next generations to avoid vicious cycles. You might not know it, but you

have renewed my faith in humanity, and every little message asking for advice even after one year that you have left the lab has been the most rewarding gift.

Last, but not least, I want to thank the University of Cologne, the SFB1403 consortium, and the IPMM graduate school. All these years they have been incredibly supportive of my education, offering the best courses and training. Thank you for all the facilities that allowed this project to develop, and all the professionals who dealt daily with the bureaucratic aspects that kept everything running. I especially want to thank Emmy, Manolis, and Hamid for creating such a supportive environment for a PhD student to develop and grow. For all the courses, travel grants, seminars, and retreats, these all shaped the professional I have become. I also thank my colleagues on the IPMM member committee, especially Jan. We tried to improve some things. We did not succeed in all of them, but we still tried and we learned a lot navigating the way.

To close this unbearably long set of acknowledgments, I want to thank my love, my partner, my husband, who has been with me at every single step. Thank you for every hug, every meal, for cooking every night even when I got home at 2 am, for fixing my bike so I could go to work, for taking me to the airport, for every WhatsApp message asking if I was coming back so you could wait for me for dinner. For every trip, and every little love gesture. For being by my side even when I was broken or without energy. For every weekend on the couch watching movies and drinking wine, or going out dancing until 5 am to celebrate life, but also copping up to me when I was working on Sundays or needed it to change a medium in the middle of the night. I will not say I could not have done this without you, but I will say that I would definitely not be this healthy, this happy, or this loved if you had not been there with me. Thank you.

It has been a long journey, but far from being finished, it is the starting point of new adventures. Thank you, science. Thank you for being so beautiful, although complicated. This is just the beginning.

Table of contents

Figures and tables index

Zusammenfassung / Abstract

Diese Dissertation untersucht die Rolle der linearen Ubiquitinierung, vermittelt durch den LUBAC-Komplex, in der Homöostase des Fettgewebes sowie bei adipositasassoziierten Erkrankungen. Adipositas ist durch eine niedriggradige chronische Entzündung und metabolische Dysfunktion gekennzeichnet, wobei Zytokine der TNF-Familie den Zelltod und die Entzündungsprozesse im Fettgewebe (Adipose Tissue, AT) fördern. Die TNF-Signalgebung wird dabei durch LUBAC streng reguliert – den einzigen E3-Ligasen, der lineare Ubiquitin (LinUb)-Ketten generiert. LUBAC besteht aus den drei Proteinen HOIP, HOIL-1 und SHARPIN. Sowohl HOIP als auch HOIL-1 besitzen E3-Ligasen-Aktivität; HOIP ist jedoch die katalytisch aktive LinUb-E3-Ligase, die die LinUb-Ketten synthetisiert, während HOIL-1 die HOIP-Aktivität durch Autoubiquitinierung moduliert. Die Funktion von LUBAC besteht darin, eine optimale NF-κB/MAPK-Signaltransduktion zu gewährleisten und den Zelltod bei TNF-Stimulation zu verhindern.

Analysen humaner Datenbanken zeigten, dass eine niedrige Expression der LUBAC-Komponenten im Fettgewebe mit Biomarkern des metabolischen Syndroms korreliert und invers mit der Caspase-8-Expression assoziiert ist, was auf eine protektive Rolle von LUBAC im Kontext von Adipositas hinweist. Zur weiteren Aufklärung des Zusammenspiels von LinUb, Zelltod und metabolischer Regulation kombinierten wir die Analyse humaner Daten mit in vitro- und in vivo-Mausmodellen sowie omics-basierten Ansätzen. Hierzu generierten wir murine Mutanten mit fehlender LinUb in Adipozyten (durch Deletion von HOIP, (*Hoip*$^{A\text{-}KO;}$) oder mit gesteigerter LinUb (durch Expression der katalytisch inaktiven HOIL-1-Mutante, *Hoil-1*^{C458A}) und setzten diese unter eine Hochfett-Diät (High-Fat Diet, HFD).

HOIP-Defizienz in Adipozyten führte zu spontaner Lipodystrophie und verschärfter metabolischer Dysfunktion unter HFD, ein Phänotyp, der durch die zusätzliche Deletion von Caspase 8 in Adipozyten (*Hoip*$^{A\text{-}KO;}$ *Casp8*$^{A\text{-}KO}$) vollständig aufgehoben wurde, was die Bedeutung apoptotischer Mechanismen bei der Entwicklung des metabolischen Syndroms hervorhebt. Im Gegensatz dazu veränderte eine erhöhte lineare Ubiquitinierung die Adipozytengröße und erhöhte die Infiltration von Immunzellen, schützte jedoch gegen bestimmte Aspekte der diätinduzierten metabolischen Dysfunktion, wie z. B. die Fettablagerung in der Leber und erhöhte Cholesterinwerte im Blut. Mechanistisch schützte die erhöhte LinUb vor TNF- und diätinduziertem Zelltod im Fettgewebe, Preadipozyten und knochenstammzellabgeleiteten Makrophagen und förderte tendenziell die mitochondriale Dichte sowie die Thermogenese in subkutanen (ScWAT) und braunem Fettgewebe (BAT).

Besonders hervorzuheben sind geschlechtsspezifische Unterschiede in den metabolischen Reaktionen auf veränderte LinUb, was die Notwendigkeit betont, geschlechtsspezifische Aspekte in der metabolischen Forschung zu berücksichtigen.

Diese Befunde zeigen, dass LinUb die Expansion des Fettgewebes unterstützt, indem sie das Überleben der Adipozyten fördert, vermutlich durch Regulation von NF-κB und Hemmung des Zelltods. Insgesamt liefern unsere Ergebnisse neue Einblicke in die Rolle der linearen Ubiquitinierung in der Biologie des Fettgewebes und der metabolischen Regulation und eröffnen potenzielle Perspektiven für das Verständnis und die Behandlung adipositasassoziierter Erkrankungen.

This PhD thesis explores the role of linear ubiquitination, mediated by the LUBAC complex, in adipose tissue homeostasis and obesity-associated disorders. Obesity is characterized by low-grade chronic inflammation and metabolic dysfunction, with TNF family cytokines driving cell death and inflammation within adipose tissue (AT). TNF Signalling is tightly regulated by LUBAC, the only E3 ligase that generates linear ubiquitin (LinUb) chains, which is composed of three proteins, HOIP, HOIL-1, and SHARPIN. Both HOIP and HOIL-1 bear E3 ligase function. Yet, HOIP is the catalytic-active Lin-Ub-E3-ligase subunit which generates LinUb, HOIL-1 modulates HOIP activity via autoubiquitination. LUBAC activity is to promote optimal NF-κB/MAPK signalling and to prevent cell death upon TNF stimulation.

Analysis of human databases revealed that low expression of LUBAC components in AT correlates with metabolic syndrome biomarkers and inversely with caspase-8 expression, suggesting a protective role for LUBAC in obesity. To further elucidate the interplay between LinUb, cell death, and metabolic regulation, we combined human data analysis with in vitro and in vivo mouse models and omics approaches. We generated murine mutants lacking LinUb in adipocytes (by deleting HOIP, $Hoip^{A\text{-}KO}$) or with exacerbated LinUb (by expressing catalytically inactive HOIL-1, $Hoil\text{-}1^{C458}$), and challenged them with a high-fat diet (HFD).

HOIP deficiency in adipocytes led to spontaneous lipodystrophy and exacerbated metabolic dysfunction under HFD, a phenotype fully rescued by Caspase 8 deletion in adipocytes ($Hoip^{A\text{-}KO};Casp8^{A\text{-}KO}$), highlighting the importance of apoptotic machinery in metabolic syndrome development. Conversely, increased linear ubiquitination altered adipocyte size and increased immune cell infiltration, while protected against certain aspects of diet-induced metabolic dysfunction, such as liver lipid deposition and blood cholesterol levels. Mechanistically, increased LinUb protected against TNF- and diet-induced cell death

in AT, preadipocytes, and bone-derived macrophages, while tended to promote mitochondrial content and thermogenesis in ScWAT and BAT.

Importantly, we noted sex-specific differences in metabolic responses to altered LinUb, underscoring the need for gender-specific considerations in metabolic research.

These findings demonstrate that LinUb supports AT expansion by enhancing adipocyte survival, likely through NF-κB regulation and inhibition of cell death pathways. Collectively, our results provide new insights into the role of LinUb in adipose tissue biology and metabolic regulation, with potential implications for understanding and treating obesity-related disorders.

Keywords: Cell death, Obesity, LUBAC, Ubiquitination, Linear chains, M1-chains, Hoip, Rnf31, Hoil-1, Rbck1, Adipocytes, Metabolic syndrome, Apoptosis, Caspase 8, NF-κB, Insulin resistance, Diabetes, Lipodystrophy .

List of Abbreviations

A20	Tumour necrosis factor alpha induced protein 3
ALAT	Alanine Transaminase
AP	Adipocyte precursor or preadipocyte
AST	Aspartate aminotransferase
AT	Adipose tissue
ATM	Adipose Tissue Macrophages
BAFF-R	B cell activating factor receptor
BAT	Brown adipose tissue
B-box	B-box type zinc finger
BCR	B cell receptor
BCL-10	B cell lymphoma 10
BeAT	Beige Adipose Tissue
BMDMs	Bone marrow-derived macrophages
cAMP	Cyclic adenosine monophosphate
CARMA1	Caspase recruitment domain membrane associated guanylate kinase protein 1
CAP-Gly	Cytoskeleton associated protein glycine rich
Casp	Caspase
CBR	Catalytic in between RING
CD	Control diet
CD40	Cluster of differentiation 40
cFLIP	Cellular FLICE-like inhibitory protein
CHX	Cycloheximide
cIAP 1/2	Cellular inhibitor of apoptosis protein 1/2
CO2	Carbon dioxide
Cre	Causes recombination
CRISPR	Clustered regularly interspaced short palindromic repeats
CYLD	Cylindromatosis
DD	Death domain
ddH20	Double-distilled water
DED	Death effector domain
DFs	Dermal fibroblasts
DIO	Diet induced obesity
DNL	De novo lipogenesis
DMEM	Dulbecco's Modified Eagle Medium
DMSO	Dimethyl sulfoxide
DNA	Desoxyribonucleic acid
DR	Death receptors
EDTA	Ethylene Diamine Tetraacetate
ERK	Extracellular signal-regulated kinase
FADD	Fas-associated protein with death domain
Gck	Glucokinase
GDP	Global gross domestic product
Glp1	Glucagon-like peptide-1

Glp1r	Glucagon-like peptide-1 receptor
GLUT	Glucose transporter
GO	Gene ontology
G-CSF	Granulocyte colony stimulating factor
GTT	Insulin Tolerance Test
GWAT	Gonadal white adipose tissue
HCC	Hepatocellular carcinoma
HEPES	2-[4-(2-hydroxyethyl)piperazin-1-yl]ethanesulfonic acid
HFD	High fat diet
HOIL-1	Heme-Oxidized IRP2 ubiquitin ligase 1 homolog
HOIP	HOIL-1 interacting protein HRP Horseradish peroxidase
IκBa	Inhibitor of NFκ-B alpha
IBMX	3-isobutyl-1-methylxanthine
IKKα	IκB kinase alpha
IKKβ	IκB kinase beta
IKKγ/NEMO	NF kappa B essential modulator
IL-1R	Interleukin 1 receptor
IκBα	Inhibitor of NF kappa B alpha
IBR	In between RING
IF	Immunofluorescence
IHC	Immunohistochemistry
IKK1/2	IB kinase 1/2
IL	Interleukin
IP	immunoprecipitation
IR	Insulin resistance
IRAK	Interleukin-1 receptor associated kinase
ITT	Insulin Tolerance Test
JNK	c-Jun N-terminal kinase
lPC	Liver parenchymal cell
LDD	Linear ubiquitin chain Determining Domain
Lepr	Leptin receptor
LT-βR	Lymphotoxin beta receptor
LTM	LUBAC tethering motif
LUBAC	Linear ubiquitin chain assembly complex
MALT1 protein 1	Mucosa associated lymphoid tissue lymphoma translocation
MASLD	Metabolic-dysfunction-associated steatotic liver disease
MAPK	Mitogen-activated protein kinase
MEFs	Murine embryonic fibroblasts VIII
MetS	Metabolic syndrome
MLKL	Mixed lineage kinase like
MyD88	Myeloid differentiation primary response 88
MONW	metabolically obese normal weight
NAFLD	Non-alcoholic fatty liver disease
Nec-1s	Necrostatin 1s
NEMO	Nuclear factor-B essential modulator

NF-κB	Nuclear factor “kappa-light-chain-enhancer” of activated B cells
NF-κB2	p100 NF kappa B subunit 2 precursor p100
NIK	NF kappa B inducing kinase
NZF	Nuclear protein localisation 4 (Npl4) zinc finger
O2	Oxygen molecule
OTU	Ovarian tumour
p38	p38 mitogen-activated protein kinase
p50	NF kappa B subunit p50
p52	NF kappa B subunit p52
PCR	Polymerase chain reaction
PIM	PUB interacting motif
PPARɣ:	Peroxisome proliferator-activated receptor ɣ
PUB	Peptide N-glycanase / UBA- or UBX-containing proteins
PRR motif	Pattern recognition receptor RHIM RIP homotypic interaction
RANK	Receptor activator of NF kappa B
RelA (p65)	v rel avian reticuloendotheliosis viral oncogene homolog A
RelB	v rel avian reticuloendotheliosis viral oncogene homolog B
RER	Respiratory exchange ratio
RIPK1/3	Receptor-Interacting Protein Kinase 1/3
RNA	Ribonucleic acid
RING	Really interesting new gene
ScWAT	Subcutaneous adipose tissue
SDS	Sodium dodecyl sulphate
SHARPIN	SHANK associated RH domain interactor
SMAC	Second mitochondrial activator of caspase
TAB 2/3	TAK1-binding protein 2/3
TAK1	Transforming growth factor beta-activated kinase 1
TBK1	TANK-binding kinase 1
TEMED	Tetramethylethylenediamine
TCR	T cell receptor
TLR	Toll-like receptor
TNF	Tumour necrosis factor
TNFR1	Tumour necrosis factor receptor 1
TPM	Transcripts per million
TRADD domain protein	Tumour necrosis factor receptor type1-associated death
TRAF2	TNF receptor-associated factor 2
TRIF	TIR-domain-containing adapter-inducing interferon-
UBA	Ubiquitin associated
UBL	Ubiquitin like
USP	Ubiquitin specific protease
VAT	Visceral adipose tissue (human)
WAT	White adipose tissue
Wt	Wild type
WHO	World HealthOrganization

XIAP	X-linked inhibitor of apoptosis
ZBP1	Z-DNA-binding protein 1
ZnF	Zinc finger
zVAD-fmk	carbobenzoxy-valyl-alanyl-aspartyl-[O-methyl]-fluoromethylketone

Abbreviations of units

%	percent
°C	Degree Celsius
A	Ampere
Bp	base pair
kCal	kilocalories
G, mg, µg, ng	gram, milligram, microgram, nanogram
h, min, sec	hours, minutes, seconds
kDa	kiloDalton
l, ml, µl	litre, millilitre, microliter
M, mM, µM, nM pM	molar, millimolar, micromolar, nanomolar, picomolar
rpm	rounds per minute
V	Volt

“The metabolic implication of linear ubiquitination during obesity-induced inflammation”

1. Bibliographic background

1.1.The obesity epidemic and associated syndromes

1.1.1.Socio-economical impacts of obesity in modern society

The prevalence of overweight and obesity is rising rapidly around the world. In 2022, 890 million adults (16% of world population) were living with obesity, while the prevalence of overweight (including obesity) in children and adolescents has risen dramatically from 8% in 1990 to 20% in 2022 (*Obesity and Overweight*, n.d.). Currently, obesity is the leading non communicable disease, which translates into higher treatment costs and early mortality, outcomes that represent not only a threat to public health but also a growing economic burden. This concern was estimated to cost 2.19% of global GDP in 2019, and is projected to rise to 3.29% by 2060, with the strongest impact expected in countries with fewer resources (Okunogbe et al., 2022).

In the past twenty years, there was a 1.72 fold increase in overweight among the adult population, and according to the World Health Organization (WHO) it is estimated that by 2030 more than one billion people (one in five women and one in seven men) will be obese, (BMI ≥ 30 kg/m2) (*World Obesity Atlas 2022*, n.d.). Shockingly, extreme mortality risk is preferentially higher in younger obese patients than in older adults (Engin, 2017), being this related mainly to cardiovascular disease and type 2 diabetes. In fact, only in 2019, diabetes accounted for 1.5 million deaths, where half of them occurred before the age of 70.

In line with this, in the period from 2000 to 2019, there was a 3% rise in age-standardised mortality rates attributed to diabetes globally, with lower-middle-income countries experiencing a particularly alarming 13% increase in mortality rates due to diabetes in this timeframe (*Diabetes*, n.d.);(*GBD Results*, n.d.). This evidence highlights the urgent need for health policies that prevent and reduce the long term consequences of excess weight in young people in order to ease the future economic and healthcare burden.

Obesity can no longer be considered a condition caused solely by an imbalance between energy intake and expenditure. It is currently acknowledged as a multifactorial condition shaped by genetic predispositions, environmental exposures, and psychological and social behaviors that together contribute to its complex etiology. In fact, the lack of effective health system responses to detect excess weight at an early stage has worsened obesity progression (*Obesity and Overweight*, n.d.), and further supports the need for multi sectoral interventions to reduce the global burden of childhood overweight, obesity, and its associated metabolic syndrome (MetS) (Noubiap et al., 2022).

In contemporary societies, the central nutritional challenge no longer lies in food scarcity but in the quality of diets. Industrialized food systems have expanded access to inexpensive calories and reduced undernutrition in many regions (Monteiro et al., 2013) (with a clear exception of areas affected by armed conflict or extreme political instability). Yet, this has not translated into optimal health outcomes. Instead, the modern dietary landscape, dominated by highly processed foods of poor nutritional value, seems to be one of the major factors in the increase of obesity, including childhood obesity (Z. H. Chen et al., 2025; Handakas et al., 2022; Louzada et al., 2015).

A major hypothesis linking food insecurity with poor dietary patterns is the substitution effect, whereby families (specially those with limited resources) replace higher quality foods (fruits, vegetables and proteins) with cheaper energy dense options (rich in refined carbohydrates and fats). In addition, this is usually aligned with time constraints, where the demands of modern life reinforce this dependence on processed foods, which offer quick and inexpensive solutions at the expense of long-term health.

The accelerating prevalence of overweight and obesity is driven by socio-economic factors and increasingly sedentary lifestyles, highlighting that obesity is not merely the consequence of personal choices. Instead, it emerges from multiple interrelated influences within broader social and economic systems that expose even children to unhealthy food environments from an early age (Costa et al., 2019; Rauber et al., 2015).

Moreover, while addressing these complex drivers will require decades of sustained public health and social policy efforts, the number of individuals living with obesity continues to rise. Consequently, it is essential to design comprehensive strategies that not only improve nutrition but also prevent the onset of metabolic syndrome and mitigate its impact in those already affected. A deep understanding of the molecular and systemic mechanisms underlying diet-related metabolic disorders is critical for developing integrated public health

approaches that could combine pharmacological, nutritional, and behavioral interventions to reduce obesity's burden on health and socioeconomic development.

1.1.2. The Metabolic Syndrome

Metabolic syndrome (MetS) is a cluster of interrelated metabolic factors that significantly increase the likelihood of cardiovascular disease, type 2 diabetes, and other health complications. While its diagnosis sometimes remains subject to debate, the classical definition in the clinic requires the presence of at least three of the following five criteria: (I) increased waist circumference, (II) elevated blood triglycerides, (III) reduced high-density lipoprotein (HDL) cholesterol, (IV) elevated fasting glucose, and (V) high blood pressure (Swarup et al., 2022)

A recent Lancet study found that in 2020, 3% of children and 5% of adolescents had MetS, while it is worth noticing that this was independent of their country's development status (Noubiap et al., 2022). Concerningly, over the past 40 years, childhood obesity and MetS have doubled in prevalence worldwide, highlighting the aforementioned obesogenic environment in which children are growing up (Al-Hamad & Raman, 2017).

Importantly, MetS is not a disease itself but a combination of risk factors, with abdominal fat accumulation being the most common and clinically significant manifestation (Després & Lemieux, 2006). And, although other factors like diet, gut microbiota, stress, lifestyle, and genetics can also contribute to the development of atherosclerotic cardiovascular disease and type 2 diabetes, the interval between the onset of obesity and the development of MetS is alarmingly shortening.

In short, as obesity progresses, excess lipids accumulate in organs not designed for fat storage, such as the liver and muscles (ectopic fat deposition). Enlarged adipocytes and other affected cells then release hormonal and inflammatory metabolites, which contribute to inflammation, tissue damage, and IR (G. A. Bray et al., 2017). Once insulin metabolism becomes impaired, the risk of developing atherosclerotic cardiovascular disease, type 2 diabetes, and neurological complications like stroke rises significantly (Abbasi et al., 2002; Galassi et al., 2006). Despite this, MetS diagnosis still primarily relies on the presence of measurable clinical indicators of cardiovascular disease and diabetes rather than solely on these underlying causes.

1.1.3.Insulin Resistance and Type 2 Diabetes

1.1.3.1 Insulin Resistance

Insulin resistance (IR) refers to the impaired biological response of target tissues to insulin stimulation. Primarily affecting the liver, skeletal muscle, and adipose tissue, IR diminishes glucose disposal efficiency, leading to compensatory overproduction of insulin by pancreatic β-cells, a condition known as hyperinsulinemia.

Since insulin also is an adipogenic hormone (Klemm et al., 2001), it also facilitates the uptake of circulating fatty acids and enhances triglyceride synthesis, which stimulates the storage of these lipids in subcutaneous fat. However, once this tissue is saturated, it can also contribute to ectopic fat in the liver, muscle, pancreas, heart, and other tissues ultimately contributing to IR (Samuel & Shulman, 2012). Hyperinsulinemia state often precedes overt diabetes and defines an asymptomatic prediabetic phase (Kahn, 1994). In line with this, current clinical evidence suggests that hyperinsulinemia, is a key factor underlying the metabolic dysfunction associated with IR (Freeman et al., 2023), including hypertension, dyslipidemia, visceral adiposity, elevated inflammatory markers, endothelial dysfunction, and a prothrombotic state (Freeman et al., 2023).

Insulin actions are mediated through its membrane-bound tyrosine kinase receptor. Upon insulin binding, the intrinsic tyrosine kinase activity of the receptor is activated, initiating a cascade of tyrosine phosphorylation involving insulin receptor substrate (IRS) proteins and subsequent activation of the phosphatidylinositol 3 kinase (PI3K)/protein kinase B (PKB/Akt) signaling axis (Saltiel & Pessin, 2002). Insulin stimulation further leads to PDK1-mediated phosphorylation of Akt at T308 and mTORC2-mediated phosphorylation at S473, fully activating Akt (Sarbassov et al., 2005). Activated Akt then phosphorylates and inhibits the tuberous sclerosis complex 2 (Tsc2) to stimulate downstream mTORC1 signaling, as well as targets glycogen synthase kinase 3 beta (GSK3β) and Forkhead Box O 1 and 3 (FoxO1/3) transcription factors (Manning & Cantley, 2007). These events enable insulin signal transduction to control metabolic enzyme activities and gene expression, ultimately modulating anabolic glucose, lipid, and protein metabolism (Samuel & Shulman, 2012).

From a molecular perspective, IR involves complex alterations in insulin receptor function and downstream signaling pathways. It is not merely the result of a loss of insulin receptors, but often includes receptor desensitization, impaired IRS phosphorylation, and disruption of mediators like PI3K and Akt (Bouzakri et al., 2003; Cozzone et al., 2008). Importantly, these

defects vary across organs, contributing to the diverse manifestations of IR in obesity and dyslipidemia, particularly liver pathology.

In adipose tissue, IR causes decreased glucose uptake and fails to inhibit lipolysis, resulting in elevated free fatty acid release, which aggravates IR in other tissues. Notably, visceral fat depots typically develop IR earlier and more severely than subcutaneous fat, increasing metabolic risk (McLaughlin et al., 2011).

In the liver, insulin promotes de novo lipogenesis (DNL) via the PI3K–AKT–mTORC1–SREBP-1 pathway. Under insulin resistance (IR), the major defect is a loss of insulin's ability to suppress hepatic glucose production, caused by impaired IRS phosphorylation and reduced PI3K–AKT signaling. Notably, blocking insulin/IRS/AKT signaling decreases hepatic lipid deposition even in IR, indicating that insulin can still regulate lipid metabolism through alternative pathways (Bo et al., 2024). In obesity, inflammation and ectopic lipid accumulation aggravate these abnormalities through inhibitory serine phosphorylation of IRS proteins. Although some mouse models show that lowering intrahepatic lipid levels or blocking lipid import can restore hepatic insulin sensitivity, hepatic IR is often considered the initiating event driving systemic and peripheral IR (Sarbassov et al., 2005).

In skeletal muscle, IR reduces insulin-stimulated glucose uptake by impairing GLUT4 translocation to the plasma membrane, a consequence of decreased IRS-1 function and compromised signaling, resulting in diminished glucose utilization and glycogen synthesis (da Silva Rosa et al., 2020).

Beyond these primary tissues, IR also affects the vascular endothelium, brain, and other organs, contributing to endothelial dysfunction, altered nitric oxide production, and dysregulated appetite, which extend IR's impact to cardiovascular and neurological complications (Rask-Madsen & Kahn, 2012).

Moreover, IR is not limited to obesity but also occurs under conditions of energy deficit, such as cancer cachexia and lipodystrophy, both characterized by systemic inflammation, fatty liver, muscle degradation, and increased lipolysis in the context of impaired anabolic insulin action (Fearon et al., 2013). Consequently, the development of therapeutic strategies to improve systemic insulin sensitivity remains critical not only for addressing obesity-related T2D, but also for novel approaches in treating wasting diseases.

1.1.3.2 Type 2 Diabetes

Insulin resistance leads to hyperglycemia. Although this can initially be compensated by increased insulin secretion, a sustained pre-diabetic state results in β-cell exhaustion and ultimately β-cell loss. Once β-cells can no longer adequately regulate blood glucose levels, persistent hyperglycemia ensues, leading to metabolic consequences (Cerf, 2013). Early symptoms are often subtle and not easily detected. The metabolic consequences of hyperglycemia at the tissue level take considerable time to result in tissue failure. The earliest and most common symptoms include polyuria (frequent urination), polydipsia (increased thirst), and fatigue. These symptoms occur because elevated blood glucose causes the kidneys to increase glucose excretion, which draws fluids from the body, resulting in dehydration and tiredness (Veauthier & Levy-Grau, 2024)

A routine clinical biomarker used to diagnose type 2 diabetes is glycated hemoglobin (HbA1c), which reflects the non-enzymatic glycation of hemoglobin by circulating glucose molecules, representing long-term glycemic control under hyperglycemic conditions. However, the etiology of type 2 diabetes remains under debate. Recent studies suggest that hyperinsulinemia might precede IR, proposing it as a potential driver rather than a subsequent consequence (Freeman et al., 2023).

T2D and obesity are normally epidemiologically linked. However, despite the fact that excess weight is a well established risk factor for T2D, most obese individuals do not develop T2D. Recent studies have uncovered several links between obesity and T2D, including proinflammatory cytokines such as TNF (Moller, 2000) and IL-6 (Bowker et al., 2020), reduction of adiponectin secretion (Y. Deng & Scherer, 2010), IR (James et al., 2021), unbalance fatty acid metabolism, and cellular stress responses. Nevertheless, the relative importance of these factors and their interactions remain unclear. In addition, genetic studies have identified common pathophysiological pathways shared between obesity and diabetes, shedding light on why some obese individuals remain metabolically healthy while others develop diabetes (Blüher, 2020; Rönn & Ling, 2015).

Obesity itself is heterogeneous, with even variations in body fat distribution and metabolic health among individuals. Overall, the development of T2D in obese individuals involves a complex interplay of genetic, environmental, and lifestyle factors, underscoring the need for further research to better understand these mechanisms and identify preventive and therapeutic strategies (Eckel et al., 2011).

1.1.4 Metabolic-Dysfunction-Associated Steatotic Liver Disease

Metabolic-dysfunction-associated steatotic liver disease (MASLD), formerly known as non-alcoholic fatty liver disease (NAFLD), has emerged as a predominant global health concern, affecting approximately 38% of the population worldwide (Targher et al., 2024; Wong et al., 2023). It is the most prominent metabolic syndrome associated with obesity, encompassing a spectrum of hepatic disorders (Swarup et al., 2022). Nonetheless, MASLD exhibits varied epidemiological and demographic characteristics worldwide, including a noteworthy portion of lean patients (Younossi et al., 2018). This subset embodies the metabolically obese normal weight (MONW) phenotype, typified by IR and heightened cardiovascular risk. Notably, MONW patients normally present diminished subcutaneous AT storage capacity, compromised mitochondrial function, and augmented hepatic de novo lipogenesis (Stefan et al., 2017), and approximately 5% of the Western population display altered metabolic traits despite maintaining a lean body composition (Conus et al., 2007).

In the MONW spectrum, lipodystrophies are groped at the extreme end. In these patients, the death of subcutaneous fat depot cells leads to pronounced ectopic lipid accumulation in skeletal muscle and liver, which in consequence exacerbate IR (Younes & Bugianesi, 2019).

Notably, IR plays a pivotal role in the development and progression of MASLD, contributing to increased fatty acid influx into the liver, enhancing fatty acid synthesis, and impairing fatty acid oxidation (Yanai et al., 2023). Reason why, obesity is an associated risk factor to this metabolic disorder.

MASLD pathophysiology involves a complex interplay of dietary factors, IR, genetic predisposition, lipotoxicity, and alterations in gut microbiota (Sarwar et al., 2018). Without proper attendance, it can progress from hepatic steatosis to non-alcoholic steatohepatitis (NASH), characterised by lobular inflammation and hepatocyte ballooning, and increasing the risk of fibrosis, cirrhosis, and the development of hepatocellular carcinoma.

Moreover, MASLD and cardiovascular disorders continue to emerge as leading causes of death in non-communicable diseases. And, although pharmacological interventions to improve hyperglycemia and dyslipidemia have potential application across metabolically unhealthy lean, overweight, and obese populations, the multifactorial prevalence of MASLD among these populations, requires refined phenotyping strategies for clinical trials (Stefan et al., 2017).

1.2.The Adipose Tissue

The adipose tissue (AT) is a dynamic endocrine organ that plays a critical role in regulating metabolism in both health and disease. It is broadly classified in white (WAT), beige (BeAT) and brown AT (BAT) according to adipocyte mitochondrial content (Ghesmati et al., 2024), which will determine the ability of these compartments to upregulate the thermogenic uncoupling mitochondrial protein 1 (UCP-1) and determine their specific metabolic function and conditionate their endocrine secretion.

More than just a storage compartment, it secretes key hormones and cytokines (adipokines) such as adiponectin, resistin, retinol-binding protein-4 (RBP4), and interleukin-6 (IL-6), that control and regulate metabolic functions in several distant organs (Galic et al., 2010).

AT is mostly composed of adipocyte precursors/preadipocytes (AP) and adipocytes, as well as various types of immune cells, including macrophages, dendritic cells, T cells, and B cells. AP are stem cells like fibroblasts that actively produce paracrine factors, hormones, and metabolic signals. They retain the capacity to differentiate into multiple lineages; however, while their adipogenic potential remains preserved (Zhu et al., 2009), their overall developmental plasticity appears to decline with age (H. P. Nguyen, Yi, & Sul, 2020). After differentiation (adipogenesis) these cells become responsive to insulin, start accumulating lipids and lose the ability to differentiate to other cell types. On the other hand AT immune cells , especially macrophages (making up about 40–50% of all immune cells in AT) also contribute to monitor and maintain the health of adipocytes, especially their sensitivity to hormones (R. Liu & Nikolajczyk, 2019; J. Lu et al., 2019).

1.2.1 Adipogenesis

Adipogenesis is the process through which multipotent progenitor stem cells differentiate into three main types of adipocytes: white, brown, and beige (also known as "brite") adipocytes (Figure 1.1). The formation of new adipocytes maintains metabolic balance by promoting healthy fat expansion through increased adipocyte number rather than harmful enlargement of existing cells. This process supports proper adipokine secretion, lipid metabolism, and insulin sensitivity, protecting against obesity-related complications.

Healthy adipose remodeling involves coordinated cellular and structural changes that preserve function and prevent inflammation and fibrosis. Impaired plasticity, however, can exceed physiological thresholds, leading to dysfunctional adipose tissue, chronic inflammation, and metabolic disease. Thus, enhancing adipose tissue plasticity by targeting

progenitor cells and differentiation pathways represents a promising strategy to improve systemic metabolic health (L. Cheng et al., 2021; Ghaben & Scherer, 2019; Ros Pérez & Medina-Gómez, 2011).

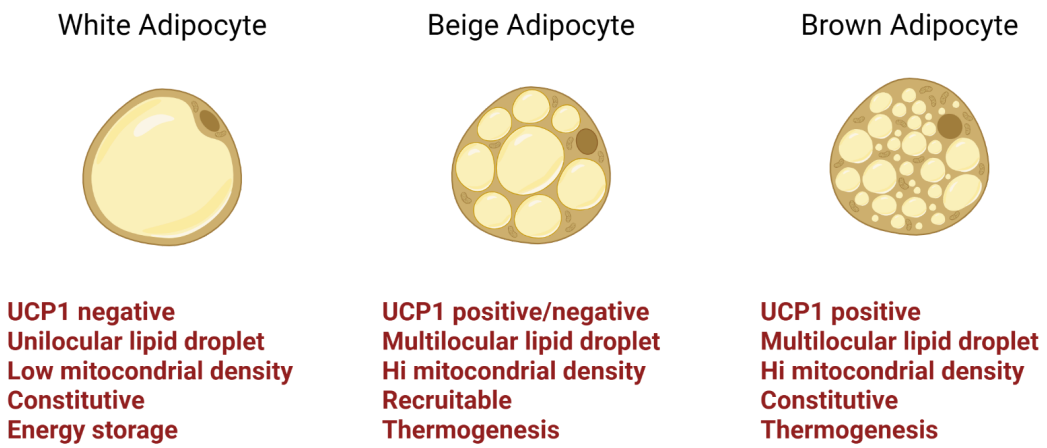

Figure 1.1: Adipocyte classification.

There are three main types of adipocytes: white, brown, and beige mainly classified by its mitochondrial content and origin. Image created in BioRender Adapted from Silva & Amato et. al (G. da N. Silva & Amato, 2022)

Adipocyte types arise from distinct developmental lineages and fulfill different physiological roles within AT (Figure 1.2). White adipocytes primarily function in energy storage and develop mainly from Myf5-negative mesenchymal progenitors (Figure 1.1 and 1.2). Their differentiation is regulated by key transcription factors including PPARγ, C/EBPα/β, TCF21, TLE3, HOXC8/9, and FABP4 (J.-E. Lee et al., 2019). In contrast, brown adipocytes, which are specialized for thermogenesis and rich in mitochondria (Figure 1.1), originate from Myf5-positive progenitors shared with muscle cells; their differentiation depends on regulators such as PRDM16, PGC1α, PPARγ, C/EBPβ, EBF2, BMP7, and UCP1 (Inagaki et al., 2016; Seale et al., 2008) (Figure 1.2). On the other hand, beige adipocytes display a hybrid phenotype with thermogenic capabilities similar to brown fat (Figure 1.1) but originate either de novo from Myf5-negative resident progenitors or via the transdifferentiation of mature white adipocytes upon external stimuli such as cold exposure, β-adrenergic agonists, irisin, or FGF21 (Pilkington et al., 2021) (Figure 1.2). Beige cells express several thermogenic markers including UCP1, CIDEA, TMEM26, CD137, TBX1, and CITED1, which highlights their functional convergence with brown adipocytes despite their distinct lineage (Pilkington et al., 2021; J. Wu et al., 2012) (Figure 1.2).

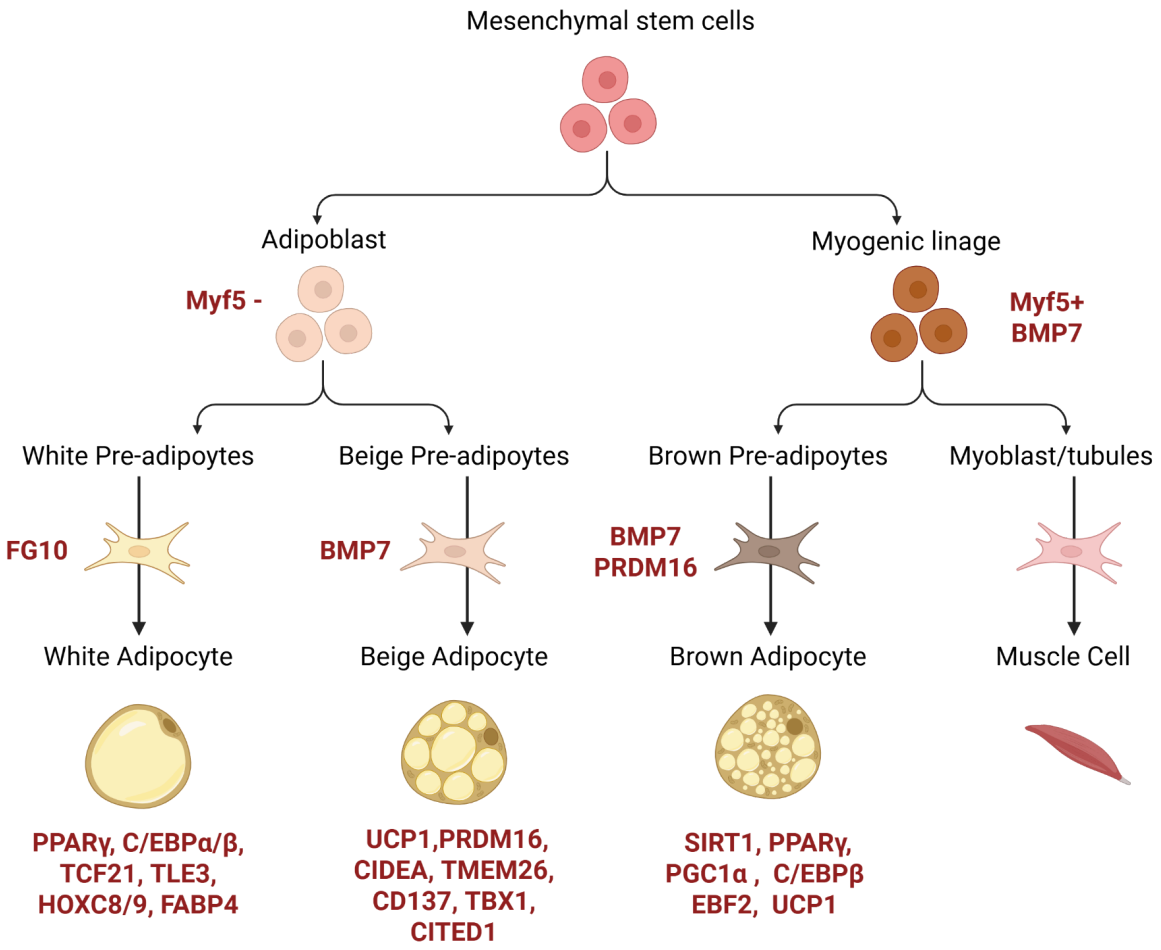

Figure 1.2: Brown, beige and white adipocytes linage

White adipocytes develop mainly from Myf5- mesenchymal progenitors and specialize in energy storage. Their differentiation is driven by transcription factors such as PPARγ, C/EBPα/β, TCF21, TLE3, HOXC8/9, FABP4, and others. Beige (brite) adipocytes either arise de novo from resident progenitors (often Myf5-) or result from the transdifferentiation of mature white adipocytes upon specific stimuli such as cold, β-adrenergic agonists, irisin, or FGF21. These cells share thermogenic properties with brown adipocytes and express key markers including UCP1, CIDEA, TMEM26, CD137, TBX1, and CITED1 Brown adipocytes originate from Myf5+ progenitors that are shared with myocytes and are dedicated to thermogenesis, being rich in mitochondria. Key regulators of this lineage include PRDM16, PGC1α, PPARγ, C/EBPβ, EBF2, BMP7, and UCP1, among other factors. Image generated in Biorender.

1.2.2.1 The browning process

Brown, beige, and white adipocytes differ in developmental origin and function. Classical brown adipocytes arise prenatally from Myf5-expressing progenitors and reside mainly in dedicated BAT depots, where they continuously produce heat. In contrast, beige and most white adipocytes derive from Myf5-negative precursors (Figure 1.2) (Billon et al., 2007). Unlike brown adipocytes, beige adipocytes are inducible postnatally within WAT and acquire thermogenic properties in response to appropriate stimuli (Figure 1.3). Environmental

factors, notably temperature, strongly regulate the abundance and phenotype of both brown and beige adipocytes. Chronic cold exposure, for example, stimulates proliferation of interscapular brown adipocytes in mice, whereas warmer temperatures induce apoptosis and "whitening" of these cells (Bukowiecki et al., 1982; Lindquist & Rehnmark, 1998).

Functionally, brown and beige adipocytes exhibit high basal thermogenic activity through the activation and expression of UCP1, which increases energy expenditure. In contrast, white adipocytes predominantly prioritize energy storage via distinct transcriptional mechanisms (Billon et al., 2007; Y.-H. Lee et al., 2012; Seale et al., 2008) (Figure 1.1).

The thermogenic programs of brown and beige adipocytes are primarily driven by activation of β-adrenergic receptors, especially the β3 subtype (Ghorbani et al., 1997; Rosell et al., 2014), although adrenergic-independent factors such as cytokines and hormones also modulate browning responses (Herz & Kiefer, 2019; Jun et al., 2020). Of note, although both brown and beige adipocytes can become white (Figure 1.3), only beige adipocytes retain an epigenetic memory, allowing rapid reactivation of their thermogenic machinery upon restimulation (Roh et al., 2018).

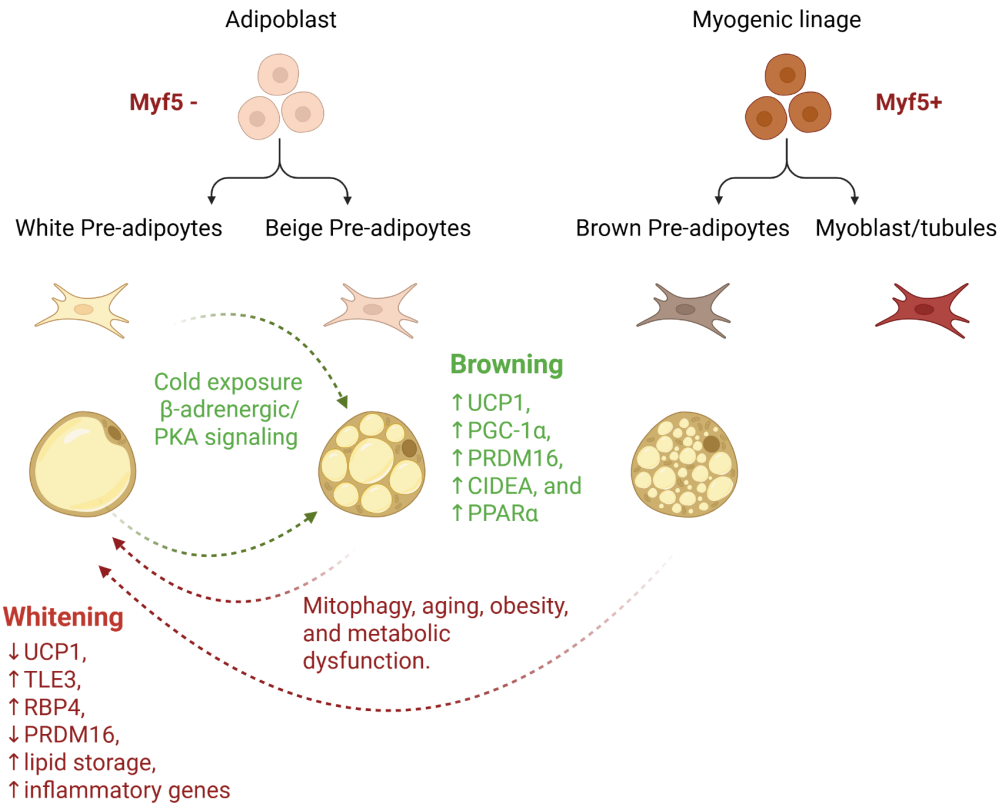

Figure 1.3 Adipocytes plasticity, browning and whitening processes.

Browning can occur both from WAT-resident progenitor cells as well as through the direct reversible transition of mature white adipocytes in response to stimuli such as cold exposure, β-adrenergic activation, exercise, or hormonal factors. In both cases, the main upregulated pathways during browning include the β-adrenergic/PKA signaling cascade, resulting in increased expression of genes like UCP1, PGC-1α, PRDM16, CIDEA, and PPARα. Whitening of Brown/Beige Adipocytes: Occurs under conditions like aging, chronic overnutrition, or lack of thermogenic stimuli. Features loss of UCP1, increased TLE3, decreased PRDM16, increased RBP4, and elevated expression of genes linked to lipid storage and adipose inflammation. Image created in Biorender.

The plasticity of adipose tissue plays a crucial role in energy balance and metabolic health by linking browning processes to leanness and enhanced metabolism. Targeting BAT activation and promoting WAT browning remain promising strategies for the treatment of obesity and diabetes. Non-pharmacological interventions such as exercise, prolonged intermittent fasting, dietary modulation of the gut microbiota, mild cold exposure, and brown adipocyte stem cell transplantation can effectively stimulate BAT activation and growth. Additionally, pharmacological approaches including β-adrenergic receptor agonists, immunomodulators that favor anti-inflammatory macrophage programming (e.g., SGLT2 inhibitors), and insulin signaling sensitizers like imatinib have demonstrated efficacy in increasing energy expenditure via WAT browning (Giralt & Villarroya, 2013; G. Li et al., 2017; Moreno-Navarrete & Fernandez-Real, 2019). Collectively, these multifaceted strategies hold great potential for restoring adipose tissue function and improving metabolic outcomes in obesity-related disorders.

1.2.2.1 BAT whitening

BAT whitening is driven by multiple factors including high ambient temperature, aging, leptin receptor deficiency, impaired β-adrenergic signaling, and lipase deficiency (Figure 1.3). Under thermoneutral conditions, whitening involves decreased mitochondrial biogenesis coupled with alterations in autophagy- and lysosome-related gene expression, impaired vascularization, increased inflammation, and endoplasmic reticulum stress (Altshuler-Keylin et al., 2016, 2016; Ginting et al., 2023; Rangel-Azevedo et al., 2022).

This process is characterized by reduced expression of thermogenic genes, mitochondrial density and mitochondrial protein production, leading to diminished non-shivering thermogenesis and a white fat-like phenotype (Altshuler-Keylin et al., 2016; Ginting et al., 2023; Y. Lu et al., 2018; Rangel-Azevedo et al., 2022; Uldry et al., 2006). Moreover, BAT whitening involves significant triglyceride accumulation primarily from de novo lipogenesis (Schlein et al., 2021), while the metabolic remodeling contributes to brown adipocyte death,

macrophage recruitment (CLS formation) and increased inflammatory processes (Kotzbeck et al., 2018; Rangel-Azevedo et al., 2022).

In sum, whitening contributes to reduced thermogenic capacity and metabolic dysfunction.

1.2.2 The White Adipose Tissue

WAT is central to the pathology of obesity-related disorders. Composed mainly by white adipocytes, secretes several metabolites that regulate functions in distant tissue like heart, liver and muscle, while its efficient storage function is key to prevent ectopic and harmful accumulation of lipids (lipotoxicity) (Azzu et al., 2020). It is classified into two main compartments according to their distinct metabolic functions, subcutaneous (ScWAT) and visceral or perigonadal/gonadal (GWAT) (Ronquillo et al., 2019). To a lesser extent, white adipocytes are also found in other locations, including the bone marrow, surrounding larger blood vessels (perivascular), forming a thin layer within the skin (dermal WAT), surrounding the heart (epicardial), within muscle tissue (intramuscular adipocytes) or in the pancreas (pancreatic adipocytes) (Hagberg & Spalding, 2024).

Generally, differences between fat depots are mainly attributed to gene expression profiles, epigenetic modifications, and varying sensitivities to adipogenic stimuli. During adipose tissue expansion, fat depots grow either by adipocyte hypertrophy (increase in size) or hyperplasia (increase in number), a mechanism influenced by the differentiation predisposition of adipocyte precursors. Notably, visceral adipose tissue precursors tend to favor hypertrophic expansion (Pellegrinelli et al., 2016), whereas subcutaneous adipocyte precursors are more efficient at adipogenesis due to their distinct gene expression profiles (Kirkland et al., 2002; Macotela et al., 2012).

Although several factors determine AT distribution and growth, such as genetic predisposition, type of diet, exercise and hormonal control, as a general rule, men tend to accumulate more in lipids GWAT, influenced by testosterone (Enzi et al., 1986), while women typically have higher ScWAT deposition, especially in the gluteo-femoral región due to oestrogen. In fact, one of the consequences of decline in oestrogen in post-menopausal women is a marked increase in GWAT deposition. Moreover, ageing also affects fat cell dynamics, reducing the differentiation of preadipocytes into mature adipocytes. This dysregulation can lead to adipose tissue dysfunction, ectopic fat deposition, inflammation, and predisposes elderly patients to metabolic disorders (Cartwright et al., 2007; Ronquillo et al., 2019; Smith & Kahn, 2016). These differences underline the importance of

gender-specific strategies to manage and prevent obesity-related metabolic disorders in aged populations.

1.2.2.1 Subcutaneous WAT

ScWAT represents the most prominent WAT depot in lean, healthy individuals. It comprises about 80% of all adipose tissue (Reddy et al., 2019) and can be divided into "upper" and "lower" regions, mainly situated in the trunk and gluteal-femoral zones, respectively.

Upper subcutaneous WAT is often grouped with visceral WAT as "abdominal fat", although it exhibits distinctive functions. ScWAT acts as a buffer for excess energy intake by storing lipids during periods of high-calorie consumption. Additionally, it serves as a temperature insulator, a barrier against infections, and a cushion protecting against impacts (Mittal, 2019).

ScWAT plays a central role in systemic metabolism by acting as a lipid buffer. Its adipocyte precursors are intrinsically distinct, showing higher proliferative capacity, elevated adipogenic transcription factors, and a permissive chromatin state that persist into adulthood as cell-autonomous traits, suggesting a strong heritable component in WAT distribution (Kahn et al., 2019; Kim et al., 2016; van Harmelen et al., 2002; Vidal, 2001). When this buffering capacity is exceeded in obesity, adipocyte hypertrophy and reduced adipogenesis trigger inflammation and ectopic lipid deposition (Patel & Abate, 2013). ScWAT also produces higher leptin levels than VAT across lean and obese states (Table 1.1) (Lefebvre et al., 1998; Spoto et al., 2014; van Harmelen et al., 2002). Regionally, greater gluteofemoral ScWAT is linked to lower insulin resistance and favorable cardiometabolic profiles independent of BMI (Huang et al., 2023; McLaughlin et al., 2011), whereas ScWAT loss in lipodystrophy increases disease risk (Mann & Savage, 2019).

Adipokine or Secreted Factor	Source Cells	Depot	Pro or Anti-Inflammatory	Lean/Obese/Both	References
Leptin	adipocytes	ScWAT > Omental	Pro	Both	(Wiest et al., 2010)
Adiponectin HMW	adipocytes	Omental > ScWAT	Anti	Both	(Kovacova et al., 2012)
PAI-1	PA	Possibly, Omental > ScWAT	Pro	Both	(X. J. Xu et al., 2012)
IL-6	PA,macrophages, activated endothelial cells, large adipocytes	GWAT > ScWAT	Pro	Obese	(Fontana et al., 2007)
TNF-α	preadipocytes, macrophages, adipocytes	Mesenteric > Omental = ScWAT	Pro	Both	(Cartier et al., 2008; X. J. Xu et al., 2012)
MCP-1	preadipocytes, macrophages	VAT > ScWAT	Pro		(Madani et al., 2009; Miller et al., 2011)
Angiotensin	fat tissue	Omental > ScWAT	Pro	Both	(Dusserre et al., 2000; van Harmelen et al., 2000)
CCL5 (RANTES)	stromal vascular fraction, adipocytes	Gastric fat> Omental = ScWAT	Pro	Both	(Madani et al., 2009)
CSF-1	endothelial cells, fibroblasts	VAT > ScWAT	Pro	Both	(Harman-Boehm et al., 2007)
Omentin	stromal vascular cells	Omental > ScWAT	Anti	Lean	(Yang et al., 2006)
RBP4	PA, adipocytes	VAT < ScWAT	Pro	Both	(Kos et al., 2011)
Chimerin	unknown	VAT < ScWAT	Unknown	Both	(Alfadda et al., 2012)
Vaspin	adipocytes	VAT > ScWAT	Anti	Both	(Hida et al., 2005)

Table 1.1: Cytokine production of the different WAT depots.

Relative expression of cytokines production of different white adipose tissue depots and its pro- or antiinflammatory functions and its upregulation during obese or lean conditions. Adapted from Tchkonia et al., 2013(Tchkonia et al., 2013). PA: preadipocytes

1.2.2.2 Visceral/Gonadal WAT

Lean, healthy individuals typically have minimal visceral/gonadal white adipose tissue (GWAT). Normally, GWAT constitutes 5–20% of the total body fat mass in humans and includes intraperitoneal (omental, mesenteric, epiploic), retroperitoneal, mediastinal, gonadal and pericardial adipose depots (Chait & den Hartigh, 2020; Hagberg & Spalding, 2024).

GWAT has a higher rate of blood flow per unit of tissue compared to ScWAT despite having poorer overall vascularization (J. Ye, 2011), which facilitates the rapid release of free fatty acids, inflammatory cytokines and other metabolites into the portal circulation. Differently from ScWAT, its physiological role seems to serve as a reservoir of innate and adaptive immune cells with direct implication in immune surveillance (Cao et al., 2021). In fact, VAT microenvironment is less favourable for adipogenesis, marked by higher oxidative stress and hypoxia, and some authors even perceived GWAT deposition as an ectopic lipid accumulation (Pou et al., 2007).

In addition, preadipocytes from GWAT have relatively higher metabolic rate (R. Liu et al., 2015), are more sensitive to lipolysis (due to increased number of β1- and β2-receptors), particularly in nonobese individuals (Arner et al., 1990; Hellmér et al., 1992), present a higher insulin-stimulated glucose uptake in-vitro (Perrini et al., 2008) and more resistance to the antilipolytic action of insulin (J. A. Johnson et al., 2001).

Last, adipokine secretion also varies between fat depots (Table 1.1). Hypertrophic adipocytes in VAT secrete more inflammatory cytokines (such as TNF and IL-6), that recruit and activate immune cells (Caër et al., 2017; Weyer et al., 2000), However, isolation studies revealed that despite having lower mRNA levels, GWAT derived adipocytes secreted three times more adiponectin (Perrini et al., 2008) showing a prominent anti-inflammatory program as well (Table 1.1).

1.2.3 The Brown Adipose Tissue

BAT is essential for nonshivering thermogenesis in mammals. Mainly located on the back side of the neck, brown adipocytes contain a high number of mitochondria and express uncoupled respiratory chain protein (UCP1) in their inner mitochondrial membranes. This

protein uncouples the proton motive force from oxidative phosphorylation to dissipate energy as heat using energy to maintain core body temperature (Cannon & Nedergaard, 2004).

BAT dynamically adapts to environmental cues, decreasing brown adipocyte numbers with inactivity and activating under cold or hormonal stimulation (Cannon & Nedergaard, 2004). Although once thought to disappear after infancy (Cereijo et al., 2015; Eckel et al., 2011), BAT remains metabolically active in adults, contributing to energy expenditure and protection against metabolic syndrome (Frontini & Cinti, 2010; Giralt & Villarroya, 2013), while during ageing, BAT loses mitochondria content and tends to shift towards beige phenotype (Sidossis & Kajimura, 2015).

Loss of brown adipocytes is also a hallmark of obesity. Obese individuals exhibit decreased BAT mass and activity due to impaired brown adipocyte differentiation, reduced proliferation, and increased apoptosis, which contributes to diminished thermogenic capacity and energy expenditure. This loss of BAT thermogenic potential exacerbates metabolic dysfunctions observed in obesity. Strategies aimed at enhancing BAT recruitment, improving mitochondrial function, or promoting beige adipocyte formation in white fat depots are promising therapeutic avenues to counteract obesity and its related metabolic complications (C.-H. Wang & Wei, 2021).

1.3 Cell Death and Inflammation

Inflammation represents a fundamental biological program. Activated in response to infection, tissue damage, metabolic stress, or functional perturbation, has the overarching aim of preserving or restoring homeostasis. Although frequently associated with pathology, inflammatory signaling is also an intrinsic component of physiological tissue adaptation and repair. At the center of these processes stands cell death. Rather than being a simple outcome of inflammation, cell death acts as a critical driver of immune activation, linking the preservation of tissue integrity to host defense. The growing recognition of this reciprocal relationship reframes inflammation and cell death not as sequential events but as interconnected processes whose dynamic interaction determines tissue fate, whether resolution, regeneration, or progression toward chronic dysfunction.

Cell death can occur through the genetically encoded programs of apoptosis, necroptosis, and pyroptosis, or as a consequence of metabolic dysregulation, as in ferroptosis (Newton et al., 2024). In contrast, cell proliferation maintains tissue integrity by replacing senescent, damaged, or infected cells; disruption of the balance between proliferation and death drives organismal dysfunction (Newton et al., 2024).

Among the key mediators of regulated cell death are death receptors (DRs), a subclass of the tumor necrosis factor receptor superfamily (TNFRSF) defined by their intracellular death domain (DD) (Walczak, 2013). Classical members include TNFR1, Fas/CD95, TRAIL-R1/DR4, TRAIL-R2/DR5, and DR3 (Annibaldi & Walczak, 2020).

Upon ligand binding, DRs assemble apical protein complexes through DD adaptors such as Fas-associated death domain (FADD) and Tumour necrosis factor receptor type1-associated death domain protein (TRADD) to initiate cytotoxic signaling and apoptosis (Wilson et al., 2009). Yet despite their name, DRs also drive diverse noncytotoxic processes including proliferation, differentiation, chemokine release, inflammation, and tumor-promoting activities. These functions are actively regulated by adaptor networks and receptor trafficking rather than solely through suppression of apoptosis (Galluzzi et al., 2012; Guicciardi & Gores, 2009).

In this thesis, the focus will be on TNFR1-mediated pathways governing cell death and NF-κB/MAPK signaling in the context of metabolic disease.

1.3.1 TNFR1-Induced Cell Death

TNFR1 is expressed on many cell types and has important roles in pathogen defense (Rothe et al., 1993; Stutz et al., 2021; Wajant et al., 2003) but sustained activation of this receptor can also fuel chronic inflammation. Although TNFR1 is named for its role in inducing cell death (tumor necrosis factor), under normal physiological conditions, TNFR1 signaling predominantly promotes inflammation and cell survival (Ting & Bertrand, 2016). Unlike other death receptors such as Fas (CD95) and TNF-related apoptosis-inducing ligand receptors (TRAIL-R1/DR4 and TRAIL-R2/DR5), which form a multiprotein assembly known as the death-inducing signaling complex (DISC) (Walczak, 2013), that latter initiates extrinsic apoptosis by recruiting adaptor proteins such as FADD and caspase-8 (Casp-8) (Walczak, 2013). TNF binding to TNFR1 primarily triggers the formation of complex I through interactions of the death domain (DD) (Micheau & Tschopp, 2003; Newton et al., 2024). (Figure 1.4). This induces receptor aggregation and the recruitment of multiple adaptor proteins that activate NF-κB and MAPK signaling pathways (described in the following section) (Figure 1.4). This activation drives the expression of pro-survival and pro-inflammatory genes, including anti-apoptotic proteins which inhibit the formation of cell death-inducing complexes (Hughes et al., 2016).

After trimerization, TRADD and RIPK1 are recruited to TNFR1 via homotypic DD interactions, with TRADD subsequently recruiting E3 ligases TRAF2 and TRAF5 (Figure 1.5). TRAF2 plays a crucial role in recruiting the cellular inhibitor of apoptosis proteins cIAP1 and cIAP2 through its interaction motif (CIM) (Hsu et al., 1996; Vince et al., 2009; Wajant & Scheurich, 2001). These ligases catalyze the addition of K63-, K11-, and K48-linked polyubiquitin chains to RIPK1 and cIAP1, which prevents RIPK1 autophosphorylation and maintains its engagement with the complex (Annibaldi et al., 2018; Bertrand et al., 2008; Dynek et al., 2010). These ubiquitin chains facilitate the recruitment of the linear ubiquitin chain assembly complex (LUBAC) and the kinase complex TAK1/TAB2/TAB3. LUBAC conjugates M1-linked polyubiquitin chains to components of complex I, including RIPK1, TRADD, and TNFR1, reinforcing the stability of the complex (Draber et al., 2015; Gerlach et al., 2011). This enhanced ubiquitination promotes efficient recruitment and activation of the IKK complex (which consists of NEMO, IKKα, and IKKβ) leading to downstream activation of NF-κB (Zinngrebe et al., 2014) (Figure 1.5). Activation of TAK1 and IKK within complex I triggers NF-κB and MAPK signaling pathways that drive the expression of pro-inflammatory genes (Figure 1.5) such as Ccl2, Ccl3, Ccl5, Csf2, Cxcl1, Cxcl2, Il1b, Il6, Nos2, and Tnf, as well as pro-survival genes including Bclx and Cflar (Newton et al., 2024).

Under specific stress or pathological conditions, destabilization of complex I can trigger the formation of its cytosolic form, the TNFR complex II (Figure 1.4). Complex II assembles upon dissociation of complex I and consists of RIPK1, FADD, and procaspase-8 (Casp-8) (R. Guo et al., n.d.; Hughes et al., 2016; Kantari & Walczak, 2011; Kuwana et al., 1998) (Figure 1.4). Procaspase-8 is recruited and undergoes proximity-induced dimerization, initiating autocatalytic cleavage at specific aspartate residues and generating active subunits (p43/p41 and p10/p12). This cleavage releases Casp-8 in its active form, enabling it to cleave and activate executioner caspases such as caspase-3 (Casp3), leading to apoptosis. Concurrently, Casp-8 cleaves Gasdermin D (GsdmD) at its inactivating site, thereby preventing canonical pyroptosis, another highly inflammatory form of programmed cell death (Taabazuing et al., 2017) (Figure 1.4).

The activation of Casp-8 is tightly controlled by the cellular FLICE-inhibitory protein (c-FLIP), an enzymatically inactive homolog of Casp-8. c-FLIP isoforms form heterodimers with Casp-8 at complex II, modulating its activation (Hillert-Richter et al., 2024). The long isoform (c-FLIPL) can prevent full Casp-8 processing and inhibit apoptosis while allowing limited catalytic activity that supports non-apoptotic roles such as NF-κB activation. This balance determines cell fate toward survival or death and acts as a critical regulatory checkpoint (Martinez-Lagunas et al., 2023; Hughes et al., 2016).

Casp-8 also cross-talks with mitochondria by cleaving BID to truncated BID (tBID), promoting outer mitochondrial membrane permeabilization and amplifying apoptotic signaling via cytochrome c release and caspase-9 activation (Kantari & Walczak, 2011; Kuwana et al., 1998). In addition, Gasdermin E (GsdmE) can be cleaved by caspase-3, inducing plasma membrane and mitochondrial membrane pore formation that amplifies cell death responses (Rogers et al., 2017, 2019) (Figure 1.4).

Although apoptosis is traditionally considered a non-inflammatory form of cell death, caspase activation can provoke inflammation (Dannappel et al., 2014; Kumari et al., 2014; Rickard et al., 2014). The accumulation of apoptotic bodies can lead to secondary necrosis and the release of pro-inflammatory signals (Rock & Kono, 2008; M. T. Silva et al., 2008). Simultaneously, Casp-8 acts as a critical checkpoint preventing necroptosis by cleaving and inactivating autophosphorylated RIPK1 (Figure 1.4). Failure of this checkpoint allows RIPK1 to recruit RIPK3 via RHIM domain interactions, leading to RIPK3 activation. Activated RIPK3 phosphorylates the pseudokinase MLKL, which forms pores in the plasma membrane, inducing necroptotic cell death (Figure 1.4) (Murphy et al., 2014; Sun et al., 2012). This

process triggers immune cell recruitment through release of intracellular contents and pro-inflammatory mediators (Hildebrand et al., 2014; Tanzer et al., 2020).

Caspase-1 (Casp1) plays a pivotal role in inflammation and cell death. Initially was recognized for processing of interleukin-1β (IL-1β) and interleukin-18 (IL-18), essential cytokines in immune responses (Takeuchi & Akira, 2010). In the early 2000s, caspase-1 was shown to mediate a novel programmed cell death with pore formation and release of pro-inflammatory cytokines, termed pyroptosis. Canonical pyroptosis requires priming by signals such as toll-like receptor 4 (TLR4) activation by lipopolysaccharides (LPS), which upregulates inflammasome components NLRP3, ASC, and caspase-1. Upon activation by danger-associated molecular patterns (DAMPs) like ATP or NLRP3, oligomerizes with ASC and pro-caspase-1, forming the inflammasome complex. Caspase-1 is activated and cleaves Gasdermin D (GsdmD), whose N-terminal fragment forms membrane pores to execute pyroptosis (Figure 1.4). Caspase-1 also processes pro-IL-1β into its mature form, released through GsdmD pores (Figure 1.4).

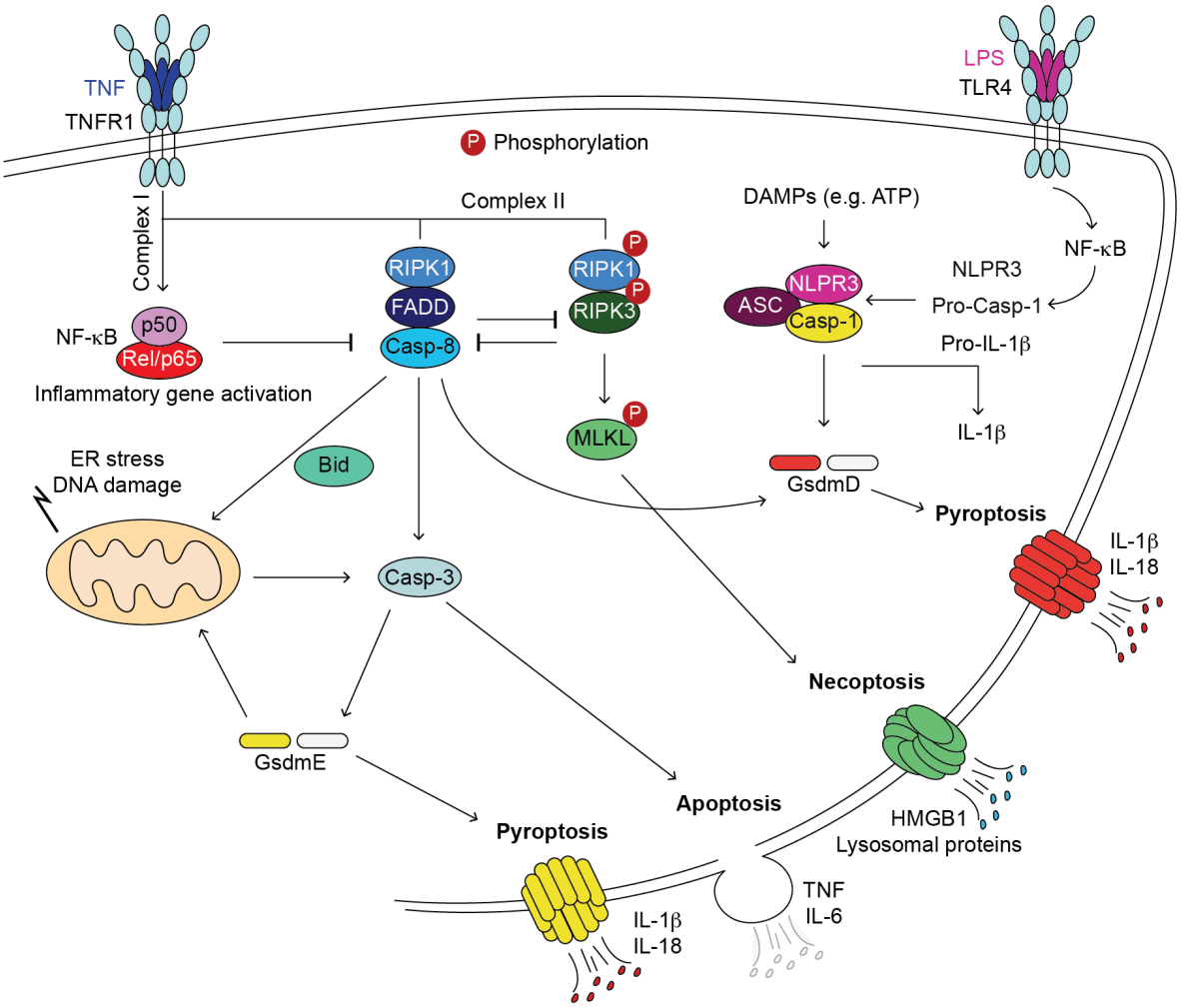
TNF
TNFR1
LPS
TLR4
P Phosphorylation
Complex I
Complex II
DAMPs (e.g. ATP)
NF-κB
RIPK1
FADD
Casp-8
RIPK1
RIPK3
NLPR3
ASC
Casp-1
Pro-Casp-1
Pro-IL-1β
NF-κB
p50
Rel/p65
Inflammatory gene activation
MLKL
IL-1β
GsdmD
Pyroptosis
ER stress
DNA damage
Bid
Casp-3
IL-1β
IL-18
Necoptosis
GsdmE
Apoptosis
HMGB1
Lysosomal proteins
Pyroptosis
TNF
IL-6
IL-1β
IL-18

Figure 1.4: Different cell death modalities upon activation of receptors of the TNFR1 family. (Hildebrandt et al., 2022)

Activation of NF-κB prevents formation of cell death complexes, however, under pathological conditions, TNF can induce the formation of complexes that promote cell death. Apoptosis is triggered by a complex formed from RIPK1, FADD, and caspase-8 (Casp-8). This leads to cleavage and activation of caspase-3 (Casp3), resulting in apoptosis. In some cases, caspase-8 also cleaves Gasdermin D (GsdmD), triggering pyroptosis, an inflammatory form of programmed cell death. Necroptosis is initiated when RIPK1 recruits and activates RIPK3 by autophosphorylation. RIPK3 then phosphorylates MLKL, which forms pores in the plasma membrane leading to rupture. Apoptotic and necroptotic pathways suppress each other by Caso8 activation. Canonical pyroptosis requires an initial priming step that increases the expression of inflammasome components such as NLRP3, ASC, and caspase-1. This is often achieved through toll-like receptor 4 (TLR4) activation by lipopolysaccharides (LPS). Danger signals like ATP activate NLRP3, which oligomerizes with ASC and pro-caspase-1 to form the inflammasome complex. This activates caspase-1, which cleaves Gasdermin D to form membrane pores inducing pyroptosis, and processes pro-IL-1β to its mature form, which is then released through these pores. Pyroptosis can also be induced by Gasdermin E (GsdmE), which is cleaved and activated by caspase-3. Gasdermin E amplifies cell death by forming pores not only in the plasma membrane but also in mitochondrial membranes. Phosphorylated proteins are indicated by "P."

Thus, TNF-induced cell death via complex II formation represents a regulated backup pathway that occurs when survival and inflammatory signals from complex I fail, highlighting the dual role of TNFR1 signaling in controlling inflammation and cell fate.

1.3.2 The NF-κB pathway

The NF-κB signalling pathway plays a central role in regulating immunity, inflammation, cell survival, differentiation, proliferation, and stress responses. Through transcriptional control, NF-κB influences a wide range of genes that shape both protective and pathological outcomes (T. Liu et al., 2017). The NF-κB transcription factor is composed of homo- or heterodimers formed by the family members p50 (p105/NF-κB1), p52 (p100/NF-κB2), RelA (p65), RelB, and c-Rel. In resting conditions, these dimers are kept inactive in the cytoplasm by inhibitors of NF-κB (IκB) proteins (Oeckinghaus & Ghosh, 2009) (Figure 1.5). Activation occurs through a wide range of stimuli, including pathogen-associated molecular patterns (PAMPs), damage-associated molecular patterns (DAMPs), and pro-inflammatory cytokines such as IL-1β, LPS, TNF, TRAIL, and CD95L (T. Liu et al., 2017) (Figure 1.5). These stimuli activate the IκB kinase (IKK) complex, which consists of the catalytic subunits IKKα (IKK1) and IKKβ (IKK2), together with the regulatory subunit NEMO/IKKγ (Israël, 2010). The IKK complex phosphorylates IκB proteins, marking them for ubiquitination and proteasomal degradation, thereby releasing NF-κB dimers. Free dimers then translocate into the nucleus to bind κB sites and initiate transcription of target genes (Hoesel & Schmid, 2013) (Figure 1.5).

NF-κB signalling can proceed through two distinct pathways. The canonical pathway is rapid, driven mainly by degradation of IκB proteins, and mediated by p50/p65 or p50/c-Rel heterodimers in an IKKβ- and NEMO-dependent manner (Figure 1.5). It underlies immediate responses to stimuli and must be tightly regulated, since chronic activation drives inflammatory and autoimmune disorders, metabolic diseases, and cancer (Baker et al., 2011; J. Chen & Chen, 2013; Karin, 2006). In contrast, the non-canonical pathway is slower, activated mainly by TNF superfamily members such as CD40L, RANKL, BAFF, and LIGHT. It is independent of NEMO and instead relies on IKKα and NF-κB-inducing kinase (NIK) (Figure 1.5). Normally, NIK is continuously degraded, but stimulation leads to its stabilization, phosphorylation of IKKα, and processing of p100 to p52, which pairs with RelB to regulate transcription (Vallabhapurapu et al., 2008; Zarnegar et al., 2008) (Figures 1.5). Additionally, TBK1 and IKKε are non-canonical IKKs induced by cytokines such as TNF, IL-1, and IL-6, as well as LPS. TBK1 is broadly expressed, whereas IKKε shows tissue-enriched expression in lymphoid organs, blood, and pancreas (Peters et al., 2000; Pomerantz & Baltimore, 1999; Shimada et al., 1999; Tojima et al., 2000).

Because NF-κB activation influences powerful survival and inflammatory pathways, it is tightly regulated by multiple feedback loops. Two of the most important negative regulators are IκBα and A20, both induced by NF-κB itself. They ensure oscillatory dynamics in response to autocrine and paracrine cytokine signals such as TNFα and IL-1β (Pękalski et al., 2013) (Figure 1.5).

Beyond immunity and inflammation, NF-κB plays a key role in maintaining cell viability. Upon TNFR1 engagement, NF-κB drives the transcription of anti-apoptotic genes, including A20, Bcl-xL, and c-FLIP, and suppresses sustained JNK signalling (G. Tang et al., 2001) (Figure 1.5). When NF-κB activation is absent or impaired, TNFR1 signalling shifts toward caspase-dependent apoptosis, as described by the sequential assembly of the death-inducing complex (Micheau & Tschopp, 2003). This protective role of NF-κB explains why its activation must balance between appropriately promoting survival while avoiding pathological over-activation.

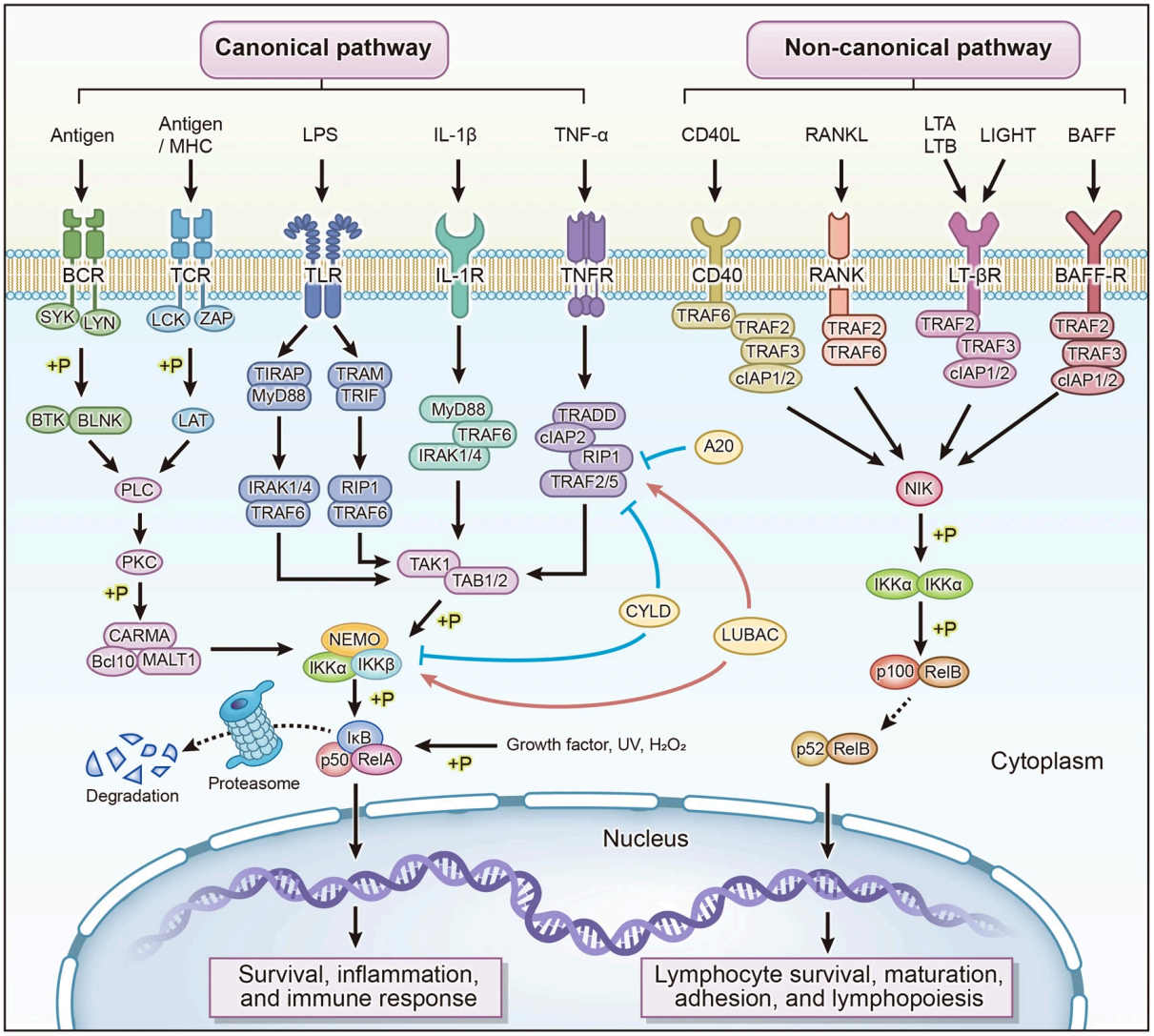

Figure 1.5: Activation of NF-κB pathway (Q. Guo et al., 2024)

Canonical NF-κB signaling is activated by membrane receptors including BCR, TCR, TLR, IL-1R, and TNFR. BCR and TCR trigger activation of the CARMA1/BCL-10/MALT1 complex, while TLR, IL-1R, and TNFR activate the TAK1/TAB complex. Both complexes phosphorylate the IKKα/IKKβ/NEMO (IKKγ) complex, leading to phosphorylation, ubiquitination, and proteasomal degradation of IκBα. This degradation releases the p50/RelA NF-κB dimer, which translocates to the nucleus to induce gene transcription involved in cell survival, inflammation, and immune responses. Non-canonical NF-κB signaling is activated by a specific subset of TNF receptor superfamily members, including CD40, RANK, LT-βR, and BAFF-R. These receptors trigger stabilization and accumulation of NF-κB-inducing kinase (NIK), which phosphorylates and activates IKKα. Activated IKKα then phosphorylates the NF-κB2 precursor p100, leading to its ubiquitination and proteasomal processing into p52. The p52 subunit forms a heterodimer with RelB, which translocates to the nucleus to regulate gene expression involved in lymphocyte development, survival, and maturation. (Q. Guo et al., 2024)

1.3.3 Linear ubiquitination at TNFR1 signalling

1.3.3.1 The Ubiquitin System

Ubiquitination is a conserved post-translational modification that regulates protein stability and activity by attaching ubiquitin, a small 76-amino acid protein, to target proteins through a cascade of enzymatic reactions. This process begins with an isopeptide bond formation between the C-terminal glycine of ubiquitin and a lysine residue on the substrate (Kulathu & Komander, 2012), and the reaction is orchestrated by three sequential enzymes: the ubiquitin-activating enzyme (E1), the ubiquitin-conjugating enzyme (E2), and the ubiquitin ligase (E3) (Figure 1.6). The E1 enzyme initiates the process by catalysing the ATP-dependent activation of ubiquitin, forming a thioester bond with ubiquitin's C-terminal carboxyl group and its own active cysteine residue. The activated ubiquitin is then transferred to the active site cysteine of the E2 enzyme, and after the E3 enzyme facilitates the transfer of ubiquitin from the E2 to the substrate (Kennedy et al., 2022) (Figure 1.6).

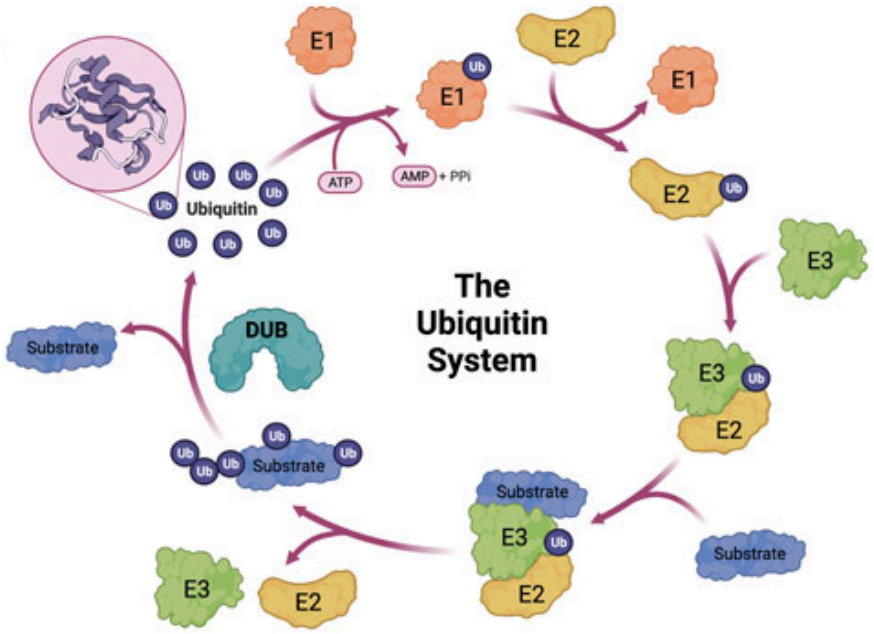

Figure 1.6: The ubiquitin cycle (Kennedy et al., 2022)

The ubiquitin system operates through a cascade of enzymes where E1 (orange) activates ubiquitin, which is then transferred to E2 (yellow) and finally conjugated to substrate proteins (blue) by E3 ligases (green), with ubiquitin molecules shown in purple. This ATP-dependent process attaches ubiquitin to substrates, tagging them for various cellular fates. Deubiquitinating enzymes (DUBs, teal) dynamically remove ubiquitin from substrates, allowing ubiquitin recycling and regulation of ubiquitin signaling.

This occurs via one of its seven lysines (K6, K11, K27, K29, K33, K48, and K63) or its N-terminal methionine (M1) in a tail to head bond (Figure 1.7). Depending on the amino acid

used as substrate, the different ubiquitin chains adopt distinct tridimensional conformations. Lys6-, Lys11-, and Lys48-linked ubiquitin chains for example form compact, rigid, and packed structures, whereas Lys63- and Met1-linked chains adopt more flexible, extended, and open conformations (Hrdinka & Gyrd-Hansen, 2017). Each of these complex topologies result in unique cellular consequences, demonstrating the versatility and regulatory potential of the ubiquitin system in eukaryotic cells (Dikic et al., 2009; Komander & Rape, 2012; Swatek & Komander, 2016) (Figure 1.7).

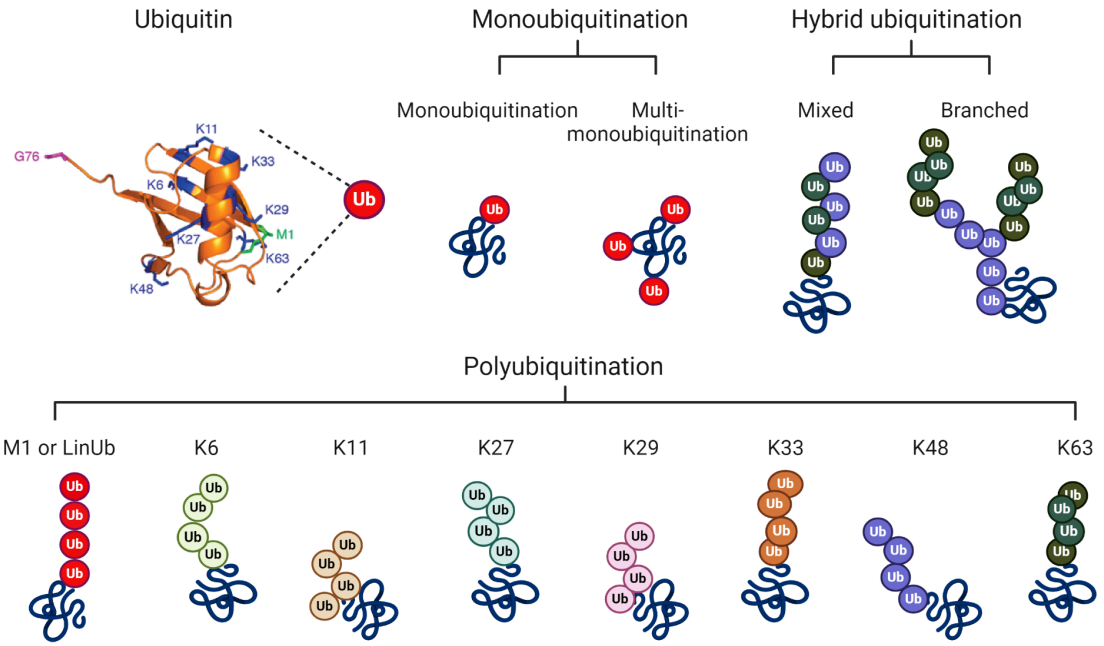

Figure 1.7: The different ubiquitination patterns.

Ubiquitination can occur as the attachment of a single ubiquitin molecule to one or more lysine residues on a target protein, a process called monoubiquitination. In contrast, polyubiquitination involves the addition of ubiquitin molecules into chains linked through one of seven lysine residues: K6, K11, K27, K29, K33, K48, or K63 or the N-terminal methionine (M1) in a head-to-tail fashion. Furthermore, hybrid ubiquitin chains comprising different linkage types exist, increasing the complexity and specificity of ubiquitin-mediated signaling. Each chain type forms a distinct three-dimensional structure, allowing diverse cellular responses. Image generated by Biorender.

Proteins containing ubiquitin binding domains (UBDs) are known as ubiquitin receptors. Most UBDs bind to a hydrophobic patch located around Isoleucine 44 of ubiquitin, but other residues in this region also contribute to binding (Husnjak & Dikic, 2012).

The precision of the ubiquitin code is also attributed to the E3 ligases. The human genome encodes two E1 enzymes (Schulman & Harper, 2009), nearly 40 E2 enzymes (Y. Ye & Rape, 2009), and over 600 E3 enzymes (W. Li et al., 2008). Normally, E3 enzymes are categorised into three main groups based on their domain structure and the ubiquitin transfer mechanism: (1) homologous to E6-AP C-terminus (HECT) that transfer ubiquitin to the substrate in a two-step process, first to the E3's active cysteine and then to the substrate; (2) really interesting new gene (RING), and (3) U-box, that both directly transfer ubiquitin from the E2 to the substrate. Additionally, there is another family of E3 ligases called RING-in-between-RING (RBR), which contains two RING domains separated by an in-between-RING (IBR) domain. RBR E3s act as HECT-RING hybrids, initially binding the E2 with one RING domain, transferring ubiquitin to the second RING domain, and finally attaching it to the substrate (Kulathu & Komander, 2012; Stieglitz et al., 2012; Wenzel et al., 2011)

Ubiquitination is reversible by a family of nearly 100 deubiquitinases (DUBs) that remove ubiquitin modifications, regulate substrate function, and recycle free ubiquitin (Komander et al., 2009; Reyes-Turcu et al., 2009). The versatility and specificity of ubiquitin linkages, along with the precise regulation by E3 ligases and DUBs, underscore the complexity of ubiquitin-mediated signalling pathways.

1.3.3.2 The LUBAC Complex assembly and its regulators

Linear ubiquitin chains (LinUb) are critical signaling scaffolds that regulate diverse biological processes, including pro-inflammatory signaling, antiviral interferon responses, regulated cell death, xenophagy, cell survival, innate and adaptive immune responses, and autophagy (Aalto et al., 2022). In fact, genetic defects that disrupt the regulation of LinUb chains lead to severe immune-related disorders (Fiil & Gyrd-Hansen, 2021). So far, LUBAC is the only known Ub ligase in vertebrates that assembles Met1-Ub (Jahan et al., 2021). Composed by three core protein subunits: Heme-oxidized IRP2 ubiquitin ligase-1 (HOIL-1 also known as RBCK1), HOIP (also called RNF31), and SHARPIN (Gerlach et al., 2011; Haas et al., 2009; Ikeda et al., 2011; Rittinger & Ikeda, 2017; Tokunaga et al., 2009, 2011) attaches LinUb downstream several immune receptors.

The integrity and catalytic activity of LUBAC depend on intricate interactions between its components. Both HOIL-1 and HOIP belong to the RBR subclass of RING E3 ubiquitin ligases (Walczak et al., 2012). HOIP functions as the central architectural and catalytic subunit, assembling M1-linked ubiquitin chains via its RING2 domain and the unique linear

ubiquitin chain-determining domain (LDD). HOIL-1's E3 ligase activity restricts HOIP's promiscuity to ensure precise ubiquitin chain formation (K. Song & Li, 2021), while SHARPIN acts as a stabilizing accessory protein.

HOIL-1 and SHARPIN bind to HOIP's ubiquitin-associated (UBA) domains through their ubiquitin-like (UBL) domains and also interact with each other via their LUBAC-tethering motifs (LTMs). These interactions relieve HOIP autoinhibition, stabilize the catalytically competent trimeric complex, and enhance its activity (Figure 1.8) (Fiil & Gyrd-Hansen, 2021; L. Gao et al., 2023).

HOIP's NZF domain facilitates substrate recognition, and its C-terminal RBR-LDD region orchestrates the specific assembly of M1-linked ubiquitin chains. This region operates through a two-step mechanism involving both RING and HECT E3-type activities, classifying HOIP as a HECT/RING hybrid ligase (Stieglitz et al., 2012, 2013). The RING1 domain recognizes ubiquitin-loaded E2, transferring ubiquitin to a conserved cysteine on the RING2 domain, forming a transient thioester intermediate before conjugation to the substrate or donor ubiquitin (Stieglitz et al., 2012, 2013).

HOIL-1 contributes to linear ubiquitin chain formation via its NZF domain, requiring both its UBL and NZF domains for full E3 ligase activity (Fujita et al., 2018; Gomez-Diaz et al., 2021; Peltzer et al., 2018; Stieglitz et al., 2012). Notably, mutations within these domains yield distinct phenotypes, with specific genotype-phenotype associations observed in HOIL-1 deficiencies (Cenacchi et al., 2019), as discussed subsequently.

SHARPIN stabilizes the TNFR1 complex I by interacting with both HOIP and HOIL-1. Its UBL domain binds to HOIP's UBA domain (Figure 1.8), while its NZF domain enhances LUBAC recruitment to TNFR1 (Kirisako et al., 2006; S. Shimizu et al., 2016). This coordinated network of domain interactions ensures LUBAC's structural integrity and catalytic efficiency.

LUBAC-mediated signaling is critically regulated by several key deubiquitinases (DUBs). Most notably OTULIN, A20, and CYLD. OTULIN directly associates with LUBAC by binding to the PUB domain of the HOIP subunit (Figure 1.8). Under resting conditions, OTULIN itself is linearly ubiquitinated by LUBAC at specific lysine residues (K64, K66), which stabilizes the OTULIN-HOIP interaction. This interaction ensures that LUBAC activity is restrained before immune stimulation. Disruption of OTULIN binding or OTULIN's linear ubiquitination leads to excessive NF-κB activation and inflammation, highlighting OTULIN's essential role as a negative feedback regulator of LUBAC activity (Fiil & Gyrd-Hansen, 2021; L. Gao et al.,

2023). Interestingly, loss of OTULIN does not result in enhanced NF-κB signaling prior to stimulation because excessive linear ubiquitin chains impair proper TNF receptor complex assembly due to steric hindrance (Draber et al., 2015).

CYLD is another important DUB that regulates both K63- and LinUb chains. Recruited to LUBAC via the adaptor SPATA2, binds to LinUb chains with less affinity than OTULIN. In addition, CYLD-SPATA2 and OTULIN binding through PIM-PUB domain interaction is mutually exclusive (Figure 1.8).

A20 (also known as TNFAIP3) functions as a negative regulator of LUBAC-dependent NF-κB activation by preventing the interaction between LUBAC and its adaptor NEMO. Importantly, this regulatory role is independent of A20's enzymatic deubiquitinase (DUB) activity. In the TNFR1 complex, A20 binds linear ubiquitin (LinUb) chains through its C-terminal zinc finger 7 (ZF7) domain, protecting them from degradation (opposing to CYLD) (Figure 1.8) (Draber et al., 2015; Fiil & Gyrd-Hansen, 2021; Priem et al., 2019).

Additionally, A20 contains an N-terminal OTU domain with DUB activity (Verhelst et al., 2014) that preferentially cleaves K48- and K11-linked ubiquitin chains (Komander & Barford, 2008; S.-C. Lin et al., 2008; Mevissen et al., 2013) (Figure 1.8). Moreover, this OTU domain, together with a C2-C2 zinc finger E3 ligase domain, can also remove K63-linked ubiquitin chains from key signaling molecules such as RIP1, TRAF6, and NEMO, disrupting the IKK complex, thereby downregulating the inflammatory response (Boone et al., 2004; Hitotsumatsu et al., 2008; E. G. Lee et al., 2000; Wertz et al., 2004).

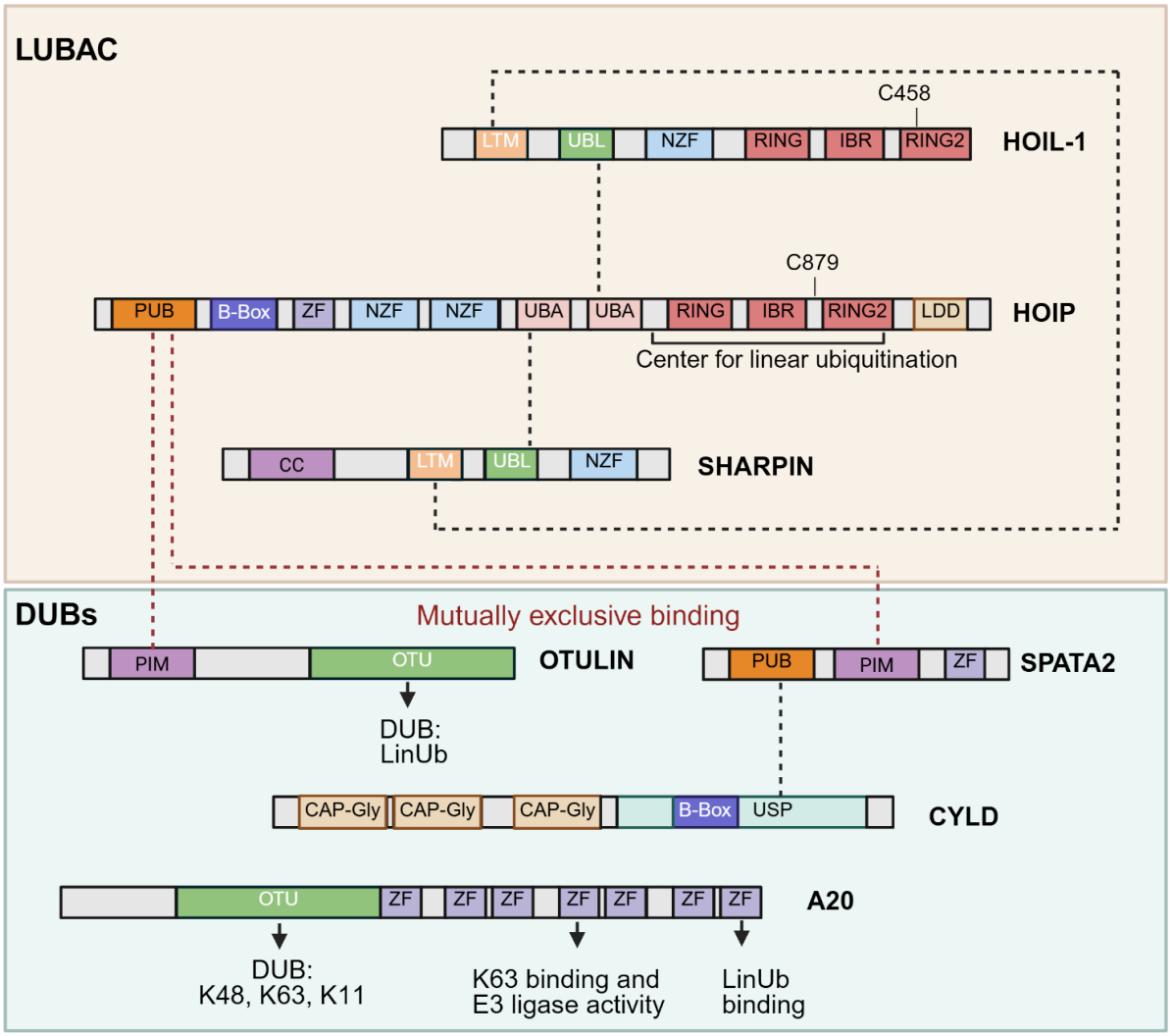

Figure 1.8: Schematic representation of the domain organisation of LUBAC subunits and associated DUBs.

HOIL-1 and SHARPIN interact with HOIP through their UBL-UBA domain interactions. Simultaneously, HOIL-1 and SHARPIN stabilize the complex by heterodimerizing through their LTM domains. OTULIN and CYLD (in complex with SPATA2) are the best-characterized DUBs that disassemble LinUb chains. OTULIN exclusively disassembles LinUb chains, whereas CYLD-SPATA2 is less specific and also disassembles Lys63-Ub and other linkages (not shown). OTULIN negatively regulates LUBAC binding via its N-terminal PIM. The OTU domain of OTULIN possesses DUB activity that cleaves linear Ub chains. The interaction of OTULIN and CYLD-SPATA2 with HOIP is mutually exclusive, as both compete for binding to the PUB domain of HOIP via their PIM motifs. A20 does not directly bind LUBAC; however, its ZF7 domain specifically binds LinUb chains, protecting them from cleavage by other DUBs such as CYLD. Additionally, its ZF4 domain binds K63-linked polyUb and functions as an E3 ligase catalyzing formation of K48-linked chains targeting proteins for proteasomal degradation. Simultaneously, the OTU domain of A20 selectively cleaves K48-, K63-, and K11-linked Ub chains. Catalytic cysteines in HOIP and HOIL are indicated by numbering based on the human protein sequence. Slashed lines indicate interacting domains.

Abbreviations: B-box, B-Box-type zinc finger; CAP-Gly, cytoskeleton-associated protein–glycine rich; CBR, catalytic in-between RING; CYLD, cylindromatosis; DUB, deubiquitinase; HOIL-1, heme-oxidized IRP2 ubiquitin ligase-1; HOIP, HOIL-1-interacting protein; IBR, in-between RING; LDD, linear ubiquitin chain-determining domain; LTM, LUBAC-tethering motif; Glys, Glysine; NZF, nuclear protein localization 4 zinc finger; OTU, ovarian tumor domain; PIM, PUB-interacting motif; PUB, peptide:N-glycanase/UBA- or UBX-containing proteins; RING, really interesting new gene; SPATA2, spermatogenesis-associated protein 2; UBA, ubiquitin-associated; UBL, ubiquitin-like; Ub, ubiquitin; USP, ubiquitin-specific protease; ZnF, zinc finger; LinUb, linear ubiquitination.. Adapted from (Jahan et al., 2021; Karri et al., 2024)

1.3.3.3 LUBAC prevents cell death and inflammation

Functionally, LUBAC plays a pivotal role in orchestrating the balance between immune activation and programmed cell death downstream of various immune receptors, with tumor TNFR1 being the most studied.

Downstream TNFR1, LUBAC-mediated linear ubiquitination of signaling molecules like RIPK1 prevents the assembly of a pro-death signaling complex (complex II) and favors NF-κB-dependent cell survival pathways (Figure 1.9). The importance of LUBAC components is reflected in phenotypes resulting from their loss: knockout of *Hoip* or *Hoil-1* causes embryonic lethality due to dysregulated apoptosis and necroptosis, while Sharpin loss leads to hyperactive inflammatory signaling, resulting in multiorgan inflammation and dermatitis (Peltzer et al., 2014, 2018; Taraborrelli et al., 2018). Rescue of lethality in LUBAC-deficient models requires simultaneous deletion of critical death effectors caspase-8 and MLKL but not ablation of TNFR1 alone, indicative of LUBAC regulating cell death signaling downstream of multiple receptors, including TRAIL, CD95, and Toll-like receptors TLR3 and TLR4 (Jahan et al., 2021; Taraborrelli et al., 2018).

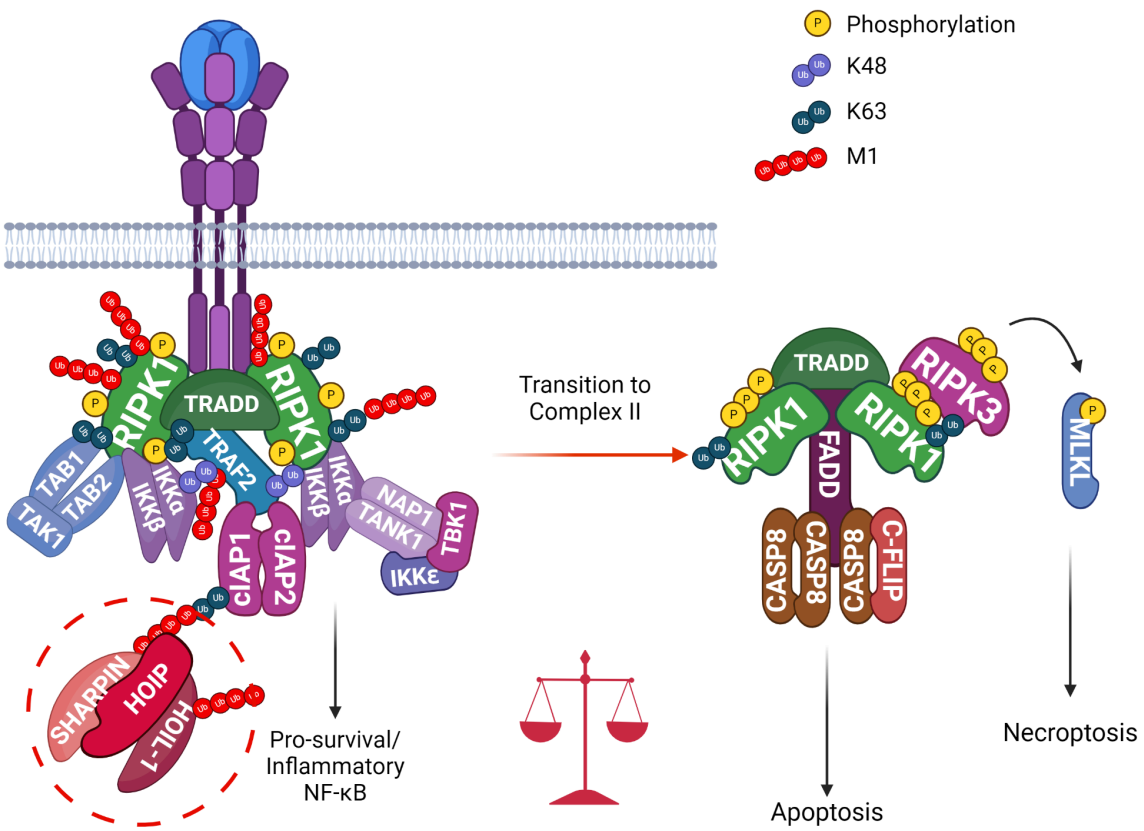

Figure 1.9: LUBAC regulates the balance between life and death.

Upon ligand binding, TNF-R1 forms a membrane-bound complex-I. LUBAC is recruited to complex-I through Lys63-Ub conjugated by cIAP1/2 on RIPK1 and possibly other proteins. In turn, LUBAC assembles Met1-Ub on RIPK1, TRADD, NEMO, and TNF-R1 itself. The absence of LUBAC destabilises TNFR1 complex I, attenuates NF-κB, and increases cell death rates upon TNF stimulation either through Caspase8 (Casp8) activation (apoptosis) or RIPK3 and MLKL phosphorylation (necroptosis). Image generated in Biorender.

The critical nature of linear ubiquitin chain regulation is underscored by the severe human diseases associated with its perturbation. Mutations affecting LUBAC activity or its regulatory mechanisms cause immunodeficiency, autoinflammation (notably OTULIN-related autoinflammatory syndrome), amylopectinosis, glycogen storage diseases, cardiomyopathies, and increased cancer susceptibility (Boisson et al., 2012). However, although the role of LiUb in NF-κB signaling and cell death is well-established, recent studies reveal LUBAC's involvement in a broader array of cellular processes beyond immune signaling, including Wnt signaling, protein quality control, autophagy/xenophagy, metabolic regulation, and chromosome alignment (Chu et al., 2021; Jahan et al., 2021; Rivkin et al., 2013; van Well et al., 2019; M. Wu et al., 2019; Z. Wu et al., 2022). These expanding functions highlight LinUb as a crucial and versatile regulator and open new avenues for research.

1.3.3.3.1 HOIP

Although HOIP is the main catalytic component of LUBAC, its activity requires the presence of at least one other LUBAC component, either HOIL-1 or SHARPIN, for proper activation (Ikeda et al., 2011). Both the deficiency of HOIP and loss of its catalytic function (*Hoip*^{C879S}) result in embryonic lethality (Emmerich et al., 2013; Peltzer et al., 2014). Correspondingly, human mutations in HOIP cause severe phenotypes like multi-organ autoinflammation, immunodeficiency, and amylopectinosis (Boisson et al., 2015).

The first case presented a missense mutation (L72P in the PUB domain) that led to HOIP deficiency and reduced HOIL-1 and SHARPIN levels. The clinical features included multiorgan autoinflammation, immunodeficiency, amylopectinosis, systemic lymphangiectasia, and transient metabolic symptoms responsive to a low-fat diet. In addition, patients' fibroblasts showed impaired NF-κB activation while monocytes exhibited hyperresponsiveness to IL-1β and defective B cell antibody responses (Boisson et al., 2015). The second case showed reduced LUBAC expression, altered cytokine production, transcriptional changes, and immunological defects including persistent dermatitis and splenomegaly (Oda et al., 2019). In mouse modes, proteomic studies reveal about ninety interactors per HOIP domain across various mouse tissues, highlighting tissue-specific functions (Fu et al., 2024), and reveal tissue-specific consequences of HOIP deletion. Liver-specific knockout for example leads to hepatocyte apoptosis and inflammation progressing to tumorigenesis (Y. Shimizu et al., 2017), while pancreatic beta cell-specific deletion causes no spontaneous phenotype or diabetes susceptibility (Veli et al., 2024). Immune cell–specific deletions further clarify distinct roles: B-cell HOIP deficiency impairs development (Y. Sasaki et al., 2013), T-cell deletion disrupts maturation(Okamura et al., 2016; Teh et al., 2016), and regulatory T-cell deletion causes severe immune dysregulation (Teh et al., 2016). Interestingly, macrophage-specific HOIP activity alleviates chemically induced colitis, whereas intestinal epithelial cell deficiency has minimal effects (Sakamoto et al., 2023).

Overall, HOIP is essential to prevent autoinflammation, cancer, and immunodeficiency, and to develop proper B cell memory in both mice and humans. Nevertheless, its functions are highly tissue-specific.

1.3.3.3.2 HOIL-1

The RBCK1 gene encodes for a 510-aminoacid protein called "Ring-B-box-coiled-coil protein interacting with protein C-Kinase-1" (also known as HOIL1). HOIL-1 functions alongside

HOIP to mediate linear ubiquitination. Is predominantly a mono ubiquitination E3 ligase that attaches the first ubiquitin to the substrate. This initial step then allows the elongation and/or branching by HOIP, and other E3 ligases forming heterotypic ubiquitin chains (Kelsall et al., 2019; Rodriguez Carvajal et al., 2021).

HOIL-1 forms oxyester bonds between the C-terminus of ubiquitin and serine and threonine residues in its substrates. Recombinant HOIL-1 has been shown to ubiquitinate itself at several serine and threonine residues, including Ser365 (Kelsall et al., 2019). In addition, it can also ubiquitinate unbranched polysaccharides and maltose in-vitro (Kelsall et al., 2022).

Its activity is essential for LUBAC regulation. Besides controlling HOIP activity, it catalyses its own monoubiquitylation and is proposed to monoubiquitinates SHARPIN by an oxyester bond (Kelsall et al., 2019; Tatematsu et al., 2008). In addition, IRAK1, IRAK2, and MyD88 have also been identified as physiological substrates of HOIL-1 during Toll-like receptor signalling (Kelsall et al., 2019), and results fundament for TNF-, IL-1β-, and CD40L-induced NF-κB signalling.

Mutations causing loss of expression or loss of function of the N-terminal regions of HOIL-1 have been identified in patients with autoinflammation and immunodeficiency (Nilsson et al., 2013). By contrast, mutations in the middle or C-terminal regions have been reported in Polyglucosan body myopathy-1 (PGBM1) without immunodeficiency (Nilsson et al., 2013; Phadke et al., 2020). Since the N-terminal region plays a crucial role in complex formation, it leads to severe acute inflammation (Fujita et al., 2018) it is speculated that mutations in that region drastically reduce LUBAC expression in comparison with those in the mid- or C-terminal, explaining why these two regions might have different implications regarding HOIL-1 loss of function.

In the clinic, recessive mutations in human are linked to two distinct clinical phenotypes: (1) early-onset fatal immunodeficiency characterised by chronic autoinflammation, invasive bacterial infections, severe dilated cardiomyopathy, and myopathy with polyglucosan storage in cardiac, skeletal, smooth muscle, and liver (Boisson et al., 2012) and (2) childhood or juvenile-onset polyglucosan body myopathy type 1 (PGBM1), associated with dilated cardiomyopathy and cardiac failure, often requiring transplantation (Boisson et al., 2012; Cenacchi et al., 2019; Krenn et al., 2018; Nilsson et al., 2013; Phadke et al., 2020; K. Wang et al., 2013)

Differently to the immunodeficiency, Rbck1-dependent PGBM1 phenotype seems to arise from the progressive accumulation of toxic polyglucosan bodies in cardiac muscle and other

tissues, such as the brain, with some patients also displaying cognitive impairment (L. Chen et al., 2021; Phadke et al., 2020). Symptoms start early childhood, with patients present exercise intolerance and hepatosplenomegaly, and high liver profile (AlAnzi et al., 2022). Later on, PGBM1 patients exhibit indigestible polyglucosan bodies in muscle biopsies resistant to α-amylase and proteinase-k treatment (Nilsson et al., 2013). To date, approximately 15 families have been reported with PGBM1, showing various null mutations associated with different phenotypes. None of these patients had episodes of sepsis or chronic auto-inflammation, but some had various immunological disturbances (recurrent laryngitis, psoriasis, granulomatous disease) (Cenacchi et al., 2019). However, two unrelated patients with a homozygous truncating mutation in the middle part of the gene suffered from a childhood onset cardiomyopathy and displayed signs of auto-inflammation and immunodeficiency (Krenn et al., 2018).

The expression of HOIL-1 is critical for the stability of HOIP in murine cells and vice versa (Fujita et al., 2018; Peltzer et al., 2018). Hence, in-vivo the deletion of any of these two components completely abolishes the expression of the other and results in embryonic lethality. However, the E3 ligase-inactive mouse model *Hoil-1*^{C458S}/*Hoil-1*^{C458A} does not compromise other LUBAC component expression (Cohen et al., 2020; Fuseya et al., 2020; Kelsall et al., 2019, 2022). These mice are born at normal Mendelian frequencies, presenting only mild splenomegaly upon ageing, and do not exhibit any overt phenotype at 6 months old death. When they start accumulating polyglucosan bodies in the brain and other organs (Kelsall et al., 2019, 2022; Nitschke et al., 2022).

Lack of HOIL-1 catalytic activity increases M1-chains and NF-κB activation in consequence. Surprisingly in macrophages it reduces the production of pro-inflammatory cytokines and chemokines, without affecting anti-inflammatory cytokine IL-10 (Cohen et al., 2020). So far, it is established that lack of HOIL-1 activity protects against LPS and TNF shock and salmonella infections (Fuseya et al., 2020), most likely due to pro-survival gene expression and prevention of cell Last, in another version of this mutant HOIL-1L-ΔRING1, which also exhibit loss of HOIL-1 E3 ligase activity, developed systemic lupus erythematosus (SLE) and Sjögren's syndrome in a female-dominant fashion (Fuseya et al., 2024). Hence, HOIL-1 catalytic activity seems to have cell type specific functions which vary according to stimuli.

1.3.3.3.3 SHARPIN

SHAPIN function is fundamental for immune cell regulation and its loss sensitises to TNF-induced cell death in vitro. It participates in many critical physiological activities such as

B cells activation and platelet aggregation. It is associated with various disorders such as chronic dermatitis, tumour development, and Alzheimer's disease (B. Yu et al., 2022).

In the liver, LUBAC is essential for the survival of hepatocytes. SHARPIN downregulation of hepatic SHARPIN by shRNA leads to hepatocyte apoptosis (similar to the HOIP hep model), in fact, its expression is significantly reduced in the fulminant hepatitis model (injection of carbon tetrachloride or acetaminophen)(Yamamotoya et al., 2017),

In mice, a loss-of-function mutation in Sharpin leads to chronic proliferative dermatitis (cpdm) which develops around 3-6 weeks of age, together with multiorgan inflammation in liver, gut, intestine, lung, joints, and oesophagus, and immunodeficiency (HogenEsch et al., 1993; Rickard et al., 2014; Seymour et al., 2007; Tokunaga et al., 2011). This mutation in a spontaneous base pair deletion in exon 1, leads to complete loss of protein expression, which causes defective NF-κB signalling upon TNF, CD40L, and IL-1β stimuli and increased TNF-induced cell death.

Cpdm dermatitis is characterized by epidermal hyperplasia, hyperkeratosis, parakeratosis, inflammation, and increased keratinocyte cell death (Rickard et al., 2014). This is subsequently followed by an aberrant immune response, including absence of Peyer's patches in the intestine, loss of splenic marginal zones, and splenomegaly. Cpdm mice also exhibit systemic chronic inflammation, with accumulation of eosinophils, macrophages, and regulatory T cells (HogenEsch et al., 2001; Redecke et al., 2016; Teh et al., 2016).

The inflammatory syndrome in Sharpin Cpdm/cpdm mice can be prevented by loss of TNF or TNFR1 (but not TNFR2), or by inactivating the kinase activity of RIPK1 (Berger et al., 2014; Dannappel et al., 2014; Kumari et al., 2014). However, TNFR1 deletion does not fully rescue the skin phenotype (Kumari et al., 2014). Loss of interleukin-1 receptor 1 (ILR1) or Casp8 combined with BID deficiency also does not fully suppress inflammation, although Casp8 heterozygosity significantly delays dermatitis. Necroptosis inhibition via Ripk3 or Mlkl deletion partially ameliorates the multi-organ phenotype, with near complete suppression achieved by combined Ripk3 deletion and Casp8 heterozygosity. However, triple deficiency of Sharpin, Ripk3, and Casp8 causes perinatal lethality (Rickard et al., 2014), consistent with similar embryonic lethality observed in $Ripk3^{-/-}Casp8^{-/-}Hoil\text{-}1^{-/-}$ mice, underscoring LUBAC's vital role during development (Peltzer et al., 2018).

In humans only two cases of SHARPIN mutation were recorded. The first one with a frameshift mutation that led to undetectable levels of SHARPIN protein and impaired LUBAC expression ex-vivo. This patient showed signs of autoinflammation, immunodeficiency, and

mild hepatic glycogen storage but unexpectedly did not exhibit the dermatological manifestations seen in Sharpin-deficient mice. It was treated with TNF inhibitors successfully ameliorating the autoinflammation A second individual with biallelic SHARPIN deficiency and similar clinical findings was identified but did not visit the NIH before succumbing to the disease (Oda et al., 2024)

1.3.3.3.4 OTULIN

OTULIN, also known as Gumby or FAM105B, is a cysteine protease deubiquitinase from the OTU family that specifically cleaves linear ubiquitin chains via substrate-assisted catalysis, showing a 100-fold preference for M1 over K63 chains (Rivkin et al., 2013).

Initially described as a negative regulator of LUBAC signaling, OTULIN deficiency leads to increased inflammation. However, it also acts to inhibit both cell death and inflammation by deubiquitinating LUBAC and enhancing its stability, thereby supporting NF-κB and MAPK signaling while restraining cell death (Heger et al., 2018), however the effects of these activities appear to be highly cell- and tissue-specific.

Patients with OTULIN-related autoinflammatory syndrome (ORAS) carrying homozygous missense or premature stop variants in the OTULIN are born prematurely and show signs of disease at a short age (Damgaard et al., 2016; Nabavi et al., 2019; Zinngrebe et al., 2022). They suffered from fever, subcutaneous fat inflammation (panniculitis), failure to thrive, diarrhoea, and arthritis accompanied by increased levels of leukocytes, neutrophils, and C-reactive protein (CrP) (Damgaard et al., 2016, 2019; Nabavi et al., 2019).

Variants affecting OTULIN's catalytic activity, results in uncontrolled increased linear ubiquitin linkages and embryonic lethality in mice (Heger et al., 2018; Rivkin et al., 2013). In addition to its known roles, novel ubiquitin-independent functions of OTULIN are starting to emerge, expanding the range of cellular pathways, such protein sorting and trafficking in the endocytosis through retromer protein SNX27 (Stangl et al., 2019).

Moreover, one ORAS patient carrying a homozygous missense mutation in OTULIN additionally suffered from steatosis and hepatocyte degeneration with abnormal liver values suggesting that functioning OTULIN is essential for liver health (Damgaard et al., 2020; Zinngrebe et al., 2022). This was further corroborated by mice models with liver-specific deletion of OTULIN, showing a similar disease phenotype with liver inflammation, steatohepatitis, apoptosis, complete glycogen storage depletion, and ultimately leading to the formation of hepatocellular carcinoma (Damgaard et al., 2020; Verboom et al., 2020).

Surprisingly, in mice, the pathology in OTULIN-deficient livers was independent of TNFR1 signalling (Damgaard et al., 2020). Instead, steatohepatitis in was associated with aberrant mTOR activation.

Collectively, these results reveal that OTULIN is critical for maintaining liver homeostasis and suggest that M1-linked polyubiquitin chains may play a role in the regulation of mTOR signalling and metabolism, at least in the liver (Damgaard et al., 2020).

1.3.3.3.5 A20

A20, plays a critical role in regulating the NF-κB signalling pathway and inflammatory responses, encoding a negative feedback regulator of the canonical NF-κB pathway. Its deficiency is linked to several autoimmune and autoinflammatory diseases such as systemic lupus erythematosus, Sjögren's Syndrome, Crohn disease , rheumatoid arthritis, type 1 diabetes and psoriasis (Fukaya et al., 2016; Musone et al., 2008; Plenge et al., 2007; Sisto et al., 2011; Tejasvi et al., 2012; Wellcome Trust Case Control Consortium, 2007). And although loss-of-function mutations in A20, are associated to early-onset autoinflammatory diseases (Zhou, Wang, et al., 2016), mutation in A20 are also reported to induce ulcers, liver fibrosis, hypothyroidism, arthralgia, and archosyrinx and even autoimmune hepatitis (G.-M. Li et al., 2019). In fact, studies in mice have shown that A20 in the liver contributes to liver regeneration after partial hepatectomy and acute toxic hepatitis through combined anti-apoptotic, anti-inflammatory, and pro-proliferative functions.

Deletion of A20 in the liver leads to spontaneous chronic liver inflammation without fibrosis or carcinomas, while increasing susceptibility to chemically or HFDt-induced hepatocellular carcinoma development (Catrysse et al., 2016). On the contrary, myeloid A20 deficiency protects mice from diet-induced obesity and IR, promoting the expansion of ATMs in adipose tissue while increasing their metabolization of palmitate in vitro and in vivo (Catrysse et al., 2021), so its functions seem to be highly tissue specific.

1.4 NF-κB and metabolic syndrome

The NF-κB pathway is one of the most well-characterized mediators linking inflammation and metabolic responses. Extensive studies have demonstrated its crucial role in the liver, adipose tissue, central nervous system, and macrophages, highlighting its involvement in the development of inflammation-associated metabolic diseases such as obesity, insulin resistance, and atherosclerosis (Baker et al., 2011; Ben et al., 2019).

In fact, for several decades NF-κB modulation has been proposed for novel treatment approaches for IR (Baker et al., 2011).

Nowadays, thanks to use of animal models, especially conditional transgenic mice, we can dissect tissue specific functions of NF-κB modulation provided significant insights into these mechanisms (Hildebrandt et al., 2022) some of the most relevant ones are listed below. Of note, this section is an amplified version of a review publication of my own (Hildebrandt et al., 2022), and my contributions to this work are fully reflected here. Permission to include and adapt this published material in my thesis has been obtained.

1.4.1 Canonical NF-κB during metabolic syndrome

1.4.1.1 IKKβ

As early as 1870, salicylate, an inhibitor of IKKβ, was shown to lower glucose levels in diabetic patients(Rena & Sakamoto, 2014; Shoelson et al., 2006), a hypothesis later supported by murine obesity models (E. Park et al., 2007; Yuan et al., 2001). In genetically obese mice and rats, salicylate's inhibition of IKKβ enhances insulin signaling and reduces inflammation by overcoming TNF-induced insulin resistance (D. Cai et al., 2005; Yuan et al., 2001). Similarly, reduced IKKβ signaling (*Ikkβ*$^{+/-}$) in genetically obese db/db mice and Zucker$^{fa/fa}$ rats lowers free fatty acids and improves insulin sensitivity, indicating that attenuation of IKKβ-mediated inflammation ameliorates metabolic dysfunction(Yuan et al., 2001).

Later on, IKKβ was shown to impaired insulin signalling by directly phosphorylating and inhibiting insulin receptor substrates (IRS) (D.-F. Lee et al., 2008). However, the targeted deletion of IKKβ in adipocytes in mice on a HFD leads to an exaggerated diabetic phenotype with systemic inflammation. This results in dystrophic AT and ectopic lipid deposition, indicating that IKKβ is vital for adipocyte survival and adipose tissue remodelling during

obesity. While mice with constitutive activation of IKKβ in adipocytes both show increased energy expenditure under basal conditions (Jiao et al., 2012).

On the other hand, hepatocyte-specific deletion of IKKβ in mice on a HFD and genetically obese$^{ob/ob}$ mice improves glucose tolerance and insulin response specifically in the liver (Arkan et al., 2005). While the same authors also show that loss of IKKβ in myeloid cells protects against IR (Arkan et al., 2005). Suggesting that NF-κB signalling in myeloid cells is crucial for systemic obesity-induced inflammation.

1.4.1.2 p65

p65 activation is associated with hepatic steatosis and insulin resistance during HFD (Zeng et al., 2016). In line with this, inhibition of NF-κB by siRNA against the p65 subunit protects HFD-fed mice from hepatic steatosis and IR without affecting body weight gain. Notably, p65 siRNA predominantly affected NF-κB transcriptional activity in the liver but not in the WAT, while also enhanced the activity of AMPK and activated genes involved in autophagy in the liver (Zeng et al., 2016).

On the other hand, p65 inactivation in adipocytes and macrophages attenuates the adipose inflammatory response in lean but not in obese mice (Z. Gao et al., 2015). In contrast, p65 overexpression in adipocytes leads to increased energy expenditure in basal conditions, enhances insulin sensitivity, and protects from weight gain upon a HFD despite increasing local and systemic inflammation (T. Tang et al., 2010)..

Moreover, in brown adipocytes, p65 RNA levels increase during differentiation. In a mouse model with p65 overexpression in brown adipocytes, cells exhibited a reduction in apoptosis and an increase in uncoupling activity. Concomitantly, inactivation of NF-κB in brown adipocytes (KO specific for BAT) led to intolerance to cold exposure (Peng et al., 2022).

Thus, p65 plays a complex and context-dependent role in metabolic regulation, influencing inflammation, insulin sensitivity, and energy balance across different tissues.

1.4.1.3 A20

A20 knockout mice are cachectic and die prematurely due to excessive multi-organ inflammation (Turer et al., 2008). However, in the liver, A20 protects hepatocytes from apoptosis in experimental hepatitis and hepatocarcinoma (Catrysse et al., 2016). In addition, A20 overexpression (attenuating NF-κB activity) ameliorates HFD-induced lipid accumulation, ROS, inflammation, hypertrophy, fibrosis, and cardiac dysfunction by

protecting cardiac cells from HFD-induced apoptosis (W. Xu et al., 2018). On the contrary, loss of A20 in myeloid cells results in protection against HFD-induced IR and increased energy expenditure due to elevated ATM metabolism (Catrysse et al., 2021). Surprisingly, although mice presented increased inflammation by NF-κB activation, the myeloid A20 deficiency mice lacked the characteristic CLS surrounding dead adipocytes upon HFD.

All these findings highlight the tissue-specific roles of the canonical NF-κB pathway in regulating inflammation, IR, and overall metabolic health (Hildebrandt et al., 2022; Kwon et al., 2014; S.-H. Park et al., 2016).

1.4.2 Non-Canonical NF-κB during metabolic syndrome

1.4.2.1 TBK1/IKKε

Non-canonical IκB kinases (IKKs) TBK1 and IKKε have essential roles as regulators of innate immunity and cancer, however, some studies have also implicated these kinases in glucose homeostasis and adaptive thermogenic and mitochondrial biogenesis during obesity-induced inflammation (Mowers et al., 2013; Shin & Choi, 2019). In fact, TBK1 and IKK-ε RNA and protein levels increase during HFD in AT, while the expression of IKK-ε also increases in liver (Chiang et al., 2009).

Moreover, IKKε-deficient mice gain less weight upon HFD and are protected against IR (Chiang et al., 2009). These mice exhibit reduced inflammation in the liver and WAT with lower expression of proinflammatory genes in adipocytes and ATMs, while displaying increased thermogenesis and enhanced expression of UCP-1 (Chiang et al., 2009). While, in another study, using the TBK1/IKKε inhibitor amlexanox (Reilly et al., 2013), researchers also observed increased thermogenesis and energy expenditure, which the lead to weight loss, improved insulin sensitivity, and decreased steatosis in obese mice fed with HFD (Möller et al., 2020).

Furthermore, inhibition of TBK1 and IKKε enhanced regeneration of pancreatic β-cells in multiple species including zebrafish, mice, and humans, and improved glycemic control by preventing β-cell demise in streptozotocin (STZ)-induced diabetic model (J. Xu et al., 2018).

However, Myeloid cell conditional Tbk1 KO mice spontaneously developed AT and metabolic disorders at old ages (T. Gao et al., 2022). This was associated with increased adipose tissue M1 macrophage infiltration and proinflammatory cytokine expression. In consequence

they displayed exacerbated hepatic inflammation and IR, when they were fed with HFD (T. Gao et al., 2022).

1.4.2.2 NIK

It has been reported that NIK activity is abnormally elevated in the skeletal muscle of obese people (Choudhary et al., 2011) and overactivated in mice liver during HFD or genetic obese models (Sheng et al., 2012). In line with this, in-vitro studies enhancing NIK expression in cultured L6 myotubes, reported an induced dose-dependent insulin-resistance (Choudhary et al., 2011). Showing a decrease in glucose uptake do to lower PI3 kinase activity and protein kinase B/Akt phosphorylation. Of note, this was reversed by adiponectin treatment (Choudhary et al., 2011).

In addition, a recent publication showed that NIK inhibition by B022 prevented HFD-induced IR in skeletal muscle (X. Chen et al., 2023). While liver-specific inhibition of NIK markedly improved hyperglycemia and glucose intolerance during HFD challenge. On the other hand, hepatocyte-specific overexpression of NIK was sufficient to promote glucose intolerance (Sheng et al., 2012).

In sum, the non-canonical NF-κB pathway plays a distinct and critical role in regulating metabolic and inflammatory processes during metabolic syndrome, with its activation exerting context-dependent effects on tissue-specific inflammation, energy metabolism, and insulin sensitivity.

1.4.3 NF-κB/MAPK and browning

NF-κB signalling plays a critical role in reprogramming the fat cell transcriptome towards inflammation in response to overnutrition and metabolic stress (Griffin, 2022). While many authors claim a detrimental role of this proinflammatory pathway in thermogenesis, general inhibition of canonical NF-κB signalling in adipocytes leads to a massive increase in adipocyte apoptosis under metabolic stress, followed up by secondary inflammation. As a matter of fact, NF-κB activity is increased during brown adipocyte differentiation through elevation of p65 (RelA), while is also transcriptionally upregulated during cold stimulation (Peng et al., 2022). Locally enhanced concentrations of NF-κB mediators like TNF, IL-1, and IL-6 suppress lipid storage, reducing lipid uptake and promoting lipolysis and fatty acid release via several pathways (Kolb, 2022). While IL-6 seems to be fundamental for beige adipocytes to reach an autocrine optimal level of differentiation (Carrière et al., 2014).

From murine mutant models we know that constitutive activation of IKKβ in AT prevents DIO by increasing fatty acid oxidation and thermogenesis-related genes in BAT and muscle (Jiao et al., 2012). In addition, the enhanced transcriptional activity of NF-κB elevates energy expenditure, decreases adipose tissue growth and reduces adipogenesis (T. Tang et al., 2010). While the loss of the NF-κB inhibitor A20 in myeloid cells increased energy expenditure due to elevated ATM metabolism (Catrysse et al., 2021).

Further support of the fundamental role of NF-κB during thermogenesis comes from the knowledge on MAPK signalling. ERK is associated with increased mitochondrial function and white adipocyte browning (Y. Liu et al., 2024). Its phosphorylation during cold exposure prevents brown adipocyte apoptosis, and increases beta3 adrenergic receptors (predominant regulators of rodent BAT thermogenesis) (Cero et al., 2021; Hong et al., 2018). In addition, ERK full deletion increases weight gain upon HFD (A. S. Khan et al., 2017), suggesting a fundamental role in MAPK in prevention of obesity.

On the other hand, in the case of non-canonical NF-κB, decreased signalling by deleting IKKe, increases energy expenditure and thermogenesis via expression of UCP1 in HFD fed mice (Chiang et al., 2009). Gene expression analyses indicate that IKKe knockout actually reduces expression of inflammatory cytokines, and changes expression of certain regulatory proteins and enzymes involved in glucose and lipid metabolism (Chiang et al., 2009).

Taken together, loss of metabolic homeostasis in fat tissue initiates a local pro-inflammatory response that seems to be fundamental to enhance both adipocyte survival and thermogenesis to counteract excess lipid uptake. Further on, secretion of pro-inflammatory mediators from macrophages and other immune cells contributes to tissue remodelling and adipocyte renewal. However, sustained proinflammatory cytokines secretion overcomes the need of pro-survival signalling, and can lead to detrimental sustained inflammation and disrupt tissue function.

1.4.4 Remarks on NF-κB regulation during metabolic syndrome

The literature unequivocally demonstrates that NF-κB signalling not only regulates inflammation during obesity but is also directly linked to energy expenditure. The tissue-specific roles of the NF-κB pathway in regulating inflammation, IR, and overall metabolic health have been established in numerous mouse models, with distinct outcomes based on the cellular context within different metabolic tissues.

In fact, the role of NF-κB seems to be highly tissue-specific. In the liver, NF-κB activation negatively impacts insulin sensitivity and promotes glucose intolerance, while inhibition of NF-κB in hepatocytes enhances insulin signalling and reduces hepatic steatosis. In ATMs, NF-κB activation prevents ATM death during obesity, highlighting its anti-apoptotic role, but can also lead to excessive proinflammatory cytokine secretion and increase macrophage infiltration. Conversely, in AT, this pathway is essential for adipocyte survival and proper tissue function, while it can also increase thermogenesis in BAT.

These findings underscore the critical importance of the NF-κB pathway in regulating inflammation and metabolic health.

In addition, therapeutic interventions targeting NF-κB and its associated kinases have shown significant promise. Small molecule NF-κB inhibitors like amlexanox undoubtedly increase thermogenesis and energy expenditure, resulting in weight loss and enhanced insulin sensitivity. On the other hand, the antihyperglycemic effects of drugs such as salicylates are indisputably linked to their anti-inflammatory effects on NF-κB signalling, and recent research suggests that direct activation of AMPK contributes to their antihyperglycemic and antihyperlipidemic actions. On the other hand, antagonist strategies against NF-κB related cytokines, such as TNF and IL-1β have been studied in the context of obesity. Randomized clinical trials with Anakinra (anti-IL-1β) have demonstrated a sustained reduction in systemic inflammation and improvement in type 2 diabetes patients(Larsen et al., 2007; Osborn et al., 2008). Similarly, retrospective observations in rheumatoid arthritis patient cohorts showed that anti-TNF therapy improves insulin sensitivity(Seriolo et al., 2008). Despite this, clinical trials with Anakinra for type 2 diabetes have remained in phase 2 since 2006 (*ClinicalTrials.Gov*, n.d.). Meanwhile, due to its highly immunosuppressive effects, anti-TNF therapy is limited to cases of extreme inflammation where the side effects outweigh the potential metabolic benefits.

Another promising candidate for metabolic disease treatment is IL-6 inhibition, which has been effective in rheumatoid arthritis (Narazaki et al., 2017) and shows potential for treating type 2 diabetes by targeting insulin resistance (Velikova et al., 2021). However, since IL-6 can also induce lipolysis, its role in metabolic syndrome remains controversial (Wueest & Konrad, 2020).

In conclusion, NF-κB undeniably plays a key role in metabolic inflammation, exhibiting diverse effects depending on the specific cell type or organ involved. The precise thresholds of NF-κB activity that drive beneficial adipose tissue remodeling versus those detrimental to

energy balance and metabolic health remain unclear. While NF-κB activation and prevention of cell death may initially act to restore energy homeostasis and regulate fat mass, paradoxically, they can also promote adipose tissue cell death. Understanding the specific cell death pathways influenced by NF-κB in metabolic syndrome and defining the mechanisms by which NF-κB modulates cell survival and death in obesity represent significant challenges in metabolic research.

1.5 Cell death during obesity-Induced inflammation

Adipose tissue (AT) expansion during obesity results in mechanical, metabolic, and inflammatory stress that leads to adipocyte cell death (Strissel et al., 2007). This triggers the chronic low-grade inflammation characteristic of obesity-associated metabolic disorders (Catharina et al., 2018; Hotamisligil, 2017; Swarup et al., 2022). Hypertrophic adipocytes are metabolically unfavorable due to increased mitochondrial catabolism causing oxidative and ER stress (Patti & Corvera, 2010). They also suffer from inadequate vascularization leading to hypoxia and fibrosis(Halberg et al., 2009), and release FFA, adipokines, and pro-inflammatory molecules contributing to dyslipidemia, glucose intolerance, and hypertension (Stenkula & Erlanson-Albertsson, 2018; Tchernof & Després, 2013).

Furthermore, multiple metabolic checkpoints, which also regulate cell death and survival including AMPK-TORC1, HIF-1, ER stress pathways, and p53, are altered in obesity (Green et al., 2014). Highlighting the intercross regulation of cell death processes and metabolism.

In recent years, multiple studies have revealed novel roles for cell death machinery genes in regulating energy homeostasis and insulin sensitivity, many linked directly to the TNFR1 complex (Gautheron et al., 2016; Karunakaran et al., 2020; Luk et al., 2023). Some authors propose that insulin resistance arises as a consequence of adipocyte death-driven inflammation during obesity (Alkhouri et al., 2010). Cytokine signaling, particularly via the TNF family, mediates adipose tissue cell death, with NF-κB playing a pivotal role in regulating both inflammation and macrophage survival (Catrysse & van Loo, 2017; Luk et al., 2023). Aberrant adipocyte death exacerbates metabolic syndrome and contributes to lipodystrophies, while anti-TNF therapies have shown promise in restoring adipose tissue mass and reducing inflammation in these conditions (Boronat-Toscano et al., 2022; Haque et al., 2002; Trujillo et al., 2005).

TNF is a classical, pleiotropic, pro-inflammatory cytokine and the first "adipokine" described to be produced by AT. Its production is regulated during obesity and is proposed to contribute to obesity-associated metabolic disease (Sethi & Hotamisligil, 2021). TNF reduces adipocyte size, prevents adipocyte differentiation, and interferes with insulin-stimulated glucose uptake by reducing glucose transporter 4 (GLUT4) expression and inhibiting insulin receptor autophosphorylation (Coppack, 2001). In vivo mouse models TNF depletion during HFD feeding increases weight gain but results in lower liver steatosis and IR (Salles et al., 2012). In fact, its depletion leads to increased epididymal AT fat storage, while reducing liver fatty acid uptake (Salles et al., 2012). However, TNFR1 knockout HFD-fed models showed

that disruption of TNFR1 signaling leads to accelerated progression from steatosis to non-alcoholic steatohepatitis (NASH) (Lambertucci et al., 2018). Thus, TNF signaling appears to be key for fat mobilization, but its pleiotropic role in inflammation, cell death, and survival makes data interpretation a bit more challenging.

IL-6 also has a complex role in metabolic regulation and, specifically, in fat oxidation (Pal et al., 2014). In animal models, IL-6 receptor expression is increased in WAT compared with subcutaneous adipose tissue (Ji et al., 2014) while, in humans, IL-6 has been shown to mediate VAT loss during exercise (Wedell-Neergaard et al., 2019), and its supplementation stimulates fatty acid release and oxidation (van Hall et al., 2003). And, although traditionally considered a proinflammatory cytokine, IL-6 has been shown to mediate improvements in insulin sensitivity (Benrick et al., 2012). In fact, IL-6 KO mice had increased obesity onset, which is partially reversed by IL-6 administration (Wallenius et al., 2002). Curiously, IL-6 seems to reduce lipid accumulation in AT and seems to be an autocrine response of adipocytes to avoid hypertrophy.

While inflammation is typically a protective mechanism against pathogens and danger signals, in the context of obesity, it refers to the activation of the immune system. This localised inflammatory response is characterised by an increased presence of immune cells, predominantly macrophages, leading to the expression of the already mentioned cytokine genes and elevated levels of pro-inflammatory mediators (Sethi & Hotamisligil, 2021). In fact, local infiltration of macrophages in CLS are the first indicators reporting adipocyte cell death in the AT.

Beyond question inflammation plays a pivotal role in metabolism, with intricate connections between cell death modalities and metabolic processes (Sethi & Hotamisligil, 2021). The local inflammatory alterations in AT are believed to be extended to systemic inflammation, introducing terms like "metaflammation" and "immunometabolism" to highlight the intimate link between excess fat accumulation and inflammatory dynamics.

This dynamic interplay between metabolism, cell death, and inflammation underscores the complexity of physiological and pathological processes, reason why addressing these gaps will be crucial for advancing our understanding and developing targeted therapeutic interventions.

Nowadays, thanks to use of animal models, especially conditional transgenic mice, we can dissect tissue specific functions of cell death effectors and acquire significant insights into these mechanisms (Hildebrandt et al., 2022) some of the most relevant ones are listed

below. Of note, this section is an amplified version of a review publication of my own (Hildebrandt et al., 2022), and my contributions to this work are fully reflected here. Permission to include and adapt this published material in my thesis has been granted.

1.5.1 Macrophages infiltration during obesity

Immune cells in AT play essential roles in maintaining adipocyte integrity, metabolic function, and hormonal sensitivity. Among these, macrophages are the most abundant and exhibit remarkable plasticity, rapidly responding to tissue-derived or environmental signals when homeostasis is disrupted. In fact, they play a key role during obesity, clearing adipocytes cellular debris, a necessary event to replace hypertrophic cells (Strissel et al., 2007). However macrophages not only remodel the extracellular matrix but also buffer lipolysis by uptaking and storing excess lipids, which they either gradually release into circulation or use as fuel (Boutens & Stienstra, 2016; K. D. Nguyen et al., 2011; Rao et al., 2014; Vogel et al., 2022).

Foam macrophages, characterized by lipid droplets accumulation in their cytoplasm, giving them a foam-like appearance, are typically activated in a pro-inflammatory state (Florance & Ramasubbu, 2022). They accumulate lipids and form multinucleated giant cells and are key players in lipid handling and tissue homeostasis in obese WAT (Florance & Ramasubbu, 2022; Hildreth et al., 2021; Vogel et al., 2022). The formation of these specialized structures suggests that the regulated cell death of adipocytes plays an important role in restoring WAT homeostasis (Figure 1.10). In fact, adipocyte and macrophage senescence is highly detrimental for adipogenesis (Q. Li et al., 2021; Matacchione et al., 2022; Palmer et al., 2019), while at the same time pro-survival NF-κB related activation is upregulated in AT of obese murine models (Hill et al., 2015), implying that an effective and controlled cell death program is needed to eliminate exhausted and stressed cells in the context of obesity,

In obese individuals, macrophages can constitute up to 40-50% of WAT cells, with their infiltration strongly correlated with BMI and adipocyte size (Weisberg et al., 2003). However, during obesity chronic low-grade inflammation in WAT reduces adiponectin secretion and promotes the production of pro-inflammatory cytokines such as TNF, iNOS, IL-6, and IL-1β, which polarize macrophages towards a pro-inflammatory (M1-like) state (Figure 1.10) (Item & Konrad, 2012; A. M. F. Johnson & Olefsky, 2013; Lumeng et al., 2007). This inflammation is more pronounced in GWAT compared to ScWAT, correlating with a higher risk of metabolic complications (Murano et al., 2008).

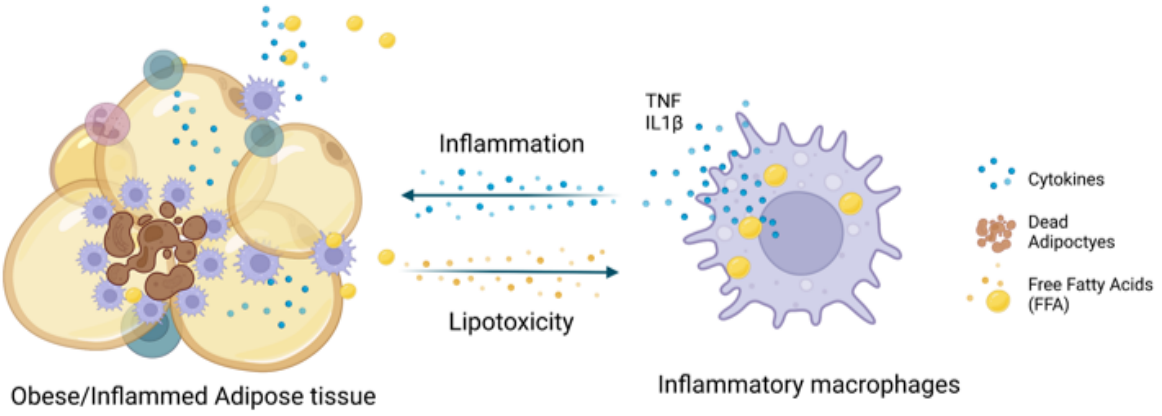

Figure 1.10 Adipocyte cell death and macrophages cross-talk during obesity.

Obesity leads to adipocyte hypertrophy and subsequent low-grade inflammation. This not only reduces adiponectin secretion and triggers the production of pro-inflammatory molecules such as TNF, iNOS, IL-6, and IL-1β, but also leads to adipocyte death. Stressed and dying adipocytes secrete these factors to attract macrophages, which normally surround them and form crown-like structures (CLS). These CLS are characterized by polarizing macrophages to a pro-inflammatory state (M1-like) that ultimately contributes to local inflammation. Adapted from (Hildebrandt et al., 2022).

Moreover, despite its scavenger function macrophages regulate several metabolic pathways in adipocytes through cytokine secretion. M1 macrophages are capable of suppressing UCP1 induction in BAT and iWAT, decreasing thermogenesis (Bae et al., 2014) and secrete inflammatory cytokines that exacerbate local inflammation (Lumeng et al., 2007). On the contrary, M2-like antiinflammatory ATM produce cytokines that protect adipocytes from TNF-induced IR (Lumeng et al., 2007), while at the same time, contribute to thermogenesis during cold exposure (K. D. Nguyen et al., 2011).

In summary, chronic low-grade inflammation driven by macrophage scavenging of adipocyte debris is essential to prevent lipid spillover, while macrophage-mediated inflammatory signaling is fundamental to restoring adipose tissue homeostasis (Cinti et al., 2005).

1.5.1.2 Apoptosis during obesity

Adipocyte death is now recognized as a crucial initial event that drives macrophage infiltration into adipose tissue and the development of IR associated with obesity in both mice and humans (Alkhouri et al., 2010). In obese animals and humans, 90% of macrophages infiltrate the AT arrange in CLS (Cinti et al., 2005). Despite the frequent occurrence of adipocyte death in WAT during obesity, the specific impacts of different types of cell death, especially those induced by ligands of the TNF family, remain underexplored.

The Fat Apoptosis Through Targeted Activation of Caspase-8 (FAT-ATTAC) model provides significant insights into the effects of Caspase-8-mediated apoptosis in WAT. In this model, induced expression and activation of Caspase-8 lead to local inflammation and adipocyte death, accompanied by pronounced glucose intolerance (Pajvani et al., 2005). This damage, while reversible with the cessation of Caspase-8 activation, leaves behind persistent glucose intolerance. This suggests that even though endogenous preadipocytes can regenerate adipose tissue, transient stress in WAT can have lasting or even permanent effects on systemic inflammation and metabolism. Furthermore, FAT-ATTAC mice crossed with ob/ob mice exhibit impaired lipid uptake by adipocytes, independent of leptin signalling or food intake, leading to lipotoxicity in peripheral organs. Notably, FAT-ATTAC mice display increased infiltration of adipose tissue macrophages (ATM), predominantly alternatively activated anti-inflammatory M2-like macrophages upon Caspase-8 activation (Fischer-Posovszky et al., 2011). This indicates that while adipocyte apoptosis triggers significant macrophage influx into WAT, these macrophages are mainly anti-inflammatory in nature under forced Caspase-8 activation (Fischer-Posovszky et al., 2011).

Other models also underscore the role of WAT apoptosis in metabolic inflammation. Mice deficient in FADD specifically in adipocytes show protection against glucose intolerance and IR in WAT, liver, and muscle when subjected to a HFD or on an ob/ob background (Zhuang et al., 2016). These mice also exhibit reduced WAT inflammation and increased energy expenditure. This phenotype is attributed to FADD's role in suppressing PPARγ-mediated gene expression, as PPARγ inhibition increases mitochondria, energy expenditure, and lipolysis in WAT by elevating cAMP levels. This suggests that FADD may interfere with adipogenesis and healthy expansion of WAT during obesity independently of apoptosis.

In line with the role of apoptosis in obesity-induced inflammation, a study shows that genetic deletion of Bid, which links death receptor with mitochondrial-cell death pathways, significantly reduces caspase activation and adipocyte apoptosis in response to HFD. Consequently, BID-deficient mice exhibit little to no ATM infiltration and are protected against the development of IR and hepatic steatosis, independent of body weight gain (Alkhouri et al., 2010). In addition, $Casp3^{-/-}$ mice subjected to diet-induced hepatic steatosis and/or fibrosis, display attenuated liver damage (Thapaliya et al., 2014; Zilu et al., 2019).

In sum, while the exacerbated apoptotic model (FAT-ATTAC) set a precedent that apoptosis can lead to metabolic syndromes, the protective mechanisms of blocking apoptosis observed in other models indicates a possible contribution of adipocytes cell death to metabolic inflammation in the context of obesity.

1.5.1.3 Necroptosis during obesity

Necroptosis, also known as programmed necrosis, is a regulated cell death pathway triggered by stimuli such as TNF, Fas, TRAIL, or specific Toll-like receptor ligands when apoptosis is inhibited. This form of cell death is highly pro-inflammatory, as it results in the release of intracellular "danger signals" that amplify inflammation. Notably, while most pro-necroptotic stimuli are inherently inflammatory (inducing cytokine and chemokine production) necroptosis itself may, in some contexts, dampen inflammatory cytokine output (Kearney & Martin, 2017).

In metabolic diseases, receptor-interacting protein kinase 3 (RIPK3) and its substrate, mixed lineage kinase domain-like protein (MLKL), have been implicated in conditions such as alcoholic and non-alcoholic steatohepatitis (Gautheron et al., 2014; Roychowdhury et al., 2013), atherosclerosis (J. Lin et al., 2013), and ischemic injury in heart and kidney(Linkermann et al., 2013; Luedde et al., 2014). However, their precise roles in obesity, metabolic syndrome, and type 2 diabetes remain unclear.

Though necroptosis markers are rare in human metabolic pathologies, obese individuals exhibit elevated RIPK3 and phosphorylated MLKL levels (Gautheron et al., 2016). Contrasting with its pro-inflammatory roles, RIPK3 deficiency in HFD-fed mice surprisingly leads to worsened glucose intolerance and insulin resistance due to liver damage. Overexpression of RIPK3 may be protective by limiting adipocyte apoptosis and inflammation. Interestingly, complete caspase-8 deficiency protects RIPK3-null mice from metabolic inflammation, highlighting adipocyte apoptosis as a key driver (Gautheron et al., 2016).

Moreover, beyond necroptosis, RIPK3 seems to also supports mitochondrial biogenesis and fatty acid oxidation in tumor-associated macrophages (Islam et al., 2022; L. Wu et al., 2020), suggesting additional roles in obesity-induced inflammation involving apoptosis regulation, inflammation, and energy homeostasis.

Human and mouse studies associate RIPK1 polymorphisms with obesity, correlating with BMI (Karunakaran et al., 2020). Reduction of RIPK1 expression in mice confers resistance to weight gain and metabolic defects under HFD. Similarly, pharmacological inhibition of RIPK1 kinase activity improves insulin resistance and glucose intolerance without altering weight (H. Xu et al., 2019).

To add complexity, findings from MLKL knockout models are mixed. Several studies report that MLKL deficiency protects against inflammation, hepatic steatosis, and metabolic dysfunction in HFD models (Saeed et al., 2019; X. Wu et al., 2020; H. Xu et al., 2019), while others report no liver protection but improved insulin sensitivity (Ohene-Marfo et al., 2024). These phenotypes appear independent of necroptosis, as MLKL modulates hepatic insulin sensitivity and lipid metabolism beyond inflammatory roles (Tye et al., 2025; H. Xu et al., 2019). Additionally, MLKL regulates proteins involved in lipid uptake and transport(Tye et al., 2025). Its deficiency impairs white adipocyte differentiation but not beige, in contrast to RIPK3 deletion, which does not affect adipogenesis (Magusto et al., 2022). Moreover, MLKL inhibits adipocyte differentiation and autophagy (Magusto et al., 2022; X. Wu et al., 2020) and restricts lipid accumulation in macrophages within atherosclerotic plaques (Rasheed et al., 2020).

Despite advances in understanding MLKL's and RIPK3's roles in liver injury and lipid metabolism, their classical necroptotic function in adipocytes during obesity-related inflammation remains unresolved.

1.5.1.4 Pyroptosis during obesity

Subsequent investigations revealed pyroptosis to be orchestrated by inflammasome complexes in response to diverse danger signals, involving sensor proteins like NLRP3, AIM2, or NLRC4, culminating in caspase-1 activation, gasdermin D (GSDMD) cleavage, and membrane pore formation (Kelley et al., 2019). This process triggers cell rupture, releasing pro-inflammatory cytokines and DAMPs, amplifying inflammation and immune responses (T. Deng et al., 2021).

As research unfolds, the intricate regulatory mechanisms of pyroptosis have unveiled its significance not only in pathogen defence but also in inflammatory diseases, spurring novel therapeutic strategies aimed at modulating this pathway to mitigate tissue damage and treat inflammatory conditions.

In the field of metabolism, the intricate interplay between cell death and inflammation extends to obesity-associated pathology. Components of the NLRP3 inflammasome, notably caspase-1, emerge as pivotal regulators in sensing danger signals linked to obesity (Wani et al., 2021). In animal studies, blocking caspase-1 activity results in decreased weight gain, decreased inflammation, and improved insulin sensitivity (Morrison et al., 2016; Stienstra et al., 2010), while blocking NLRP3 in obese mice models lead to a decrease in inflammation, blood glucose and insulin levels (Chiazza et al., 2016; Unamuno et al., 2021).

IL-1β, in particular, stands out as a key player in mediating the detrimental metabolic effects of obesity and presents a potential therapeutic target (Sauter et al., 2008). Clinical trials employing IL-1Ra (anakinra) have demonstrated promising outcomes in patients with diabetes, although without significant improvements in insulin sensitivity, underscoring the complex involvement of the IL-1 cytokine family in obesity-related inflammation and IR (Tack et al., 2012).

Moreover, the N-terminal fragment of Gasdermin D (GSDMD), representing its activated form, is elevated in patients with NASH and NAFLD (B. Xu et al., 2018). Loss of GSDMD protects mice from steatohepatitis induced by methionine-choline deficient diet or HFD. However, GSDMD knockout in HFD-fed mice does not protect against obesity-induced adipose tissue inflammation or systemic metabolic dysfunction; instead, these mice show mildly worsened glucose intolerance and increased fat mass, partially due to suppressed PPARγ expression. While liver inflammation decreases in GSDMD-deficient mice, adipose tissue inflammation remains unaffected (Ma et al., 2022).

Data on Gasdermin E (GSDME) deletion in metabolic disease models is more limited. In the atherosclerotic ApoE model, GSDME ablation in macrophages reduces LDL-induced inflammation and pyroptosis (Wei et al., 2023). Conversely, deletion of GSDME exacerbates HFD-induced obesity, impairs adipose function, and worsens glucose intolerance and insulin resistance, partly by dysregulating adipose triglyceride lipase (ATGL) expression (Wei et al., 2024).

In the context of obesity, where dysregulated metabolism fosters a pro-inflammatory milieu, the role of pyroptosis, a form of regulated necrosis, gains particular relevance. Pyroptosis, characterised by the activation of inflammasomes and subsequent release of pro-inflammatory cytokines, intersects with metabolic dysregulation to exacerbate adipose tissue inflammation and IR (Koenen et al., 2011; H. Wang et al., 2014). Understanding the interplay between pyroptosis and metabolic dysfunction in obesity holds promise for uncovering novel therapeutic strategies to mitigate obesity-related complications.

1.5.2 Linear ubiquitination during metabolic syndrome

The NF-κB pathway is involved in both inflammatory and metabolic responses, representing an entry point to study metabolic diseases and develop novel treatment strategies (Baker et al., 2011). LinUb is a fundamental regulator of NF-κB signalling allowing gene activation and preventing death complex formation. However, while the role of NF-κB signalling and several components of the cell death machinery during metabolic syndrome has been explored with

genetic mice models (Hildebrandt et al., 2022), the implications of LUBAC during metabolic syndrome have not yet been described.

Several components of LUBAC or its regulators have been implicated in metabolism. For example, key glycolytic enzymes like hexokinase-1 (HK1), hexokinase-2 (HK2), and liver-type phosphofructokinase (PFKL) were found to be linearly ubiquitinated, suggesting linear ubiquitination directly regulates glucose metabolism (Fu et al., 2024). Furthermore, HOIP liver-specific protein-protein interactions (PPIs) were found to participate in ribose phosphate metabolic processes, probably by modulating certain regulators, such as sterol carrier protein 2 (SCP2) and AMP-activated protein kinase catalytic subunit alpha-2 (PRKAA2) (Fu et al., 2024) .In addition RNF31 was found to be a relevant as a co-regulator of steroidogenic pathways in that convert cholesterol into hormones (Ehrlund et al., 2009, 2012).

On the other hand, HOIL-1 was shown to monoubiquitinate glycogen and linear maltoheptaose (an unbranched glucose polymer) in vitro, targeting the C6 hydroxyl group of glucose residues (Kelsall et al., 2022). In this report authors hypothesise that HOIL-1 monoubiquitination may initiate the removal of unbranched glucose polymers from cells, preventing their precipitation as polyglucosan bodies, which could explain why HOIL-1 deficiencies lead to amylopectinosis. In addition HOIP and Sharpin can also bind to unbranched and infrequently branched glucose polymers, but not highly branched glycogen (Kelsall et al., 2022). Moreover, patients with Rbck1-dependt PGBM1 present hepatosplenomegaly, and high liver profile as an early symptom of their disease (AlAnzi et al., 2022), so it seems to be that linear chains regulation is fundamental for proper liver function. In addition, LUBAC expression, especially SHARPIN , are significantly reduced in the livers of mice in chemical induced-fulminant hepatitis models (Yamamotoya et al., 2017).

These recent findings suggest that the linear ubiquitination machinery, particularly the LUBAC components HOIP and HOIL-1, play a role in the regulation of glycogen metabolism by directly ubiquitinating glycolytic enzymes, modulating metabolic regulators, and targeting unbranched glucose polymers for degradation to prevent their accumulation as toxic polyglucosan bodies in the liver.

In addition, liver-specific HOIP or OTULIN deficiency leads to hepatocyte apoptosis, liver inflammation and to tumorigenesis (Damgaard et al., 2020; Y. Shimizu et al., 2017) and A20 deletion (unprotected linear chains) lead to susceptibility against chemical-induced and HFD hepatocellular carcinoma (Catrysse et al., 2016). Curiously, mice with hepatocyte-specific

OTULIN deletion showed an almost complete lack of glycogen in their livers, (Damgaard et al., 2020). While, on the other hand, HOIP loss in humans also causes hepatomegaly, high levels of blood triglycerides, fatty faeces, and wasting (Boisson et al., 2015), highlighting the metabolic implications of linear ubiquitination.

In sum, deficiency or dysregulation of linear ubiquitin chains exacerbates liver inflammation, steatosis, and fibrosis due to susceptibility to liver injury and hepatocyte cell death. However little is known on the metabolic implications of LinUb outside of this context.

To further understand the contribution of linear ubiquitination to obesity-associated disorders, we generated murine mutants lacking linear chains in mature adipocytes (*Hoip*$^{A\text{-}KO}$) or presenting exacerbated LUBAC activity *(Hoil-1*^{C458A}*)* and challenged with a HFD.

In short, *Hoip*$^{A\text{-}KO}$ mice presented a spontaneous casp8-dependent lipodystrophy-like phenotype which enhanced AFLD during obesity challenge and predisposed mice to insulin resistance upon ageing. On the other hand, increased LinUb protected challenged mice against liver steatosis and BAT whitening, possibly by preventing cell death and increasing ScWAT UCP-1 expression.

This research contributes to the knowledge of the implications and novel roles of cell death machinery in adipose tissue homeostasis,proposes LUBAC deficiencies as a possible marker of predisposition to metabolic syndrome, and highlight the intricate interplay between linear ubiquitination, inflammation, cell death, and metabolic regulation, opening new avenues for therapeutic interventions in metabolic disorders.

2. Aims

The primary aim of this thesis is to elucidate the role of LUBAC in the regulation of cell death and inflammation associated with metabolic syndrome, particularly in the context of obesity. This investigation will focus on several key objectives:

1. Understand LUBAC's role in metabolic inflammation

One of the central goals is to understand the relevance of LUBAC in metabolic inflammation. This includes exploring how linear ubiquitination affects adipose tissue homeostasis during challenges such as obesity and ageing. By examining these mechanisms, we aim to uncover insights into how LUBAC contributes to the inflammatory processes that characterize metabolic syndrome.

2. Dissect cell death modalities regulated by LUBAC in adipose tissue homeostasis

Assessing the susceptibility of adipocytes to the different TNF-induced cell death modalities and determining the broader implications of adipocyte death on metabolic health during obesity will provide a clearer picture of how cell death contributes to the development and progression of metabolic syndromes.

3. Evaluate the potential for therapeutic interventions modulating linear ubiquitination

Lastly, by enhancing linear ubiquitination, we seek to clarify its role in promoting metabolic health and identify potential treatment avenues for metabolic disorders linked to obesity. The findings underscore the importance of investigating LUBAC's function in regulating inflammation and cell death, which could lead to innovative approaches in addressing obesity-related health issues.

Through these aims, this thesis will contribute to a deeper understanding of the interplay between LUBAC, inflammation, and cell death in the context of metabolic syndrome.

3. Results

This chapter presents the results of our comprehensive investigation into the role of the Linear Ubiquitin Chain Assembly Complex in metabolic health, with a particular focus on adipose tissue as the primary organ affected during obesity. Our study employed a multi-faceted approach, combining human data analysis with in-depth mouse model experiments to elucidate the impact of linear ubiquitination on metabolic homeostasis.

We began by examining RNA expression levels of LUBAC components in human adipose tissue samples, correlating these with key metabolic parameters such as insulin sensitivity, lipid profiles, and inflammatory markers. This analysis aimed to uncover potential relationships between LUBAC activity and metabolic dysregulation in obese patients.

To further delineate the precise contribution of linear ubiquitination to obesity-associated disorders, we generated and characterized two murine models: one lacking LUBAC activity by depleting HOIP specifically in adipocytes (*Hoip*$^{A\text{-}KO}$), and another with enhanced linear ubiquitination capacity (*Hoil-1*^{C458A}). These two models were subjected to a HFD challenge to assess the impact of altered linear ubiquitination on metabolic outcomes during obesity.

Additionally, we evaluated *Hoip*$^{A\text{-}KO}$ mice under normal fed conditions and across different age groups to investigate the implications of linear ubiquitin chain loss on the onset of metabolic syndrome during aging.

Through these diverse approaches, this project contributes significant insights into the novel roles of the cell death machinery in adipose tissue homeostasis and proposes Linear Ubiquitination as a pro-survival mechanism in adipocytes to prevent metabolic syndrome.

This comprehensive study aimed to provide insights into the role of LUBAC in obesity-related metabolic dysfunction.

3.1. LUBAC expression in adipose tissue correlates with metabolic health in obese patients

In collaboration with Dr. Anne Hoffmann and Matthias Blüher, we evaluated gene expression of LUBAC components using RNAseq data from visceral and subcutaneous adipose tissue from the Leipzig Obesity Biobank (LOBB). RNA expression levels of LUBAC components were examined in conjunction with metabolic parameters, including insulin sensitivity, lipid

profiles, and inflammatory markers, to uncover correlations between LUBAC activity and metabolic dysregulation across three distinct cohorts of obese and/or lean patients.

These cohorts included:

1. A cross-sectional cohort of lean and obese individuals (N = 1479)

2. A cohort comparing metabolically healthy and unhealthy obese subjects (N = 42)

3. A two-step bariatric surgery cohort of 65 morbidly obese subjects before and after dramatic weight loss

The most relevant results of this comprehensive study are presented here, providing insights into the role of LUBAC in obesity-related metabolic dysfunction in humans.

3.1.1 LUBAC expression in Cross-sectional cohort: normal and overweight Adipose Tissue

The cross-sectional cohort comprising of 1,479 subjects who were either normal or overweight was comprised of 31 lean subjects with a BMI of 25.7 ± 2.7 kg/m2, where 52% were women, and the average age was 55.8 ± 13.4 years old, and 1448 obese volunteers with a BMI: 49.2 ± 8.3 kg/m2, where 71% were women and the average age was 46.9 ± 11.7 years old.

In this cohort, LUBAC components, HOIL-1 (Rbck1), HOIP (Rnf31) and SHARPIN, exhibit a robust positive correlation among them in obese adipose tissue, suggesting a mutual regulation on the expression of the complex in adipose tissue (Figure 3.1.1). Notably, all LUBAC components showed a negative association with the expression of TNFRSF19, Fas, and TNFR11a (RANK), being Fas described as an inhibitor of adipocyte browning (Wueest et al., 2024), TNFRSF19 as an inhibitor of adipogenesis through Wnt signalling (Gire et al., 2024; Qiu et al., 2010) and RANK signalling associated with browning inhibition in ScWAT (Matsuo et al., 2020). Conversely, they exhibit a positive correlation with TNFSF13 and TNFSF12, both characteristic of obese patients without T2D mellitus (T2DM) (Shunkina Skuratovskaia et al., 2021) and TNFAIP6, associated with matrix remodelling, anti-inflammatory and tissue protective properties (Day & Milner, 2019). Interestingly, elevated plasma levels of TNFSF12 were also linked to decreased glucose levels and reduced body mass index (BMI) (Shunkina Skuratovskaia et al., 2021). Last, CSF3 (G-CSF) and TNF itself were negatively associated with LUBAC expression, both associated with inflammation and insulin resistance (Ordelheide et al., 2016).

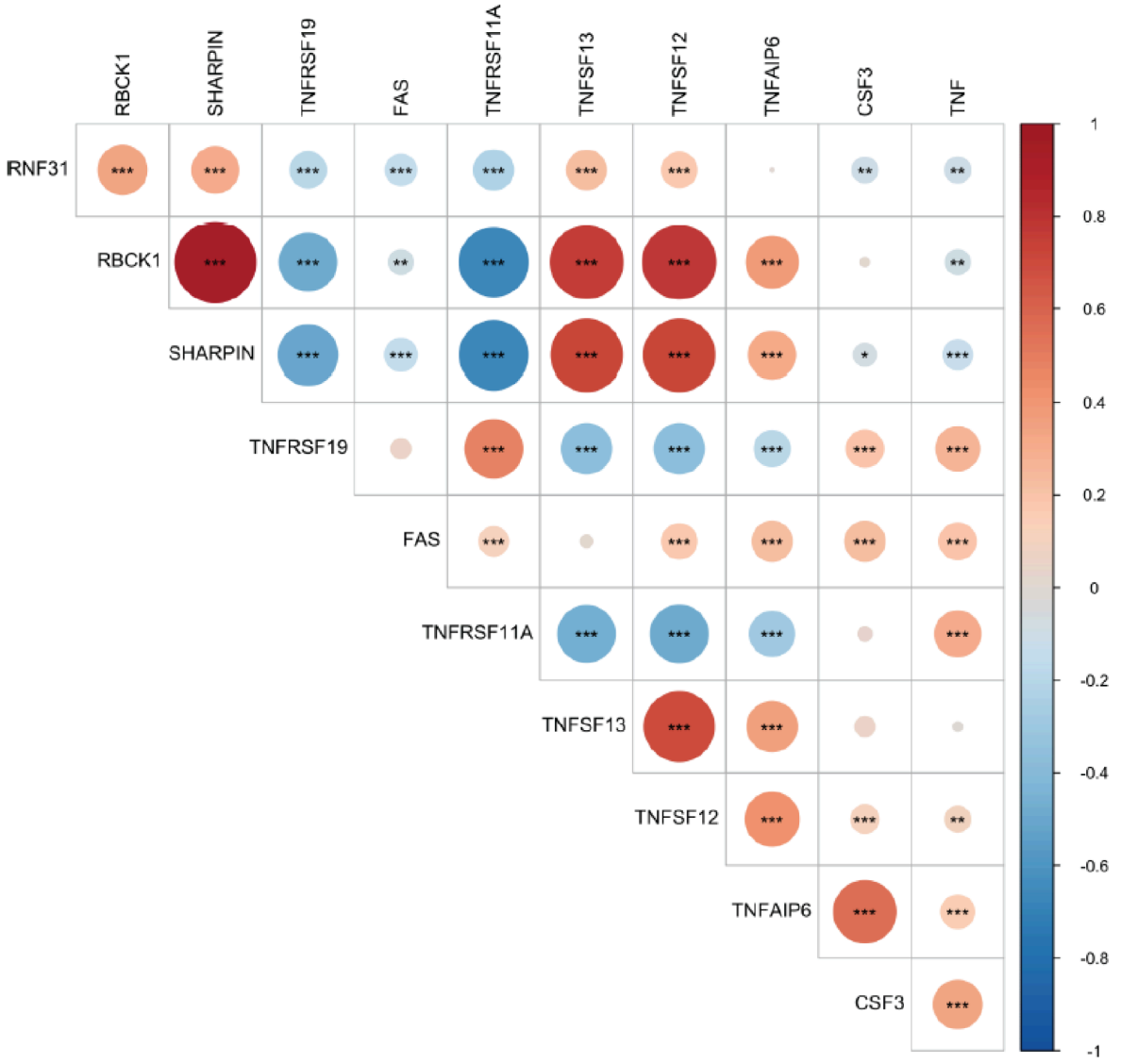

Figure 3.1.1 LUBAC components are negatively correlated with inflammatory genes in Adipose Tissue.

Correlation matrix plot of RNA expression levels in white adipose tissue of the cross-sectional cohort with lean and obese individuals. Correlations were assessed by non-parametric Spearman's test, (*) p<0,05, (**) p<0,01, (***) p<0,001, (****) p<0,0001 (ns) not significant.

On the other hand, LUBAC components are negatively correlated with Casp8 and MLKL expression, inferring a protection against TNF-induced cell death in obese adipose tissue (Figure 3.1.2). Curiously, they are also negatively associated with C-FLIP (cflar), which controls caspase-8 activity and has an anti-apoptotic. On the contrary, LUBAC positively correlates with FADD, whose activation is associated with improved IR, and decreased triglyceride storage (Zhuang et al., 2016) and NINJ1, a protein known to be increased in

db/db mice, but its role in human AT is still unknown (N. K. Sharma et al., 2016). However, in a SNIPs study, higher insulin sensitivity was associated with lower adipose NINJ1 transcript expression, however, it is most likely that the source of this membrane protein comes from stromal vascular fraction rather than adipocytes itself (N. K. Sharma et al., 2016). At the same time, RIPK1 and RIPK3, both known to be upregulated during obesity, also positively relate to LUBAC expression, which may be a result of adipose tissue expansion and potentially protection from adipocyte apoptosis as previously described for RIPK3 (Gautheron et al., 2016).

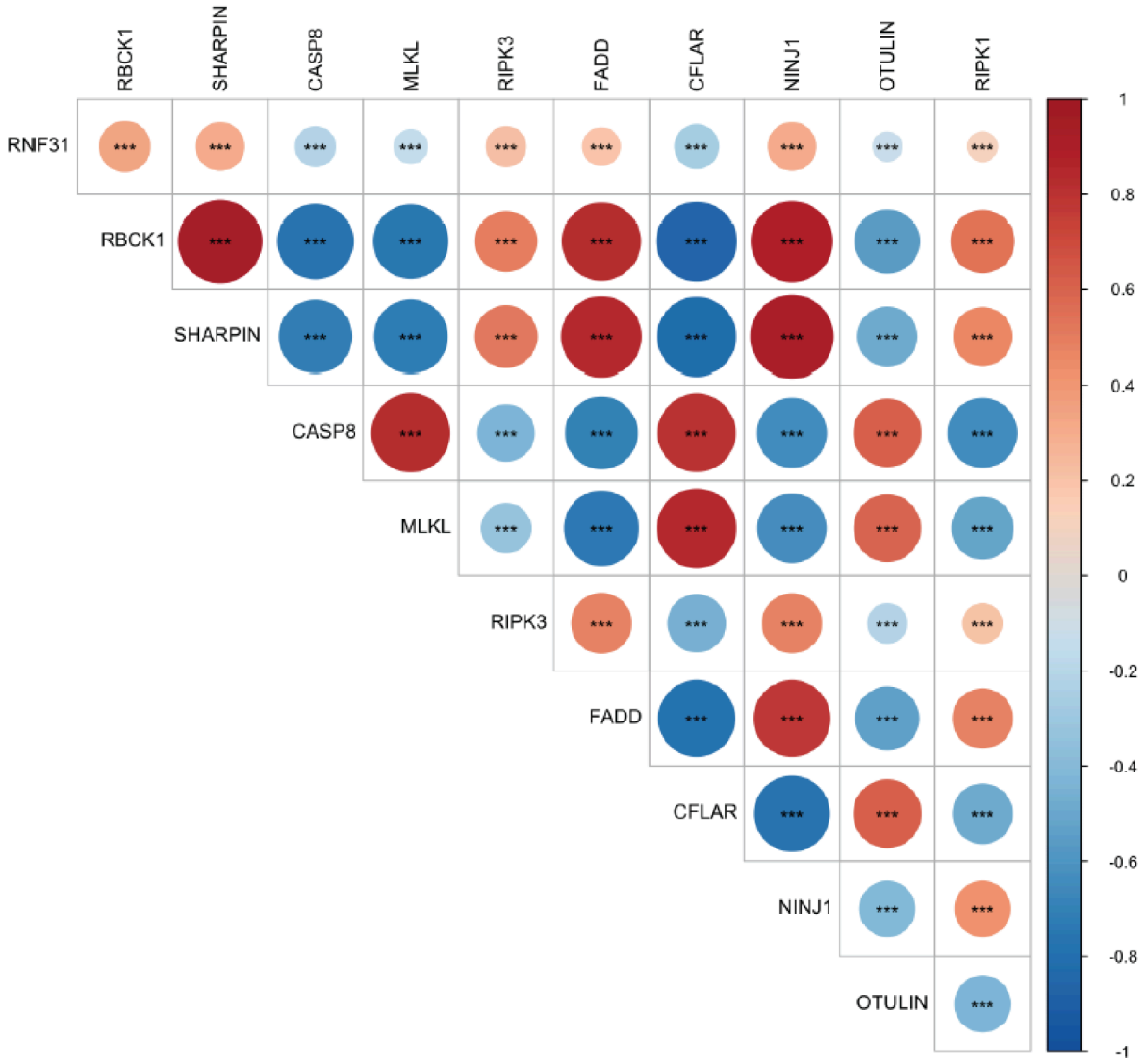

Figure 3.1.2 HOIP and HOIL-1 expression is negatively correlated with cell death effectors in Adipose Tissue.

Correlation matrix plot of RNA expression levels in white adipose tissue of the cross-sectional cohort with lean and obese individuals. Correlations were assessed by non-parametric Spearman's test, (*) p<0,05, (**) p<0,01, (***) p<0,001, (****) p<0,0001 (ns) not significant.

Regarding NF-κB activation, SARPIN and HOIL-1 are negatively correlated with IKBKB (IKKb), a central coordinator of inflammatory responses through activation of NF-κB but also essential for adipocyte survival (S.-H. Park et al., 2016), TBK1, a controversial regulator of inflammation in obese adipose tissue (Zhao et al., 2018), TNKS a negative regulator of GLUT4 expression and adiponectin in adipocytes (Yeh et al., 2009), and OTULIN a negative regulator of LUBAC activity (Figure 3.1.3). On the other hand, LUBAC is positively associated with, TRADD a required component of TNFR1 for NF-κB activation (Hayden & Ghosh, 2014), that regulates of cell death (independently of FADD can caspase-8) (Bender et al., 2005), BIRC2, which is associated with adipocyte survival in adult WAT (Röszer, 2021) and NAP1L1, a gene proposed to be a transcription regulator of genes involved in lipid and glucose metabolism (Ho et al., 2011; Hochberg et al., 2015) (Figure 3.1.3).

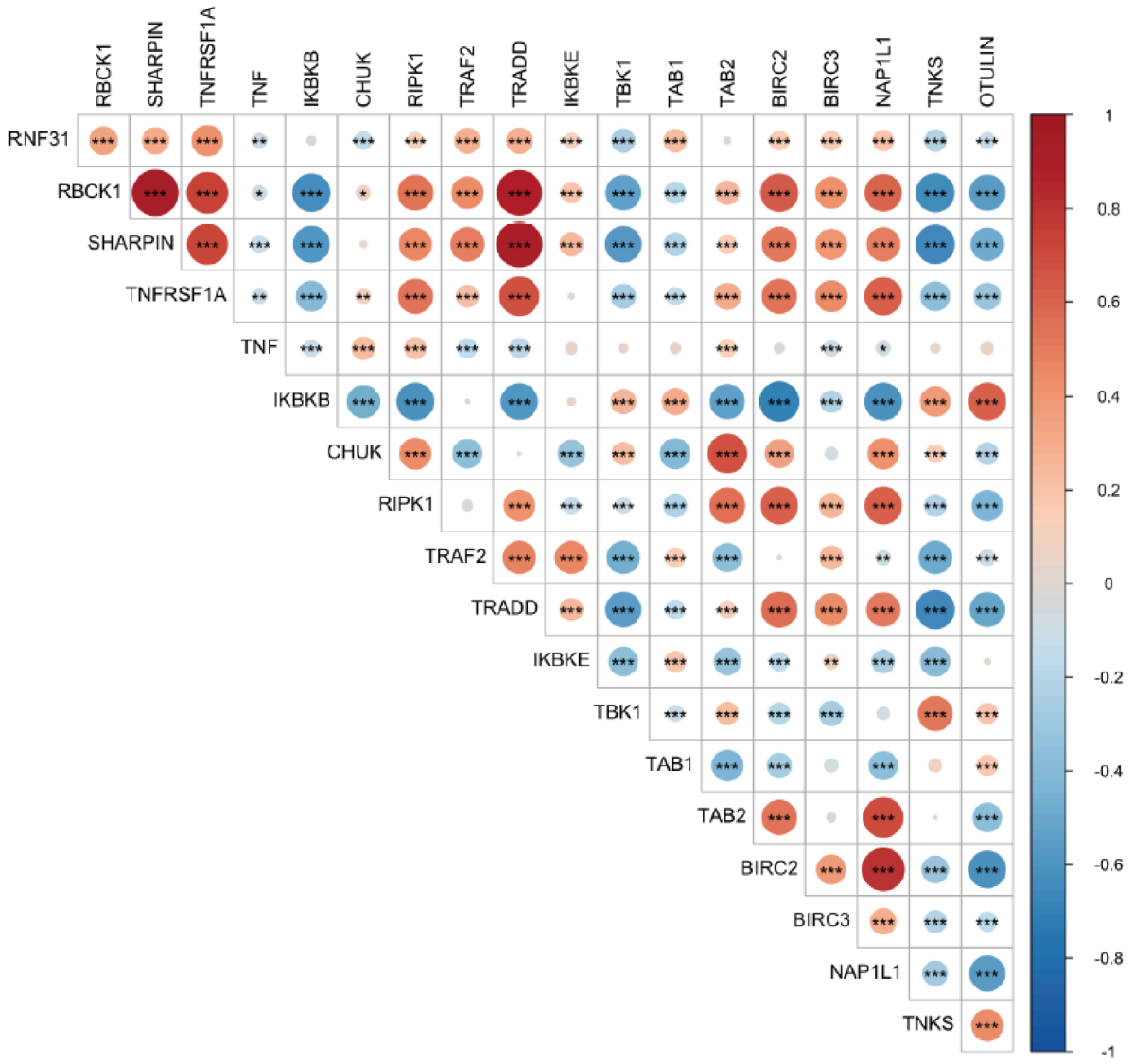

Figure 3.1.3 Correlation matrix of LUBAC components and NF-κB AT in AT of cross-sectional cohort.

Correlation matrix plot of RNA expression levels in white adipose tissue of the cross-sectional cohort with lean and obese individuals. Correlations were assessed by non-parametric Spearman's test, (*) p<0,05, (**) p<0,01, (***) p<0,001, (****) p<0,0001 (ns) not significant.

Furthermore, LUBAC expression IN at seems to positively correlate with adiponectin expression, the main antiinflammatory cytokine produced by adipocytes, while is negatively associated with Leptin receptor (Figure 3.1.4).

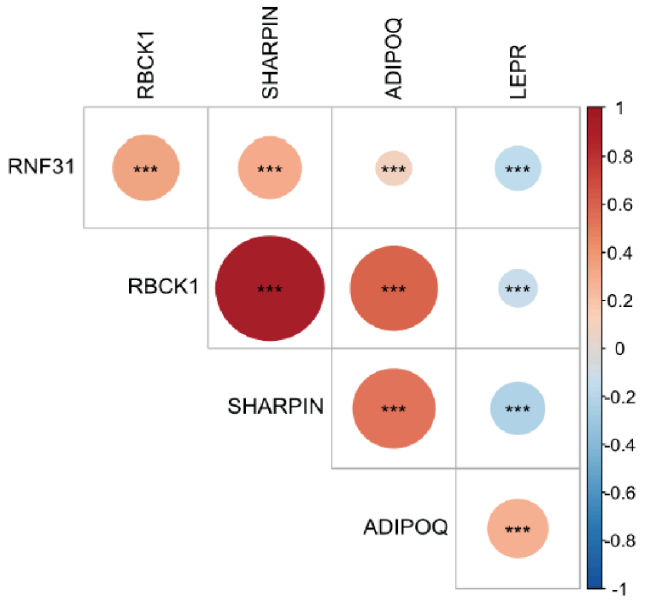

Figure 3.1.4 LUBAC components correlate with adipokines RNA expression in Adipose tissue.
Correlation matrix plot of RNA expression levels in white adipose tissue of the cross-sectional cohort with lean and obese individuals. Correlations were assessed by non-parametric Spearman's test, (*) p<0,05, (**) p<0,01, (***) p<0,001, (ns) not significant.

Comparing LUBAC gene expression with standard metabolic parameters, HOIP and HOIL-1 expression in male visceral fat was negatively correlated with Leptin blood levels (Figure 3.1.5 and 3.1.6). Moreover, LUBAC expression in male SC AT was associated with smaller hip circumference e.g., less ScWAT deposition (Figure 3.1.5).

On the other hand, in both the broad population and obese cohort we can observe a strong correlation between all of the components of the complex in VAT of males with IL-6 blood levels (Figure 3.1.5 and 3.1.6). Noteworthy, VAT expansion is associated with increased immune inflammatory response while IL-6 is associated with visceral fat mobilisation and fatty acid oxidation (Hoover et al., 2021) contributing to FFA and leptin release from adipocytes during HFD (Wueest & Konrad, 2018), however, its role in metabolic syndrome is still quite controversial (Wueest & Konrad, 2020). In addition, adiponectin in blood, had a strong positive correlation with HOIP and HOIL-1 expression in VAT (Figure 3.1.6).

From the graphs we can also observe some other significant tendencies, with lower correlation power. These include less CrP mainly in females (Figure 3.1.5)., lower LDL in blood in males (VAT) (Figure 3.1.5 and 3.1.6). Curiously, BMI was negatively correlated with HOIP expression in VAT, especially in females (Figure 3.1.5).

In the same line, LUBAC components tend to be negatively correlated with LDL Cholesterol in VAT of males (Figure 3.1.5), while HbA1c was negatively associated with HOIP and HOIL-1 in VAT from females (Figure 3.1.5 and 3.1.7).

Furthermore, in the correlation heat map we observed a mild tendency of HOIP and HOIL-1 expression in VAT with liver damage enzymes, indicating a possible role of linear chains in AT against liver steatosis (Figure 3.1.5 and 3.1.8).

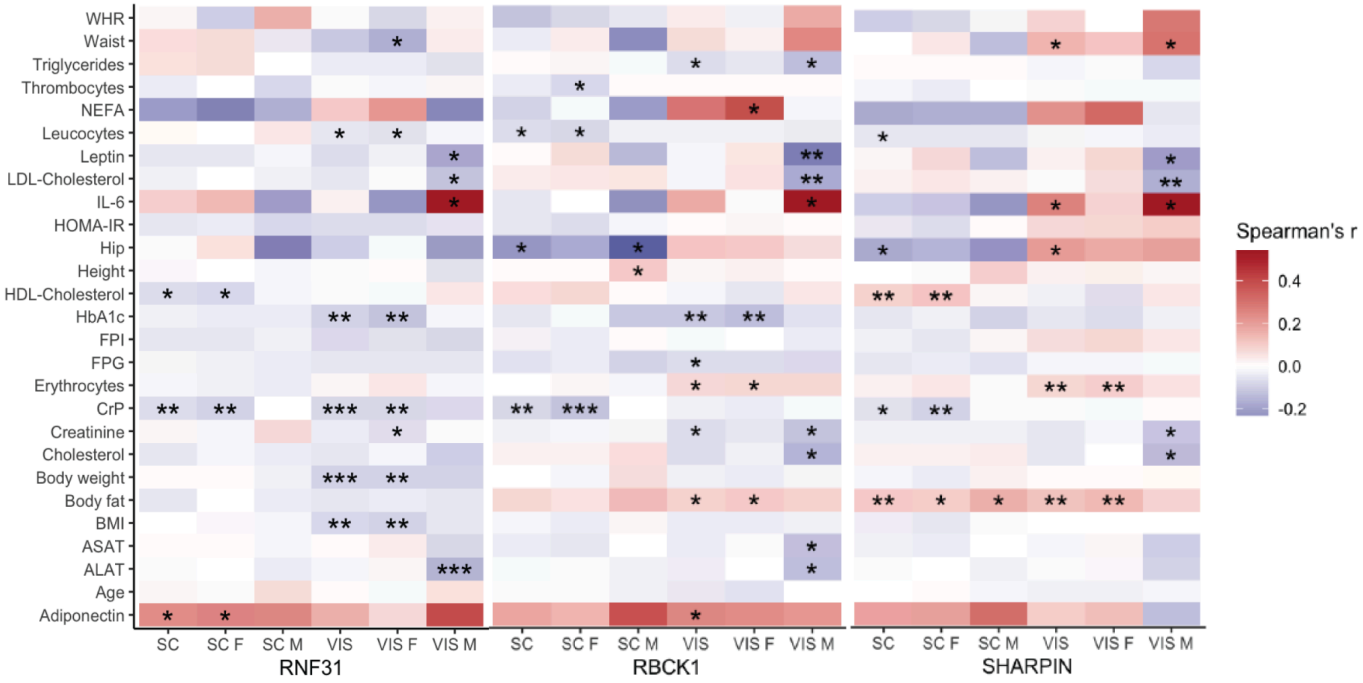

Figure 3.1.5 Correlation matrix of LUBAC components in AT of cross-sectional cohorts with metabolic syndrome parameters.

Correlation matrix of RNA expression levels in white adipose tissue of the cross-sectional cohort with lean and obese individuals. Subcutaneous adipose Tissue (SC), Visceral adipose tissue (Vis), Female (F), Male (M). Correlations were assessed by non-parametric Spearman's test, (*) p<0,05, (**) p<0,01,(***) p<0,001 blanc: not significant. .

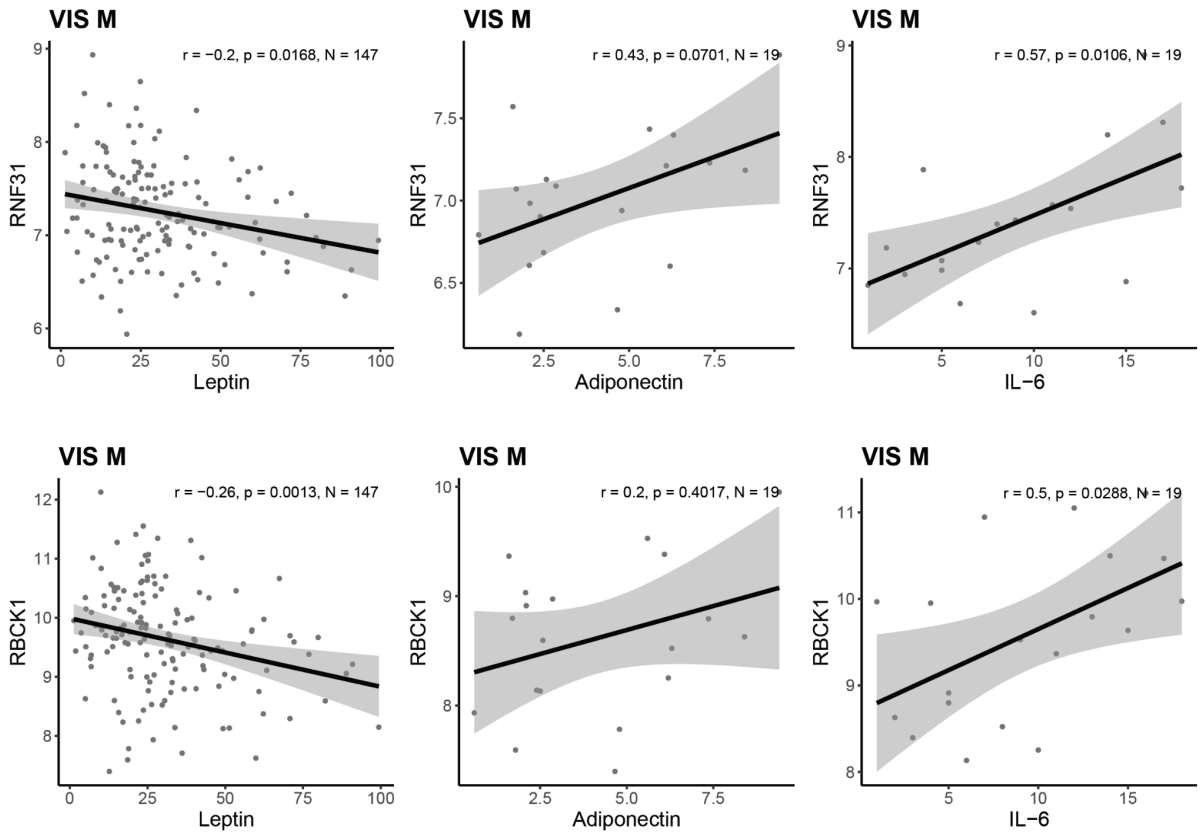

Figure 3.1.6 Adipokines values in blood correlated to HOIP and HOIL-1 RNA expression in AT.

Correlation plots of RNA expression levels in white adipose tissue with metabolic parameters using the cross-sectional cohort data with lean and obese individuals. Visceral adipose tissue (Vis), Male (M). Correlations were assessed by non-parametric Spearman's test.

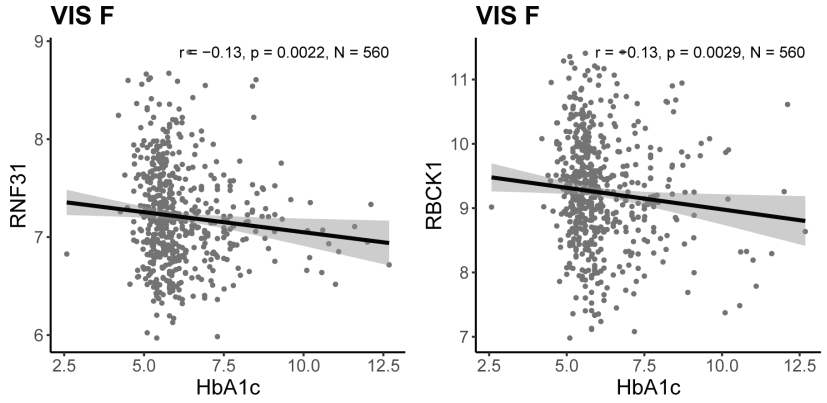

Figure 3.1.7 Diabetic market values in blood correlated to HOIP and HOIL-1 RNA expression in AT.

Correlation plots of RNA expression levels in white adipose tissue with metabolic parameters using the cross-sectional cohort data with lean and obese individuals. Visceral adipose tissue (Vis) Female (F). Correlations were assessed by non-parametric Spearman's test.

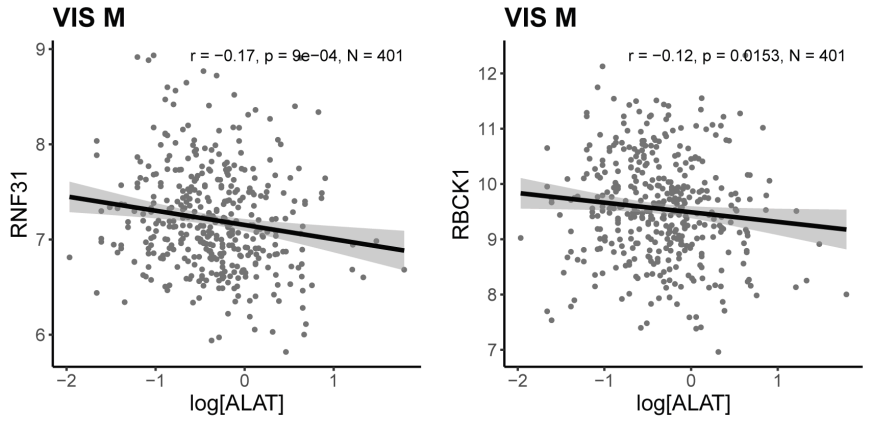

Figure 3.1.8 Liver damage enzyme values in blood correlated to HOIP and HOIL-1 RNA expression in AT.

Correlation plots of RNA expression levels in white adipose tissue liver damage enzyme Alanine Transaminase (ALAT) using the cross-sectional cohort data with lean and obese individuals. Visceral adipose tissue (Vis), Male (M) Correlations were assessed by non-parametric Spearman's test.

Last, when gene expression is distributed by BMI, we can observe a decrease of HOIP in VAT of obese patients, while at the same time, a preferential upregulation of SHARPIN and HOIL-1 in obese VAT compared to ScWAT (Figure 3.1.9).

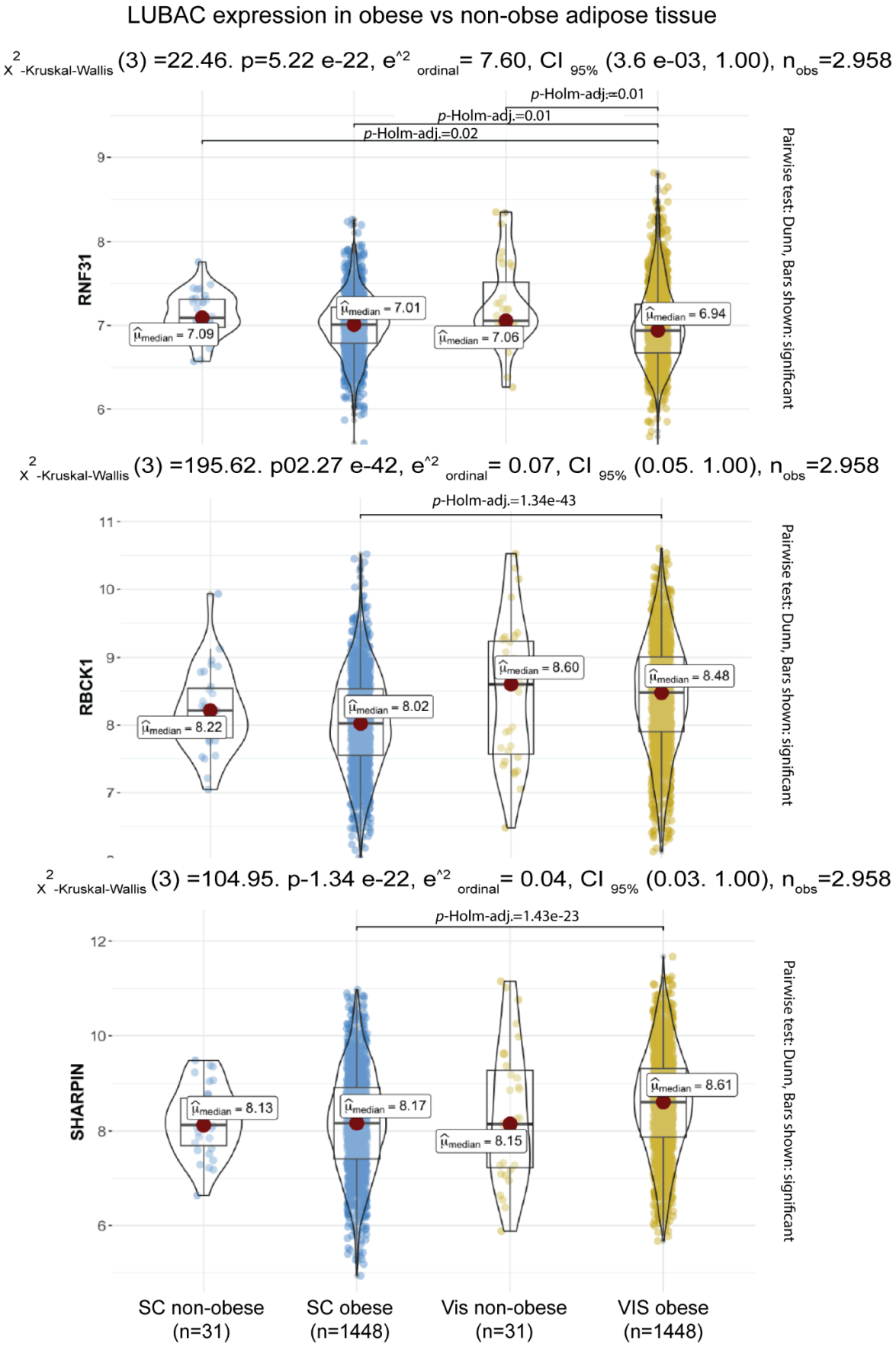

Figure 3.1.9 LUBAC expression in ScWAT and VAT adipose tissue lean vs obese.

RNA expression levels in white adipose of the cross-sectional cohort data with lean and obese individuals. Subcutaneous adipose tissue (SC/ScWAT), Visceral adipose tissue (VIS/VAT), Correlations were assessed by non-parametric Kruskal-Wallis H-test.

In general terms, in a cross sectional cohort, there is an apparent downregulation of HOIP during obesity in VAT with a preferential upregulation of LUBAC genes in VAT of obese patients in comparison to ScWAT. However, the patients with increase in LUBAC components expression in AT tend to be associated with anti-inflammatory adipokine circulation in blood, increased glucose and lipid metabolism genes, and pro-survival NF-κB activation through TNFR1 complex. At the same time, increase in LUBAC components in AT downregulates the expression of complex II cell death effectors Casp8 and MLKL (despite mild increase of RIPK3). In sum, LUBAC gene upregulation in VAT could be a pro-survival mechanism in VAT adipocytes and seem to be downregulated during obesity.

3.1.2 LUBAC expression in AT of metabolically healthy vs unhealthy obese cohort

The metabolically healthy vs unhealthy obese cohort, consisted of 31 insulin-sensitive subjects (IS) (71.43% female; age: 47.2 ± 7.7 years old; BMI: 47.3 ± 8.1 kg/m2; FPG: 5.7 ± 0.3 mmol/l; FPI: 113.7 ± 45.7 pmol/l) and 43 insulin-resistant patients (IR) (71% female; age: 38.8 ± 11.1 years old; BMI: 45.9 ± 6.9 kg/m2; FPG: 5.2 ± 0.2 mmol/l; FPI: 27.9 ± 13.5 pmol/l).

From this analysis, we observed an increase of Rbck1 expression in IS obese patients in comparison to IR (Figure 3.1.10). For the other LUBAC components the difference was not significant (data not shown)

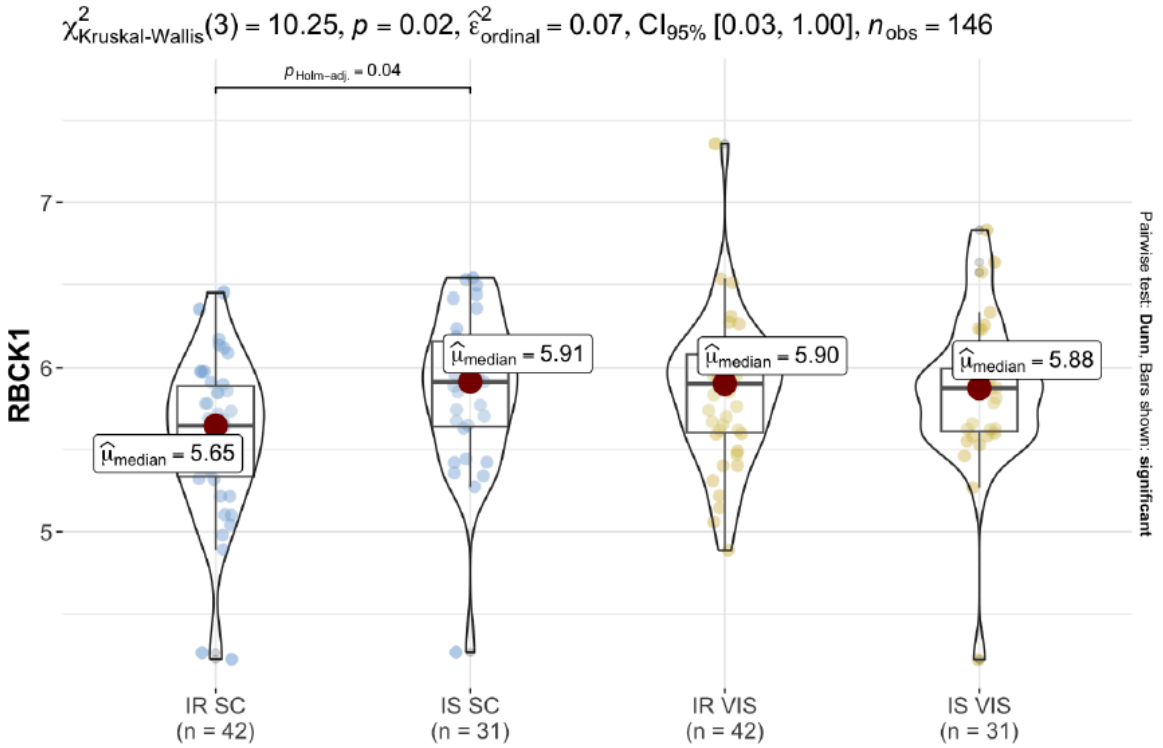

Figure 3.1.10: HOIL-1 gene expression adipose tissue of obese insulin sensitive or insulin resistant patients.

RNA expression levels in white adipose of the obese Insulin resistant (IR) or insulin sensitive (IS) obese patients before. Subcutaneous adipose tissue (SC) ,Visceral adipose tissue (Vis), Correlations were assessed by non-parametric Kruskal-Wallis H-test.

Furthermore, Leptin and IL-6 secretion were positively associated with expression of HOIP in male VAT of IR individuals (Figure 3.1.11). While vaspin, a cytokine that has been found to be significantly increased in mice with obesity and IR (Dimova & Tankova, 2015), was negatively correlated with HOIP in VAT of male IR cohort (Figure 3.1.11).

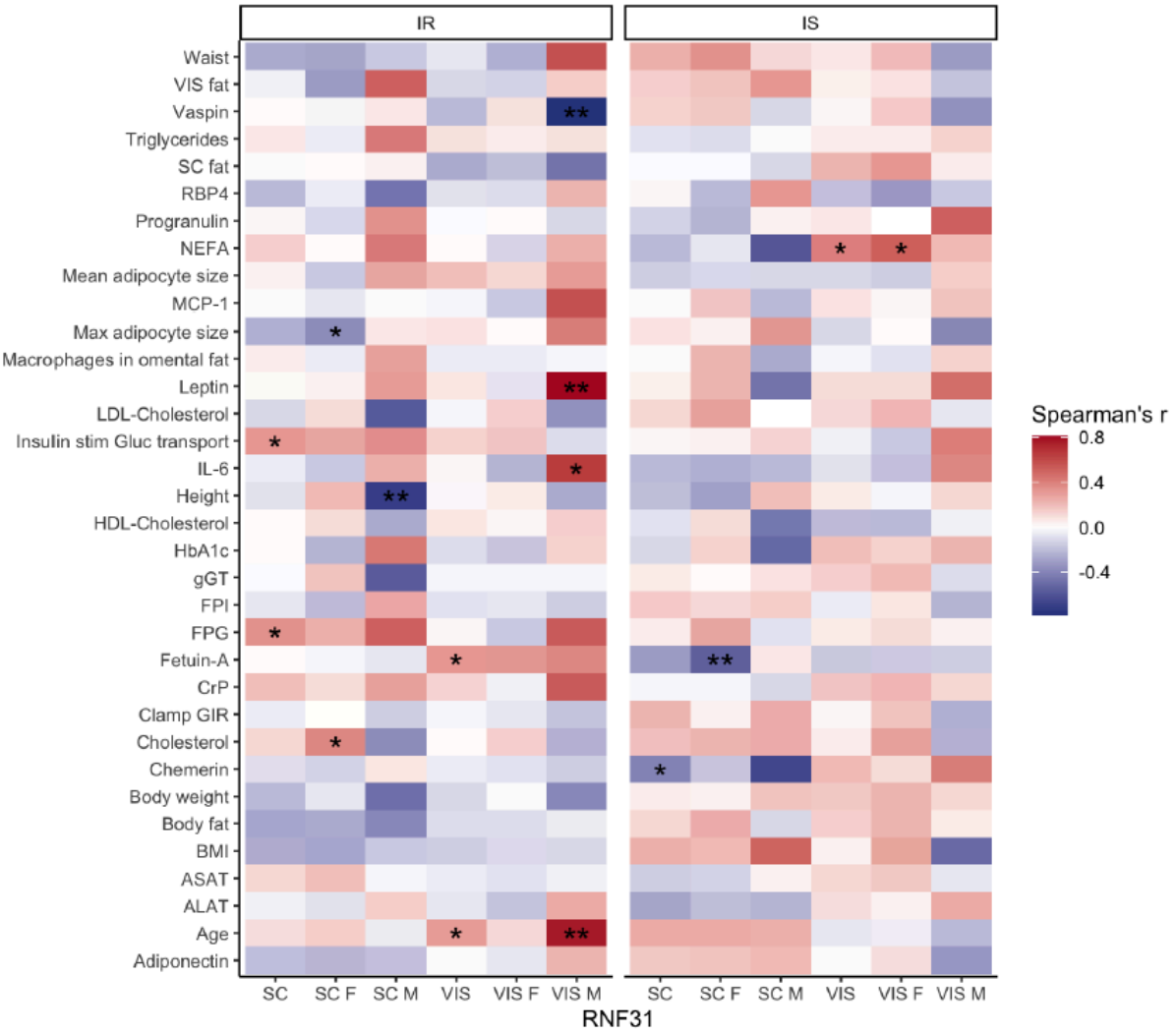

Figure 3.1.11: HOIP gene expression adipose tissue of obese insulin sensitive or insulin resistant patients vs metabolic parameters.

Correlation matrix between gene expression on adipose tissue of sensitive (IS) or insulin resistance (IR) obese patients and metabolic parameters. Subcutaneous adipose Tissue (SC), Visceral adipose tissue (Vis), Female (F), Male (M). Correlations were assessed by non-parametric Spearman's test, (*) p<0,05, (**) p<0,01,(***) p<0,001 blanc: not significant.

In the case of IS ScWAT, less SC fat was associated with increased HOIL-1 and SHARPIN levels, while the opposite was true for VAT in males (Figure 3.1.12 and 3.1.13). A similar situation is observed for AScWAT and ALAT (in IS) and IL6 levels (in IR), where female HOIL-1 and SHAPIN expression in ScWAT was associated with lower liver damage and IL6, while on the contrary was observed in male VAT (Figure 3.1.12 and 3.1.13). This highlights the differences between the different AT compartments during metabolic syndrome regarding gender. Of note, most of the correlations that are observed in the IS obese patients, and are not present in the IR subset. Despite this, Hb1Ac, IL-6 blood levels and visceral fat

deposition were positively associated with increased HOIL-1 and SHAPIN in ScWAT in IR males (Figure 3.1.12 and 3.1.13).

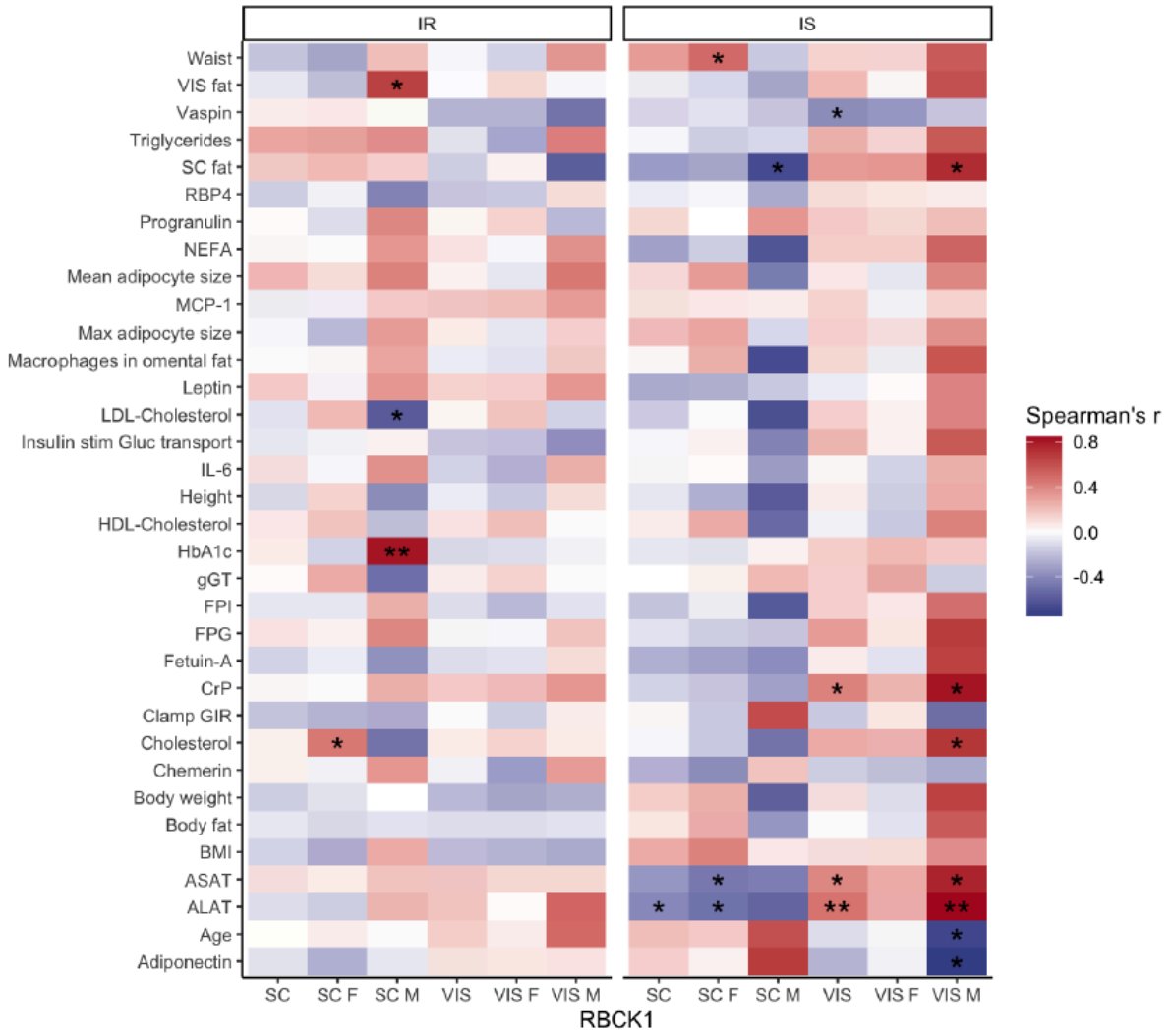

Figure 3.1.12: HOIL-1 gene expression adipose tissue of obese insulin sensitive or insulin resistant patients vs metabolic parameters.

Correlation matrix between gene expression on adipose tissue of sensitive (IS) or insulin resistance (IR) obese patients and metabolic parameters. Subcutaneous adipose Tissue (SC), Visceral adipose tissue (Vis), Female (F), Male (M). Correlations were assessed by non-parametric Spearman's test, (*) p<0,05, (**) p<0,01,(***) p<0,001 blanc: not significant.

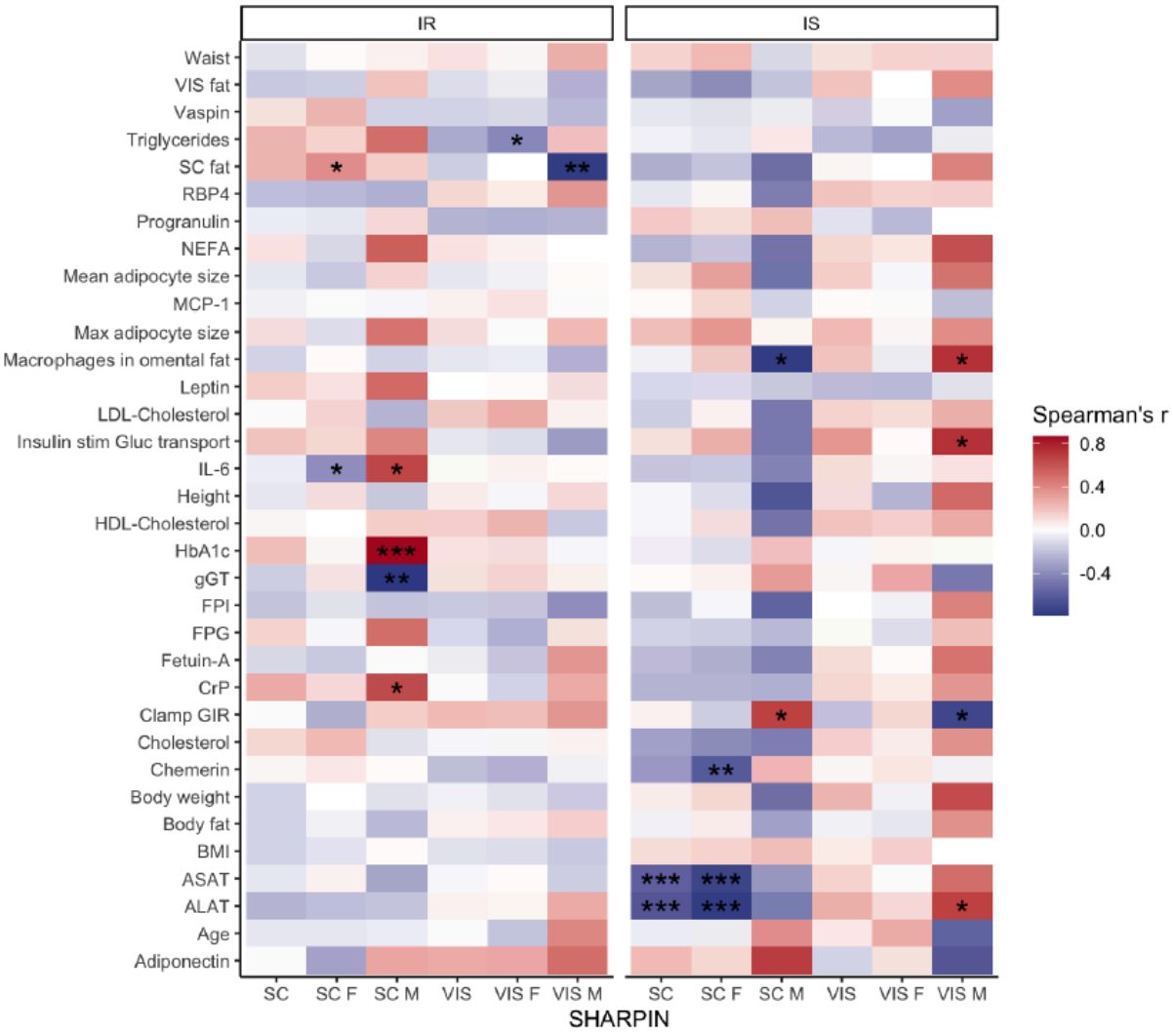

Figure 3.1.13: SHARPIN gene expression in adipose tissue of obese insulin sensitive or insulin resistant patients vs metabolic parameters.

Correlation matrix between *Sharpin* gene expression on adipose tissue of sensitive (IS) or insulin resistance (IR) obese patients and metabolic parameters. Subcutaneous adipose Tissue (SC), Visceral adipose tissue (Vis), Female (F), Male (M). Correlations were assessed by non-parametric Spearman's test, (*) p<0,05, (**) p<0,01,(***) p<0,001 blanc: not significant. .

In sum, obese females with increased LUBAC in ScWAT seem to be more protected against liver damage in the IS cohort, while males with increased LUBAC in VAT respond in the opposite direction. At the same time all LUBAC components were positively correlated with the diabetic marker in ScWAT of IR males, but not in females. Of note, the HOIP correlations that show statistical significance were mainly in the IR cohort where HOIL-1 and SARPIN were in IS, while Rbck1 the main regulator of LUBAC activity is enhanced in IS vs IR. These observations indicate sex differences of LinUb in the different AT compartments during obesity.

3.1.3 LUBAC expression in AT in morbid obesity before and after bariatric surgery

The two-step bariatric surgery cohort, consisting of 65 morbidly obese subjects (66% women; BMI>40 kg/m2) who underwent two-step bariatric surgery. The average preoperative BMI and age of the cohort patients were 54.5 ± 9.3 kg/m2 and 44.1 ± 9.2 years, respectively. After surgery, the cohort patients had an average BMI of 40.9 ± 7.2 kg/m2 and an average age of 47.1 ± 9.9 years. Patients lost an average of 40.2 ± 21.2 kg between the two surgeries. Preoperatively, T2D (T2D) was diagnosed in 28 patients, postoperatively T2D was only present in 18 patients.

From this analysis we can observe a negative correlation of HOIP and HOIL-1 expression in the AT with body fat in morbid obese patients, inferring that patients with increased LUBAC activity have less body fat percentage (Figure 3.1.14), while HOIP in ScWAT also negatively correlated with waist circumference (Figure 3.1.15).

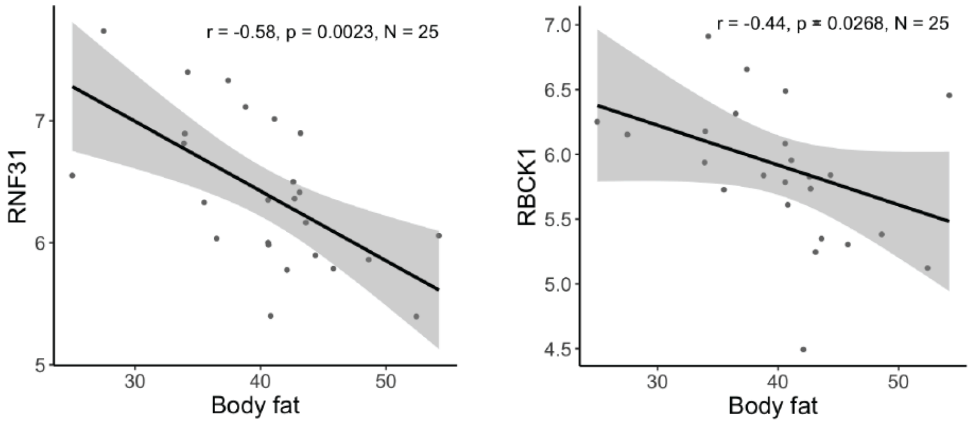

Figure 3.1.14 HOIP and HOIL-1 ScWAT expression vs Body fat composition in morbid obese males.

Correlation plots of RNA expression levels in white adipose tissue of obese and morbid obese patients before bariatric surgery with Body fat percentage. Correlations were assessed by non-parametric Spearman's test.

In addition, Rbck1 levels in ScWAT were upregulated after weight loss (Figure 3.1.16).

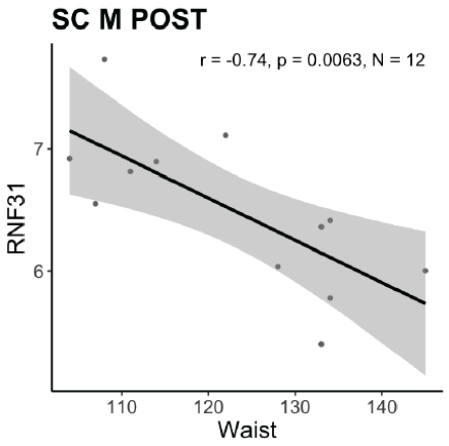

Figure 3.1.15 Correlation plot of HOIP expression in the ScWAT vs waist circumference of morbid obese patients post bariatric surgery.

Correlation plots of RNA expression levels in white adipose tissue of obese and morbid obese patients after (post) bariatric surgery with waist circumference. Correlations were assessed by

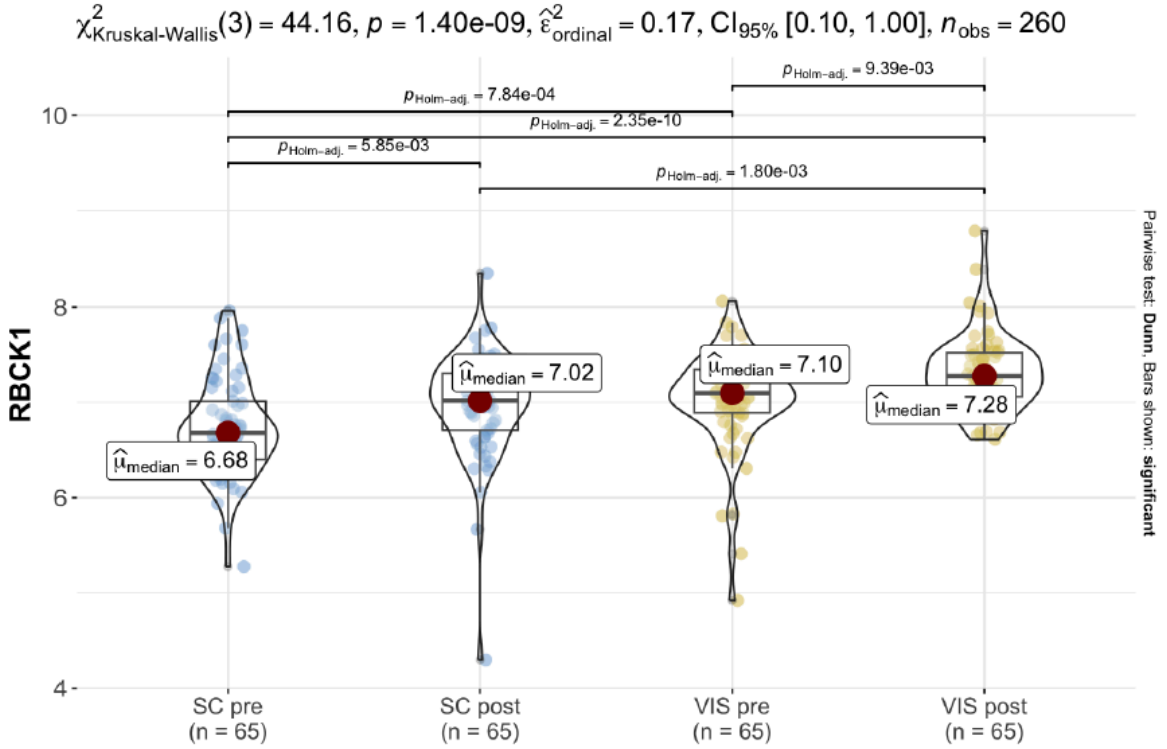

non-parametric Spearman's test.

Figure 3.1.16 HOIL-1 expression in the AT of morbid obese patients pre and post bariatric surgery.

RNA expression levels in white adipose of the obese and morbid obese patients before (pre) and after (post) bariatric surgery. Subcutaneous adipose tissue (SC) ,Visceral adipose tissue (Vis), Correlations were assessed by non-parametric Kruskal-Wallis H-test.

In line with these observations, HOIP expression in ScWAT was also correlated with smaller waist circumference after bariatric surgery (Figure 3.1.17). Curiously, in ScWAT of males increase in Rbck1 is also associated with higher triglycerides and IL-6 blood levels in concordance with VAT fat mobility and lipogenesis. In addition, VAT of males seems to be associated with less cholesterol levels in blood post surgery (Figure 3.1.17).

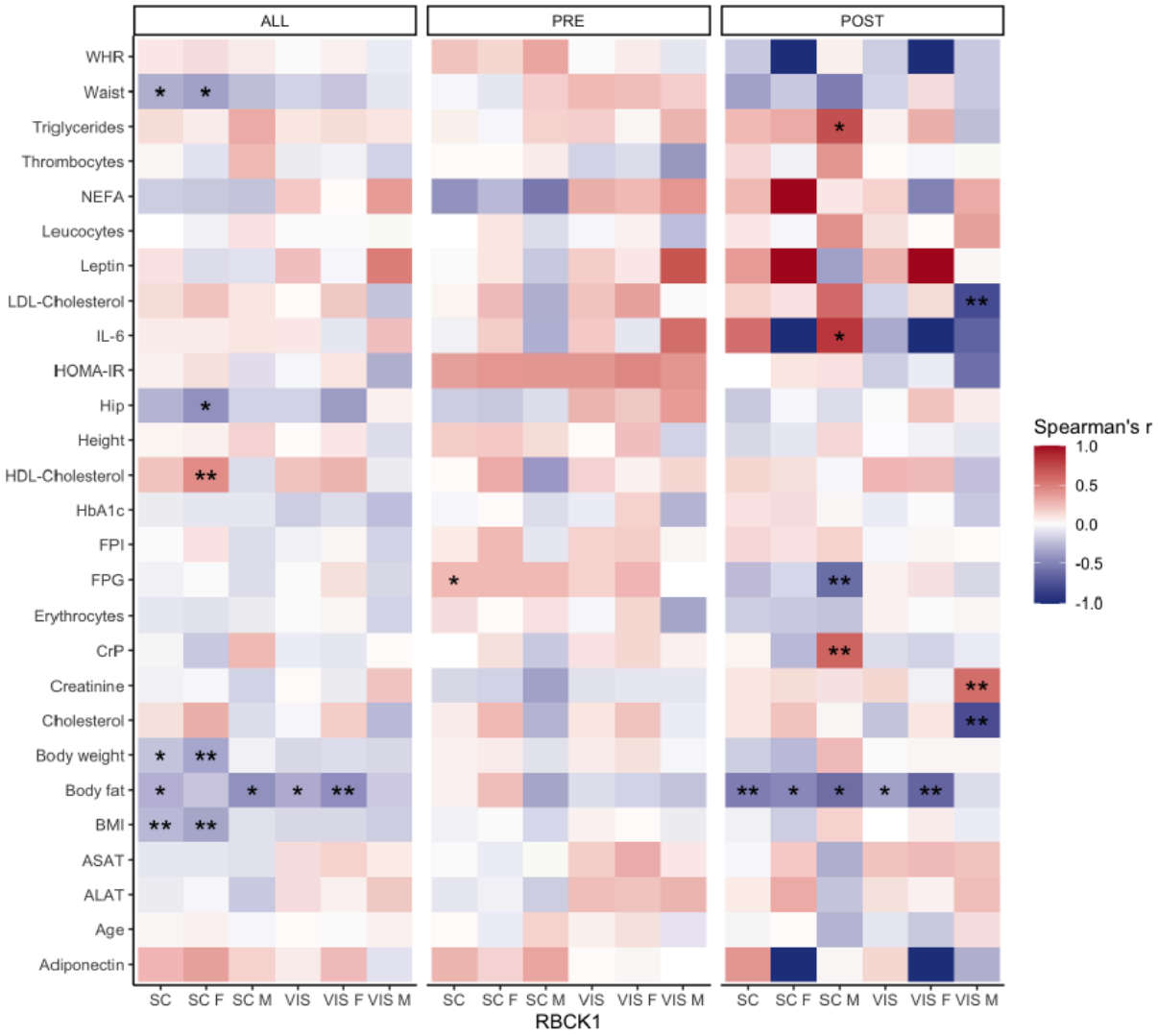

Figure 3.1.17 HOIL-1 expression in the AT correlated with metabolic parameters in morbid obese patients pre and post bariatric surgery.

Correlation matrix between gene expression in adipose tissue of obese patients before (pre) and after (post) bariatric surgery and metabolic parameters. Subcutaneous adipose Tissue (SC), Visceral adipose tissue (Vis), Female (F), Male (M). Correlations were assessed by non-parametric Spearman's test, (*) p<0,05, (**) p<0,01,(***) p<0,001 blanc: not significant.

3.1.4 Summary section 3.1

From human data analysis it seems that LUBAC expression is a protective mechanism of adipocyte survival during obesity, probably by enhancing NF-κB pro-survival role, possibly promoting lipogenesis and insulin sensitivity.

Notably, HOIL-1 expression was elevated in obese individuals with insulin sensitivity, suggesting a potential protective response through its upregulation. Intriguingly, HOIL-1 levels also rise in adipose tissue following weight loss after bariatric surgery. Collectively, these findings indicate that higher expression of LUBAC-related genes is associated with reduced fat mass and improved metabolic health in morbid obesity.

Interestingly, males with upregulation of VAT LUBAC also correlated with increased weight loss and enhanced lipogenesis, while obese females present less liver damage enzymes and better insulin response if they present high LUBAC activity is ScWAT. From this analysis it also becomes clear that the LinUb may regulate metabolic processes differently depending on the adipose tissue compartment and gender.

These observations go in line with literature, where NF-κB results fundamental to adipocytes survival and prevention of ectopic lipid accumulation, while females and males respond differently to excess on calorie intake.

3.1.5 Author contribution section 3.1

Dr. Anne Hoffmann and Prof.Dr. Matthias Blüher, evaluated gene expression of LUBAC components using RNAseq data from visceral and subcutaneous adipose tissue from the Leipzig Obesity Biobank (LOBB). We would also like to extend our acknowledgements to Falko Noé, Prof. Dr. Christian Wolfrum and Dr. Adhideb Ghosh from the Institute of Food, Nutrition and Health in Zurich, Switzerland, for being kind enough to grant us access to their database. Last, scientific interpretation and data analysis together with figure assembly were performed by the author of this thesis under supervision of Prof. Nieves Peltzer.

3.2. Linear Ubiquitination regulates adipocyte survival: Impact on Cell Death and NF-κB Signaling

The different associations between LUBAC component expression and improved metabolic parameters in obese patients suggested a protective role of the linear ubiquitination machinery during metabolic stress. These findings potentially indicate that patients with naturally higher LUBAC expression might have an advantage in managing obesity-related metabolic co-morbidities.

Given LUBAC's dual importance in preventing cell death and activating NF-κB signaling downstream of TNF receptors, we sought to elucidate the implications of LinUb in adipocytes, the primary cells composing adipose tissue.

First we evaluated the TNF response in murine differentiated adipocytes, assessing which TNF-induced cell death modalities these cells undergo in-vitro. Next, we uncovered how the absence of linear ubiquitination affects adipocyte differentiation. Last, we assessed how the loss of linear chains impacts adipocyte NF-κB activation and survival under TNF stimulation.

This analysis aimed to elucidate the molecular mechanisms underlying LUBAC's potential protective effects in obesity and related metabolic disorders, focusing on adipocyte differentiation and survival under TNF stimulation.

3.2.1. Characterization of TNF-Induced cell death modalities in murine adipocytes

Apoptotic machinery is found in essentially every cell type (Huttlin et al., 2010), however is not the sole cell death modality downstream TNFR1 (Vanden Berghe et al., 2014). TNF can also trigger necroptosis, in a number of cell types, especially when caspases are not available or inactivated (Z. Cai et al., 2014; He et al., 2009). To explore the capability of adipocytes to undergo both TNF-dependent cell death pathways, we differentiated mouse 3T3-L1 preadipocytes in-vitro and challenged them with apoptotic (TNF+BV6 or TB) and necroptotic (TNF+BV6+Zvad or TBZ) stimuli (Figure 3.2.1). These are highly standardised treatments to sensitise cells to TNF-induced cell death. In short, Smac mimetics or cIAP1-2 inhibitor (BV6), depletes cIAP1 and 2 and its corresponding E3-ligase activities at TNFR1 complex I (Petersen et al., 2007). This destabilises the complex and favours cell death, mainly by apoptosis. Upon caspase inhibition by Z-VAD-fmk (Zvad), caspase-8 is no longer able to cleave and inactivate RIPK1, thereby unleashing necroptosis. Last, Necrostatin-1 (Nec-1s) was used to inhibit RIPK1 activity and abolish both BV6-mediated apoptosis and

caspase-inhibition mediated necroptosis (Ri). We assessed cell death by PI incorporation monitored by Incucyte (preadipocytes) or FACS (adipocytes) as well as by viability as detected by CTG assay (Figure 3.2.1 A).

First, we could detect clear apoptosis induction in both preadipocytes and adipocytes (Figure 3.2.1B and D). In 3T3-L1 preadipocytes, TZ and TBZ robustly triggered necroptosis, which was effectively blocked by the RIPK1 inhibitor (Ri) (Figure 3.2.1B–C). Notably, TZ did not reduce viability in differentiated 3T3-L1 adipocytes (Figure 3.2.1C), while BV6 addition to TZ failed to enhance sensitivity to cell death in these cells. Intriguingly, PI uptake assays revealed that TBZ induced strong necroptosis in mature adipocytes, comparable to preadipocytes levels, while necroptosis in adipocytes progressed with significantly faster kinetics than apoptosis (Figure 3.2.1F 6 vs 24 hs). Western blot analysis further supported these findings, cleaved caspases emerged after 6 hours of treatment, while phospho-RIPK1 and phospho-MLKL (necroptosis markers) were detectable as early as 2 hours (Figure 3.2.1G).

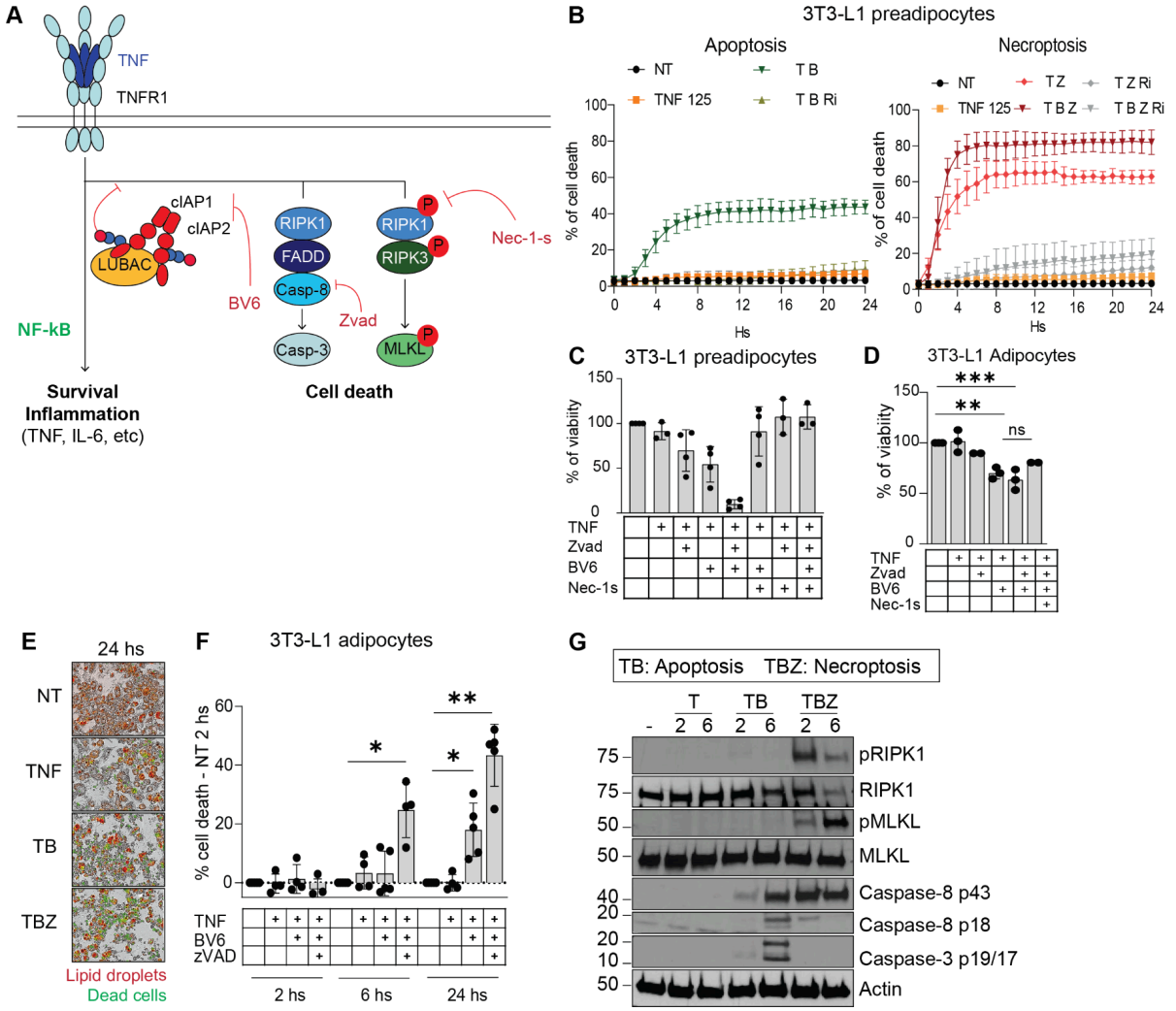

Figure 3.2.1: 3T3-L1 differentiated adipocytes undergo apoptosis and necroptosis in-vitro.

A-Diagram of TNF-induced cell death treatments. B-Percentage of 3T3-L1 preadipocyte cell death after treatment with apoptotic (TNF+BV6) or necroptotic stimuli (TNF+BV6+Zvad) and RIPK1 inhibition by Nec-1s (Ri) measured by Sytoxgreen incorporation in Incucyte, treatments are normalised to time 0 (n=5). C-D- Percentage of viability of 3T3-L1 mouse preadipocytes (n=4) or adipocytes (n=3) after 24 hs. E -Representative pictures of mouse adipocytes after 24 hs of treatment, green: death cells, orange: lipid droplets.F-Percentage of cell death of 3T3-L1 differentiated mouse adipocytes stimuli measured by Flow cytometry. Not treated 2 hs condition was taken as basal level of cell death and removed from each independent experiment (n=4). G-Protein lysates from 3T3-L1 differentiated mouse adipocytes.Statistical analysis: 1-way ANOVA against NT applying Bonferroni correction for multiple comparisons or 2-way ANOVA grouped by diet, with Bonferroni correction for multiple comparisons, p-values GP: (#) p-<0,0001, (***), p-<0,0002;(**) p-<0,0021; (*) p-<0,0332; (ns) p->0,0333.

3.2.2 Implication of loss of linear ubiquitination on human derived adipocytes

TNF is a crucial cytokine in obesity and adipose tissue biology, playing a significant role in regulating adipocyte function and metabolism (Sethi & Hotamisligil, 2021). The LUBAC

complex is a key mediator of TNF signaling, regulating the balance between gene activation and cell death upon TNFR1 engagement. To elucidate the consequences of linear ubiquitination in adipocytes, we depleted HOIP in human preadipocytes and differentiated them in vitro. This approach aimed to evaluate the implications of linear ubiquitination in adipogenesis, NF-κB signaling, and cell death responses.

3.2.2.1 HOIP deletion in human preadipocytes does not interfere with adipogenesis

In a fruitful collaboration with Julia Zinngrebe and Pamela Fisher-Posovszky from Ulm University we generated mutated human derived preadipocytes lacking *HOIP* and differentiated them ex-vivo (Figure 3.2.2.A). Surprisingly, HOIP deletion in adipocytes did not impact HOIL-1 and SHARPIN expression as it was previously reported in other cell types (Figure 3.2.2 B). From the different lines generated from human preadipocytes HOIP1.1.1 was selected since the E3 ligase activity was completely abolished in comparison with HOIP1.1.2, probably due to impartial deletion of HOIP in the latter (Figure 3.2.2.B). As expected HOIP deletion in preadipocytes decreased TNF-induced linear ubiquitination in both KO cell lines (Figure 3.2.2.D). Empty vector (EV) was used as control for all the experiments (Figure 3.2.2).

We further corroborated that the lack of linear ubiquitination does not impair adipocyte differentiation. When cells were cultured with differentiation media, HOIP KO and EV control cells showed comparable lipid content (ORO staining) and expression levels of adipogenic markers assessed by immunoblotting and qPCR (Figure 3.2.2.E-G). While a slight increase in Pparg and Fabp4 expression was observed in HOIP 1.1.1 KO cells at day 7 of differentiation, by day 14, both control and KO groups displayed equivalent adipogenic marker levels and differentiation percentages, suggesting the initial transcriptional variations do not compromise the overall differentiation process (Figure 3.2.2.G).

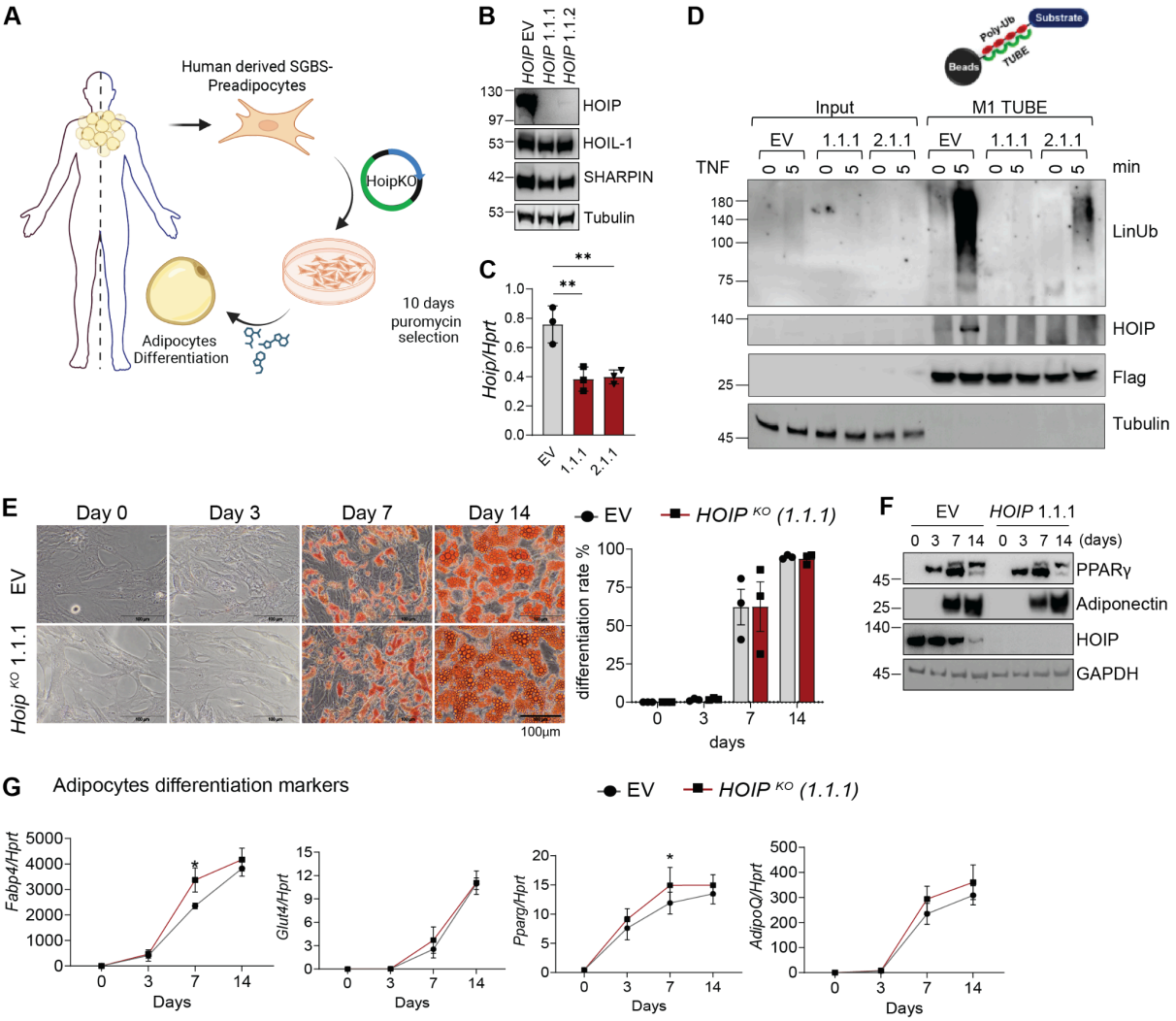

Figure 3.2.2 Hoip deletion in human preadipocytes does not interfere with adipogenesis.

A-Schematic diagram of SGBS cells derived from the stromal vascular fraction of the subcutaneous adipose tissue from a patient with Simpson-Golabi-Behmel syndrome (SGBS) later genetically engineered and differentiated into mature adipocytes. B-Protein lysates from genetically engineered human preadipocytes. C-Rnf31 RNA levels of genetically engineered human preadipocytes normalised to Hprt (n=3). D-M1-TUBE pulldown from genetically engineered human preadipocytes E-Red-oil-staining of human adipocytes at different stages of differentiation and its quantification (n=3). F-Protein lysates from genetically engineered human adipocytes at different stages of differentiation.G- qPCR of adipogenesis markers from human adipocytes at different stages of differentiation (n=3). (EV) empty vector. Statistical analysis: 1-way ANOVA against NT applying Bonferroni correction for multiple comparisons or 2-way ANOVA grouped by diet, with Bonferroni correction for multiple comparisons, p-values GP: (#) p-<0,0001, (***), p-<0,0002;(**) p-<0,0021; (*) p-<0,0332; (ns) p->0,0333.

3.2.2.2 Lack of LinUb impairs NF-κB and sensitizes to TNF-induced cell death in both preadipocytes and adipocytes

There are extensive reports on the role of NF-κB in adipocyte differentiation and its contribution to obesity-induce-inflammation and metabolic syndrome (Griffin, 2022;

Weidemann et al., 2015). Since LUBAC activity does not only prevent cell death upon TNF stimulation, but also allows NF-κB-mediated gene activation, we studied the consequences of LinUb deletion in the NF-κB axis. In EV control *Hoip* expression was upregulated upon TNF stimulation, but no response was observed in Hoip KO 1.1.1 (Figure 3.2.3 A). In addition, impaired NF-κB-mediated gene activation was observed in KO 1.1.1 preadipocytes or adipocytes upon increasing doses of TNF (Figure 3.2.3 B and D). In line, MAPK and NF-κB activation markers were decreased upon loss of HOIP in both pre and differentiated adipocytes (Figure 3.2.3 C and E), in line patient derived cells reports (Oda et al., 2019). Strikingly, despite NF-κB attenuation $Hoip^{A\text{-}KO}$ adipocytes were able to fully differentiate (Figure 3.2.2), suggesting that adipogenesis is independent of canonical NF-κB/MAPK activation in human derived preadipocytes.

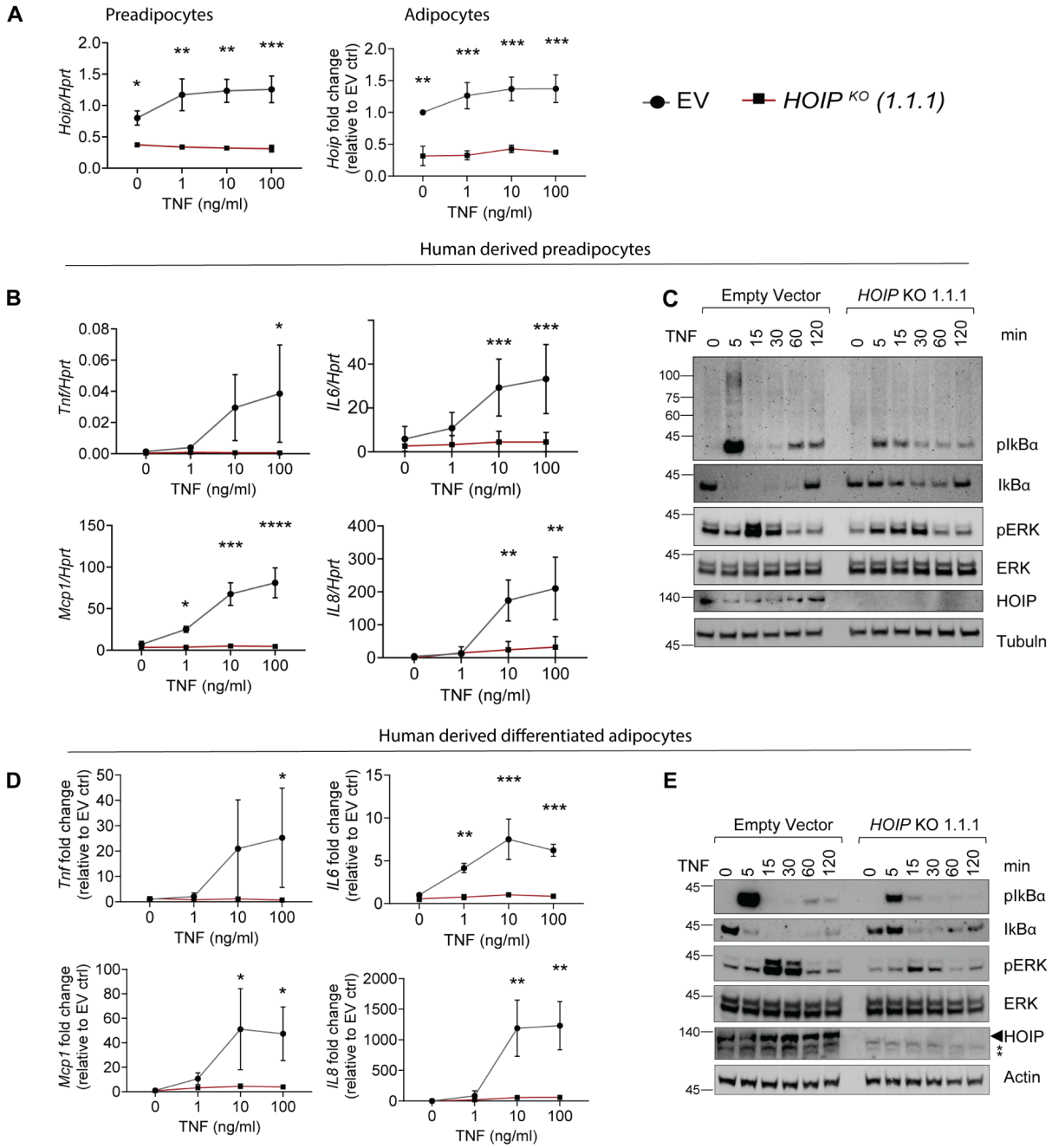

Figure 3.2.3 *Hoip* deletion impairs NF-κB activation in human derived preadipocytes and adipocytes.

A- Rnf31 RNA levels of genetically engineered human preadipocytes and adipocytes in response to TNF normalised to Hprt (n=3). B- NF-κB activation markers measured by qPCR in genetically engineered human preadipocytes after TNF stimulation.C-Protein lysates from genetically engineered human preadipocytes in response to TNF. D- NF-κB activation markers measured by qPCR in genetically engineered human differentiated adipocytes after TNF stimulation.E-Protein lysates from genetically engineered human differentiated adipocytes in response to TNF. Statistical analysis: 1-way ANOVA against NT applying Bonferroni correction for multiple comparisons or 2-way ANOVA grouped by diet, with Bonferroni correction for multiple comparisons, p-values GP: (#) p-<0,0001, (***), p-<0,0002;(**) p-<0,0021; (*) p-<0,0332; (ns) p->0,0333.

HOIP deletion in human cells was not sufficient to induce cell death upon TNF treatment only, which goes in line with previous reports using human fibroblast (Oda et al., 2022). To sensitise cells to TNF induce cell death we inhibited protein translation using cycloheximide (CHX) to prevent the synthesis of short-lived anti apoptotic proteins, or we incubate the cells with cIAP1-2 inhibitor (BV6), a well known TNF-dependent cell death sensitizer (Petersen et al., 2007) that acts upstream linUb regulation (Figure 3.2.1 A). For both treatments we compare cell viability in absence or presence of *HOIP* with increasing doses of TNF. Surprisingly, in absence of HOIP, caspase inhibition (Zvad) partially rescued TNF+CHX cell death execution instead of further sensitizing (Figure 3.2.4 C and D), suggesting a partial dependence on LinUB for necroptosis execution, as previously reported (Weinelt et al., 2024).

As expected, cells lacking LinUb were further sensitised to TNF-induced cell death in a dose dependent manner (Figure 3.2.4 A and C). Interestingly, lack of LinUb also sensitised preadipocytes to TNF-induced cell death in a serum deprivation medium, possibly due to the role of canonical NF-κB pro-survival dependency on proliferative cells (Figure 3.2.4 A) (Luo et al., 2005).

Surprisingly, despite being more sensitive to TNF-induced cell death, *Hoip*^{KO} pre- and mature adipocytes were significantly (even though, not entirely) rescued by caspase inhibition (Figure 3.2.4 B and D, red bars). This suggests a prevalence of caspase dependent pathways in *Hoip*^{KO} cells. This observation goes in line with recent publications that suggest linear chains are a checkpoint for necroptosis regulation downstream of activation of MLKL in human cells (Weinelt et al., 2024).

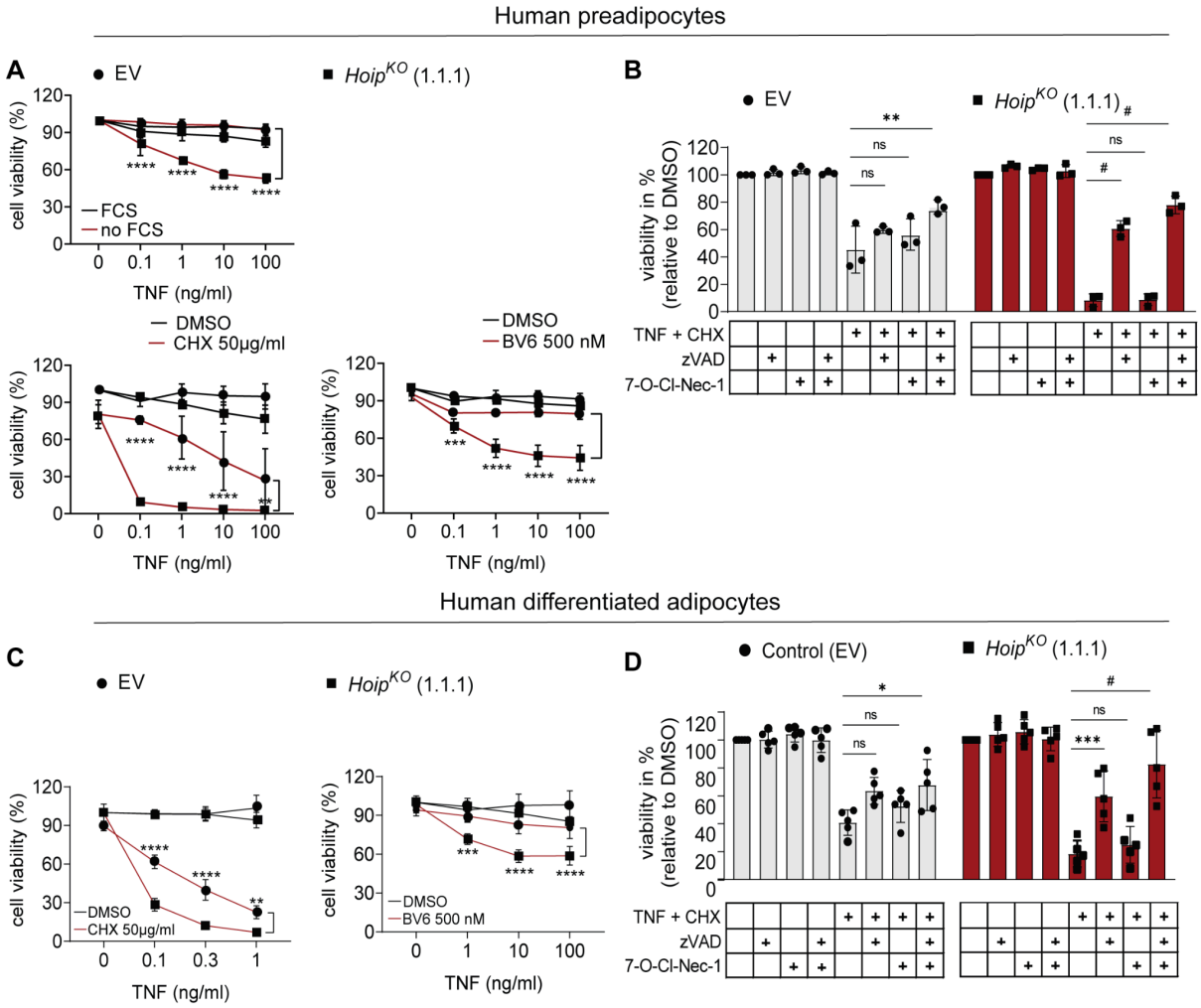

Figure 3.2.4 *Hoip* deletion sensitises human derived preadipocytes and adipocytes to TNF-induced cell death.

A- Percentage of viability of human engineer preadipocytes upon serum deprivation, CHX or BV6 treatment with increasing doses of TNF. B- Percentage of viability of human engineer preadipocytes using 10ng/ml of TNF in combination with CHX, BV6 and 7-O-Cl-Nec-1 after 24 hs.(n=3). C-Percentage of viability of human engineer differentiated adipocytes upon CHX or BV6 treatment with increasing doses of TNF. D- Percentage of viability of human engineer differentiated adipocytes using 10ng/ml of TNF in combination with CHX, BV6 and 7-O-Cl-Nec-1 after 24 hs.(n=3). Statistical analysis: 1-way ANOVA against NT applying Bonferroni correction for multiple comparisons or 2-way ANOVA grouped by diet, with Bonferroni correction for multiple comparisons, p-values GP: (#) p-<0,0001, (***), p-<0,0002;(**) p-<0,0021; (*) p-<0,0332; (ns) p->0,0333.

3.2.3 Summary section 3.2

Our experiments demonstrated that both 3T3-L1 preadipocytes and differentiated adipocytes undergo TNF-induced apoptosis and necroptosis, with mature adipocytes showing a stronger and faster tendency towards necroptosis.

Notably, an interesting discrepancy emerged between our findings in murine adipocytes and human adipocytes. While mouse adipocytes readily undergo necroptosis, human adipocytes viability assays suggest a prevalence of caspase dependent pathways in *Hoip*^{KO} cells. Although this differential sensitivity has been previously observed in LUBAC-deficient patients' cells were largely sensitized to apoptosis with limited propensity to necroptosis (Oda et al., 2022).

Furthermore, our results also revealed that the lack of linear ubiquitination does not interfere with adipogenesis, while instead, it sensitizes both human preadipocytes and adipocytes to TNF-induced cell death and downregulates canonical NF-κB signaling.

3.2.4 Author contribution section 3.2

Dr. Julia Zinngrebe and Prof. Dr. Pamela Fischer-Posovszky from Ulm University Medical Center, Ulm, Germany performed all the experiments in transfected human cells, including differentiated mutant adipocytes. Experiments performed in mouse 3T3 and 3T3 differentiated cells, data analysis, interpretation, visualization and curation were performed by the author of this thesis.

3.3 Linear ubiquitination is fundamental for adipose tissue homeostasis

LUBAC expression in the adipose tissue appears to be important to support metabolic health in obese humans. Since LUBAC results fundamental to prevent aberrant cell death during embryogenesis (Peltzer et al., 2014, 2018), and growing literature highlights the implication of adipocyte cell death during metabolic syndrome (Afonso et al., 2023; Gautheron et al., 2016; Hildebrandt et al., 2022; Karunakaran et al., 2020; Luk et al., 2023; Trujillo et al., 2005), we speculate that linear ubiquitination (LinUb) may protect against metabolic syndrome through a cell death-dependent mechanism. To investigate this hypothesis, we generated mice lacking HOIP, the catalytic component of LUBAC, specifically in mature adipocytes (*Hoip*$^{fl/fl;}$*AdipoqCre*, hereafter called *Hoip*$^{A\text{-}KO}$) (Figure 3.3.1.A). These mice were challenged with HFD to assess the impact of HOIP deficiency on metabolic outcomes during obesity. Additionally, we evaluated the implications of linear ubiquitin chain loss during ageing under unchallenged conditions and characterized sex-specific differences in metabolic homeostasis of *Hoip*$^{A\text{-}KO}$ mice.

Our findings highlight the critical role of linear ubiquitination in maintaining adipocyte homeostasis and preventing cell death-driven inflammation during obesity and ageing.

3.3.1 Linear chains prevent metabolic syndrome during obesity challenge

3.3.1.1 Adipocyte-specific HOIP deficiency causes lipodystrophy and impaired adipose tissue expansion under HFD

Hoip$^{A\text{-}KO}$ mice failed to gain weight under HFD, reaching a plateau at 8 weeks of diet (Figure 3.3.1.B). This was independent of food intake and caloric expenditure (Figure 3.3.1.C-D-E).

The respiratory exchange ratio (RER) is the ratio between the metabolic production of carbon dioxide (CO_2) and the uptake of oxygen (O_2). Since the oxidation of lipids requires higher O_2 consumption than carbohydrates with a quite constant CO_2 production, RER can be used as an indirect measurement to determine the main source of energy in mice. During HFD feeding, metabolism acutely shifts from circadian (alternating carbohydrate and fat usage) to a predominance of fat utilisation (Jais et al., 2016), the higher oxygen consumption for beta-oxidation then translates into a lower RER (Jais et al., 2016; Marvyn et al., 2016). In this study *Hoip*$^{A\text{-}KO}$ mice showed similar RER in HFD fed conditions as compared to their

controls (Figure 3.3.1.E), indicating a normal metabolization of both fatty acids and carbohydrates during light and dark circles. Hence, no exacerbated energy expenditure explains the differences in body weight gain between HFD groups. In contrast, *Hoip*$^{A\text{-}KO}$ CD-fed mice showed a decrease in RER only during light cycles (Figure 3.3.1.D), suggesting a preference for fat use as fuel during dark-cycle.

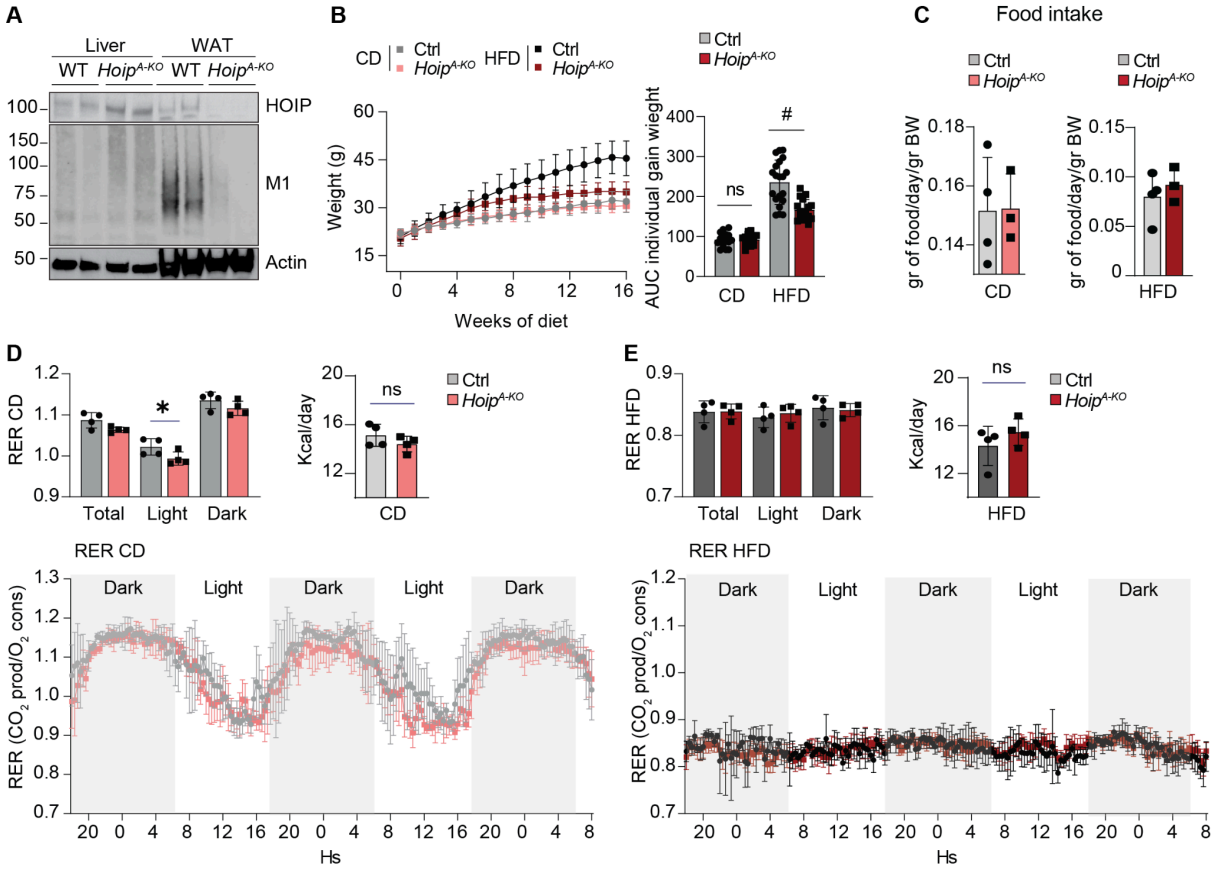

Figure 3.3.1: *Hoip*$^{A\text{-}KO}$ mice fail to gain weight under HFD independently of food intake.

A- Protein lysates of 16 weeks old *Hoip*$^{A\text{-}KO}$ chow diet fed female mice and their littermate controls (n=2). B- Gain weight of *Hoip*$^{A\text{-}KO}$ males and its littermate controls upon CD and HFD (n=10-16). C- Average of 3 days of food intake per mouse, normalised to total body weight measured in phenomaster metabolic cages (n=3-4). D and E- Respiratory exchange ratio (RER) and indirect caloric expenditure of *Hoip*$^{A\text{-}KO}$ males and its littermate controls upon CD and HFD (n=4). Statistical analysis: T-test or 2-way ANOVA grouped by diet applying Bonferroni correction for multiple comparisons. p-values GP: (#) p-<0,0001, (***), p-<0,0002;(**) p-<0,0021; (*) p-<0,0332; (ns) p->0,0333.

Despite less weight gain, the earlier hyperglycemia of *Hoip*$^{A\text{-}KO}$ in both CD and HFD-fed conditions (Figure 3.3.2.A-B), suggested that loss of LinUb could lead to a prediabetic state (*Featured JAX Mice Models of Type 2 Diabetes & Obesity*, n.d.). To further determine the

extent of defects in glucose uptake or insulin action in liver and skeletal muscle, we performed oral glucose tolerance test (oGTT) and insulin tolerance test (ITT) (M. Li et al., 2022) before and after the diabetic onset (8 and 16 weeks). Two different doses of insulin were used between diets, since 0,75 U/kg was causing hypoglycemia in all CD-fed mice interfering with the measurement. HFD-fed *Hoip*$^{A\text{-}KO}$ mice presented a lower response to insulin stimulation from 8 weeks onwards (Figure 3.3.2.C and D), while impaired glucose clearance was only observed after 16 weeks HFD (Figure 3.3.2.E and F). Last, no differences in GTT/ITTwere observed under normal fed conditions at any of the given time points (Figure 3.3.2.C-F), indicating the need of a sustained challenge to develop IR.

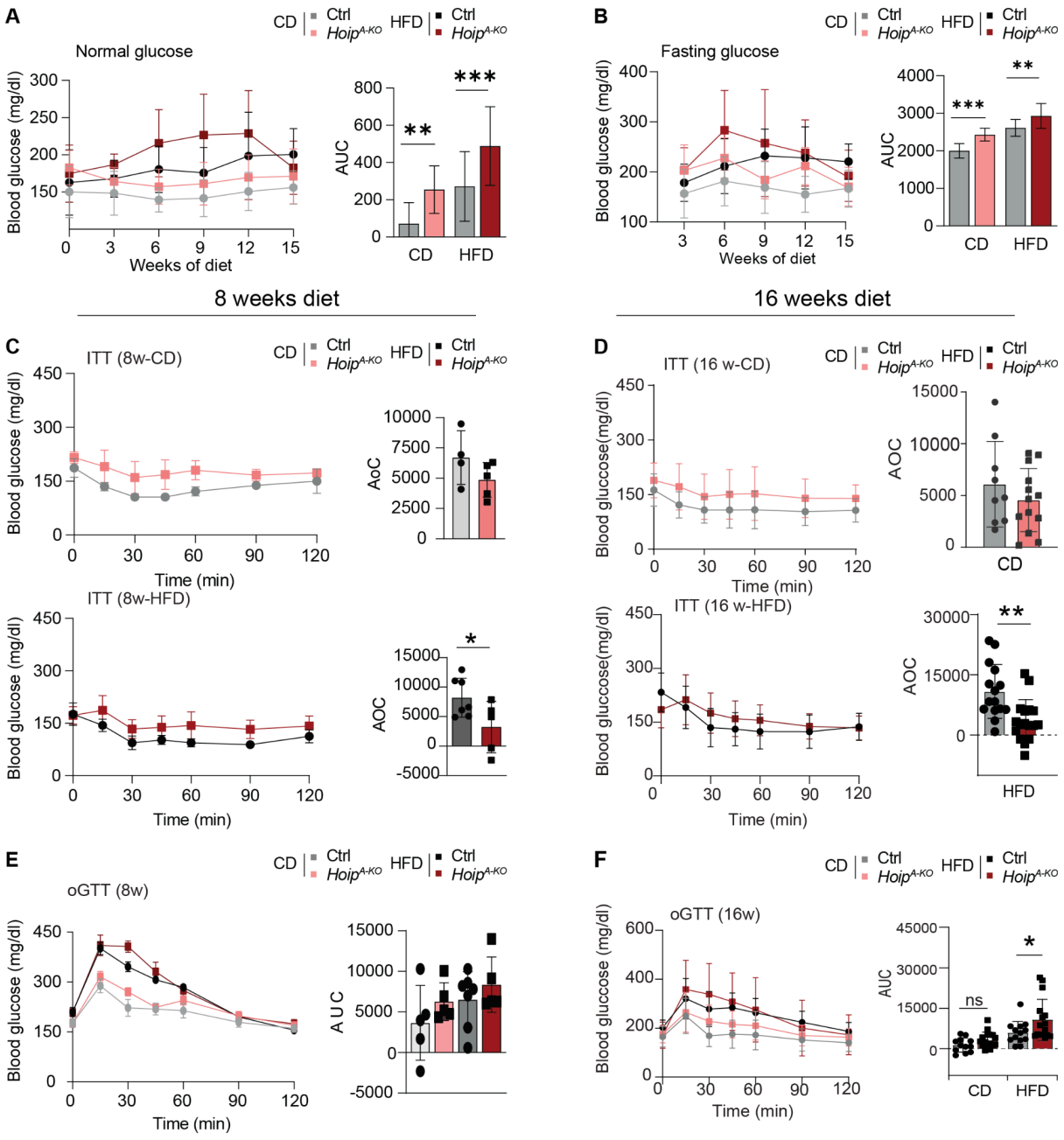

Figure 3.3.2: Insulin and glucose metabolism in *Hoip*$^{A\text{-}KO}$ mice under HFD.

A- Normal fed glucose monitoring during 16 weeks of diet (n=10-12). B- Fasting glucose monitoring during 16 weeks of diet (n=10-12). B- Gain weight of *Hoip*$^{A\text{-}KO}$ males and its littermate controls upon CD and HFD (n=10-16). C- Insulin Tolerance Test of mice after an 8-weeks diet (n= 5-6). D- Insulin Tolerance Test of mice after 16-weeks diet (n= 10-12). D- Oral Glucose Tolerance Test of mice after an 8-weeks diet (n= 5-6). F- Oral Glucose Tolerance Test of mice after 16-weeks diet (n= 10-12). Statistical analysis: T-test or 2-way ANOVA grouped by diet applying Bonferroni correction for multiple comparisons. p-values GP: (#) p-<0,0001, (***), p-<0,0002;(**) p-<0,0021; (*) p-<0,0332; (ns) p->0,0333.

HFD feeding induced an increase in LinUb in the ScWAT of both *Hoip*$^{A\text{-}KO}$and WT controls (Figure 3.3.3.A). As expected, mice lacking HOIP specifically in mature adipocytes display reduced LinUb smearing in the lysates compared to WT controls, confirming impaired LUBAC activity in the targeted cells. Notably, the LinUb signal in *Hoip*$^{A\text{-}KO}$ mice still moderately increased under HFD, suggesting that other cell types in the AT microenvironment could be contributing to LinUb levels in response to diet-induced stress. In addition, *Hoip*$^{A\text{-}KO}$ lysates show a marked reduction in the adipocyte marker perilipin, consistent with adipocyte loss or dysfunction. These findings indicate that HFD triggers an increase in LUBAC-mediated signaling in AT, that HOIP deletion in mature adipocytes leads to a selective depletion of this cell population, and the reduced LinUb activity suggest a necessary contribution of adipocyte-LUBAC-activity during metabolic challenge.

As observed in Figure 3.3.1 HFD-fed *Hoip*$^{A\text{-}KO}$ remained lean, with a clear impairment of adipose tissue expansion already from normal fed conditions (Figure 3.3.3.B). When normalising to total body weight, the gonadal compartment seem to be the most affected AT showing a reduced size in basal CD condition at short age (8 weeks diet e.g. 14-15 weeks of age) (Figure 3.3.3.C), while a longer time point (16 weeks diet e.g. 22-23 weeks of age) of HFD challenge was required to show differences in ScWAT (Figure 3.3.3.C and D).

BAT was unaffected in *Hoip*$^{A\text{-}KO}$ during HFD (Figure 3.3.3.C and D). Concomitantly with the loss of WAT, we observed significantly enlarged liver, heart and spleen in *Hoip*$^{A\text{-}KO}$ upon 16 weeks of HFD (Figure 3.3.3.D). Curiously, hepatomegaly was also observed under CD in a shorter stage (8 weeks), while splenomegaly can be detected at 16 weeks under the same condition (Figure 3.3.3.C and D).

.

.

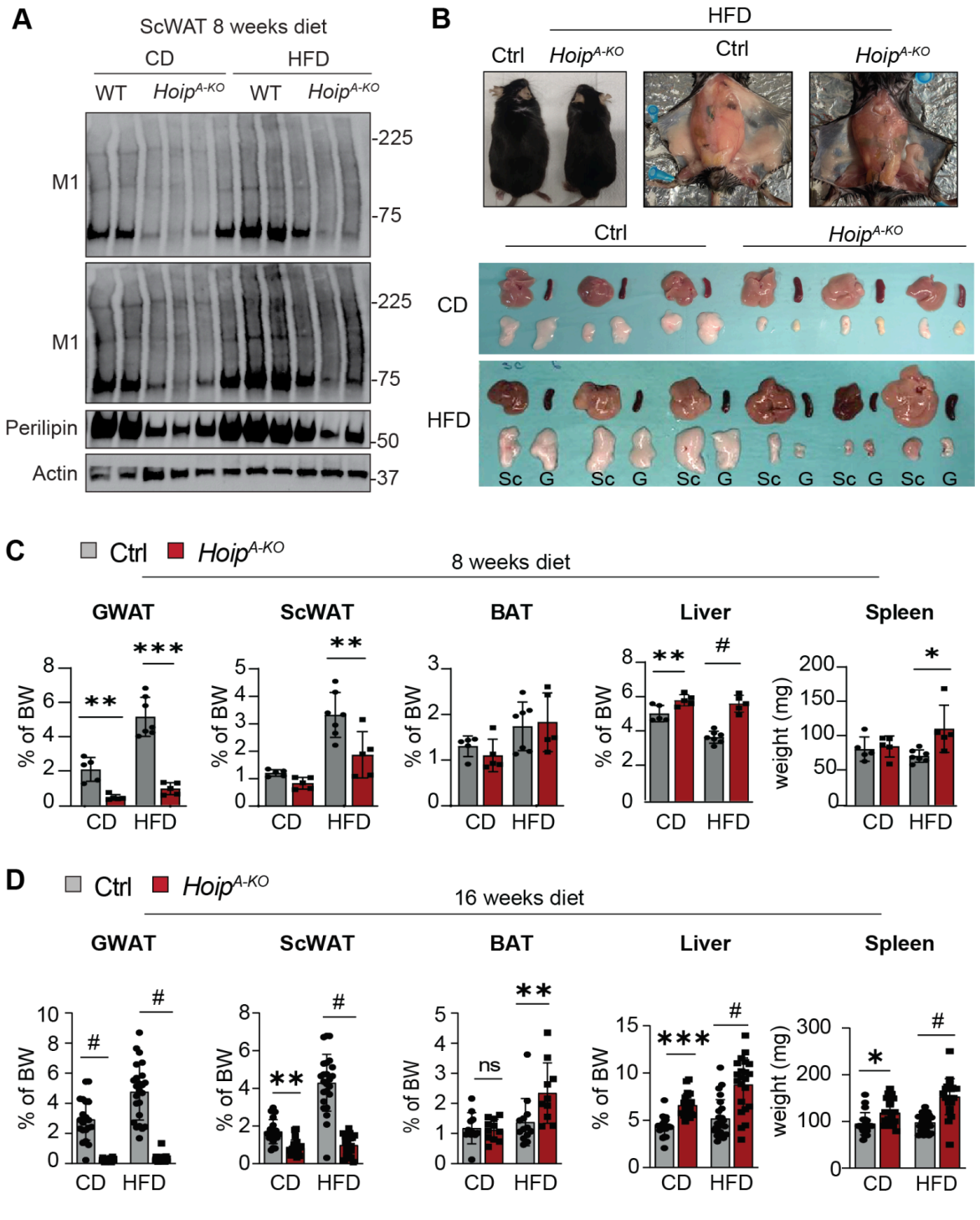
A
ScWAT 8 weeks diet
CD
HFD
WT
Hoip^A-KO
WT
Hoip^A-KO
M1
-225
-75
M1
-225
-75
Perilipin
-50
Actin
-37
B
HFD
Ctrl
Hoip^A-KO
Ctrl
Hoip^A-KO
Ctrl
Hoip^A-KO
CD
HFD
Sc G Sc G Sc G Sc G Sc G Sc G
C
Ctrl
Hoip^A-KO
8 weeks diet
GWAT
ScWAT
BAT
Liver
Spleen
% of BW
weight (mg)
CD HFD
D
Ctrl
Hoip^A-KO
16 weeks diet
GWAT
ScWAT
BAT
Liver
Spleen
% of BW
weight (mg)
CD HFD

Figure 3.3.3 Tissue weights in *Hoip*$^{A\text{-}KO}$ mice under HFD.

A- Protein lysates of ScWAT of male mice after 8 weeks of diet (n=3). B- Representative pictures of male mice after 16 weeks of diet. C- Tissue weights normalised to total body weight (except spleen) after 8 weeks of diet. (n= 5-6). F- Tissue weights normalised to total body weight (except spleen) after 16 weeks of diet (n= 10-16). Statistical analysis: 2-way ANOVA grouped by diet applying Bonferroni correction for multiple comparisons. p-values GP: (#) p-<0,0001, (***), p-<0,0002;(**) p-<0,0021; (*) p-<0,0332; (ns) p->0,0333.

To explore more in detail how loss of HOIP resulted in metabolic dysfunction, a pathohistological assessment of the different AT compartments was performed.

Histological assessment revealed that after 16 weeks of HFD, the impairment of WAT expansion was accompanied by structural abnormalities with increased cell infiltration, high degree of heterogeneity in the size of adipocytes and a decrease in total number of adipocytes (Figure 3.3.4.A-C). *Hoip*$^{A\text{-}KO}$ mice displayed both hypertrophic and small adipocytes in both ScWAT and GWAT, which points to a high degree of tissue remodelling, potentially due to dying adipocytes(Figure 3.3.4.A-C). Brown adipocytes were also hypertrophic, and whitening of the BAT can be observed in the H&E in *Hoip*$^{A\text{-}KO}$ mice, while there is a complete depletion of the dermal adipose tissue layer in the skin (Figure 3.3.4.A). All of these changes in *Hoip*$^{A\text{-}KO}$ mice were observed independently of the diet, but exacerbated by it.

Next, we examined other issues that could be indirectly affected by loss of HOIP in adipocytes. *Hoip*$^{A\text{-}KO}$ mice suffered from islet hyperplasia in pancreas in line with increased insulin in blood and increase in the diabetic marker HbA1c and with the onset of IR (Figure 3.3.4.A, D and E). Whilst no differences in dyslipidemia were observed in comparison to their littermate controls, besides an earlier increase in blood triglycerides at 8 weeks of HFD (Figure 3.3.4.F).

Last, serum adipokine levels were also highly affected by HOIP deletion (Figure 3.3.4.G). *Hoip*$^{A\text{-}KO}$ mice fail to induce serum leptin levels upon obesity as well as adiponectin levels. In the case of the latter, this effect was independent of the diet since mice lack serum adiponectin in both CD and HFD conditions, possibly explaining the already mentioned exacerbated diabetic onset (Rabe et al., 2008). Surprisingly, despite presenting a lipodystrophy-like phenotype with aberrant AT architecture, FFA levels in blood remain similar to controls (Figure 3.3.4.H).

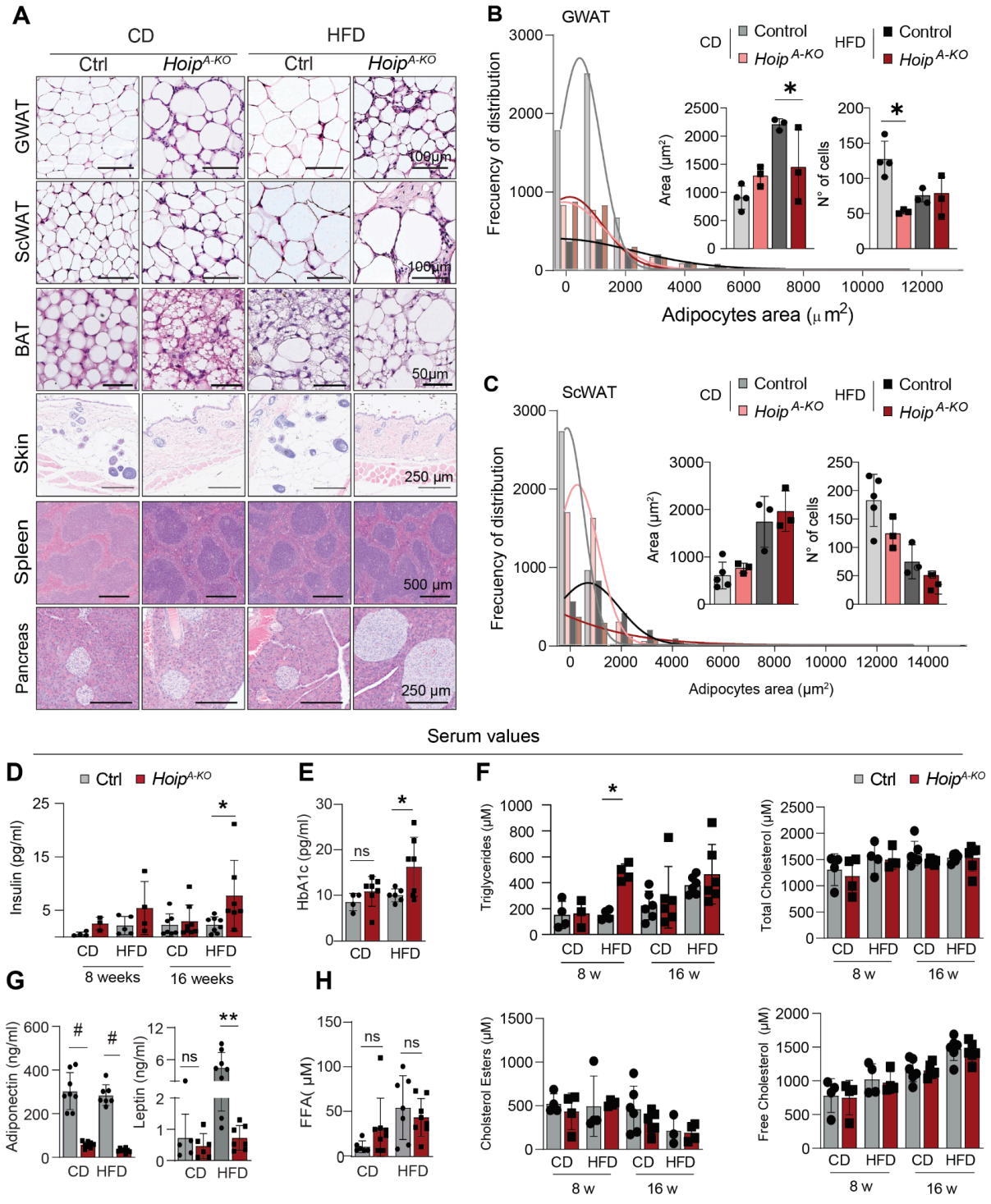

Figure 3.3.4: HOIP in adipocytes prevents lipodystrophy-associated metabolic dysfunction.

A- Representative pictures H&E staining of male mice after 16 weeks of diet . B- Adipocyte cumulative distribution of GWAT after 16 weeks of diet (n=3). C- Adipocyte cumulative distribution of ScWAT after 16 weeks of diet (n=3). D- Serum levels of insulin (n=5-8). E- Blood levels of the diabetic marker HbA1c after 16 weeks of diet (n=4-8). F- Blood serum levels of Triglycerides and Cholesterol (n=5-6). G- Adipokines serum concentration after 16 weeks of diet (n=5-8). H- Free Fatty Acids in blood after 16 weeks of diet (n=5-8). Statistical analysis: T-test for simple comparisons or 2-way ANOVA grouped by diet applying Bonferroni correction for multiple comparisons. p-values GP: (#) p-<0,0001, (***), p-<0,0002;(**) p-<0,0021; (*) p-<0,0332; (ns) p->0,0333

3.3.1.2 Adipocyte death and inflammation increase in adipose tissue in the absence of HOIP.

Being GWAT the main tissue affected by the deletion of HOIP in adipocytes, we selected sections of this tissue to further characterise the lipodystrophy-like syndrome. First we studied cell death responses by TUNEL staining in mice lacking HOIP under CD (Figure 3.3.5 A and B). Yet, surprisingly, there were no differences in TUNEL staining between genotypes under HFD-fed conditions. This is likely due to the fact that, under HFD, adipocytes are depleted and no remaining positive signal can be detected.

To evaluate immune cell infiltration we performed immunohistochemistry of CD45 for total immune cells (Figure 3.3.5 A and C). This staining revealed massive immune cell infiltration in the absence of HOIP, and, not surprisingly, the majority of these cells were F4/80 positive macrophages (Figure 3.3.5 A and D), forming CLS (Figure 3.3.5 A and E). CLS structures are composed mostly of M1-like macrophages, evidenced by a depletion of resident M2-like macrophages (Lindhorst et al., 2021). These structures are associated with adipose tissue inflammation and metabolic dysfunction (Yao et al., 2022). In the absence of HOIP we observed a complete depletion of CD163 (M2-like), independently of the diet (Figure 5 B and E), suggesting a polarisation towards M1 profile due to excessive adipocyte death.

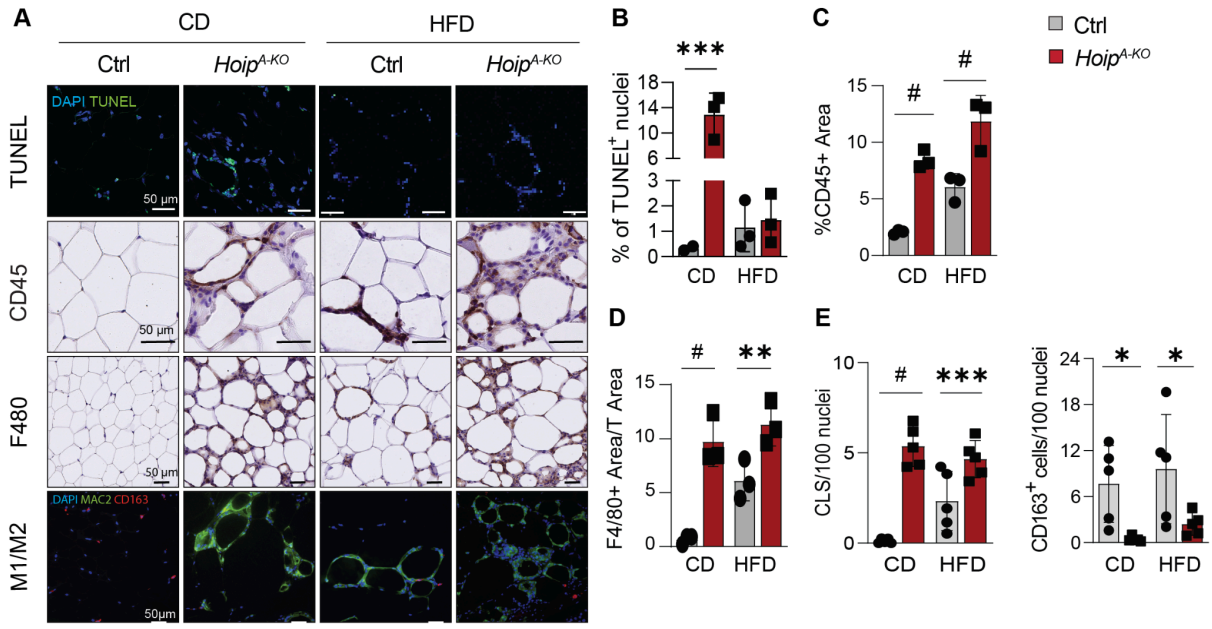

Figure 3.3.5: Loss of HOIP in adipocytes increases cell death and immune infiltration.

A- Representative pictures of TUNEL, CD45, F480 and Mac2/CD163 standings of male mice after 16 weeks of diet. B- Percentage of TUNEL+ nuclei (n=3). C- CD45 positive area normalised to total area (n=3). D- F4/80 positive area normalised to total area (n=3) E- Crow like structures and CD163 positive nuclei normalised to 100 nuclei (n=3) Statistical analysis2-way ANOVA grouped by diet applying Bonferroni correction for multiple comparisons. p-values GP: (#) p-<0,0001, (***), p-<0,0002;(**) p-<0,0021; (*) p-<0,0332; (ns) p->0,0333

To explore the nature of the metabolic dysfunction observed in *Hoip*$^{A\text{-}KO}$ mice, we performed bulk RNA sequencing (RNA-seq) of GWAT derived from *Hoip*$^{A\text{-}KO}$ mice, or littermate controls, after 16 weeks of CD or HFD. First we performed a cell type deconvolution analysis using established gene expression profiles. The analysis further revealed complete loss of adipocytes in *Hoip*$^{A\text{-}KO}$ GWAT (Figure 3.3.6 A) and a clear increase of immune cells recruitment corroborating our previous histologic observations. Moreover, among the immune cell populations, macrophages were the main immune cells found to be abundant in *Hoip*$^{A\text{-}KO}$ GWAT (Figure 3.3.6 A) . Strikingly, loss of adipocytes and increased macrophage infiltration were equally observed in both CD and HFD (Figure 3.3.6 A). Since inflammatory macrophages are associated with metabolic syndrome, we corroborated the observation of our staining using differential expression analysis (DEA). Interestingly we found that HOIP loss during CD activated inflammatory macrophages as HFD alone in littermate control (TNF, CD11c, CD36 and CCL2 receptor), with exception of ILβ which was exacerbated upon increase of adipocyte cell death rate (Figure 3.3.6 B). Unexpectedly, iNOS levels seem to decrease in *Hoip*$^{A\text{-}KO}$ mice (Figure 3.3.6 B).

Next, we tested whether local inflammatory response was translated into systemic inflammation in response to HFD and/or loss of HOIP. Surprisingly, we found only a slight overall induction of inflammatory cytokines in the serum of *Hoip*$^{A\text{-}KO}$ mice fed with both CD and HFD for 16 weeks (Figure 3.3.6 B). From the group of tested cytokines only G-CSF and IL-12 p70 were significantly elevated upon loss of HOIP under CD, which goes in line with the accumulation of M1-like macrophages in GWAT (Figure 3.3.6 B and C). To our surprise, there was no striking systemic inflammation induced by HOIP deficiency even during the HFD challenge. This indicates an active macrophage recruitment form dyeing cells, which despite polarising their phenotype to M1-like, do not contribute to inflammatory cytokine release in serum.

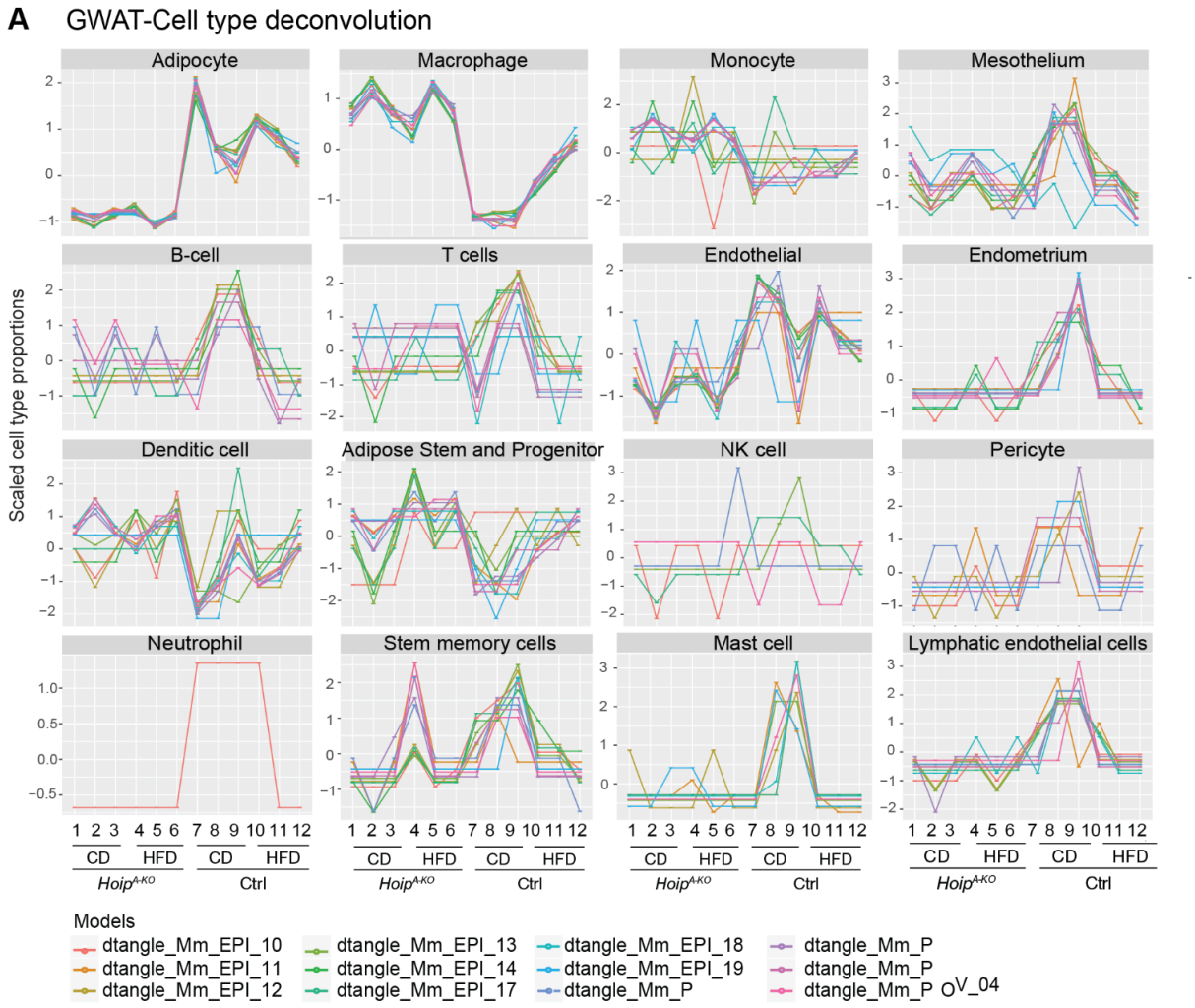
A
GWAT-Cell type deconvolution
Scaled cell type proportions
Adipocyte
Macrophage
Monocyte
Mesothelium
B-cell
T cells
Endothelial
Endometrium
Denditic cell
Adipose Stem and Progenitor
NK cell
Pericyte
Neutrophil
Stem memory cells
Mast cell
Lymphatic endothelial cells
1 2 3 4 5 6 7 8 9 10 11 12
CD HFD CD HFD
Hoip^A-KO Ctrl
Models
dtangle_Mm_EPI_10
dtangle_Mm_EPI_11
dtangle_Mm_EPI_12
dtangle_Mm_EPI_13
dtangle_Mm_EPI_14
dtangle_Mm_EPI_17
dtangle_Mm_EPI_18
dtangle_Mm_EPI_19
dtangle_Mm_P
dtangle_Mm_P
dtangle_Mm_P
dtangle_Mm_P OV_04

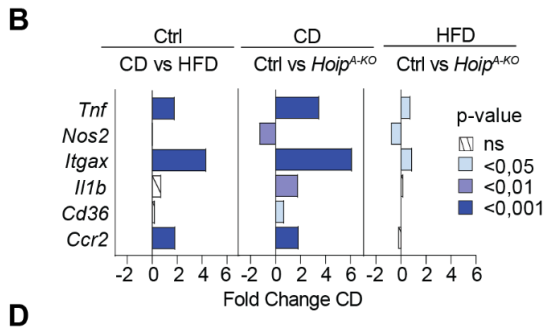
B
Ctrl
CD
HFD
CD vs HFD
Ctrl vs Hoip^A-KO
Ctrl vs Hoip^A-KO
Tnf
Nos2
Itgax
Il1b
Cd36
Ccr2
p-value
ns
<0,05
<0,01
<0,001
-2 0 2 4 6
Fold Change CD

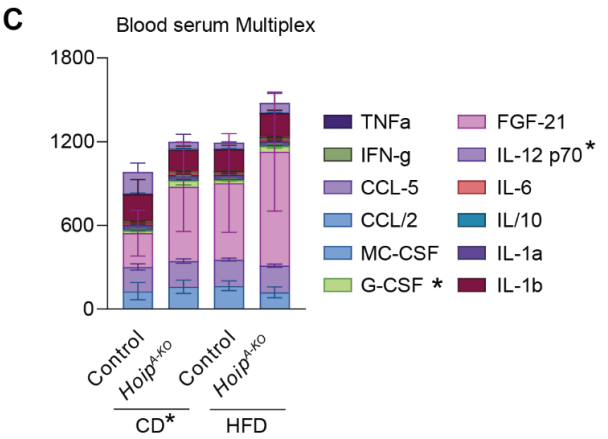
C
Blood serum Multiplex
1800
1200
600
0
TNFa
IFN-g
CCL-5
CCL/2
MC-CSF
G-CSF *
FGF-21
IL-12 p70*
IL-6
IL/10
IL-1a
IL-1b
Control
Hoip^A-KO
Control
Hoip^A-KO
CD*
HFD

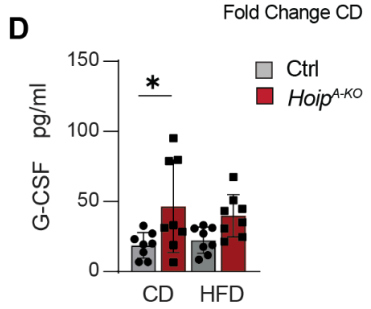
D
G-CSF pg/ml
150
100
50
0
*
Ctrl
Hoip^A-KO
CD
HFD

Figure 3.3.6 Loss of HOIP in adipose tissue increases macrophages recruitment and gene signature.

A- Cell type deconvolution using RNAseq data from GWAT of 16 week diet mice (n=3). B-DEA from bulk RNAseq from GWAT. C-Serum cytokine multiplex analysed by multiplex after 16 weeks of diet (n=5-8) D- G-CSF serum levels analysed by multiplex after 16 weeks of diet. Statistical analysis2-way ANOVA grouped by diet applying Bonferroni correction for multiple comparisons. p-values GP: (#) p-<0,0001, (***), p-<0,0002;(**) p-<0,0021; (*) p-<0,0332; (ns) p->0,0333.

Continuing with the RNAseq analysis, we found that the expression of over 3000 genes was either down- or upregulated in GWAT of *Hoip*$^{A\text{-}KO}$ mice, regardless of the diet. Gene Ontology (GO) enrichment analysis for biological processes (BP) of negatively regulated genes in *Hoip*$^{A\text{-}KO}$ GWAT pointed towards defects in metabolic pathways (Figure 3.3.7). This analysis also revealed a clear loss of genes associated with fatty acid biosynthesis, thermoregulation, response to insulin and cellular respiration (Figure 3.3.7 A). Biological processes that were upregulated in *Hoip*$^{A\text{-}KO}$ GWAT were mainly related to cell death, inflammation and extracellular matrix remodelling, with genes associated to cytokine production, immune responses and cell death proper, drastically upregulated (Figure 3.3.7 A-E). Curiously, all of these changes were irrespective of the administered diet but seem to be further detected in CD-fed mice, suggesting a partial gene signature overlapping between the loss of Hoip and the obesity challenge (Figure 3.3.7).

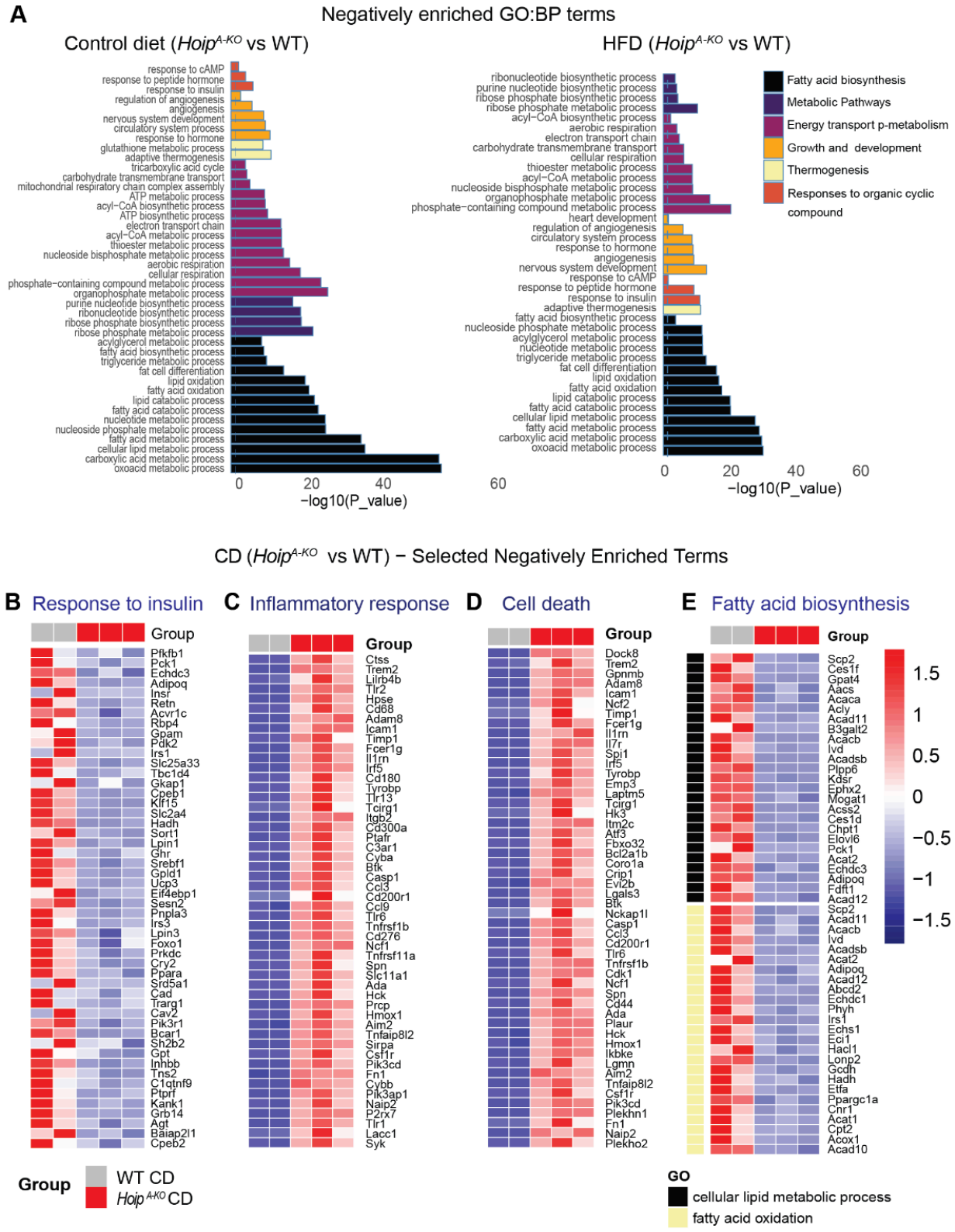
A
Negatively enriched GO:BP terms
Control diet (Hoip A-KO vs WT)
HFD (Hoip A-KO vs WT)
response to cAMP
response to peptide hormone
response to insulin
regulation of angiogenesis
angiogenesis
nervous system development
circulatory system process
response to hormone
glutathione metabolic process
adaptive thermogenesis
tricarboxylic acid cycle
carbohydrate transmembrane transport
mitochondrial respiratory chain complex assembly
ATP metabolic process
acyl−CoA biosynthetic process
ATP biosynthetic process
electron transport chain
acyl−CoA metabolic process
thioester metabolic process
nucleoside bisphosphate metabolic process
aerobic respiration
cellular respiration
phosphate−containing compound metabolic process
organophosphate metabolic process
purine nucleotide biosynthetic process
ribonucleotide biosynthetic process
ribose phosphate biosynthetic process
ribose phosphate metabolic process
acylglycerol metabolic process
fatty acid biosynthetic process
triglyceride metabolic process
fat cell differentiation
lipid oxidation
fatty acid oxidation
lipid catabolic process
fatty acid catabolic process
nucleotide metabolic process
nucleoside phosphate metabolic process
fatty acid metabolic process
cellular lipid metabolic process
carboxylic acid metabolic process
oxoacid metabolic process
0
20
40
60
−log10(P_value)
ribonucleotide biosynthetic process
purine nucleotide biosynthetic process
ribose phosphate biosynthetic process
ribose phosphate metabolic process
acyl−CoA biosynthetic process
aerobic respiration
electron transport chain
carbohydrate transmembrane transport
cellular respiration
thioester metabolic process
acyl−CoA metabolic process
nucleoside bisphosphate metabolic process
organophosphate metabolic process
phosphate−containing compound metabolic process
heart development
regulation of angiogenesis
circulatory system process
response to hormone
angiogenesis
nervous system development
response to cAMP
response to peptide hormone
response to insulin
adaptive thermogenesis
fatty acid biosynthetic process
nucleoside phosphate metabolic process
acylglycerol metabolic process
nucleotide metabolic process
triglyceride metabolic process
fat cell differentiation
lipid oxidation
fatty acid oxidation
lipid catabolic process
fatty acid catabolic process
cellular lipid metabolic process
fatty acid metabolic process
carboxylic acid metabolic process
oxoacid metabolic process
0
20
40
60
−log10(P_value)
Fatty acid biosynthesis
Metabolic Pathways
Energy transport p-metabolism
Growth and development
Thermogenesis
Responses to organic cyclic compound
CD (Hoip A-KO vs WT) − Selected Negatively Enriched Terms
B Response to insulin
Group
Pfkfb1
Pck1
Echdc3
Adipoq
Insr
Retn
Acvr1c
Rbp4
Gpam
Pdk2
Irs1
Slc25a33
Tbc1d4
Gkap1
Cpeb1
Klf15
Slc2a4
Hadh
Sort1
Lpin1
Ghr
Srebf1
Gpld1
Ucp3
Eif4ebp1
Sesn2
Pnpla3
Irs3
Lpin3
Foxo1
Prkdc
Cry2
Ppara
Srd5a1
Cad
Trarg1
Cav2
Pik3r1
Bcar1
Sh2b2
Gpt
Inhbb
Tns2
C1qtnf9
Ptprf
Kank1
Grb14
Agt
Baiap2l1
Cpeb2
C Inflammatory response
Group
Ctss
Trem2
Lilrb4b
Tlr2
Hpse
Cd68
Adam8
Icam1
Timp1
Fcer1g
Il1rn
Irf5
Cd180
Tyrobp
Tlr13
Tcirg1
Itgb2
Cd300a
Ptafr
C3ar1
Cyba
Btk
Casp1
Ccl3
Cd200r1
Ccl9
Tlr6
Tnfrsf1b
Cd276
Ncf1
Tnfrsf11a
Spn
Slc11a1
Ada
Hck
Prcp
Hmox1
Aim2
Tnfaip8l2
Sirpa
Csf1r
Pik3cd
Fn1
Cybb
Pik3ap1
Naip2
P2rx7
Tlr1
Lacc1
Syk
D Cell death
Group
Dock8
Trem2
Gpnmb
Adam8
Icam1
Ncf2
Timp1
Fcer1g
Il1rn
Il7r
Spi1
Irf5
Tyrobp
Emp3
Laptm5
Tcirg1
Hk3
Itm2c
Atf3
Fbxo32
Bcl2a1b
Coro1a
Crip1
Evl2b
Lgals3
Btk
Nckap1l
Casp1
Ccl3
Cd200r1
Tlr6
Tnfrsf1b
Cdk1
Ncf1
Spn
Cd44
Ada
Plaur
Hck
Hmox1
Ikbke
Lgmn
Aim2
Tnfaip8l2
Csf1r
Pik3cd
Plekhn1
Fn1
Naip2
Plekho2
E Fatty acid biosynthesis
Group
Scp2
Ces1f
Gpat4
Aacs
Acaca
Acly
Acad11
B3galt2
Acacb
Ivd
Acadsb
Plpp6
Kdsr
Ephx2
Mogat1
Acss2
Ces1d
Chpt1
Elovl6
Pck1
Acat2
Echdc3
Adipoq
Fdft1
Acad12
Scp2
Acad11
Acacb
Ivd
Acadsb
Acat2
Adipoq
Acad12
Abcd2
Echdc1
Phyh
Irs1
Echs1
Eci1
Hacl1
Lonp2
Gcdh
Hadh
Etfa
Ppargc1a
Cnr1
Acat1
Cpt2
Acox1
Acad10
1.5
1
0.5
0
−0.5
−1
−1.5
Group
WT CD
Hoip A-KO CD
GO
cellular lipid metabolic process
fatty acid oxidation

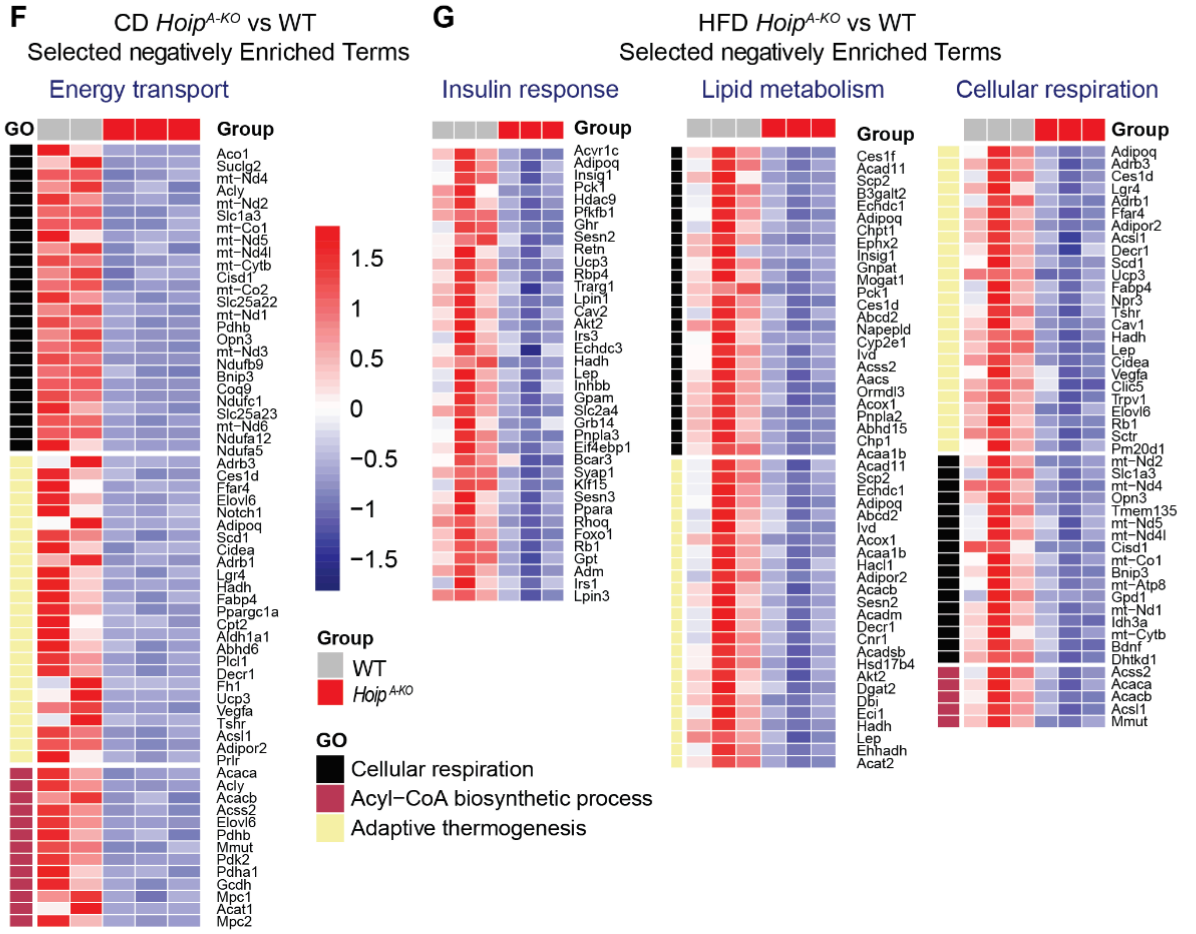

Figure 3.3.3.7: Hoip deletion in adipocytes increases inflammatory and cell death gene expression.

Bulk RNAseq analysis of GWAT. For Hoip$^{A\text{-}KO}$ GWAT of 3 mice pooled for RNA extraction, controls were treated the same way for consistency. One of the CD Hoip$^{A\text{-}KO}$ was excluded from the analysis due to technical reasons (n = 2 or 3 pools of 3 mice). A-Negatively enriched GO terms genes CD Hoip$^{A\text{-}KO}$ vs WT, HFD Hoip$^{A\text{-}KO}$ vs wt. Heatmaps of selected pathways from Negatively enriched genes CD (Hoip$^{A\text{-}KO}$ vs WT)B-Insulin response, C-Inflammatory response, D-Cell death, E- Fatty acids biosynthesis. F- Energy transport. G- HFD (Hoip$^{A\text{-}KO}$ vs WT) for Insulin response , lipid metabolism and cellular respiration.

From the positively enriched GO assessment we can observe that both CD and HFD conditions present an upregulation of a similar pattern in cell death, cytokine production and immune responses (Figure 3.3.8 A-D). However these differences are again more striking in the CD group, specially for immune response (Figure 3.3.8.A and B). This data suggest an obesity-like transcriptional profile in *Hoip$^{A\text{-}KO}$* mice already from basal condition.

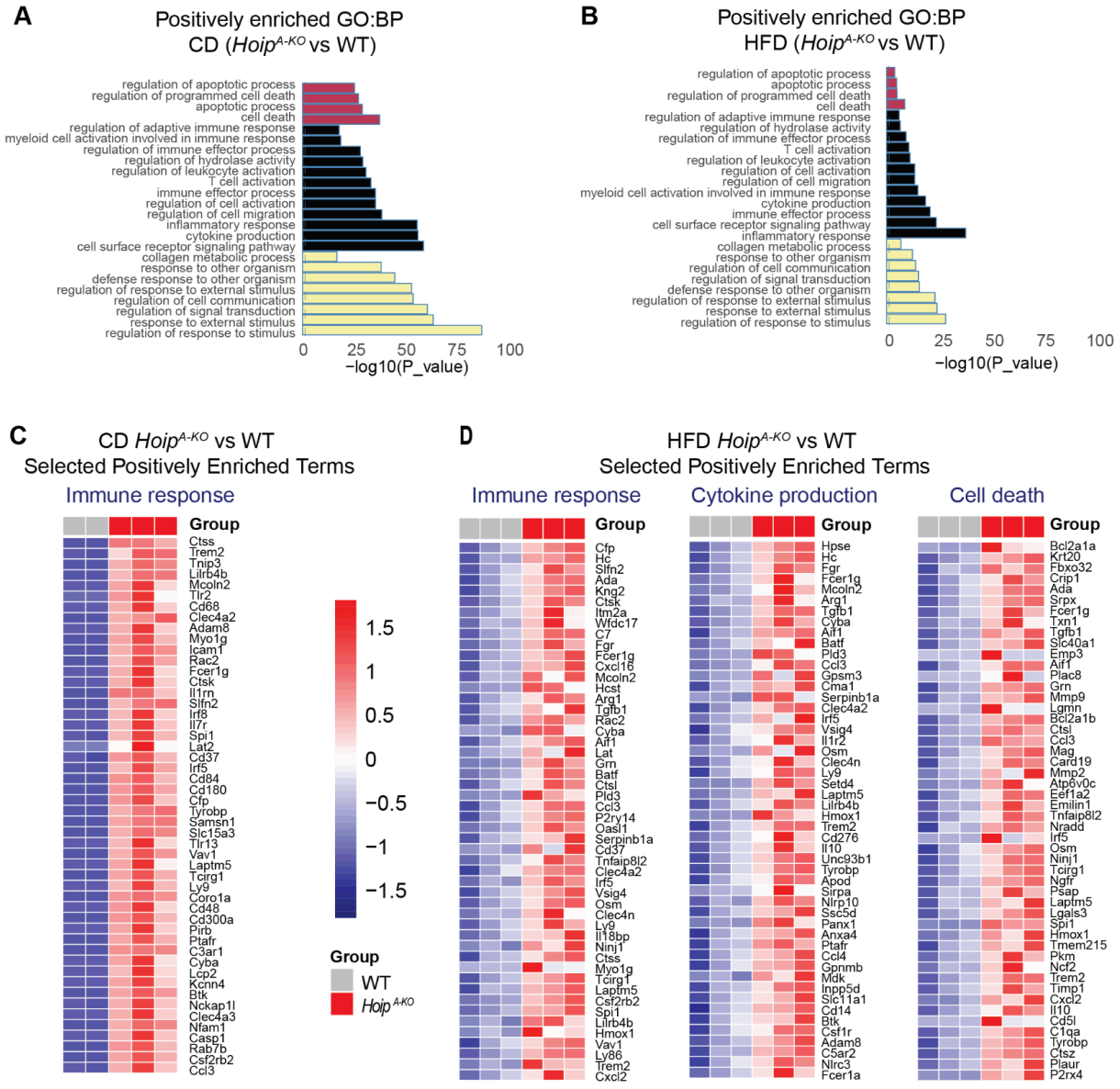

Figure 3.3.8 Hoip deletion in adipocytes increases cell death in inflammation.

Bulk RNAseq analysis of GWAT. For *Hoip*$^{A\text{-}KO}$ GWAT of 3 mice needing to *be pooled for RNA extraction, controls were treated the same way for consistency. One of the CD Hoip*$^{A\text{-}KO}$ pools was excluded from the analysis (n = 2 or 3 pools of 3 mice). Positively enriched GO terms genes of A-CD (*Hoip*$^{A\text{-}KO}$ vs WT), B-HFD (*Hoip*$^{A\text{-}KO}$ vs WT). Heatmaps of selected pathways from Positively enriched GO terms genes of CA-Immune response, CD (*Hoip*$^{A\text{-}KO}$ vs WT). D-HFD (*Hoip*$^{A\text{-}KO}$ vs WT), Immune response, Cytokine production and Cell death.

As an internal control, to evaluate which was the response only to the diet we also compared which signatures were enriched or decreased in the wt littermate controls upon obesity challenge. Surprisingly results go in line with our observation, showing similar pathways than the *Hoip*$^{A\text{-}KO}$ during control diet. This supports the hypothesis of an overlapping gene signature between the metabolic stress of the challenge and the lack of linear chains in adipocytes (Figure 3.3.7 3.3.8 and 3.3.9).

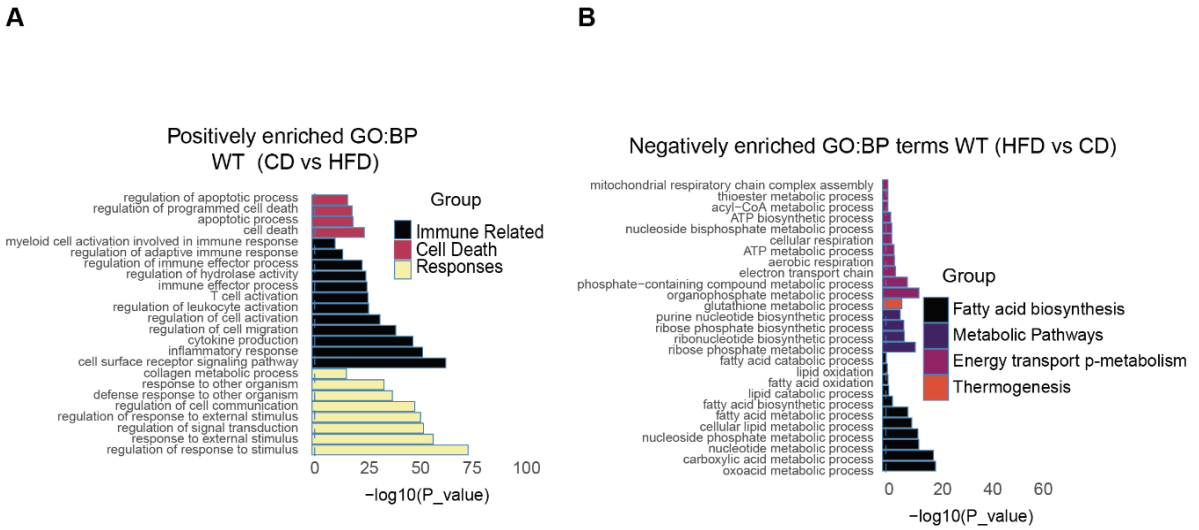

Figure 3.3.9 Obesity challenge increases cell death and immune response gene expression while reducing thermogenesis.

Bulk RNAseq analysis of GWAT (n=3 pools of 3 mice). A- Positively enriched GO terms genes of WT mice under HFD. B-Negatively enriched GO terms genes of WT mice under HFD.

Given these observations, using the data obtained in our volcano plots (Figure 3.3.10 A and B), we performed a correlation plot (Figure 3.3.10 C) comparing the gene signature of the most significant up-regulated and down-regulated genes in (I) CD *Hoip*$^{A\text{-}KO}$ vs WT (green) and (II) WT HFD vs CD (blue). In the next step, we selected only the genes that were significant only in both comparisons and overlapped them. The analysis shows a strong positive correlation between CD *Hoip*$^{A\text{-}KO}$ and WT HFD, illustrating the gene signatures perfectly aligned in a diagonal (red). This encouraged us to hypothesise that HOIP deficiency could spontaneously cause a state of obesity-related metabolic dysfunction in the absence of a HFD-feeding. Hence, we studied the phenotype of *Hoip*$^{A\text{-}KO}$ mice during ageing under normal chow diet (NCD). Results on this study can be found in section 3.3.4.

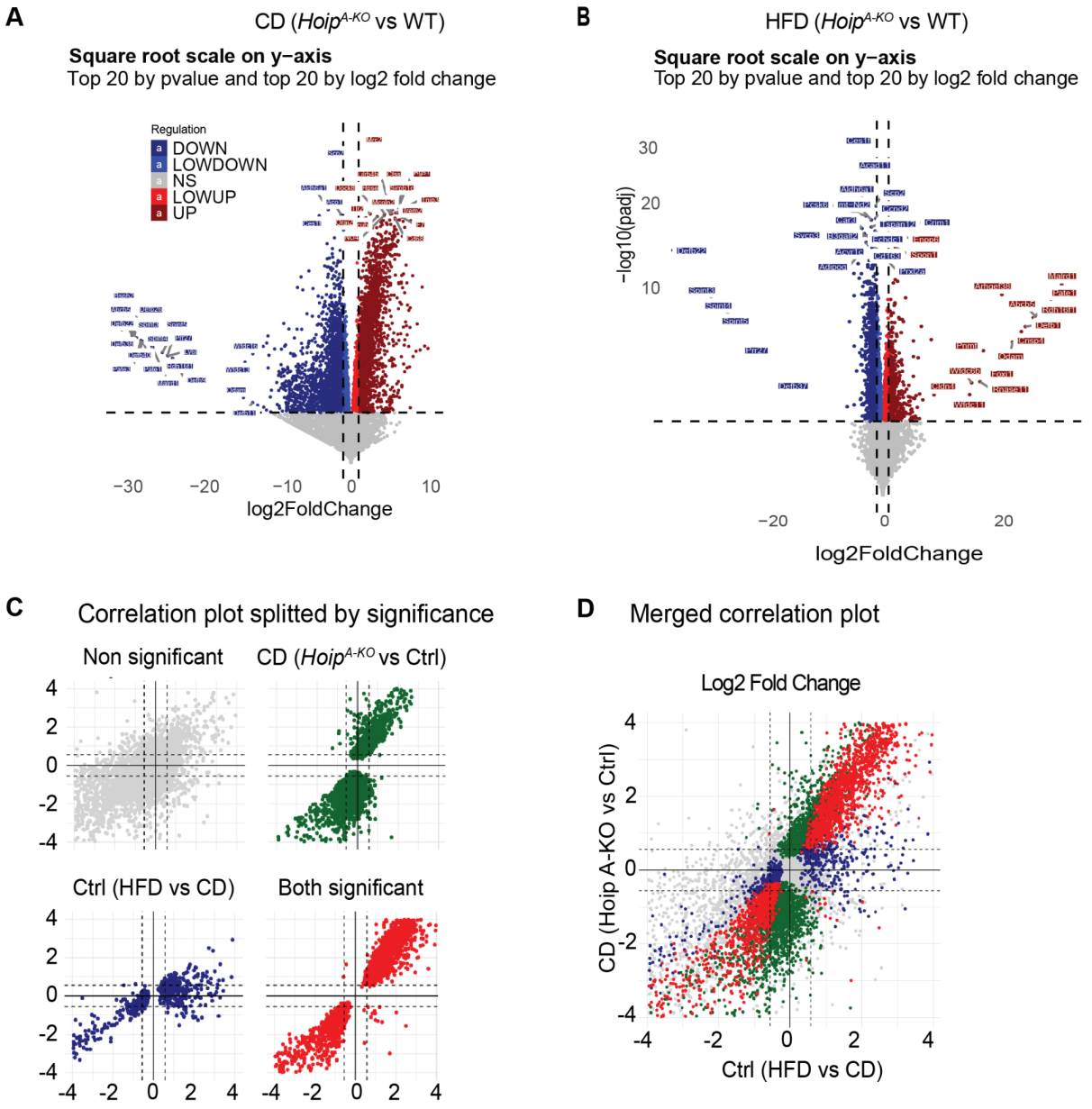

Figure 3.3.10 Hoip deletion in adipocytes mimics obese gene signature

Bulk RNAseq analysis of GWAT. For *Hoip*$^{A\text{-}KO}$ GWAT of 3 mice needing to be pooled for RNA extraction, controls were treated the same way for consistency. One CD *Hoip*$^{A\text{-}KO}$ pool was excluded from the analysis (n = 2 or 3 pools of 3 mice). Volcano plots of the most significant upregulated and downregulated genes A-CD (*Hoip*$^{A\text{-}KO}$ vs WT), B-HFD *(Hoip*$^{A\text{-}KO}$ vs WT). C-Correlation plots from RNAseq of mice after 16 weeks of diet; significant genes for the following comparison are indicated in colour: green CD (*Hoip*$^{A\text{-}KO}$ vs WT); blue WT (CD vs HFD); red both CD (*Hoip*$^{A\text{-}KO}$ vs WT) and WT (CD vs HFD).

3.3.1.3 Lack of linear chains in adipose tissue sensitises mice to MASLD during obesity challenge

To further understand the metabolic consequences of the loss of linUb in adipocytes, we evaluated the effect of this mutation in distant tissues.

Starting with the BAT already from basal condition we can observe a disruption of the BAT architecture with increased signs of inflammation. In response to the diet , there is a massive whitening of the central región of the tissue with the presence of enlarged and hypertrophic white adipocytes. This is known to occur during HFD as observed in the wt littermate control and is clearly exacerbated by the loss of LinUb. (Figure 3.3.11.A)

In the hepatic evaluation, *Hoip*$^{A\text{-}KO}$ mice displayed massive steatosis both under CD and HFD feeding for 16 weeks (Figure 3.3.11 B-C), with an increased total cholesterol accumulation already from basal conditions (Figure 3.3.11 D), Yet, only after 16 weeks of HFD, this was translated into increased liver damage enzymes (Figure 3.3.11 E). Last, there were no obvious differences in small intestine or colon inflammation due to the mutation (Figure 3.3.11 F-H).

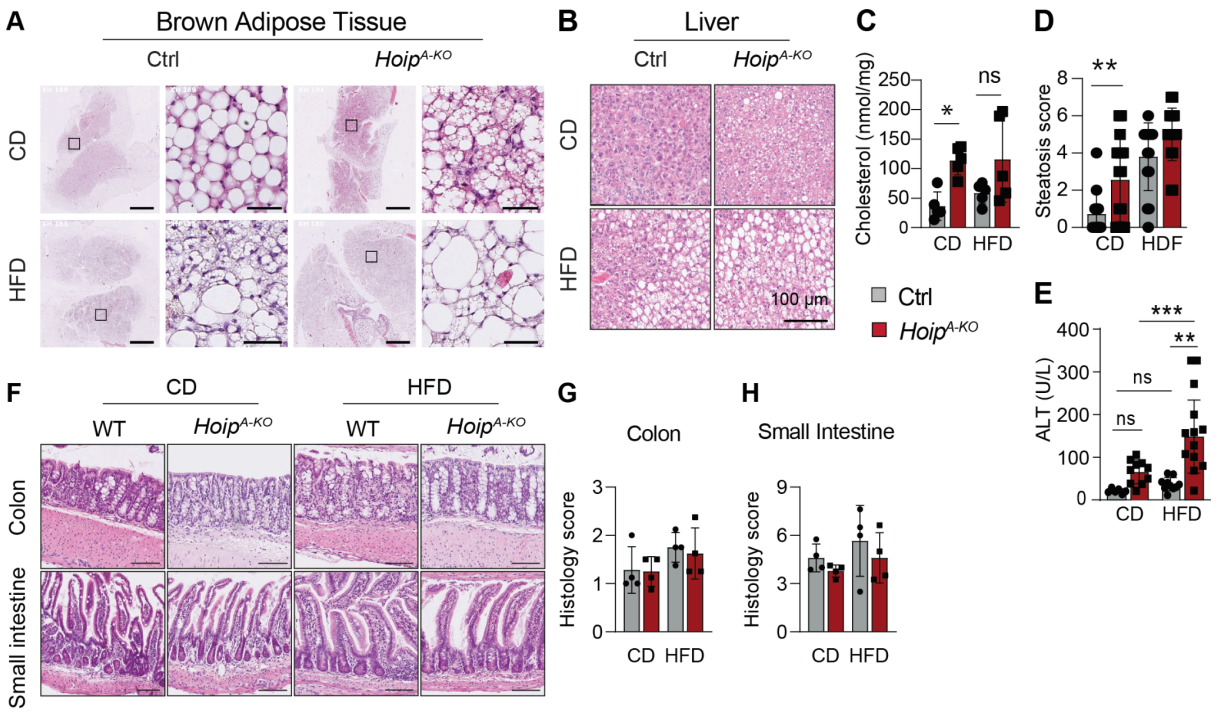

Figure 3.3.11: Loss of HOIP in adipose tissue affects distant tissues

A- Representative H&E pictures of brown adipose tissue after 16 weeks of diet. B Representative H&E pictures of liver after 16 weeks of diet. C- Total liver cholesterols levels after 16 weeks of diet (n=5). D- Steatosis score of liver after 16 weeks of diet (n=8-10). E- ALT serum levels after 16 weeks of diet. F- Representative H&E pictures of small intestine and colon after 16 weeks of diet. Histological score assessment of G-Colon and H- Small intestine (average of jejunum, ileum and duodenum. Statistical analysis: 2-way ANOVA grouped by diet applying Bonferroni correction for multiple comparisons. p-values GP: (#) p-<0,0001, (***), p-<0,0002;(**) p-<0,0021; (*) p-<0,0332; (ns) p->0,0333

In MASLD, initial lipid accumulation is generally benign, as inert lipid species such as triglycerides and cholesterol esters predominate. Under normal conditions, the liver takes up lipids from circulation (including FFAs released from WAT) and, together with fatty acids derived from de novo lipogenesis (using carbohydrates), synthesizes triglycerides and other complex lipids. In contrast, steatohepatitis is characterized by elevated levels of free cholesterol, diacylglycerols, and/or ceramides. The excessive accumulation of these lipids can trigger inflammatory cascades and promote insulin resistance in hepatocytes.

Based on observations of hepatic steatosis and significant increases in liver cholesterol during carbohydrate-enriched diets (CD), and considering the role of adipose tissue–liver crosstalk in MASLD, mediated by fatty acids and endocrine factors (Heeren & Scheja, 2021), we performed lipidomic analysis to assess the metabolic consequences of lipodystrophy in our mutant mouse model.

We observed significantly elevated levels of triglycerides (TAG), Diacylgliceroids (DAG) and cholesterol esters (CE) in *Hoip*$^{A\text{-}KO}$ mice (Figure 3.3.12 A, C and D). On the other hand, the Triglycerides and Cholesterol lipidic signatures differ from the littermate controls (independently of the diet), being short chain saturated (SFA) (14:0, 16:0 and 18:0) or monounsaturated fatty acids (MUFAs) (16:1 and 18:1) the most prominent among the mutants (Figure 3.3.12 A and E), at exception of cholesterols where also longer chains (20:0, 20:1, 20:2) are clearly observed (Figure 3.3.12 E and F).

During HFD there is a marked increase on TAGs and DAGs (Figure 3.3.12 A, B, C and D), specially on 16:0, 18:0, 18:1 and 18:2 which are the most abundant fatty acids in the dietary composition (See methods section 4.2 Diet composition). So the increase of this type of fatty acid can be explained by direct absorption from the diet. However in the Z-scores triglycerides and cholesterols (that compare the abundance of each lipidic species separately)(Figure 3.3.12 B and F), we can observed that HFD fed *Hoip*$^{A\text{-}KO}$ also present an increase in long chains unsaturated (20:0), MUFAs (20:1) and polyunsaturated (20:2, 20:3) fatty acids (PUFAs), which in the context of a dystrophic AT, suggest that the liver of *Hoip*$^{A\text{-}KO}$

mice are able to elongate and desaturate fatty acid chains, but these species are being actively accumulated in hepatic tissue.

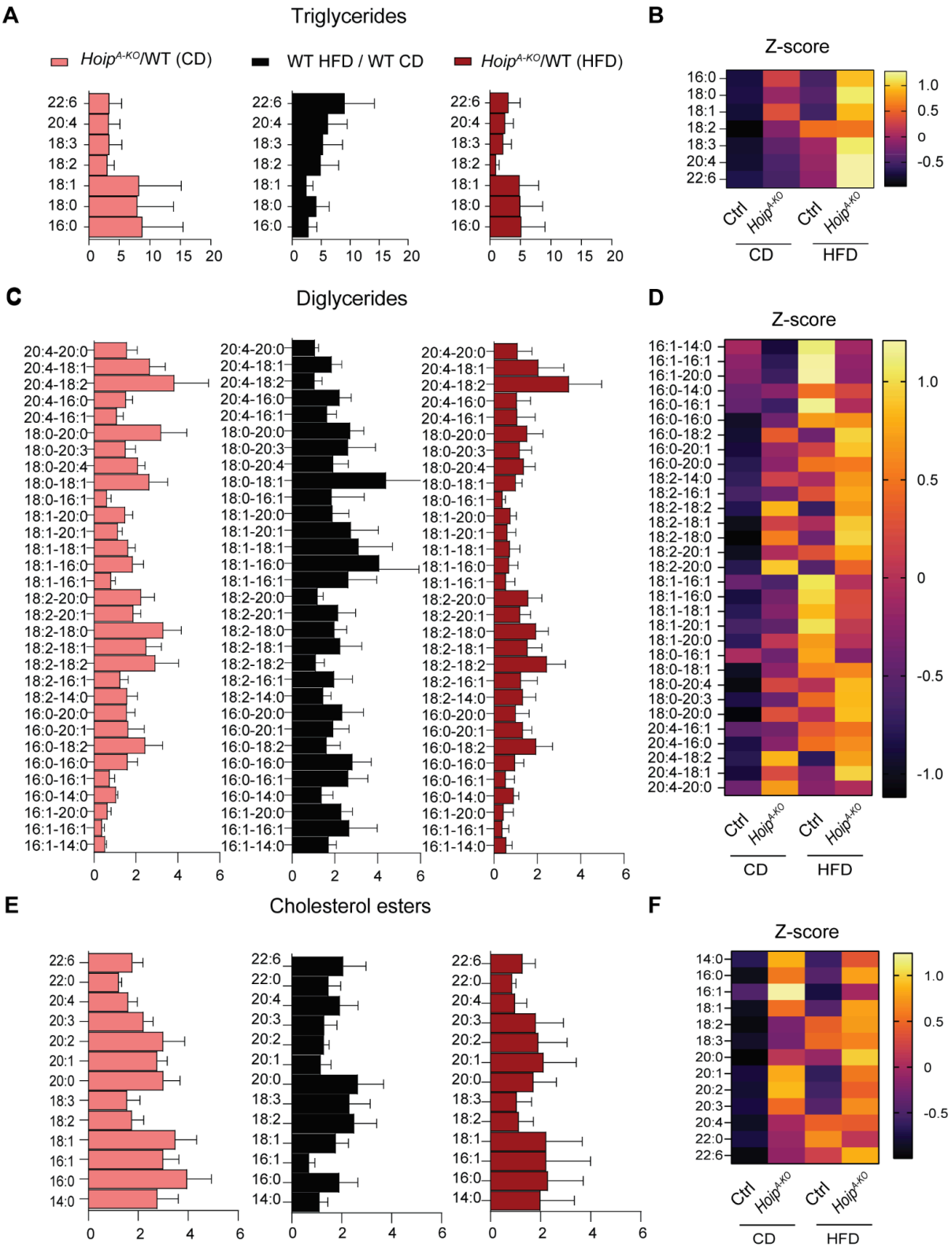

Figure 3.3.12: Loss of *Hoip*$^{A\text{-}KO}$ in adipose tissue affects liver lipid profile

Lipidomics analysis of liver after 16 weeks of diet (n=5) A- Fold change of Tryglicerides normalized to WT CD or HFD as indicated. B-Z-score of Tryglicerides normalized to mean of each lipid species. C-Fold change of Diglicerides normalized to WT CD or HFD as indicated. D-Z-score of Diglicerides normalized to mean of each lipid species. E- Fold change of Cholesterols esters normalized to WT CD or HFD as indicated. F-Z-score of Cholesterols esters normalized to mean of each lipid species. Statistical analysis: T-test for simple comparisons or 2-way ANOVA grouped by diet applying Bonferroni correction for multiple comparisons. p-values GP: (#) p-<0,0001, (***), p-<0,0002;(**) p-<0,0021; (*) p-<0,0332; (ns) p->0,0333

Steatosis during lipodystrophies is likely to occur. This ís due to two key mechanisms that are likely to be altered (1) excessive lipid flux from AT with impaired synthesis, with release of free fatty acids (FFAs) and intermediate lipids, increasing fatty acid chains in the liver; (2) a disrupted AT endocrine function that impairs lipid export mechanisms and leads to its accumulation within hepatocytes. Of note, there are no indications of increased FFA circulation or dyslipidemia in mutant mice to explain the accumulation (Figure 3.3.5). Which led us to investigate if lipogenesis was exacerbated in mutant mice.

qPCR analysis revealed no differences in de novo lipogenesis (DNL) between mutants and controls (Figure 3.3.13 and Table 3.3.1). However, regarding glycolysis genes (Table 3.3.1) Gck expression was elevated in *Hoip*$^{A\text{-}KO}$ mice on a CD, likely suggesting increased hepatic glucose phosphorylation activity to regulate hyperglycemia (Han et al., 2016) (Figure 3.3.2 A, B). GCK is critical for hepatic glucose metabolism and is upregulated by insulin (Peter et al., 2011)), so the observed Gck increase may result from a conserved, yet active insulin signaling during CD. In contrast, *Hoip*$^{A\text{-}KO}$ mice on HFD (despite systemic hyperglycemia and hyperinsulinemia) exhibited significantly reduced Gck levels, consistent with their pronounced insulin resistance (Figure 3.3.2 D, 3.3.5 A, D). Moreover, significant amounts of fatty acids can also amplify Gck activity in the liver, while long chain acyl CoA inhibits this process. Thus, this decline of Gck activity in HFD-fed mutant mice could also be exacerbated by the inhibitory effect of accumulated long-chain lipids (Figure 3.3.13 A). Thus, Gck regulation in *Hoip*$^{A\text{-}KO}$ mice seems to be influenced by both insulin signaling and hepatic lipid content in a diet dependent manner.

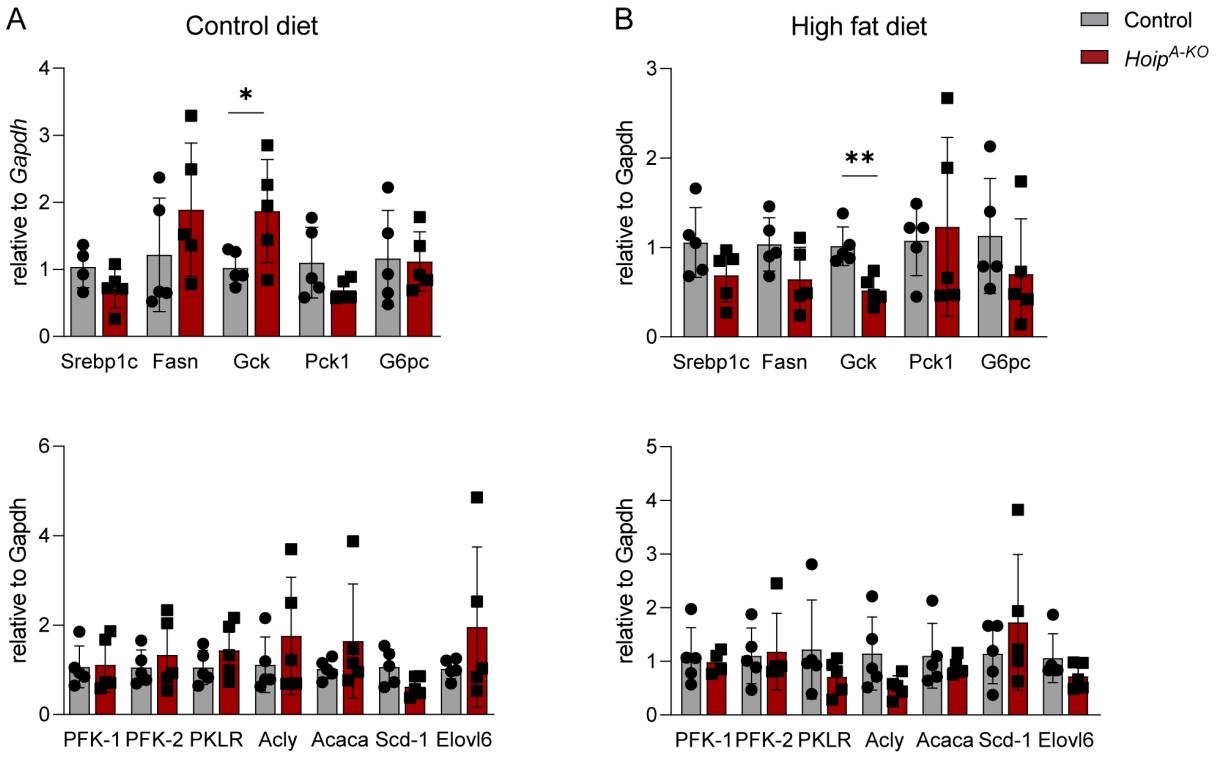

Figure 3.3.13 Gluconeogenesis and lipogenesis remain unadulterated in liver of mutant mice

qPCR levels from RNA extraction of liver of male mice after 16 weeks of diet normalised to GAPDH (ddCT). A-CD. B-HFD. Genes names and functions can be found in Table 3.3.1. (n=5). Statistical analysis. Múltiple T-test for simple comparisons of each gene. p-values GP: (#) p-<0,0001, (***), p-<0,0002;(**) p-<0,0021; (*) p-<0,0332; (ns) p->0,333.

Main process	gene ID	Name and abreviation	Function in liver
Glycolysis	103988	Glucokinase (Gck)	Catalyzes the phosphorylation of glucose to glucose 6-phosphate (G6P), essential for glucose metabolism
	18641	Phosphofructokinase-1 (PFK-1)	Key regulatory steps of glycolysis. Regulate glycolysis through allosteric inhibition,
	18640	Fructose-2,6-biphosphatase 2 (PFK-2)	Indirect regulator of glycolysis/gluconeogenesis rates
	18770	Liver pyruvate kinase (PKLR)	Provides carbon sources for FA and TAG synthesis, produces pyruvate kinase.
	14377	Glucose-6-phosphatase (G6pc)	Key enzyme in gluconeogenesis and glycogenolysis.
	18534	Phosphoenolpyruvate Carboxykinase 1 (pck1)	Limits gluconeogenesis
FA synthesis pathway	104112	ATP-citrate lyase (Acly)	Involved in acetyl-CoA biosynthetic process and carboxylic acid metabolic process
	107476	Acetyl-CoA carboxylase (Acaca)	Involved in acetyl-CoA metabolic process (fatty acid biosynthetic process; and protein homotetramerization)
	14104	Fatty acid synthase (Fasn)	Catalyze the synthesis of palmitate from acetyl-CoA and malonyl-CoA, in the presence of NADPH, into long-chain saturated fatty acids.
	20249	Stearoyl-CoA desaturase (SCD-1)	Acts in brown/ white fat cell differentiation;intervenes in monounsaturated fatty acid biosynthetic process
	170439	ELOVL fatty acid elongase 6 (Elovl6)	Catalyzes the first and rate-limiting reaction the long-chain fatty acids elongation cycle
	20787	Sterol regulatory element binding transcription factor 1 (Srebp1c)	Transcription factor that regulates genes of de novo lipogenesis and glycolysis

Table 3.3.1 Glycolysis and Fatty acid synthesis genes abbreviation, names and functions determined by qPCR in the liver of male mice after 16 weeks of diet

Taken together, our findings demonstrate that *Hoip*$^{A\text{-}KO}$ mice, despite lacking elevated plasma lipids or increased de novo lipogenesis, accumulate a wide spectrum of complex lipid species in the liver, regardless of diet. This suggests that disruption of AT–liver communication impairs hepatic lipid export, leading to progressive lipid retention within hepatocytes. Under a CD, this manifests as benign steatosis, which may predispose mice to IR; by contrast, a HFD exacerbates hepatic lipid influx, resulting in inflammation, hepatocellular injury (Figure 3.3.11), and overt IR (Figure 3.3.2). These observations indicate that defective AT signaling disrupts hepatic lipid handling independently of dietary fat, ultimately predisposing *Hoip*$^{A\text{-}KO}$ mice to metabolic dysfunction.

Notably, even though these mice remain lean on a HFD, impaired increase in cell death in adipose tissue drives MASLD, and metabolic decompensation resembling diabetic features. These findings are consistent with clinical observations in obese human subjects, providing robust evidence that LUBAC signaling is essential for protecting against metabolic dysfunction in the context of dietary challenge.

3.3.1.4 Caspase-8-mediated cell death is responsible for spontaneous Hoip-dependent lipodystrophy in males and females.

Given the implication of linUb in preventing cell death downstream TNFR1, we hypothesised that caspase deletion in adipocytes could partially rescue the lipodystrophy syndrome of *Hoip*$^{A\text{-}KO}$ mice, preventing apoptosis execution. For this reason we deleted Caspase 8 in adipose tissue together with HOIP (*Hoip*$^{A\text{-}KO}$*;Casp8*$^{A\text{-}KO}$) and evaluated these mice under unchallenged conditions.

We found no differences in weight gain between mutant groups and their wt littermates controls in both females or males at 12 weeks of age (Figure 3.3.14 A and B). Regarding glucose homeostasis, single Casp8 deletion in adipocytes led to a decrease in glycemia in both sexes, in line with previous reports (Figure 3.3.14 C and D) while *Hoip*$^{A\text{-}KO}$*;Casp8*$^{A\text{-}KO}$ mice presented similar glucose levels in compare to WT littermate controls. In addition, there were no differences in insulin (Figure 3.3.15 A and B) or glucose sensitivity (Figure 3.3.15 C and D) in either of the genders at the same age.

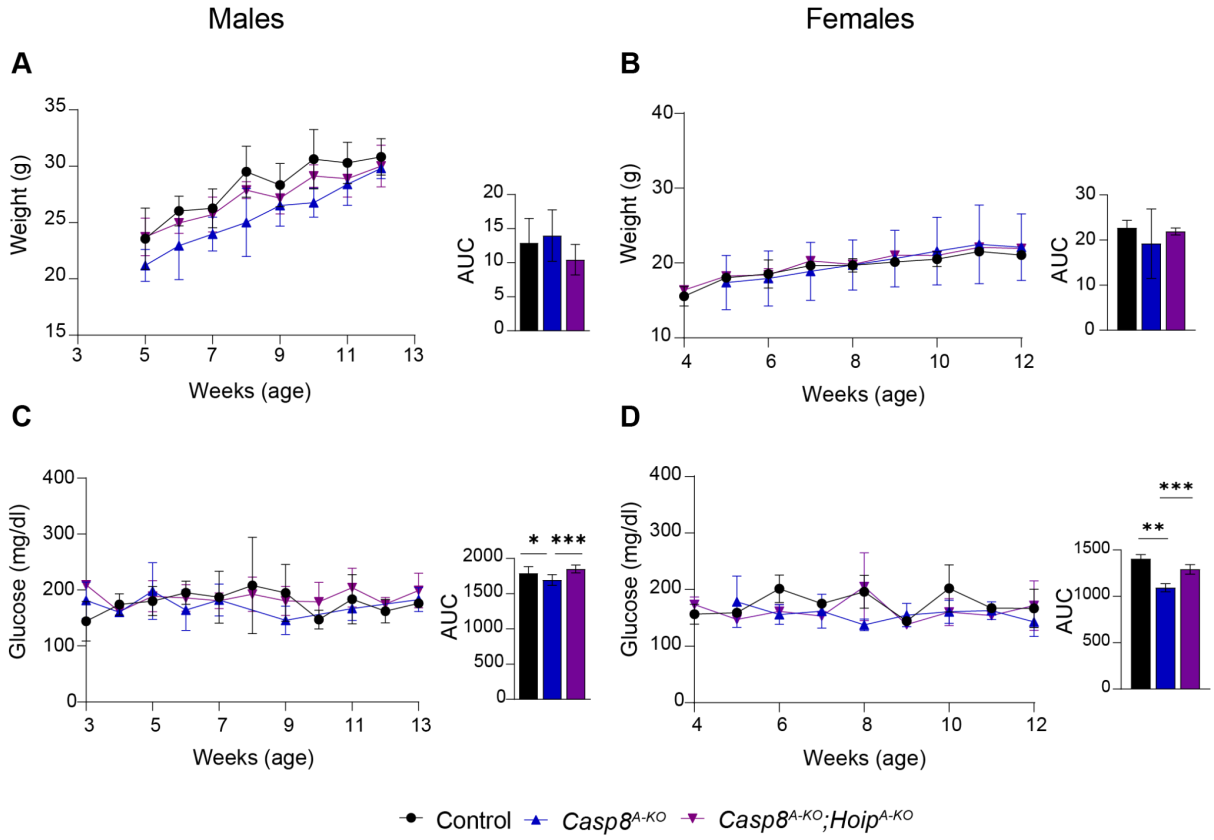

Figure 3.3.14 Casp8 deletion in adipocytes seems to decrease glycemia

Insulin tolerance test of mice under CHOW diet at 12 weeks of age, A-Females (n=7-9), B- (n=5-6). Glucose tolerance test of mice under CHOW diet at 12 weeks of age, A-Females (n=7-9), B- (n=5-6). Statistical test: 1-way ANOVA with selected comparisons (to control), applying Bonferroni correction for múltiple comparisons. p-values: (#) p-<0,0001, (***) p-<0,0002, (**) p-<0,0021, (*) p-<0,033, (ns) not significant.

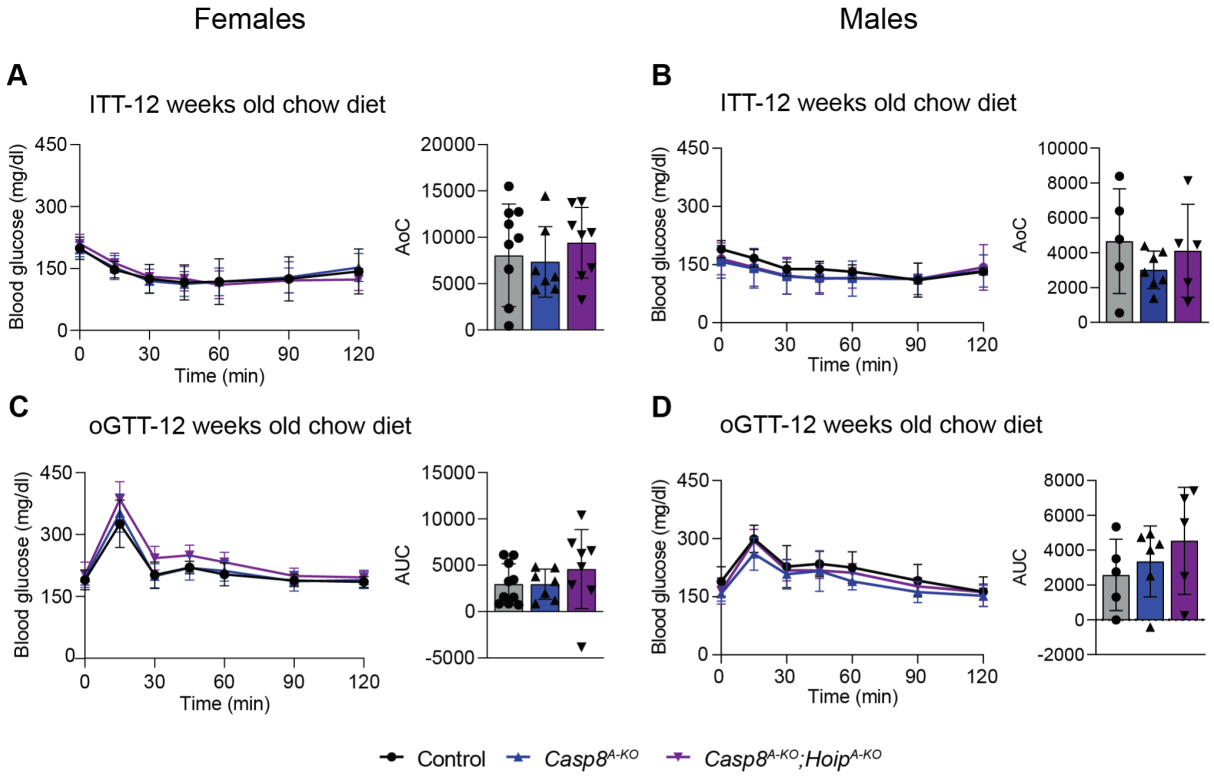

Figure 3.3.15 Casp8 and Hoip co-deletion in adipocytes do not affect glucose metabolism in basal conditions.

Insulin tolerance test of mice under CHOW diet at 12 weeks of age, A-Females (n=7-9), B- (n=5-6). Glucose tolerance test of mice under CHOW diet at 12 weeks of age, A-Females (n=7-9), B- (n=5-6). Statistical test: 1-way ANOVA with selected comparisons (to control), applying Bonferroni correction for múltiple comparisons. p-values: (#) p-<0,0001, (***) p-<0,0002, (**) p-<0,0021, (*) p-<0,033, (ns) not significant.

Since the spontaneous lipodystrophy signature was detected from 12-weeks old onwards in *Hoip*$^{A\text{-}KO}$ we choose this early stage as the first time point to evaluate tissue weights. To our surprise, we found that single deletion of casp8 completely restored fat mass in both *Hoip*$^{A\text{-}KO}$ males and females (Figure 3.3.16), however splenomegaly was exacerbated by single *Casp8*$^{A\text{-}KO}$ deletion in both groups .

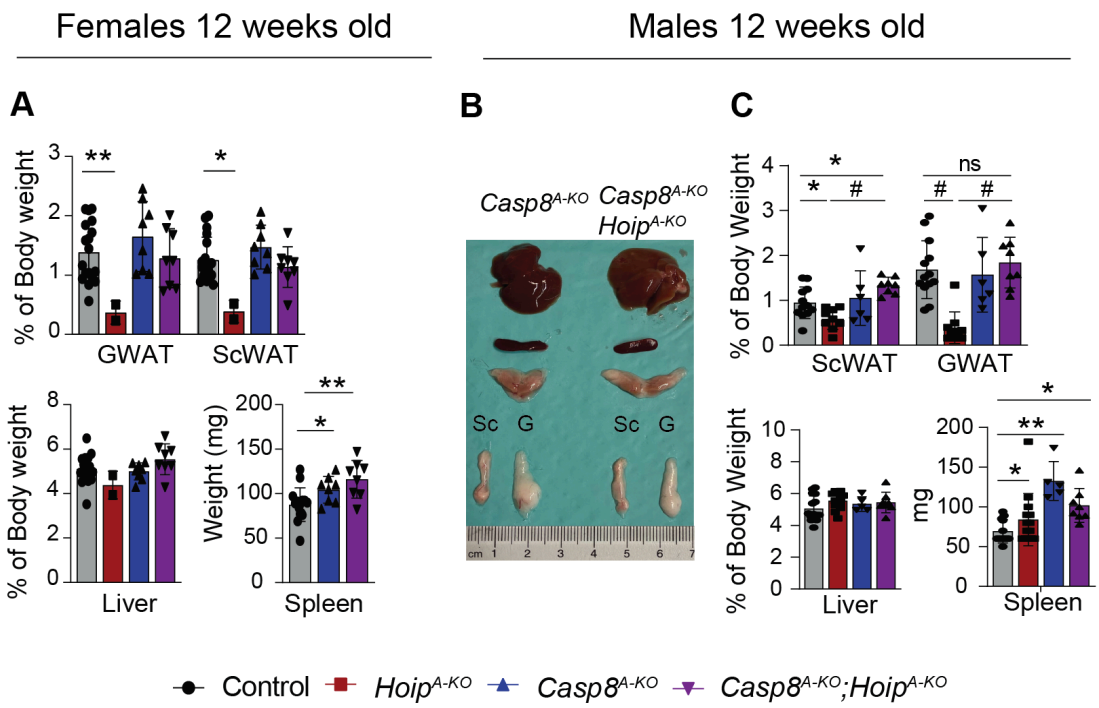

Figure 3.3.16 Casp8 and deletion in adipocytes rescues adipose tissue mass in *Hoip*$^{A\text{-}KO}$ mice but not splenomegaly

A-Tissue weights of 12 weeks old females fed with chow diet relativized to total body weight (except for spleen expressed in mg) (n=7-9), B- Pictures of male tissues at endpoint (12 weeks of age), C-Tissue weights of 12 weeks old males fed with chow diet relativized to total body weight (except for spleen expressed in mg) (n=5-6). Statistical test: 1-way ANOVA with selected comparisons (to control), applying Bonferroni correction for múltiple comparisons. p-values: (#) p-<0,0001, (***) p-<0,0002, (**) p-<0,0021, (*) p-<0,033, (ns) not significant.

A comprehensive histopathological assessment of multiple tissues was performed in both male and female mice across all genotypes. As shown in Figure 3.3.17, adipocyte morphology in ScWAT displays distinct patterns depending on genotype and sex.

In ScWAT, both male and female *Hoip*$^{A\text{-}KO}$ mice exhibited pronounced adipocyte hypertrophy compared to WT controls (Figure 3.3.17). Female *Casp8*$^{A\text{-}KO}$ mice also presented with enlarged adipocytes relative to controls, albeit to a lesser extent than observed in *Hoip*$^{A\text{-}KO}$ females. Intriguingly, double mutant *Casp8*$^{A\text{-}KO}$;*Hoip*$^{A\text{-}KO}$ mice showed near normalization of adipocyte size, suggesting a compensatory or counterbalancing effect between the two genetic modifications. In males, adipocytes in *Casp8*$^{A\text{-}KO}$ mice appeared smaller, in agreement with previous reports (Luk et al., 2023), while the *Casp8*$^{A\text{-}KO}$;*Hoip*$^{A\text{-}KO}$ genotype presented a highly heterogeneous mosaic pattern, with a mixture of small and large adipocytes.

In GWAT, female *Hoip*$^{A\text{-}KO}$ mice showed markedly hypertrophic adipocytes, but no evidence suggesting lipodystrophy, in line with their conserved tissue weight. Males, by contrast, displayed increased immune cell infiltration and significantly larger adipocytes, indicative of altered tissue homeostasis. In female *Casp8*$^{A\text{-}KO}$ mice, adipocyte size was reduced compared to controls, while the *Casp8*$^{A\text{-}KO}$;*Hoip*$^{A\text{-}KO}$ combination closely resembled the *Hoip*$^{A\text{-}KO}$ phenotype, indicating a loss of the *Casp8*$^{A\text{-}KO}$ effect in this depot. In males, lipodystrophy characteristic of *Hoip*$^{A\text{-}KO}$ mice was clearly attenuated in double mutants, which were largely indistinguishable from WT controls.

Analysis in BAT revealed that both male and female *Hoip*$^{A\text{-}KO}$ mice exhibited pronounced whitening, consistent with impaired thermogenic capacity. BAT from *Casp8*$^{A\text{-}KO}$ mice contained more compact brown adipocytes with smaller lipid droplets, aligning with an increased thermogenic state as previously described (Luk et al., 2023). However, this effect was blunted in *Casp8*$^{A\text{-}KO}$*;Hoip*$^{A\text{-}KO}$ mice, where the whitening phenotype was partially rescued. Thus, the expected thermogenic signature driven by Casp8 deletion was diminished upon concurrent Hoip ablation, suggesting that these effects counteract each other (potentially due to NF-κB).

In the skin, the marked loss of subdermal adipocytes observed in *Hoip*$^{A\text{-}KO}$ mice (in both sexes), was not rescued by Casp8 deletion, indicating that the maintenance of this adipose depot is likely dependent on LinUb function (potentially NF-κB dependent) or can execute caspase-independent cell death pathways. Of note, *Casp8*$^{A\text{-}KO}$ mice showed a trend towards decreased subdermal adipocyte content, particularly in males however, in females this effect seems to be subtle and further quantification and synchronized sampling is required for definitive assessment.

Other tissues, including liver, spleen, and pancreas, exhibited no obvious histopathological differences across genotypes in either sex.

Together, these observations highlight depot- and sex-specific effects of Casp8 and Hoip genetic ablation on AT morphology.

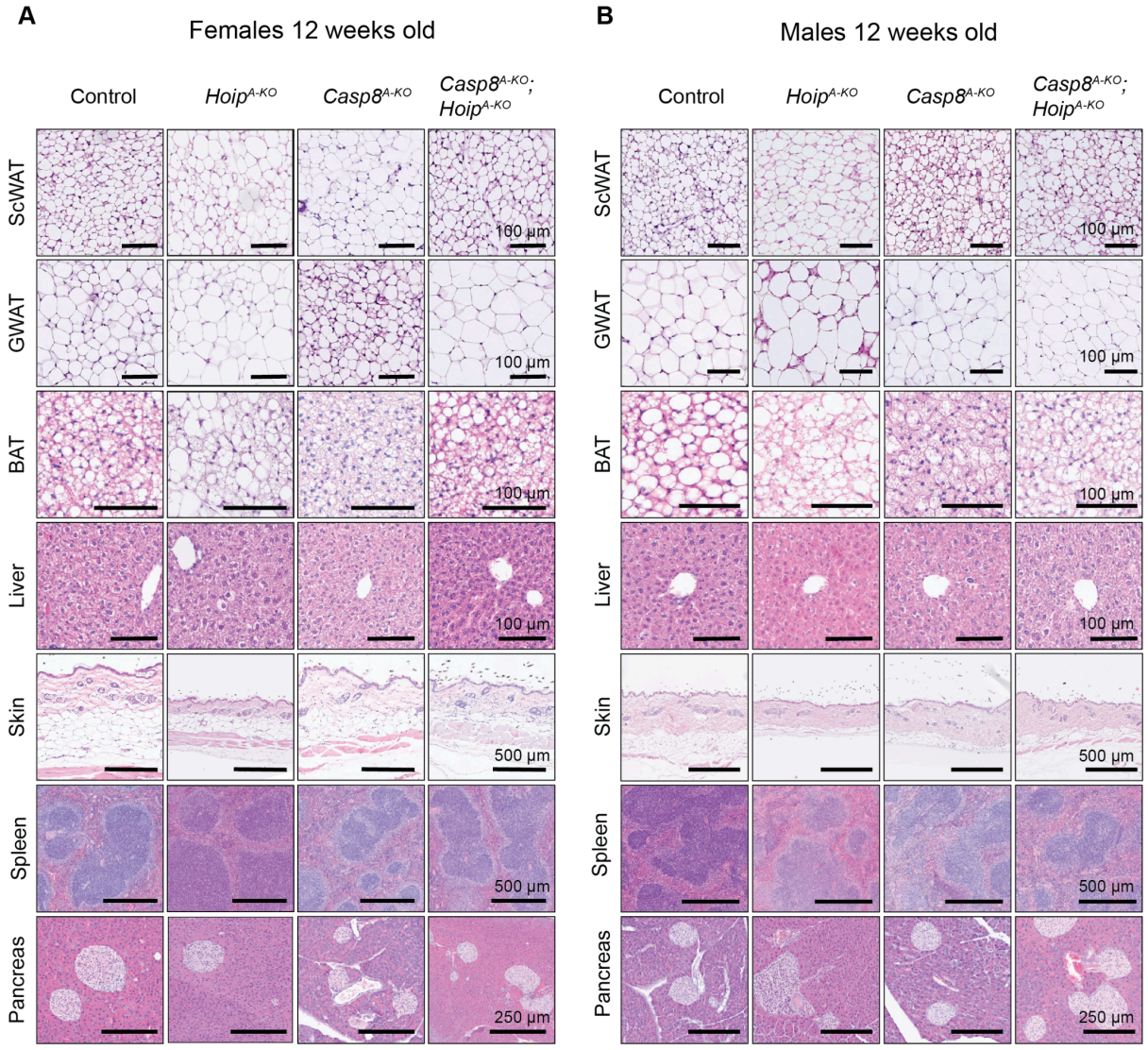

Figure 3.3.17 Casp8 deletion rescues HOIP-dependent lipodystrophy, pancreatic islet hyperplasia but no subdermal adipose tissue loss.

Representative H&E pictures from different tissues of 12 weeks old mice fed with chow diet A- Females (n = 2-9), B- Males (n = 5-7).

Given the high heterogeneity and presence of hypertrophic cells in *Hoip*$^{A\text{-}KO}$ fat depots, adipocyte distribution in GWAT and ScWAT was evaluated in these young mice. In ScWAT, deletion of caspase 8 was found to result in a decreased adipocyte size distribution in females (Figure 3.3.18.A), while this difference was not observed in males (Figure 3.3.18.B). Concurrently, *Hoip*$^{A\text{-}KO}$*;Casp8*$^{A\text{-}KO}$ female mice exhibited a distribution similar to wild-type controls, suggesting that the effect observed in ScWAT of Casp8-deficient mice might be NF-κB dependent. In GWAT, *Casp8*$^{A\text{-}KO}$ and *Hoip*$^{A\text{-}KO}$*;Casp8*$^{A\text{-}KO}$ adipocytes were found to be smaller in both sexes (Figure 3.3.18 C and D), possibly related to the aforementioned Casp8-dependent thermogenic effect (Luk et al., 2023).

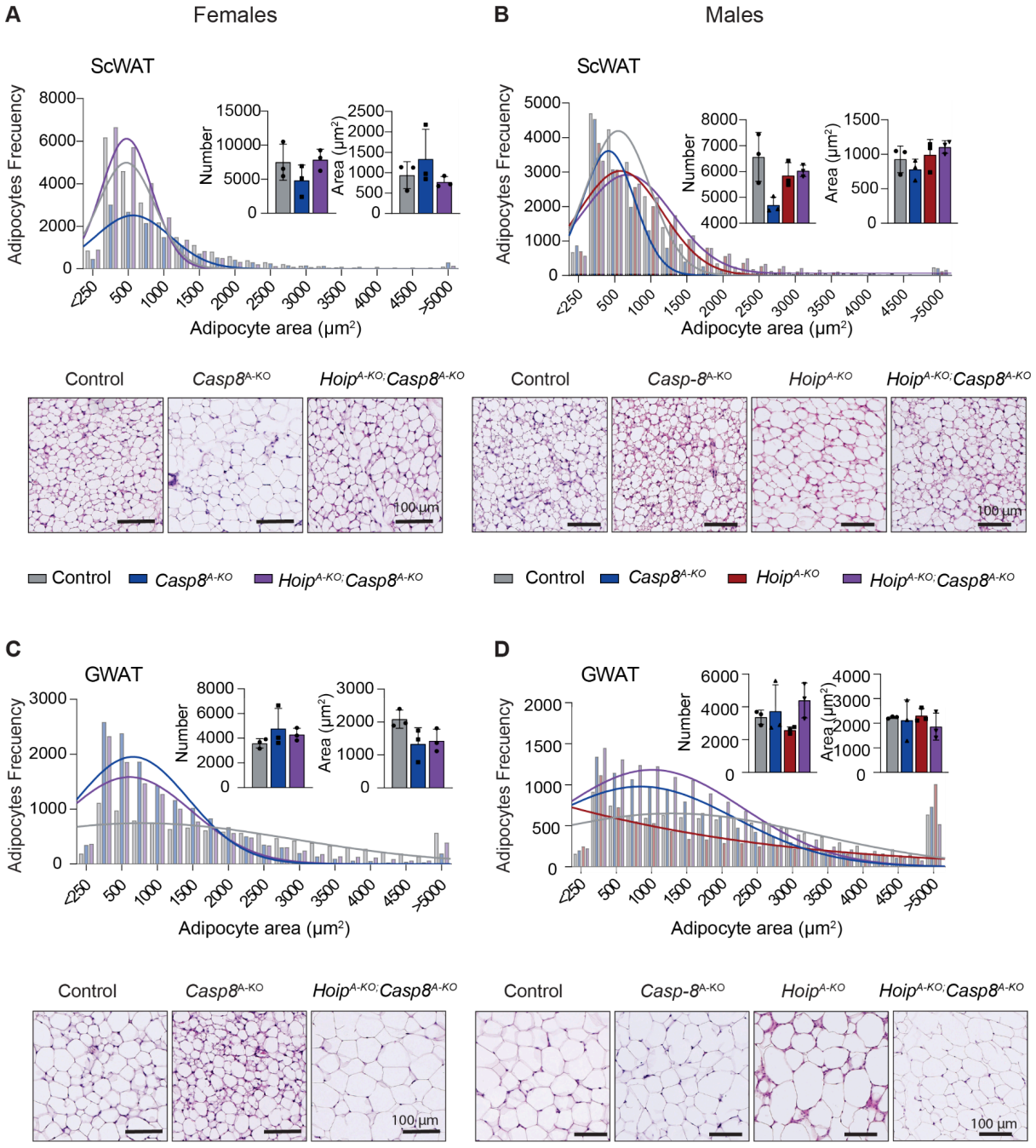

Figure 3.3.18 *Casp8*$^{A\text{-}KO}$ and *Hoip*$^{A\text{-}KO}$*;Casp8*$^{A\text{-}KO}$ mice present reduced adipocyte size in GWAT.

Adipocyte size distribution quantified from AT H&E by Adiposoft plug in (FiJi). All groups belong to 12 weeks old mice fed with CHOW diet and have n=3. A- ScWAT Females, B- ScWAT Males, C- GWAT Females, D- GWAT Males. Statistical Test: 1-way ANOVA with selected comparisons (to control), applying Bonferroni correction for múltiple comparisons. p-values: (#) p-<0,0001, (***) p-<0,0002, (**) p-<0,0021, (*) p-<0,033, (ns) not significant.

Last, in line with the restored fat mass, casp8 deletion entirely rescued the spontaneous lipodystrophy-like phenotype of *Hoip*$^{A\text{-}KO}$ mice evidenced by a clear reduction of macrophage

infiltration and complete absence of TUNEL+ cells (Figure 3.3.19 A, B and C) at 12 weeks of age.

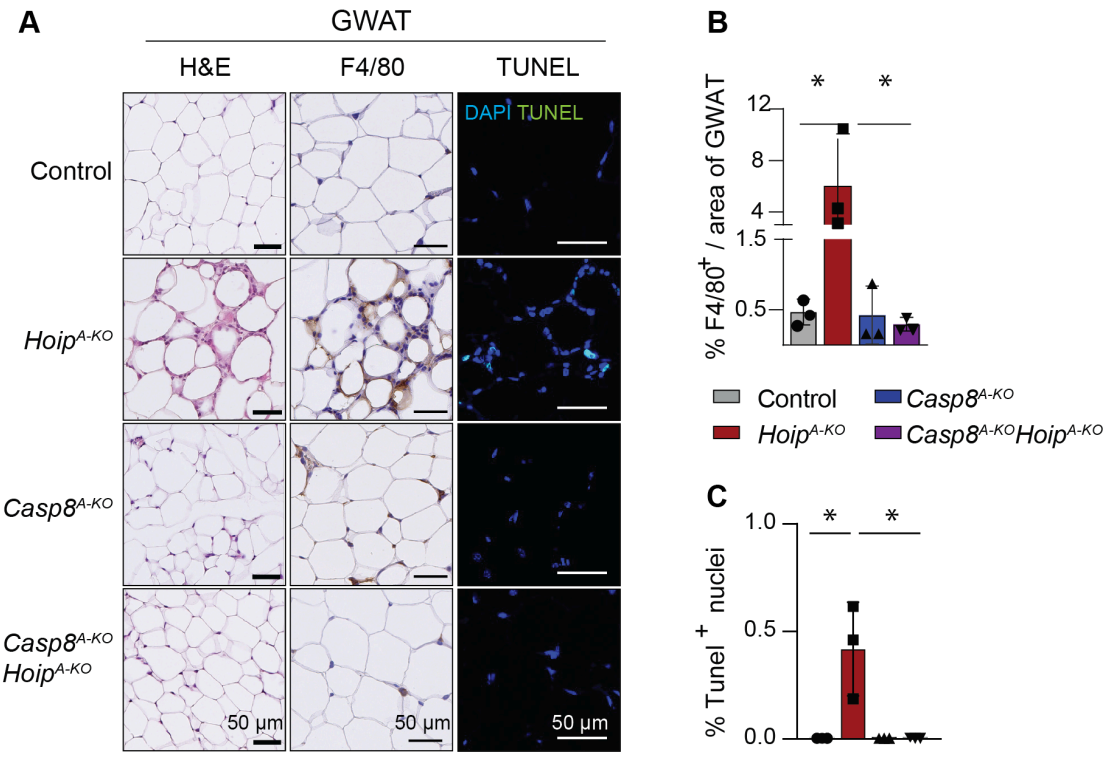

Figure 3.3.19 Casp8 adipocyte deletion rescued AT *Hoip^{A-KO}* cell death rates and subsequent macrophage infiltration.

A- Representative pictures of GWAT from 12 weeks old males fed with CHOW : H&E, F480 (IHC) and TUNEL (IF). B- F4/80 positive area normalizer to total tissue area. C-Percentage of TUNEL positive nuclei quantified by Qpath. Statistical test: 1-way ANOVA with selected comparisons (to control or to *Hoip^{A-KO}*), applying Bonferroni correction for múltiple comparisons. p-values: (#) p-<0,0001, (***) p-<0,0002, (**) p-<0,0021, (*) p-<0,033, (ns) not significant.

To sum up, deletion of caspase 8 abolished the lipodystrophy observed in *Hoip^{A-KO}* mice at 12 weeks of age. Furthermore, cell death prevention allows us to observe that LinUb might play a crucial role in adipocyte size distribution, likely attributable to its function in NF-κB regulation, since *Casp8^{A-KO};Hoip^{A-KO}* mice still presented a reduced adipocytes size, although we cannot rule out that this could be a Casp8-dependent effect (Luk et al., 2023). These findings underscore the significant interplay between Hoip and caspase 8 in maintaining adipose tissue homeostasis.

3.3.1.5 Caspase-8-mediated cell death is responsible for the metabolic dysfunction driven by HOIP deficiency during obesity

To further characterize the implications of LinUb during obesity-induced inflammation, *Hoip*$^{A\text{-}KO}$;*Casp8*$^{A\text{-}KO}$ mice were challenged with a HFD. The *Hoip*$^{A\text{-}KO}$;*Casp8*$^{A\text{-}KO}$ mice gained weight similarly to their WT littermate controls, with only a slight, non-significant decrease observed in *Casp8*$^{A\text{-}KO}$ mice (Figure 3.3.20 A), similar to a previous report (Luk et al., 2023).

Notably, *Hoip*$^{A\text{-}KO}$;*Casp8*$^{A\text{-}KO}$ but not *Casp8*$^{A\text{-}KO}$ mice presented an increased fasting blood glucose value at 8 weeks of diet (Figure 3.3.20 B) . However, this difference dissipated after 16 weeks of diet (Figure 3.3.20 B). In contrast to earlier reports, an increase in glycemia was observed in *Casp8*$^{A\text{-}KO}$ mice (Figure 3.3.20 C), which corresponded with an elevation in the glycemia marker HbA1c (Figure 3.3.20 D)

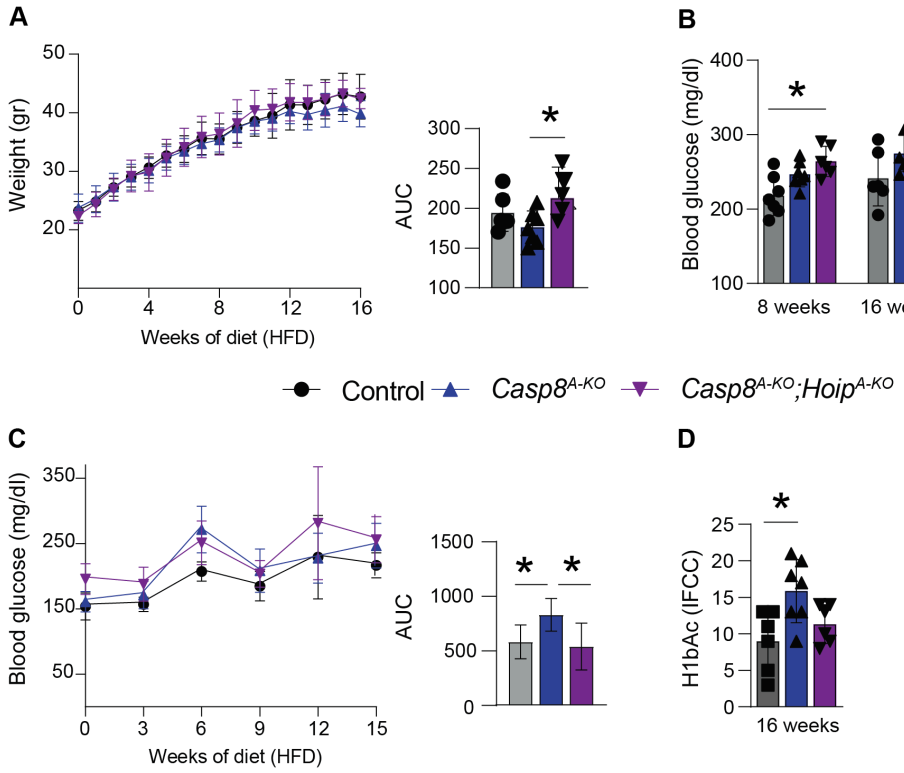

Figure 3.3.20 Casp8 co-deletion restores gain weight on *Hoip*$^{A\text{-}KO}$ mice during HFD.

A- Weight monitoring of males during HFD. B- Blood glucose values after 6 hrs of Fasting. C- Normal fed glucose evaluation males during HFD.D- Glacemia marker of mice after 16 weeks of diet. Mice were fed ad-libitum with HFD and monitored for 16 weeks (n=5-7). 1-way ANOVA applying Bonferroni correction for múltiple comparisons. p-values: (#) p-<0,0001, (***) p-<0,0002, (**) p-<0,0021, (*) p-<0,033, (ns) not significant.

Despite these observations, and contrary to previous findings (Luk et al., 2023), no differences in insulin sensitivity (Figure 3.3.21 A and C) or glucose tolerance (Figure 3.3.21 B and A) were detected among any of the groups at the evaluated timepoints.

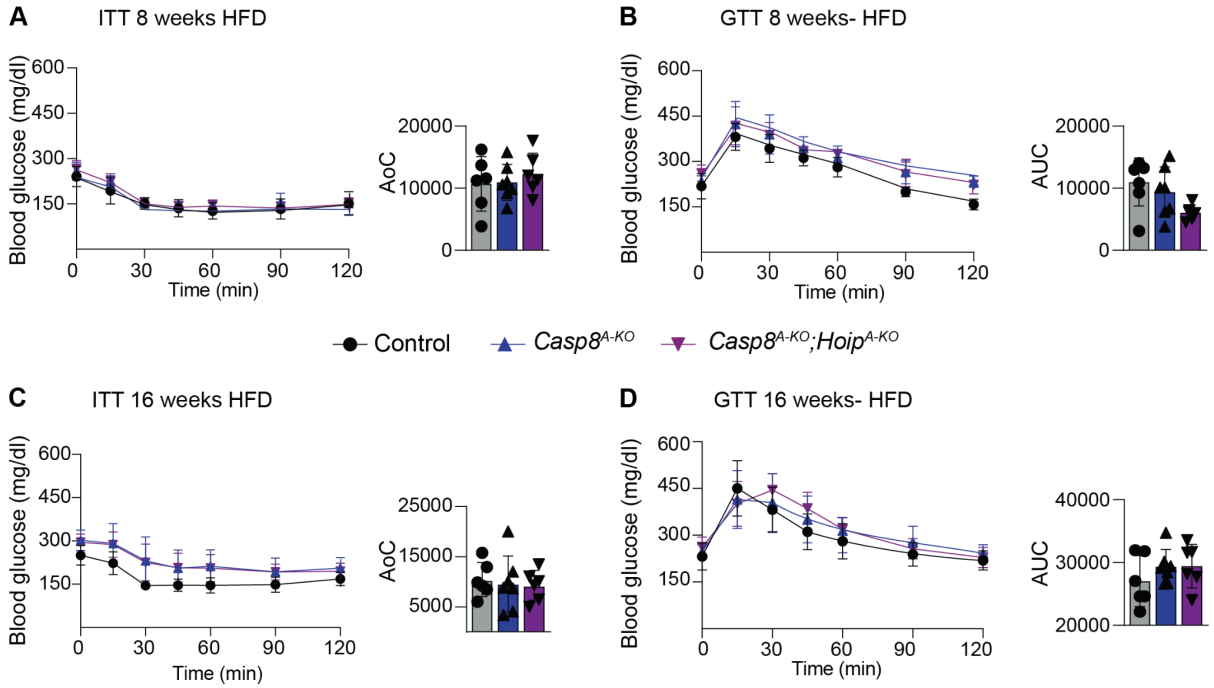

Figure 3.3.21 Casp8 and Hoip Co-deletion in adipocytes do not affect glucose metabolism during HFD.

A- Insulin tolerance test of male mice after 8 weeks of HFD (n=5-7). A- Oral glucose tolerance test of male mice after 8 weeks of HFD (n=5-7). C- Insulin tolerance test of male mice after 16 weeks of HFD (n=5-7). A- Oral glucose tolerance test of male mice after 16 weeks of HFD (n=5-7). Statistical test: 1-way ANOVA applying Bonferroni correction for múltiple comparisons. p-values: (#) p-<0,0001, (***) p-<0,0002, (**) p-<0,0021, (*) p-<0,033, (ns) not significant.

Regarding fat mass, *Hoip*$^{A\text{-}KO}$ wasting was rescued by Casp8 absence in adipocytes, with GWAT weight reaching a similar level to the *Casp8*$^{A\text{-}KO}$ control. However, as previously reported, Casp8 deletion in adipocytes led to decreased fat deposition in GWAT (Luk et al., 2023), despite no differences in ScWAT or BAT in our model (Figure 3.3.22.A). Furthermore, the hepatomegaly and splenomegaly observed in *Hoip*$^{A\text{-}KO}$ mice were completely reversed by Casp8 ablation (Figure 3.3.22.A).

Concurrently, fat mass recovery Casp8 deletion fully restored *Hoip*$^{A\text{-}KO}$;*Casp8*$^{A\text{-}KO}$ WAT endocrine function, as evidenced by adiponectin and leptin levels (Figure 3.3.22 B). However, despite this, *Hoip*$^{A\text{-}KO}$;*Casp8*$^{A\text{-}KO}$'s histological analysis revealed a highly infiltrated AT, especially in the gonadal compartment (Figure 3.3.22 C).

Unexpectedly, and contrary to previous reports, *Casp8*$^{A\text{-}KO}$ BAT was highly prone to HFD-whitening in 50% of the cases, while a similar tendency was observed in *Hoip*$^{A\text{-}KO}$;*Casp8*$^{A\text{-}KO}$ mice (Figure 3.3.22 C), which does not align with the expected and aforementioned thermogenic effect or protection against DIO in *Casp8*$^{A\text{-}KO}$. In *Hoip*$^{A\text{-}KO}$;*Casp8*$^{A\text{-}KO}$ the whitening tendency was also accompanied by increased cell infiltration, suggesting either increased adipocyte cell death or inflammatory signalling upon the loss of LinUb and Caspase activity (Figure 3.3.22 C).

Liver H&E staining revealed morphological differences in lipid distribution. Control and *Hoip*$^{A\text{-}KO}$;*Casp8*$^{A\text{-}KO}$ mice exhibited a radial distribution of clear lipid droplets from the vessel, while *Casp8*$^{A\text{-}KO}$ mice showed more prominent ballooning (swollen, rounded liver cells that are typically 1.5 to 3 times larger than normal hepatocytes, with a pale, wispy, or rarefied cytoplasm) (Figure 3.3.22 C). Nevertheless, all groups showed a similar steatotic score (Figure 3.3.22 D and E). Notably, *Hoip*$^{A\text{-}KO}$ islet hyperplasia was completely reversed by the deletion of Casp8 (Figure 3.3.22 C).Despite this, higher insulin levels HFD-fed *Hoip*$^{A\text{-}KO}$;*Casp8*$^{A\text{-}KO}$ were still present in comparison to WT littermates controls (Figure 3.3.22 F).

Similar to *Hoip*$^{A\text{-}KO}$, no obvious morphological changes were observed in the spleen. On the other hand, subdermal AT phenotype could not be rescued by Casp8 deletion, suggesting either a higher dependency on NF-κB pro-survival genes in this AT depot or the execution of other cell death modality, independent of casp8 (Figure 3.3.22 C).

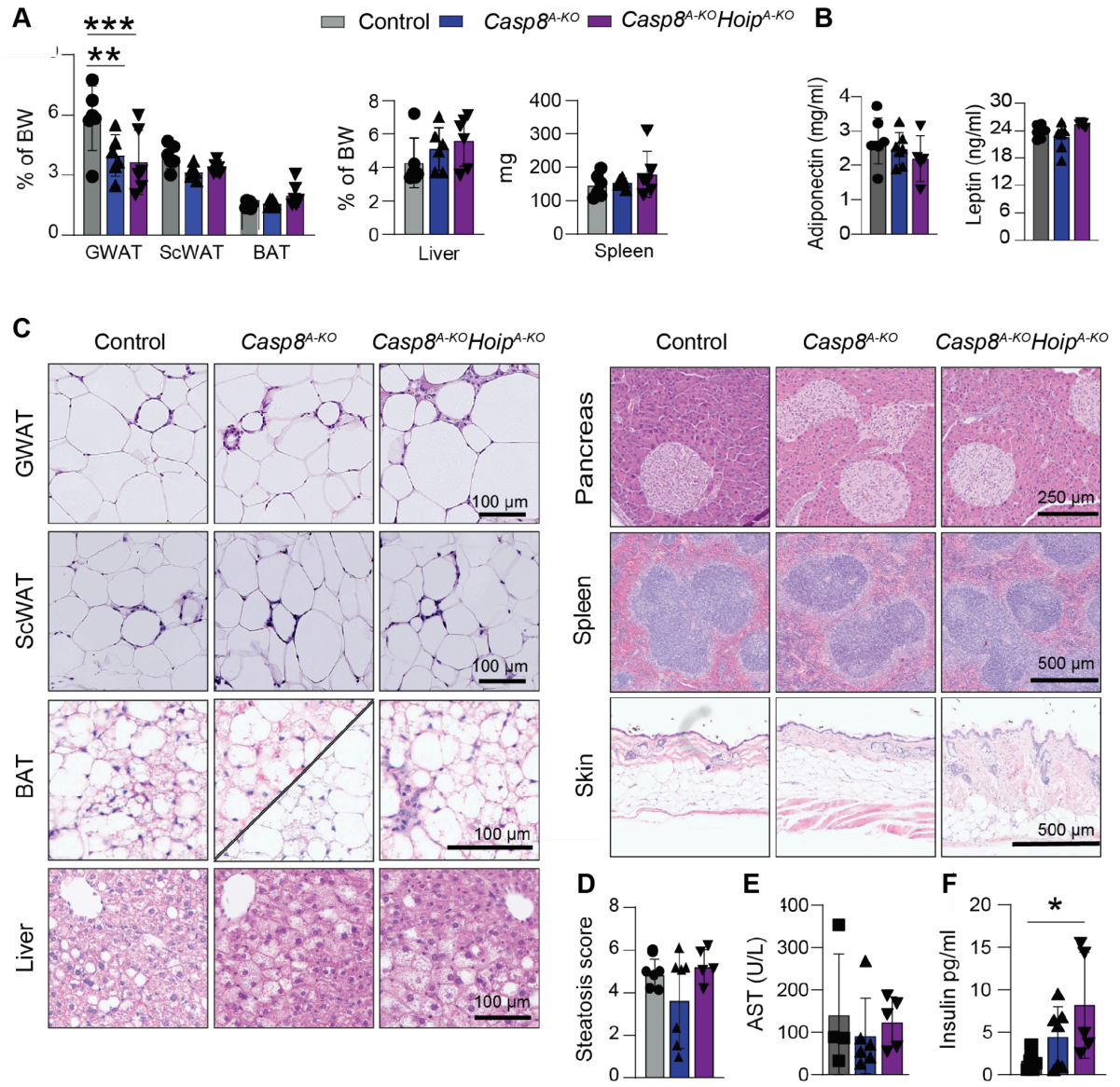

Figure 3.3.23 Casp8 deletion in adipocytes rescues *Hoip*$^{A\text{-}KO}$ AT mass and endocrine function even after HDF challenge.

A- Tissue weights of 16-weeks HFD-fed males at end point normalised to total body weight (except spleen). B- Adiponectin and Leptin serum values after 16 weeks of field. C- Representative pictures of H&E of different tissues after 16 weeks of diet. D- Steatosis scores of livers at 16 weeks of diet. E- AST serum levels at 16 weeks of diet. F- Insulin serum levels at 16-weeks if diet.Statistical test: 1-way ANOVA applying Bonferroni correction for múltiple comparisons. p-values: (#) p-<0,0001, (***) p-<0,0002, (**) p-<0,0021, (*) p-<0,033, (ns) not significant.

Evaluation of adipocyte distribution in GWAT and ScWAT of HFD-challenged mice revealed distinct patterns across the experimental groups. Analysis of adipocyte size distribution in GWAT from mice challenged with a HFD showed a consistent logarithmic distribution across all experimental groups (Figure 3.3.23 A). This likely reflects the presence of highly hypertrophic adipocytes induced by HFD (Figure 3.3.23 C). Notably, the *Casp8*$^{A\text{-}KO}$ group

exhibited a slightly reduced distribution slope, indicative of fewer very large adipocytes, yet the mean adipocyte size was not significantly different from controls. This outcome contrasts with findings in recent reports (Luk et al., 2023), and is particularly interesting given that *Casp8*$^{A\text{-}KO}$ GWAT mass was lower than controls. These results suggest that HFD has a dominant impact on GWAT adipocyte size, overshadowing effects attributable to specific genotypes.

Conversely, ScWAT displayed subtle differences among the groups. Notably, HFD-fed *Hoip*$^{A\text{-}KO}$*;Casp8*$^{A\text{-}KO}$ mice demonstrated adipocyte size Gaussian distribution, similar to WT controls, while lack of LinUb conserved the logarithmic distribution in HFD-fed *Hoip*$^{A\text{-}KO}$ mice (Figure 3.3.23 B). Furthermore, Casp8 deletion alone resulted in reduced adipocyte size in ScWAT, consistent with the previous report by Luk et al. (Figure 3.3.23 B), while in this AT depot it also prevented *Hoip*$^{A\text{-}KO}$ adipocyte hypertrophy to a similar extent to *Casp8*$^{A\text{-}KO}$ (Figure 3.3.23 D).

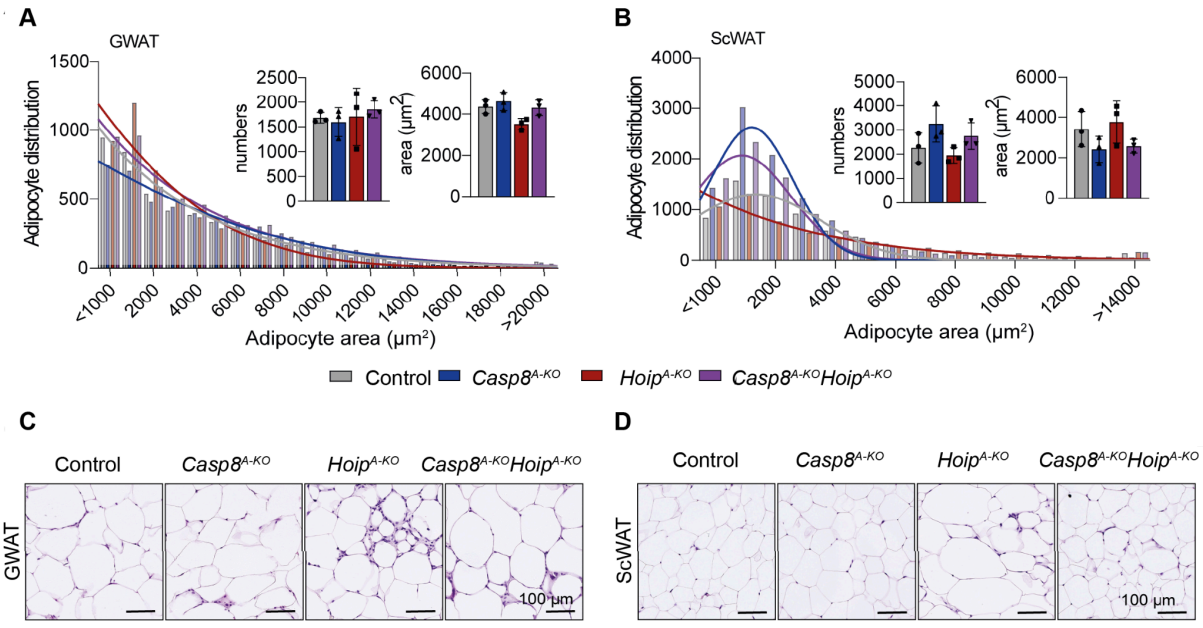

Figure 3.3.23 Caspase8 deletion decreases adipocyte size in ScWAT but not GWAT during HFD.
Adipocyte size distribution quantified from AT H&E by Adiposoft plug in (FiJi). All groups belong to 16 weeks fed with HFD and have n=3. A- GWAT B- ScWAT, C- Representative H&E GWAT Females, D- Representative H&E ScWAT. Statistical test: 1-way ANOVA applying Bonferroni correction for múltiple comparisons. p-values: (#) p-<0,0001, (***) p-<0,0002, (**) p-<0,0021, (*) p-<0,033, (ns) not significant.

Curiously, although total fat mass was normal, GWAT hypertrophy accompanied by immune cell infiltration was only partially prevented in obese *Hoip*$^{A\text{-}KO}$*;Casp8*$^{A\text{-}KO}$ mice (Figure 3.3.24

A). The observation that *Hoip*$^{A\text{-}KO}$*;Casp8*$^{A\text{-}KO}$ mice were not fully protected from GWAT hypertrophy upon HFD prompted us to evaluate whether caspase-8-independent cell death was present in these mice. TUNEL positive staining was fully blocked in HFD-fed *Hoip*$^{A\text{-}KO}$*;Casp8*$^{A\text{-}KO}$ mice, indicating that loss of caspase-8 prevents cell death caused by HOIP deficiency (Figure 3.3.24 B and C). However, the differences in the levels of caspase-3 activation between groups were overall not significant (Figure 3.3.24 C). Notably, loss of caspase-8 did not fully prevent the elevated levels of caspase-3 activation observed in HFD-fed *Hoip*$^{A\text{-}KO}$ mice, despite the rescue of TUNEL positivity. This suggests that while caspase-8 deletion was sufficient to block HOIP deficiency-induced DNA fragmentation (as detected by TUNEL), it did not completely suppress caspase-3 activation. One possible explanation is that caspase-3 may be activated by alternative, caspase-8-independent apoptotic pathways, such as those involving mitochondrial effectors like Bax and BAK, which could be triggered by the metabolic stress of the HFD itself, as all HFD groups showed similar levels of caspase-3 activation.

In addition, it is important to consider that immune cells infiltrating the GWAT are not targeted by the Casp8 or Hoip deletions and may themselves exhibit caspase-3 activation in response to the inflammatory environment, even in the absence of detectable DNA fragmentation (TUNEL negativity). This could account for the persistent caspase-3 signal despite the rescue of TUNEL staining in *Casp8;Hoip*$^{A\text{-}K}$ mice. The lack of TUNEL positivity in the presence of caspase-3 activation is intriguing and may reflect sub-lethal or non-apoptotic roles of caspase-3 in these cells, or a threshold of activation insufficient to induce DNA fragmentation detectable by TUNEL.

Taken together, these results indicate that while loss of caspase-8 can block cell death associated with HOIP deficiency and partially restore normal adipocyte distribution in ScWAT, it does not fully prevent GWAT hypertrophy or caspase-3 activation under HFD conditions. This highlights both depot-specific and pathway-specific effects of these genetic modifications in adipose tissue remodeling under metabolic stress.

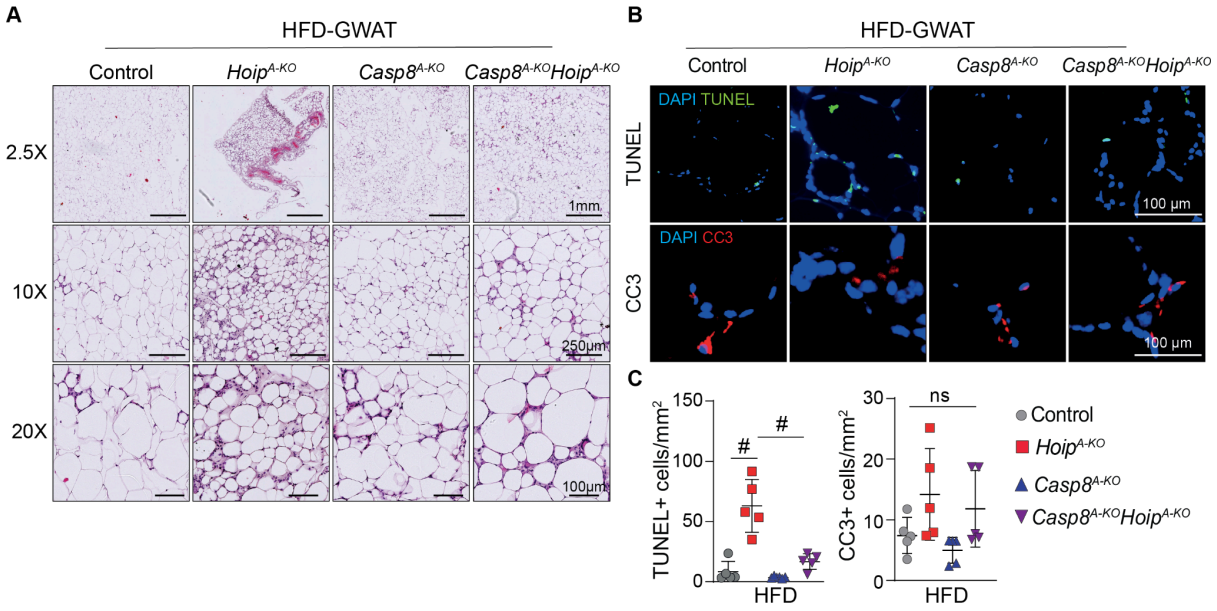

Figure 3.3.24 Caspase 8 deletion rescues adipose tissue mass and apoptotic cell death, but not tissue infiltration during HFD

A- Representative H&E pictures of GWAT at different magnifications after 16 weeks of HFD. B- Representative pictures of GWAT of TUNEL and Cleaved Caspase 3 (CC3) immunofluorescence after 16 weeks of HFD C- Quantification of immunofluorescence standings (n=5). Statistics: 1-way ANOVA applying Bonferroni correction for múltiple comparisons. p-values: (#) p-<0,0001, (***) p-<0,0002, (**) p-<0,0021, (*) p-<0,033, (ns) not significant.

To comprehensively evaluate the metabolic status of the mutant mice, a complete blood serum panel was performed after 16 weeks of HFD feeding. The analysis revealed no significant differences in hepatic or renal function markers, including albumin, urea, LDH, and AST, or triglyceride levels among the experimental groups (Figure 3.3.25 A-E). However, both *Casp8*$^{A\text{-}KO}$ and *Hoip*$^{A\text{-}KO}$*;Casp8*$^{A\text{-}KO}$ mice exhibited increased total cholesterol compared to controls (Figure 3.3.25 F). This trend was consistent across all cholesterol species, including HDL, non-HDL, and LDL (Figure 3.3.25 G-I), indicating an overall increase in lipid circulation in the bloodstream caused by Casp8 deletion. This observation highlighted a potential role for Casp8 in regulating cholesterol metabolism or transport, independent of NF-κB or its interaction with Hoip.

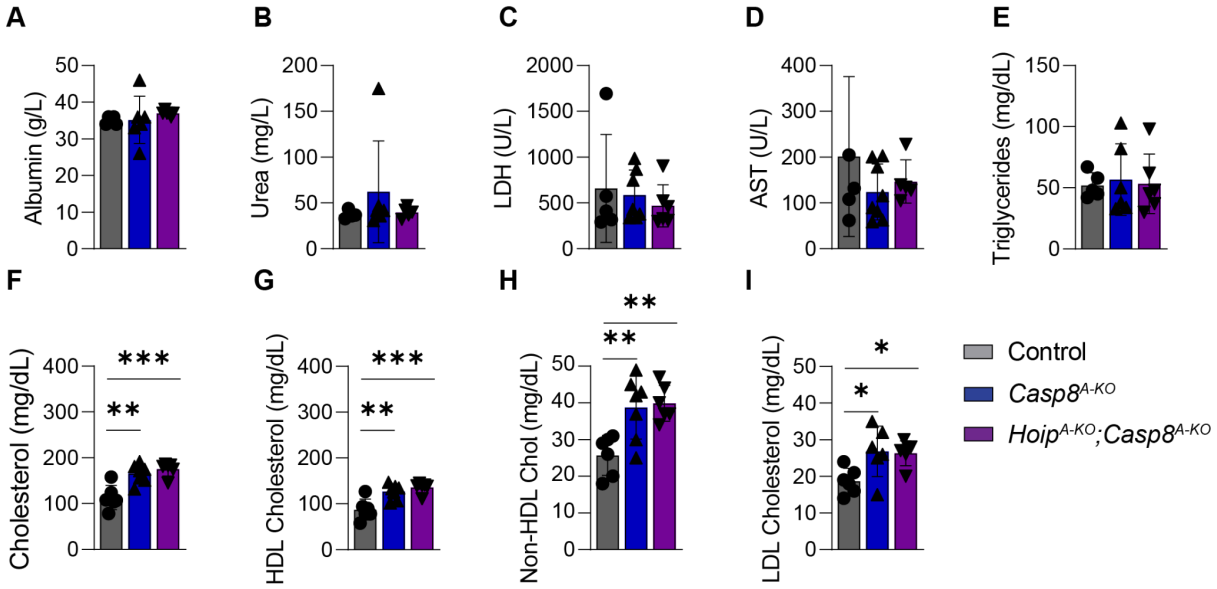

Figure 3.3.25 Caspase 8 deletion increases blood cholesterol during HFD

Blood serum values levels of males after 16 weeks of HFD (n=5-8): A-Albumin, B-Urea, C-Lactate dehydrogenase (LDH), E-Triglycerides, F-Total Cholesterol, G- High Density Lipoprotein (HDL) Cholesterol, H- Non-High Density Lipoprotein (non-HDL) Cholesterol, I- Low Density Lipoprotein (LDL) Cholesterol. Statistical test: 1-way ANOVA applying Bonferroni correction for múltiple comparisons. p-values: (#) p-<0,0001, (***) p-<0,0002, (**) p-<0,0021, (*) p-<0,033, (ns) not significant.

To sum up, our HFD-fed model revealed that loss of LinUb led to excessive Casp8-dependent apoptosis rates in obese conditions, with cell death-driven inflammation exacerbating diabetic and MASLD onset in HFD-fed *Hoip*$^{A\text{-}KO}$ mice. Intringly, although fat mass and AT endocrine function was restored, *Hoip*$^{A\text{-}KO}$*;Casp8*$^{A\text{-}KO}$ still presented adipocyte hypertrophy and excessive infiltration. Importantly, our findings also provide new insights into a potential metabolic function of Casp8 in adipocytes, particularly its impact on cholesterol homeostasis.

3.3.2. Linear ubiquitination prevent adipose tissue dysfunction during ageing

Hoip$^{A\text{-}KO}$ mice develop spontaneous lipodystrophy, a condition that in humans is strongly associated with an increased risk of metabolic syndrome later in life. Surprisingly, although the gene expression profile of GWAT in *Hoip*$^{A\text{-}KO}$ mice closely mimics that of HFD-fed WT controls, H*oip*$^{A\text{-}KO}$ mice do not spontaneously develop metabolic syndrome at the evaluated time point. Nonetheless, increased hepatic lipid accumulation, higher blood glucose levels, and elevated inflammatory gene expression in AT (M1-like CLS) are hallmarks of obesity-induced inflammation. Therefore, we hypothesize that adipocyte-specific loss of LUBAC activity initiates progressive adipose tissue dysfunction that predisposes to metabolic disease independent of dietary challenge. To test this, we examined the ageing

profile of *Hoip*$^{A\text{-}KO}$ mice by evaluating metabolic parameters and AT structure throughout their lifespan.

3.3.2.1 Sex differences in Hoip-driven lipodystrophy mouse model

Hoip$^{A\text{-}KO}$ and their littermates' controls (males and females) were monitored during 18-months. During this period weight gain was diminished by deletion of linUb in AT in both sexes (Figure 3.3.26 A and B), although HOIP deficiency did not affect normal glycemia throughout lifespan (Figure 3.3.26 C and D). Weight gain difference was first listed in females (Figure 3.3.26 A), likely attributable to females having a higher body fat percentage relative to their total body weight.

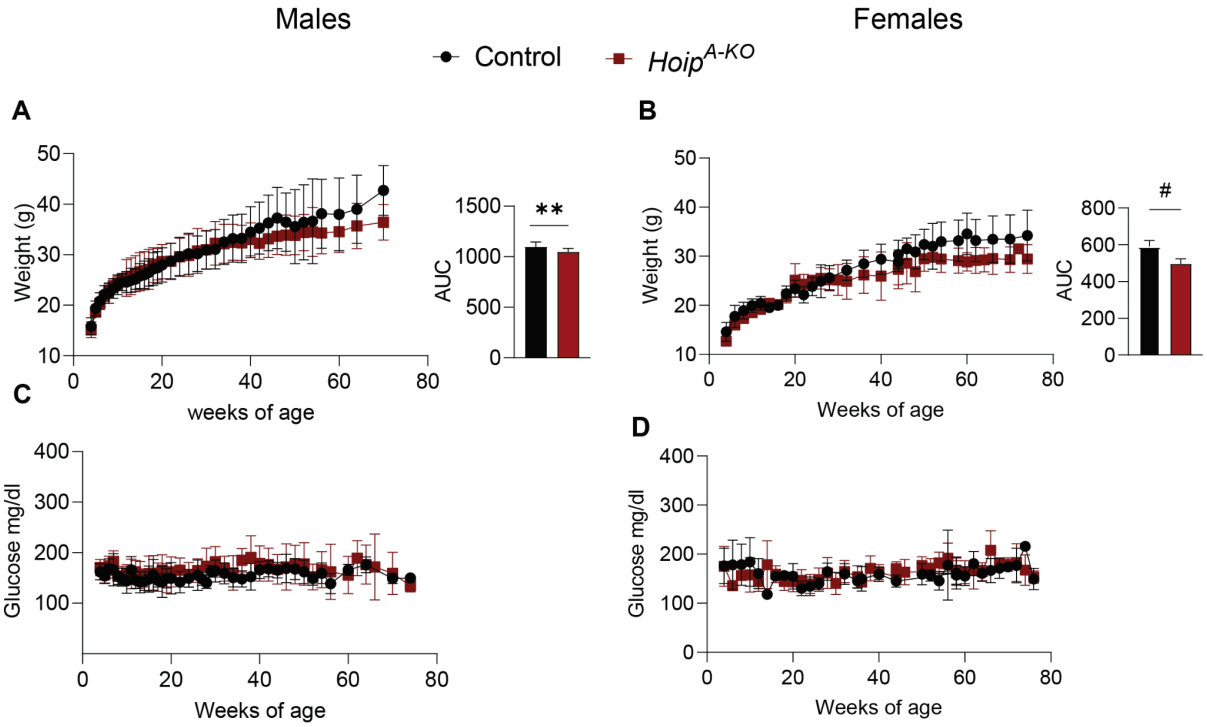

Figure 3.3.26 Weight and glucose monitoring of Hoip A-KO mice.

A and B -Weight monitoring of *Hoip*$^{A\text{-}KO}$ males (right) and females (left) with their corresponding Cre- littermate controls. C and D- Normal fed glucose evaluation of *Hoip*$^{A\text{-}KO}$ males (right) and females (left) with their corresponding Cre- littermate controls. Mice were fed ad-libitum with a chow diet and monitored for 18-months. T-test. p-values: (#) p-<0,0001, (***) p-<0,001, (**) p-<0,01, (*) p-<0,05, (ns) not significant.

Furthermore, aged *Hoip*$^{A\text{-}KO}$ mice present impaired insulin sensitivity compared to littermates controls (Figure 3.3.27 A and B) However this was not translated to glucose intolerance in any of the groups (Figure 3.3.27 C and D).

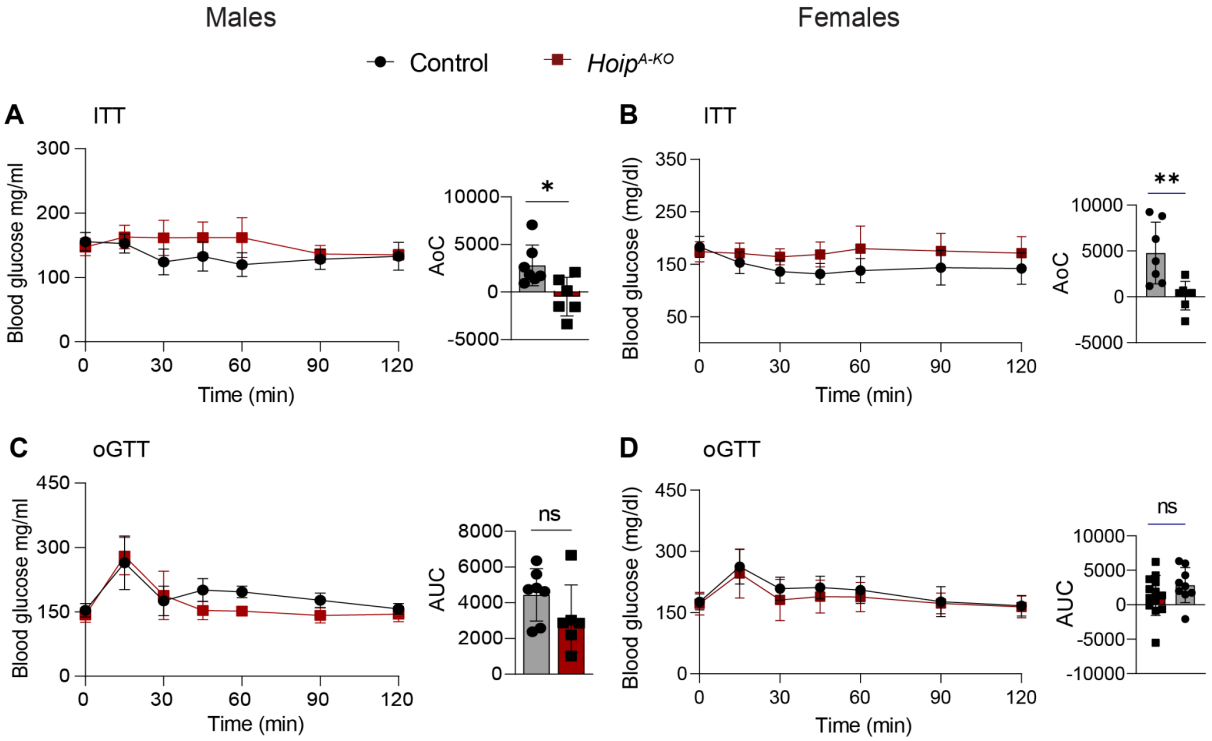

Figure 3.3.27 Insulin and oral Glucose tolerance Test in 18-months old males and females.

A and B -ITT of *Hoip*$^{A-KO}$ males (right) and females (left) with their corresponding Cre- littermate controls at 18-months old (males n=9, females n=7). C and D- Normal fed glucose evaluation of *Hoip*$^{A-KO}$ males (right) and females (left) with their corresponding Cre- littermate controls at 18-months old (males n=8-9, females n=10-12). T-test. p-values: (**) p-<0,01, (*) p-<0,05, (ns) not significant.

Regarding tissue weights, *Hoip*$^{A-KO}$ mice show reduced ScWAT and GWAT (Figure 3.3.28 A-D) with age, however we can observe that in GWAT females developed this only with ageing but not at 4 months of age, while males have it from premature age (Figure 3.3.28 A-D). In addition *Hoip*$^{A-KO}$ had splenomegaly and hepatomegaly, independent of sex (Figure 3.3.28 A-D). Regarding BAT, *Hoip*$^{A-KO}$ males presented reduced BAT at 18 months of age, while females do not show differences (Figure 3.3.28 A-D). Moreover, no differences were observed in heart weight (Figure 3.3.28 C-D).

Interestingly, females also presented enlarged thymus surrounding the heart and swallowed lymph nodes surrounding ScWAT and mesenteric AT compartments (data not shown) , indicating an altered immune response to AT loss.

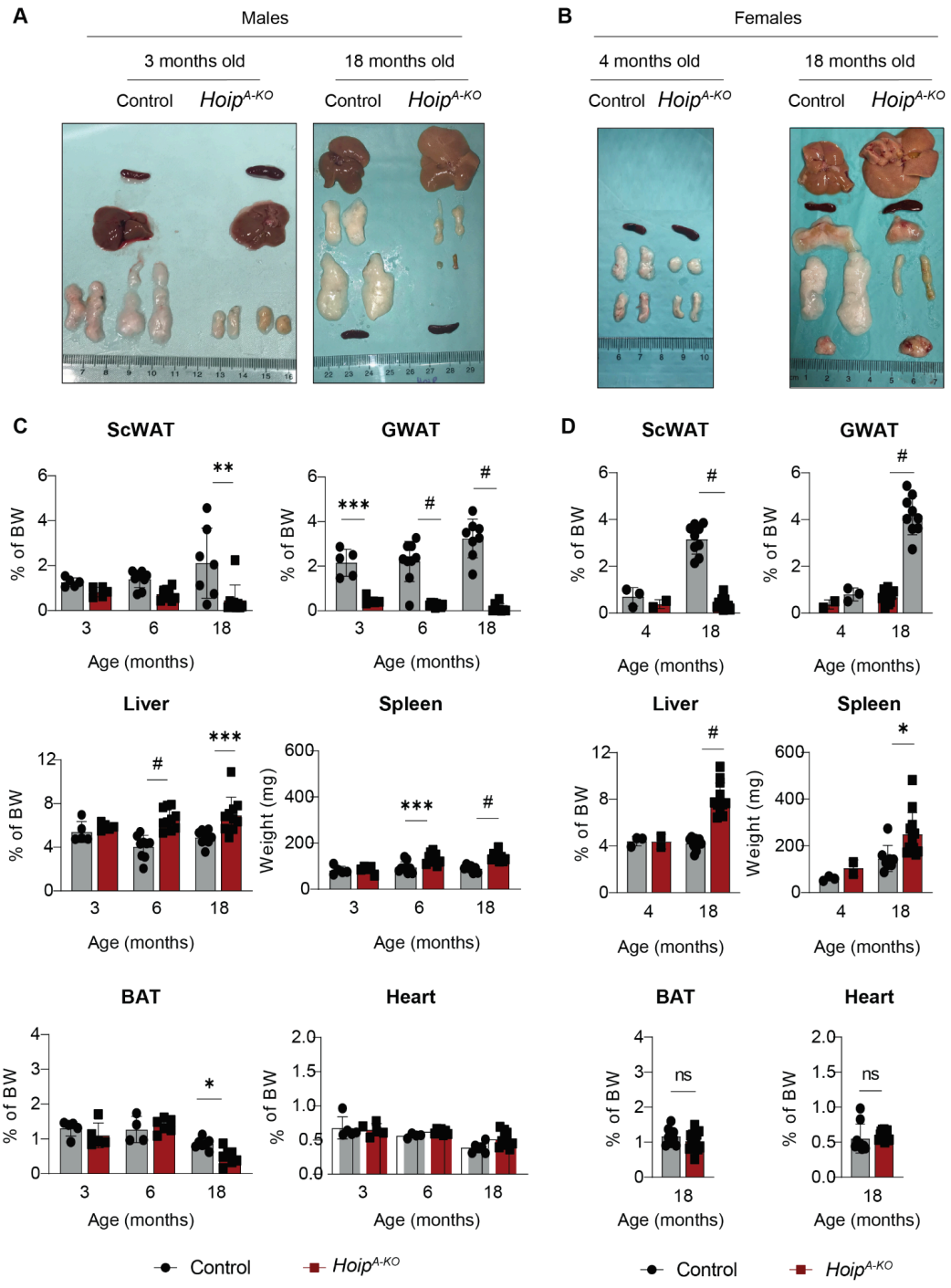

Figure 3.3.28 Tissue weights of males and females chow diet.

A and B -Representative pictures of *Hoip*$^{A\text{-}KO}$ males (right) and females (left) with their corresponding Cre- littermate controls at 3, 4 or 18-months old as indicated. Organs from top to bottom: A- 3 months old males: Spleen, Liver, WAT (right: ScWAT ; left: GWAT), 18 months: Liver, WAT, ScWAT, GWAT, spleen. B- 4 months females: Spleen, GWAT, ScWAT, 18 months females: Liver, Spleen, BAT, WAT(right : ScWAT; left: GWAT), Spleen, Thymus. C and D- Tissue weights normalised to total body weight at exception of spleen which is expressed in mg of *Hoip*$^{A\text{-}KO}$ males (right) and females (left) with their corresponding Cre- littermate controls at 3, 6 and 18-months old for males (n 5-6 ; 5-7 ; 8-9) and 4 and 18-months old for females (n 2-3 ;10-12). T-test. p-values: (#) p-<0,0001, (***) p-<0,001, (**) p-<0,01, (*) p-<0,05, (ns) not significant.

As part of a comprehensive histopathological examination, we found that, consistent with the observed loss of fat mass, both female and male *Hoip*$^{A\text{-}KO}$ mice exhibited adipocyte hypertrophy in WAT (ScWAT and GWAT), accompanied by marked immune infiltration and fibrosis (red arrows) (Figure 3.3.29 A and B). Both sexes also showed spontaneous whitening of BAT (Figure 3.3.29 C). However, mirroring depot-specific patterns of fat mass loss, GWAT in males appeared to be the most necrotic depot (Figure 3.3.29 A), whereas in females showed the greatest degree of immune cell infiltration, extracellular matrix deposition (red arrows), and architectural disruption in ScWAT (Figure 3.3.29 B). Subdermal adipose tissue was completely absent in both sexes (red arrows) (Figure 3.3.29 A and B). Despite this, no spontaneous skin lesions were observed at 18 months of age, except in two males who developed wounds (likely due to fighting) and were excluded from the study.

Hepatic steatosis was observed only in *Hoip*$^{A\text{-}KO}$ females, despite the presence of severe lipodystrophy in both sexes (Figure 3.3.29 D). Last, since intestinal inflammation (IBD/Ulcerative colitis) (Boutros & Maron, 2011), (Bhagavathula et al., 2021) is associated with metabolic syndrome we performed a complete histological score of these mice. We found that male *Hoip*$^{A\text{-}KO}$ mice displayed mild inflammation in the colon (Figure 3.3.7 E and F), a feature not observed in females. These results once more highlight sex-dependent implications in the outcome of HOIP-dependent lipodystrophy during.

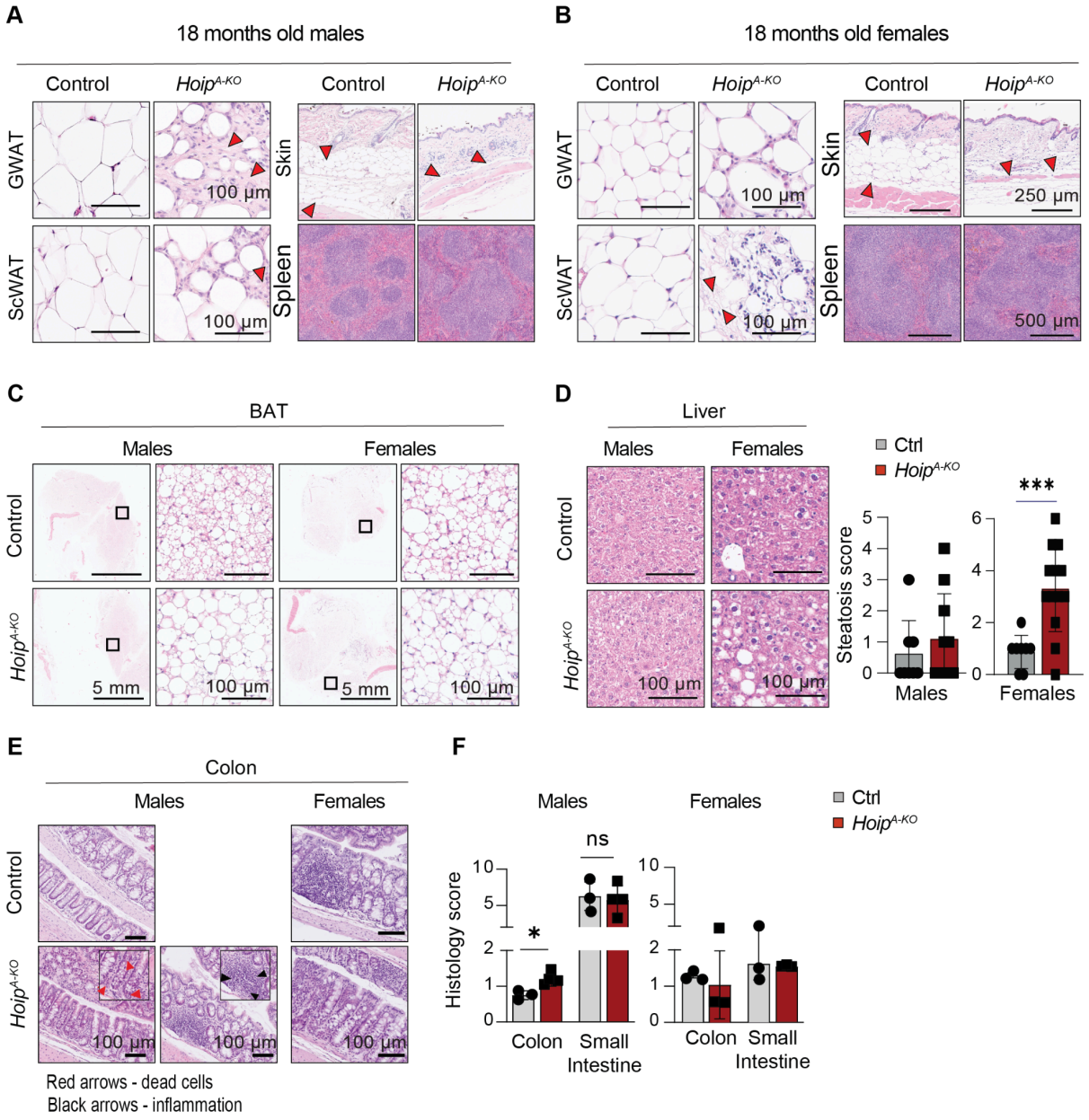

Figure 3.3.29 Representative H&E pictures of different tissues in males and females.

A and B -Representative HE staining *Hoip*$^{A\text{-}KO}$ males (right) and females (left) with their corresponding Cre- littermate controls at 18-months of age. C and D Liver Steatosis score of 18-months old males (right) and females (left) (n = 7-11). E- Representative H&E cut from Colon. F-Histological score Colon and Small intestine of 18 months-old males (n=4) and females (n=3). Statistical test: T-test. p-values: (#) p-<0,0001, (***) p-<0,001, (**) p-<0,01, (*) p-<0,05, (ns) not significant.

Surprisingly, the lipodystrophy phenotype was not translated into dyslipidemia in any of the sexes (Figure 3.3.30 A and B), while despite increased steatosis in females, old mice did not present signs of liver damage (Figure 3.3.30 A and B). Last, old *Hoip*$^{A\text{-}KO}$ presented males elevated urea in blood, which might indicate a risk of developing kidney failure (Figure 3.3.30 A)

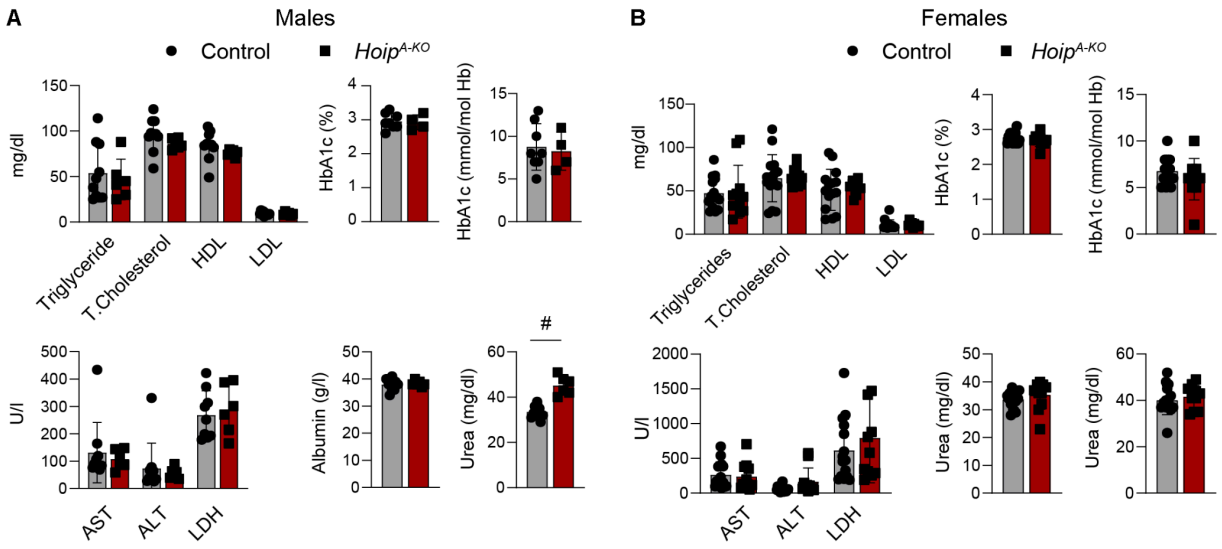

Figure 3.3.30 Blood values in *Hoip*$^{A-KO}$ males and females.

A and B -Representative HE staining *Hoip*$^{A-KO}$ males (right) and females (left) with their corresponding Cre- littermate controls at 18-months of age. C and D Liver Steatosis score of 18-months old males (right) and females (left) (n = 7-11). T-test. p-values: (#) p-<0,0001, (***) p-<0,001, (**) p-<0,01, (*) p-<0,05, (ns) not significant.

3.3.2.2 Further characterization of metabolic syndrome in Hoip-dependent lipodystrophic males

During necropsies of 18-month-old *Hoip*$^{A-KO}$ male mice, we consistently observed prostatic necrosis and hyperplasia (Figure 3.3.31 A), features commonly associated with obesity and type 2 diabetes in humans (Parsons et al., 2013; Tzenios et al., 2022) Given these findings, we expanded our analysis to evaluate additional metabolic syndrome–related comorbidities First we evaluated cardiac dysfunction a potential secondary hallmark of MetSyndrome frequently linked to ageing (C. Li et al., 2022). In our complete cardiological assessment we could not detect significant cardiac defects in terms of stroke volume (SV), effusion fraction (EF) or end diastolic volume (EDV), except for a slight, albeit significant, increase in the heart rate of the *Hoip*$^{A-KO}$ males (Figure 3.3.31 B).

Continuing with the characterization of insulin resistance we performed an insulin staining in pancreatic β-cells (Figure 3.3.31 C). β-cells exhaustion and islet hyperplasia was observed in aged *Hoip*$^{A-KO}$ evidenced by a higher islet area (Insulin +) ratio (Figure 3.3.31 C). Hormonal analysis further revealed increased insulin in blood in *Hoip*$^{A-KO}$, corroborating the insulin staining in situ, as well as lower leptin and adiponectin, altogether indicating metabolic imbalance (Figure 3.3.31 D and E). Once more, no dyslipidemia was observed in line with what we observed in HFD-fed mice (Figure 3.3.31 F).

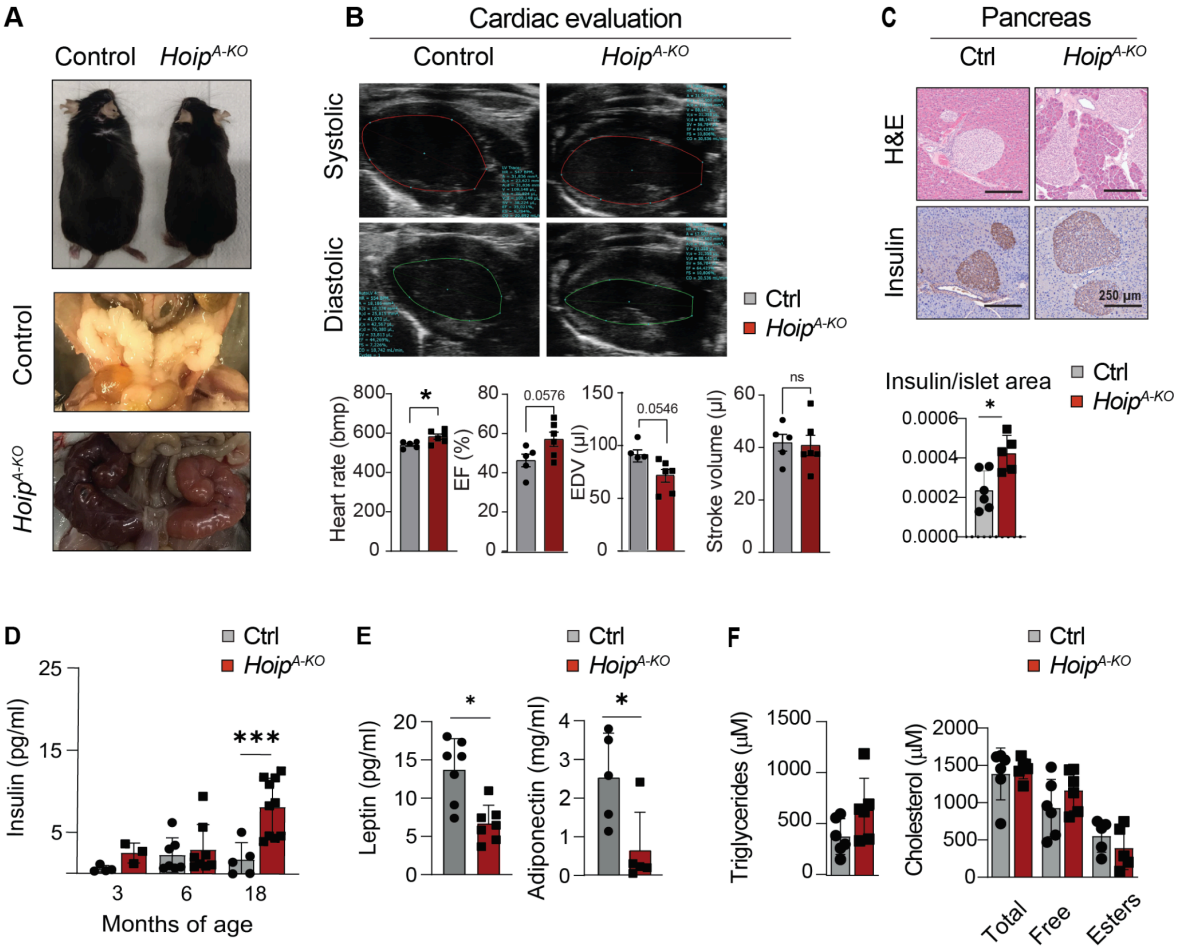

Figure 3.3.31 Further observations in *Hoip*$^{A\text{-}KO}$ males.

A- Up: Representative picture of normal fed 18 months-old males, down: seminar vesicles of 18 months-old males. B- Echocardiogram evaluation of 18 months-old males (n=5-7). C- Insulin staining of pancreas of 18 months-old males Positive insulin area was normalised to pancreas area and expressed in ratio. D- Insulin blood serum levels of normal fed 18 months-old males (n = 5-8). E-Leptin and adiponectin levels in serum of 18 months-old males (n=5-7). F-Blood Triglycerides and Cholesterol species of 18 months-old males (n=5-7) T-test. p-values: (#) p-<0,0001, (***) p-<0,001, (**) p-<0,01, (*) p-<0,05, (ns) not significant.

In sum, old *Hoip*$^{A\text{-}KO}$ presented lower insulin sensitivity in both sexes as compared to littermates, however this was not sufficient to induce hyperglycemia and T2D. On the other hand, Hoip-dependent lipodystrophy exhibited distinct sex-specific features in the onset of metabolic syndrome. In males, HOIP deficiency in adipocytes led to early GWAT compartment depletion, accompanied by marked colon inflammation and the formation of enlarged, abnormal necrotic seminar vesicles. Interestingly, these males did not display exacerbated liver steatosis or structural abnormalities in the spleen. In contrast, females with adipocyte HOIP-loss predominantly showed ScWAT necrosis (although also GWAT was affected) , and presented liver steatosis without apparent colon inflammation. These

observations highlight a gender-specific response to lipodystrophy and suggest a differential sensitization towards developing metabolic syndrome upon loss of linear ubiquitin chains.

This sexual dimorphism in the metabolic consequences caused by HOIP deficiency underscores the complexity of adipose tissue regulation and its systemic effects, emphasizing the need for gender-specific considerations in the study and treatment of metabolic disorders.

3.3.2.3 Sex differences in LUBAC expression during ageing in humans

Given that Hoip deletion led to differential outcomes in elderly males and females with clear depot and sex specific effects, we evaluate LUBAC expression in adipose tissue during ageing in humans.

In males we found an upregulation of LUBAC components during ageing (HOIP, HOIL-1 in both ScWAT and VAT, while SHARPIN only in VAT) (Figure 3.3.32 A-C and 3.3.33 A-C). Curiously these observations do not apply for females, who seem to have a more stable expression of LUBAC during lifespan. Curiously in ScWAT increased eLUBAC expression in males was in line with increased Casp8 levels (Figure 3.3.32 D), suggesting a possible activation of apoptotic programs, while no differences were observed in females. Last, we found no differences between MLKl and TNFR1 expression in ScWAT or VAT during ageing in any of the groups (Figure 3.3.32 D and E and 3.3.33 D and E).

Thus, we corroborate our observations in human adipose tissue demonstrating that LUBAC expression exhibits sex-specific differences during ageing. Our results suggest that males have a higher dependency on LUBAC activity during ageing in AT, or alternatively, that ageing-associated signaling pathways induce LUBAC expression more strongly in males. In contrast, female AT appears more resistant to such changes. This sex-dimorphic regulation of LUBAC may underlie the differential AT remodeling and metabolic outcomes observed in ageing populations and corresponding mouse models. Although we speculate that LUBAC expression in AT could contribute to prevent cell death during ageing processes, further studies are required to establish correlations between LUBAC expression and metabolic health in aged populations.

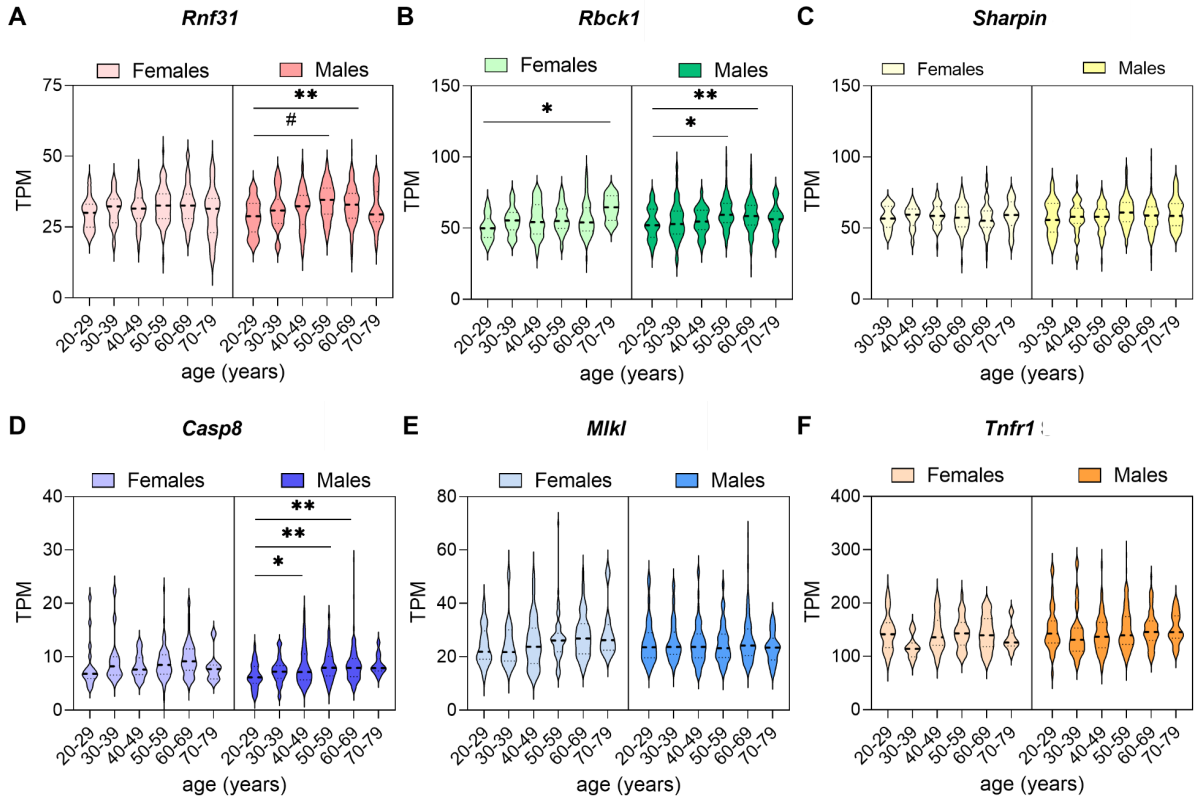

Figure 3.3.32 LUBAC components RNA expression in human ScWAT increase in male during ageing.

Transcripts per million (TPM) of A- HOIP, B-HOIL-1, C, SHARPIN, D-Caspase8, E- MLKL, F-TNFR1. GTEx Portal v8 in October 2022 on Subcutaneous WAT (ScWAT). Levels of expression of genes of interest were evaluated in adipose tissue (subcutaneous) of non-diseased individuals clustered by age.Statistical analysis: 1-way ANOVA against youngest cohort (20-29) applying Bonferroni correction for multiple comparisons. p-values GP: (#) p-<0,0001, (***), p-<0,0002;(**) p-<0,0021; (*) p-<0,0332; not clarified, p->0,0333.

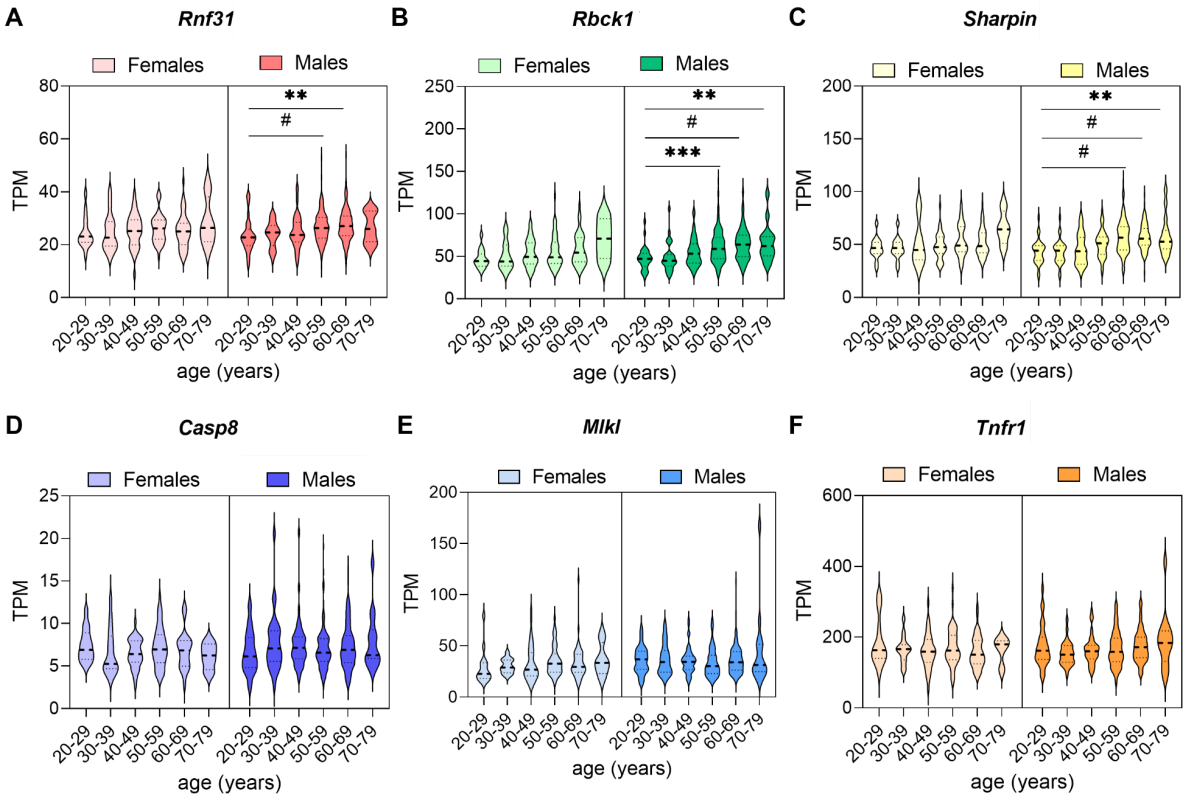

Figure 3.3.33 LUBAC components RNA expression in human GWAT increase in male during ageing.
Transcripts per million (TPM) of A- HOIP, B-HOIL-1, C, SHARPIN, D-Caspase8, E- MLKL, F-TNFR1. GTEx Portal v8 in October 2022 on Visceral/Gondal WAT (GWAT). Levels of expression of genes of interest were evaluated in adipose tissue (visceral) of non-diseased individuals clustered by age.Statistical analysis: 1-way ANOVA against youngest cohort (20-29) applying Bonferroni correction for multiple comparisons. p-values GP: (#) p-<0,0001, (***), p-<0,0002;(**) p-<0,0021; (*) p-<0,0332; not clarified,

3.3.3 Summary section 3.3

Results in section 3.3 highlight the role of linear ubiquitination in adipose tissue homeostasis. *Hoip*$^{A\text{-}KO}$ mice presented spontaneous lipodystrophy phenotype in normal fed conditions, which was dependent on caspase 8 cell death execution. In addition, HOIP was demonstrated to play a crucial role in adipocyte size, likely attributable not only to the prevention of cell death, but also to its function in NF-κB regulation.

In the case of HFD challenge, it further elucidated the metabolic consequences of HOIP deficiency, revealing that loss of linear ubiquitination leads to excessive Casp8-dependent-apoptosis under obese conditions. This cell death-driven inflammation accelerates the development of diabetes and MASLD in HFD-fed Hoip$^{A\text{-}KO}$ mice, despite their leaner phenotype. Consistent with data from human obesity studies, the absence of linear ubiquitination in adipocytes specifically intensified diabetic features during the obesity

challenge. Interestingly, despite fat mass and adipose AT function being restored in *Hoip*$^{A\text{-}KO}$*;Casp8*$^{A\text{-}KO}$ mice, these animals still exhibited enlarged adipocytes and increased immune cell infiltration, despite the absence of DNA fragmentation as indicated by TUNEL staining but no differences in caspase 3 activation, suggesting a possible sub-lethal activation of the cell death machinery. Importantly, our findings also provide new insights into a potential metabolic function o*f Casp8* in adipocytes, particularly its impact on cholesterol homeostasis. Notably, our findings on the metabolic impact of caspase 8 deletion in adipocytes contradicted some observations from previous reports (Luk et al., 2023), particularly its effects on cholesterol homeostasis.

Moreover, the spontaneous Hoip-dependent-lipodystrophy predisposes mice to metabolic complications during ageing. Aged *Hoip*$^{A\text{-}KO}$ mice exhibited reduced insulin sensitivity in both sexes compared to littermates, although this was insufficient to induce T2D. Furthermore, *Hoip*$^{A\text{-}KO}$ mice manifested distinct sex-specific features in the onset of metabolic syndrome, underscoring the need for gender-specific considerations in metabolic disorder research and treatment.

Last, LUBAC expression in human AT increases with ageing in a sex- specific manner, showing upregulation in males, while females maintain stable levels, suggesting a sex-dependet regulation that may influence AT remodeling during ageing.

Taken together, our results underscore the importance of LinUb and Casp8 in preserving adipose tissue integrity, ensuring metabolic and inflammatory balance during both obesity and aging.

3.3.4 Author contribution section 3.3

Armel Hyoubi from Peltzer lab performed the following histological stainings: F480, CD45, CC3, UCP-1 and TUNEL. Öykü Kaya as part of the Peltzer lab performed Insulin Staining and quantification in *Hoip*$^{A\text{-}KO}$ aged mice, while also contributing to establishing UCP-1 staining. Ali Abdalla performed the GWAT RNAseq and Cell type deconvolution. Julian Rodefel optimized adipocyte distribution protocol and performed all the corresponding quantifications. Elena Wagner and Holger Winkels performed the Electrocardiogram analysis including analysis and figure preparations. Matea Poggenberg prepared the intestine swiss roles and quantified the inflammation score on these samples including figure visualization. Andreas Lindhorst and Martin Gericke performed and quantified the CD163,Mac2 staining in GWAT. Yuan Wang assisted in mouse work and performed mice genotyping. Joëlle Dimmler assisted and contributed to ScWAT WB. Liane Gardeweg, Jutta Schillings, Pegi Koci,

assisted in mouse work, tissue´s H&E scanning and data curation. Jutta Schillings also performed liver qPCRs. Pegi Koci first established TUNEL staining in adipose tissue. Francesca Bonechi and Lucas Valdez Capuccino, assisted in mouse work . Micheal Singer and Tom Luedde facilitate contact with a clinic pathologist and deliver liver samples to perform the steatosis score, Dr. Aslihan Yavas, performed all the steatosis scores in this thesis. Lipidomics was performed by the CECAD facility. The remaining experiments, data analysis, interpretation, visualization and data curation were performed by the author of this thesis.

3.4. Linear ubiquitination protects against MASLD during obesity

E3 activity of HOIL-1 plays a crucial role in LUBAC regulation. HOIL-1 E3 conjugates monoubiquitin onto all LUBAC subunits, followed by HOIP E3-mediated conjugation of linear chains onto the monoubiquitin (Fuseya et al., 2020, 2024).

Mice models in which in Hoil-1 ligase activity is impaired by harbouring a mutation of C458 (C458S or C458A) are depleted from Hoil-1-dependent monoubiquitination (Fuseya et al., 2020; Kelsall et al., 2019). As a result of this mutation, there is an overall increase in LUBAC activity, which leads to enhanced NF-κB activation and provides protection against cell death. Mice carrying this mutation are fertile, born in normal Mendelian ratios, and have a typical lifespan. However, it is important to note that mice lacking HOIL-1 activity exhibit an increased interferon response, enhanced activation of T cells and macrophages, protection against liver damage and bacterial infections, and accumulate polyglucosan in the brain, heart, and other organs as they age (Fuseya et al., 2020, 2024; Kelsall et al., 2022; Petrova et al., 2021). Implications of these models in the context of metabolic syndrome have not been previously established.

Given our observations from obese patients and the association between LUBAC expression and metabolic fitness, we aimed to evaluate the impact of increased linear ubiquitination during diet-induced obesity. To this end, we utilized mice expressing catalytically inactive HOIL-1 (hereafter called *Hoil-1*^{C458A}) and challenged them with a HFD to assess the metabolic consequences of increased linear ubiquitin chains in metabolic tissues, particularly the liver and adipose tissue.

Furthermore, as *Hoip*^{KO} preadipocytes demonstrated marked sensitization to TNF-induced cell death, we expanded our investigation to evaluate the response of *Hoil-1*^{C458A} primary cells to TNF-induced stimuli. This comprehensive approach allowed us to examine the cell-type specific effects of altered linear ubiquitination in the context of metabolic stress and inflammation.

3.4.1 Increased linear ubiquitination protects against liver lipid deposition

In line with the mutation, we observed increased linear chains in adipose tissue (Figure 3.4.1.A). However, contrary to expectations, this did not affect weight gain (Figure 3.4.1.B). This result was unexpected, since previous studies have shown that activation of NF-κB in adipocytes, either by overexpression of p65 (T. Tang et al., 2010) or constitutive activation of IKKβ (Jiao et al., 2012) leads to increased energy expenditure under basal conditions,

improved insulin sensitivity and protection against weight gain upon HFD challenge (despite exacerbated local and systemic inflammation). To further corroborate our findings, we monitored food consumption during both diets and found similar feeding patterns between the groups (Figure 3.4.1.C). Additionally, no differences in normal fed or fasting glucose levels were recorded (Figure 3.4.1.D and E).

Results suggest that the increased linear ubiquitination in *Hoil-1*^{C458A} mice does not significantly impact weight gain or glycaemia when challenged with a HFD, despite the observed increase in NF-κB activation.

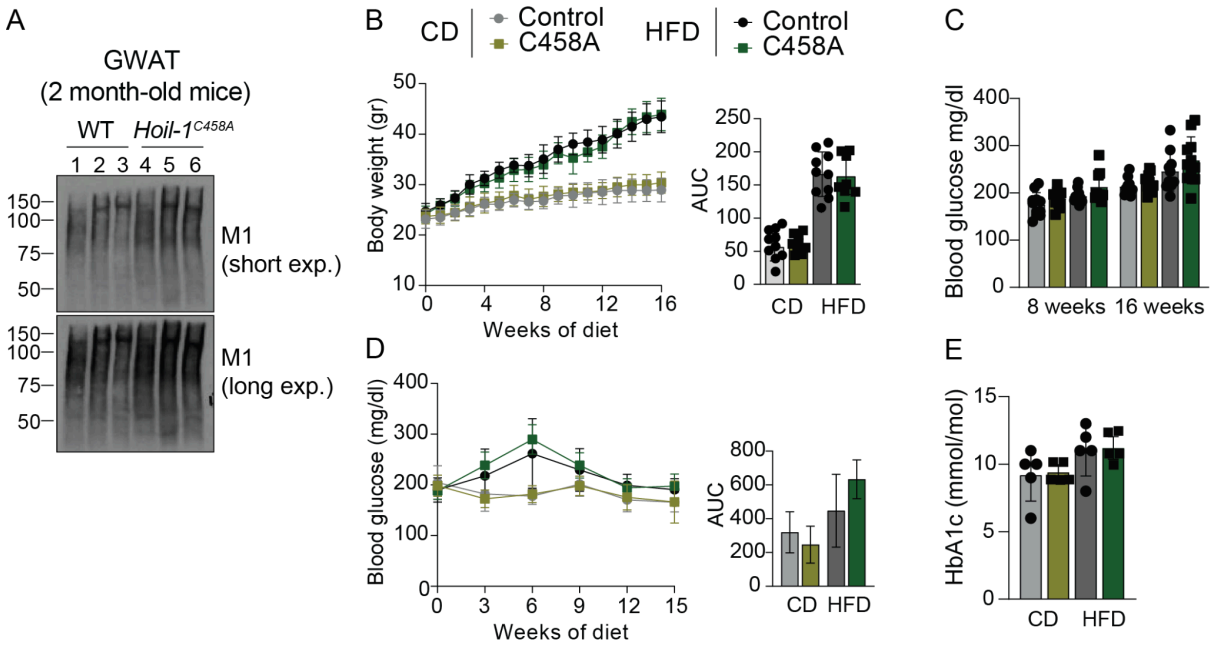

Figure 3.4.1 Increase linear chains does not interfere with weight gain or glucose homeostasis during HFD.

A- Protein lysates from GWAT of 2 months old male mice fed with chow diet (n=3) B-Gain weight curve of males fed with CD and HFD during 16 weeks (n=8-11). C- Average food consumption per day normalized to total body weight after 16 weeks measured in metabolic cages during 72 hs (n=3-4). D-Normal blood glucose monitoring during 16 weeks of diet (n=8-11). E- Blood glucose levels after 6 hs fasting (n=8-11) Statistical test: 2-way ANOVA grouped by diet applying Bonferroni correction for múltiple comparisons. p-values: (#) p-<0,0001, (***) p-<0,0002, (**) p-<0,0021, (*) p-<0,033, (ns) not significant.

Continuing with our evaluation of mutant mice, we performed a comprehensive histopathological analysis using H&E staining of several organs after 16 weeks of diet (Figure 3.4.2 A). We observed smaller adipocytes in the ScWAT during CD, which translated to decreased ScWAT mass during HFD (Figure 3.4.2 B) (Jiao et al., 2012; T. Tang et al., 2010). A similar tendency was observed in gonadal white adipose tissue (GWAT) with a

marked increase in immune infiltration, consistent with previous studies(Jiao et al., 2012; T. Tang et al., 2010). However, this did not translate into changes in tissue weight in this compartment (Figure 3.4.2 C). We did not observe weight changes in other evaluated tissues (BAT, heart, and liver), with exception of the spleen (Figure 3.4.2 C-G). An interesting observation was a slight protection against DIO-induced whitening of BAT (Figure 3.4.2 A), potentially suggesting higher or more conserved mitochondrial content compared to wild-type littermate controls (Kajimura et al., 2015), a feature typically diminished during obesity (Huo et al., 2024).

Another marked feature of mutant mice was the reduction of lipid deposition in the liver during HFD (Figure 3.4.2 A). However, this did not translate into a reduced steatotic score, possibly due to increased immune infiltration, another hallmark of this scoring system (Figure 3.4.2 A and H). We did observe a slight, though not significant, protection against liver damage, indicated by decreased blood serum values of ALT (Figure 3.4.2 I), with no differences in AST or LDH (Figure 3.4.2 J and K). Additionally, we observed similar β-cell islet sizes in the pancreas. Despite the aforementioned splenomegaly, no major differences in the white and red pulp of the spleen were observed. Last, in line with the observation in ScWAT, subdermal WAT depots appeared thinner in HFD-fed mutant mice, with reduced adipocyte size under the skin (Figure 3.4.2 A).

These findings suggest that the mutant mice exhibit altered adipose tissue distribution and composition and a potential protection against some aspects of diet-induced metabolic dysfunction, such as liver steatosis.

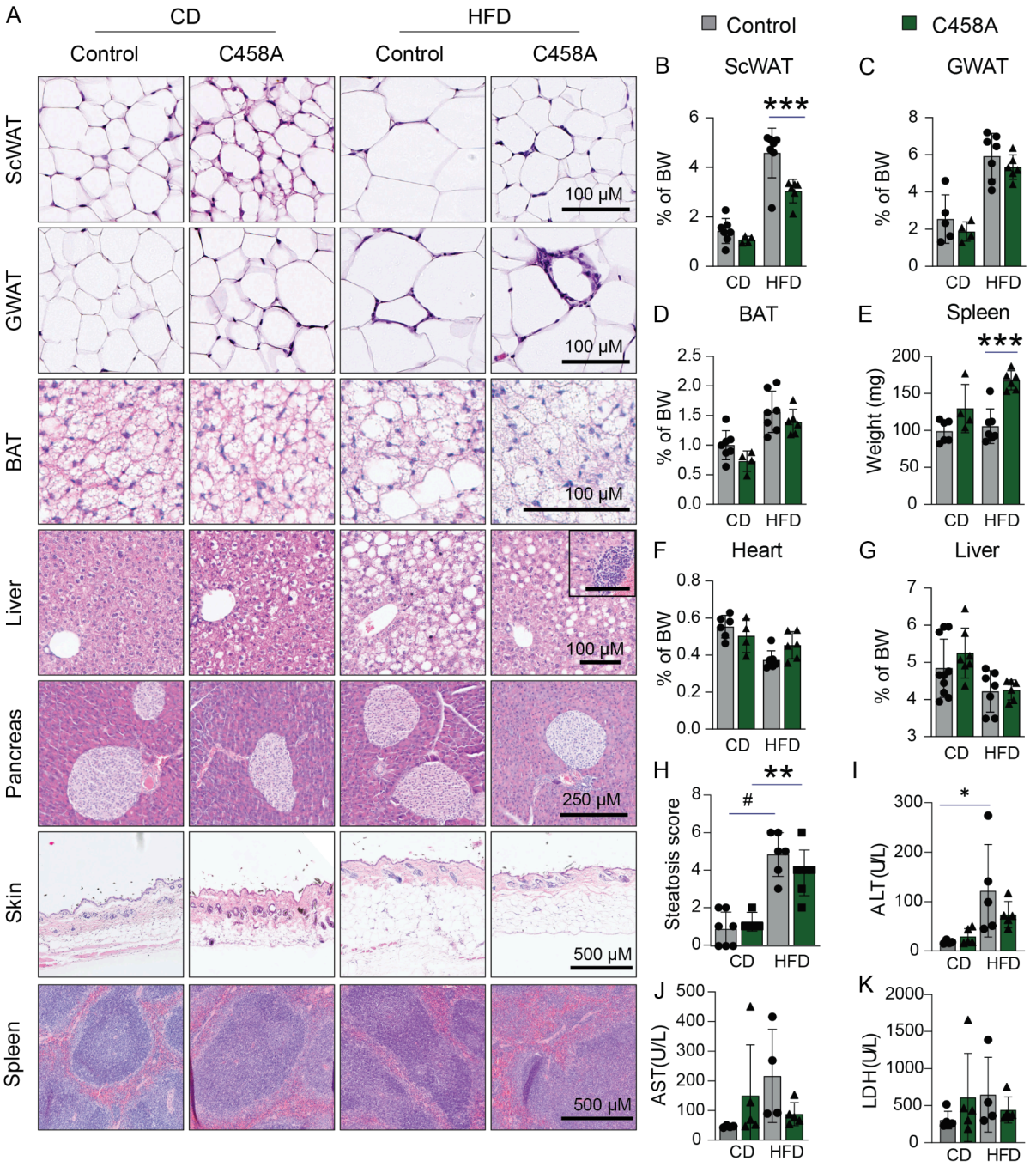
A
CD
HFD
Control
C458A
Control
C458A
ScWAT
GWAT
BAT
Liver
Pancreas
Skin
Spleen
100 μM
100 μM
100 μM
100 μM
250 μM
500 μM
500 μM
Control
C458A
B
ScWAT
% of BW
***
C
GWAT
% of BW
D
BAT
% of BW
E
Spleen
Weight (mg)
***
F
Heart
% of BW
G
Liver
% of BW
H
Steatosis score
**
#
I
ALT(U/L)
*
J
AST(U/L)
K
LDH(U/L)
CD
HFD

Figure 3.4.2 Increase linear chains prevents ScWAT expansion and protects against HFD-induce whitening.

A- Representative H&E pictures of different tissues from male mice under CD and HFD during 16 weeks (n=5-7). Tissue weight normalised to total body weight at 16 weeks of diet B-ScWAT. C-GWAT. D-BAR. E-Spleen (in mg). F-Heart. G-Liver. Statistical test: 2-way ANOVA grouped by diet applying Bonferroni correction for múltiple comparisons. p-values: (#) p-<0,0001, (***) p-<0,0002, (**) p-<0,0021, (*) p-<0,033, (ns) not significant. H-Steatosis scores of liver H&E at 16 weeks of diet. Liver damage enzyme in serum at 16 weeks of age (n=5) I-ALT. J-AST. K-LDH. Statistical test: 2-way ANOVA applying Bonferroni correction for múltiple comparisons. p-values: (#) p-<0,0001, (***) p-<0,0002, (**) p-<0,0021, (*) p-<0,033, (ns) not significant.

To further understand the liver dynamics in these mice, we conducted a comprehensive lipidomic panel of the mutants after 16 weeks on their respective diets. This analysis revealed a significant reduction in total liver triglycerides during HFD feeding (Figure 3.4.3 A), particularly in the 18:2 species corresponding to linoleic acid (Figure 3.4.3 B), a major component of very low-density lipoprotein (VLDL) and chylomicrons.

Moreover, Z-score analysis of diglyceride abundance revealed an overall decrease across all species in C458A mutants under basal conditions. Interestingly, in WT controls, HFD feeding induced a notable shift from 14 and 16 carbon species towards 18 and 20 carbon diglycerides (Figure 3.4.3 C), likely as a result of increased reesterification of existing or ingested lipids rather than de novo lipogenesis during HFD. Although mutant mice exhibited a similar trend, they consistently maintained lower levels of all diglyceride species, even under HFD conditions. Consistent with these findings, we also observed a decrease in cholesterol species containing 18 carbons and 2 unsaturated bonds (18:2) (Figure 3.4.3 C), which appeared to be the major contributor to the reduction in total cholesterol levels in mutant mice livers (Figure 3.4.3 D). The 18:2 formula corresponds to cholesteryl linoleate, a cholesterol ester of linoleic acid, which is a key component of plasma lipoproteins, particularly LDL and HDL. Despite these changes, total cholesterol levels did not show significant differences (Figure 3.4.3 E). Last, given the association of certain phosphosphingolipids, especially ceramides, with insulin resistance and inflammation during obesity, we investigated potential alterations in the pattern of these lipid species. However, no significant differences were found between the groups (Figure 3.4.3 F).

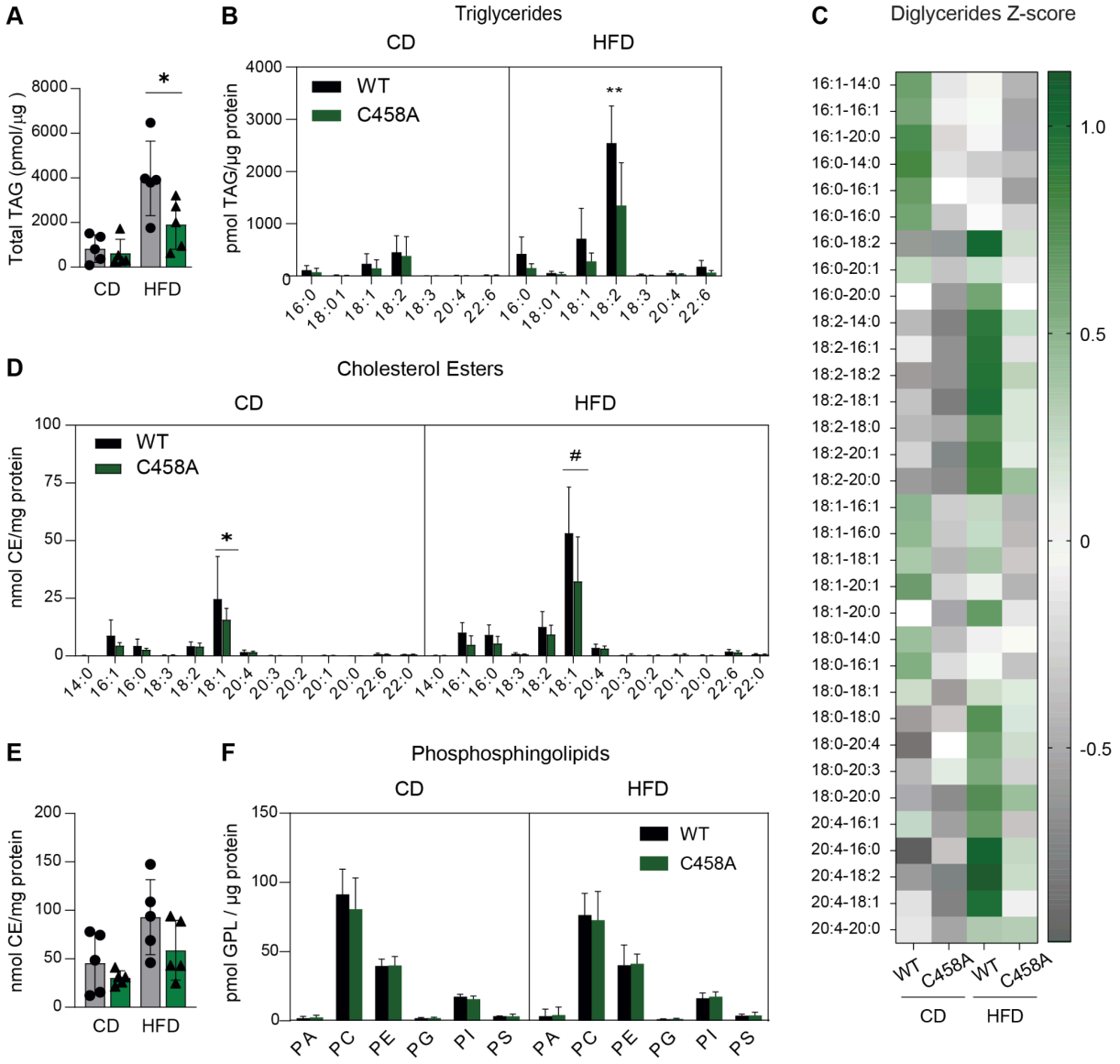

Figure 3.4.3 Increased linear ubiquitination protects against liver triglycerides and cholesterol species deposition during HFD.

Lipidomic profile of males after 16 weeks of diet (n=5): A- Total triglycerides normalized to grams of protein. B- Triglyceride species per diet and genotype normalized to grams of protein. C- Z-score of diglyceride species normalized to grams of protein. D- Cholesterol Ester (CE) species per diet and genotype normalized to grams of protein. E- Total CE normalized to grams of protein. F- Phosphosphingolipid species normalized to grams of protein. Statistical test: 2-way ANOVA grouped by diet applying Bonferroni correction for multiple comparisons. p-values: (#) p<0.0001, (***) p<0.0002, (**) p<0.0021, (*) p<0.033, (ns) not significant.

To determine whether the protection against liver steatosis could be attributed to alterations in insulin sensitivity, we further evaluated the metabolic performance of these mutant mice. No differences in basal insulin metabolism were observed under basal conditions at any of the given timepoints (Figure 3.4.4 A and C). Although we found a slight protection against insulin resistance in the mutant mice at 8 weeks of HFD feeding (Figure 3.4.4 C), this

difference was no longer appreciated at a later time point (Figure 3.4.4 D). Moreover, no significant differences in glucose metabolism were observed at either 8 or 16 weeks (Figure 3.4.4 E and F).

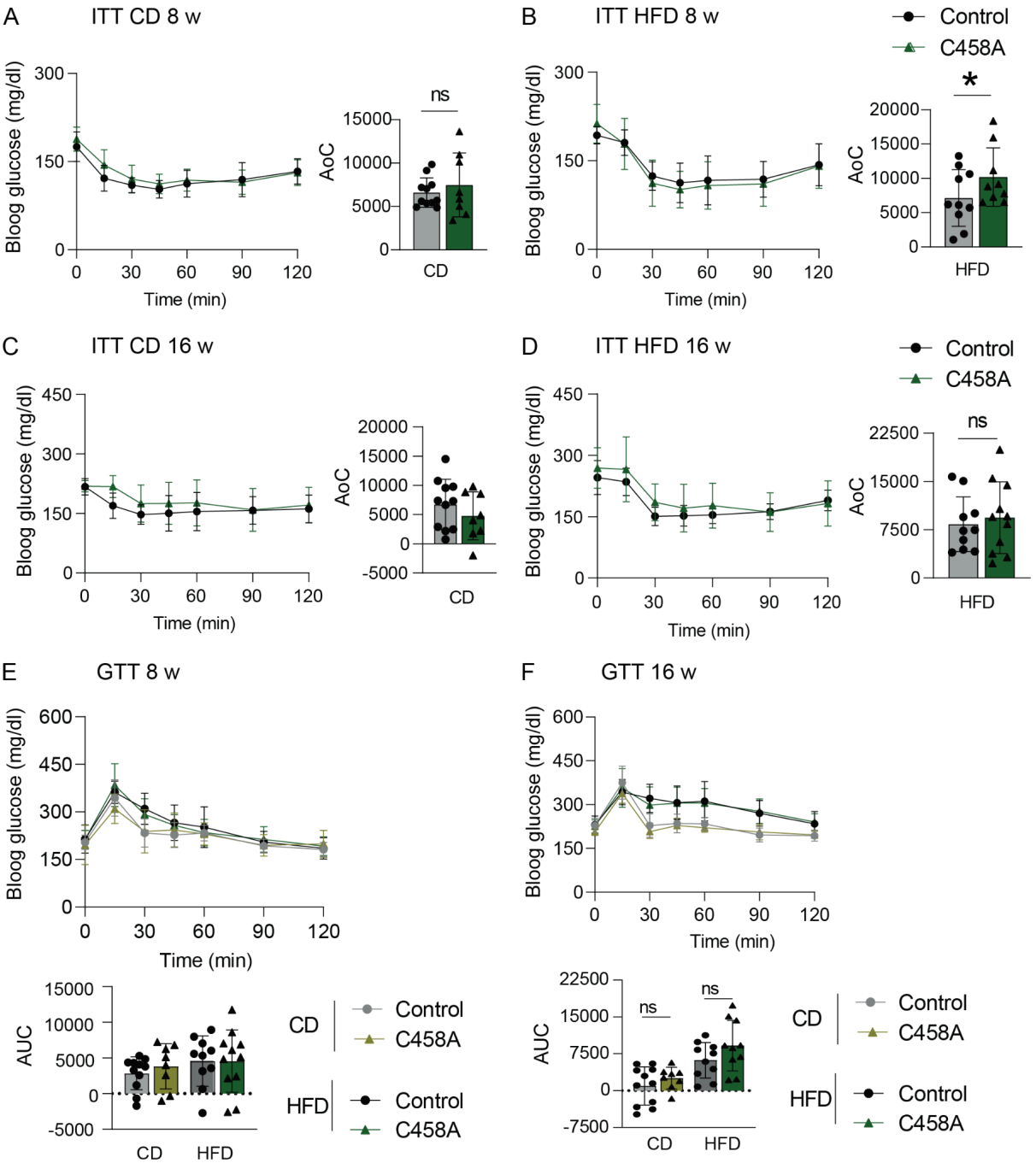

Figure 3.4.4. Increased linear chains do not affect glucose metabolism during HFD challenge.

Insulin tolerance test of male mice under CD or HFD. A- CD 8 weeks (n=8-11), B- HFD 8 weeks (n=9-12). C- CD 16 weeks (n=8-11), B- HFD 16 weeks (n=9-12). Oral Glucose tolerance test of male mice under E- 8 weeks of diet (n=8-12), D- 16 weeks of diet (n=8-12). Statistical test: 2-way ANOVA grouped by diet applying Bonferroni correction for múltiple comparisons. p-values: (#) p-<0,0001, (***) p-<0,0002, (**) p-<0,0021, (*) p-<0,033, (ns) not significant.

Changes in lipid composition could also result from alterations in lipid metabolism pathways. To further assess the metabolic state of these mice, we performed a standard blood panel checkup. Despite showing no difference in the insulin tolerance test, mutant mice exhibited decreased total insulin levels at the endpoint in the HFD groups (Figure 3.4.5 A). However, consistent with previous observations (Figure 3.4.1 and 3.4.4), no alteration in hemoglobin glycosylation was observed (Figure 3.4.5 B). Interestingly, although liver triglyceride content was lower (Figure 3.4.3), blood triglyceride levels remained unchanged (Figure 3.4.5 C). In contrast, the HFD-fed mutant group showed a significant reduction in nearly all blood cholesterol species measured, except for direct LDL (Figure 3.4.5. D-H). Notably, despite adiponectin typically being inversely correlated with fat mass content, mutant mice did not exhibit variations in circulating adiponectin levels (Figure 3.4.5 I).

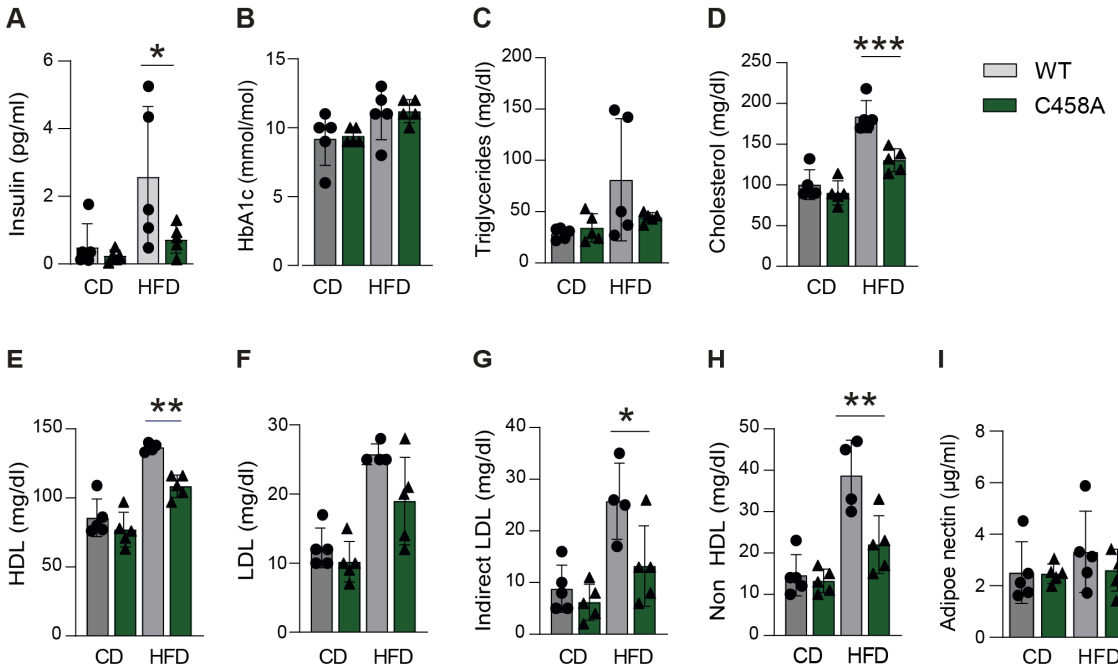

Figure 3.4.5 Increase LUBAC activity decreases blood cholesterol levels during HFD.

Blood values after 16 weeks of diet (n=4-7) A-Insulin, B- Glycosylated haemoglobin, C- Triglycerides, D- Total Cholesterol, E- High Density Cholesterol , F- Low Density Cholesterol , G- Indirect-Low Density Cholesterol , H- Non High Density Cholesterol. Statistical test: 2-way ANOVA applying Bonferroni correction for múltiple comparisons. p-values: (#) p-<0,0001, (***) p-<0,0002, (**) p-<0,0021, (*) p-<0,033, (ns) not significant.

3.4.1.2 Linear ubiquitination alters adipose tissue distribution and seems to promote thermogenesis

Enlarged adipocytes are linked to obesity-related comorbidities such as Insulin-resistance, T2D, dyslipidemia, and cardiovascular disease. Thus, measuring adipocyte size and area is crucial for understanding the metabolic impact of fat tissue expansion (Veilleux et al., 2011; Weyer et al., 2000). In mutants with increased LUBAC activity, adipocytes in the ScWAT compartment appeared smaller upon HFD compared to WT controls (Figure 3.4.6 A). This observation suggested a potential protective effect of enhanced LUBAC activity against obesity-related adipocyte hypertrophy. Despite this, our mean area and count analysis indicated no significant differences between the groups (Figure 3.4.6 A and C). Frequency histograms, which provide a more accurate representation of adipocyte size variability, showed a shift in the median towards smaller adipocytes with the Gaussian distribution in the mutant CD group. Suggesting that increased LUBAC activity might influence adipocyte size distribution even under normal dietary conditions.

In the GWAT compartment, the effects observed under CD were maintained without statistical significance in mean sizes (Figure 3.4.6 B and D). During HFD feeding, a notable alteration in the shape of the distribution curves of both groups was observed due to pronounced adipocyte size expansion (Figure 3.4.6 B), however, mutant cells presented a higher slope in their curve, a result that was also reflected in a reduced mean adipocyte area. This observation suggested that GWAT adipocytes responded differently to increased LUBAC activity compared to ScWAT adipocytes.

Adipocyte hypertrophy during HFD can ultimately lead to cell death. To further corroborate if cell death was also prevented in AT upon increased LinUb, we performed a TUNEL staining in both GWAT and ScWAT (Figure 3.4.6.A and B). As illustrated in the representative images and quantifications, increase of linear ubiquitination prevented HFD-induced cell death in both tissues (Figure 3.4.6 E and G). Intriguingly, despite lower cell death levels, an increase in immune infiltration can be observed in both challenged AT compartments evidenced by CD45+ area (Figure 3.4.6.A, B, F and H), possibly due to increased NF-κB activation.

However, since TUNEL single staining is ubiquitous towards all cell populations, we cannot exclude that also immune cells could benefit against HFD-induced cell death.

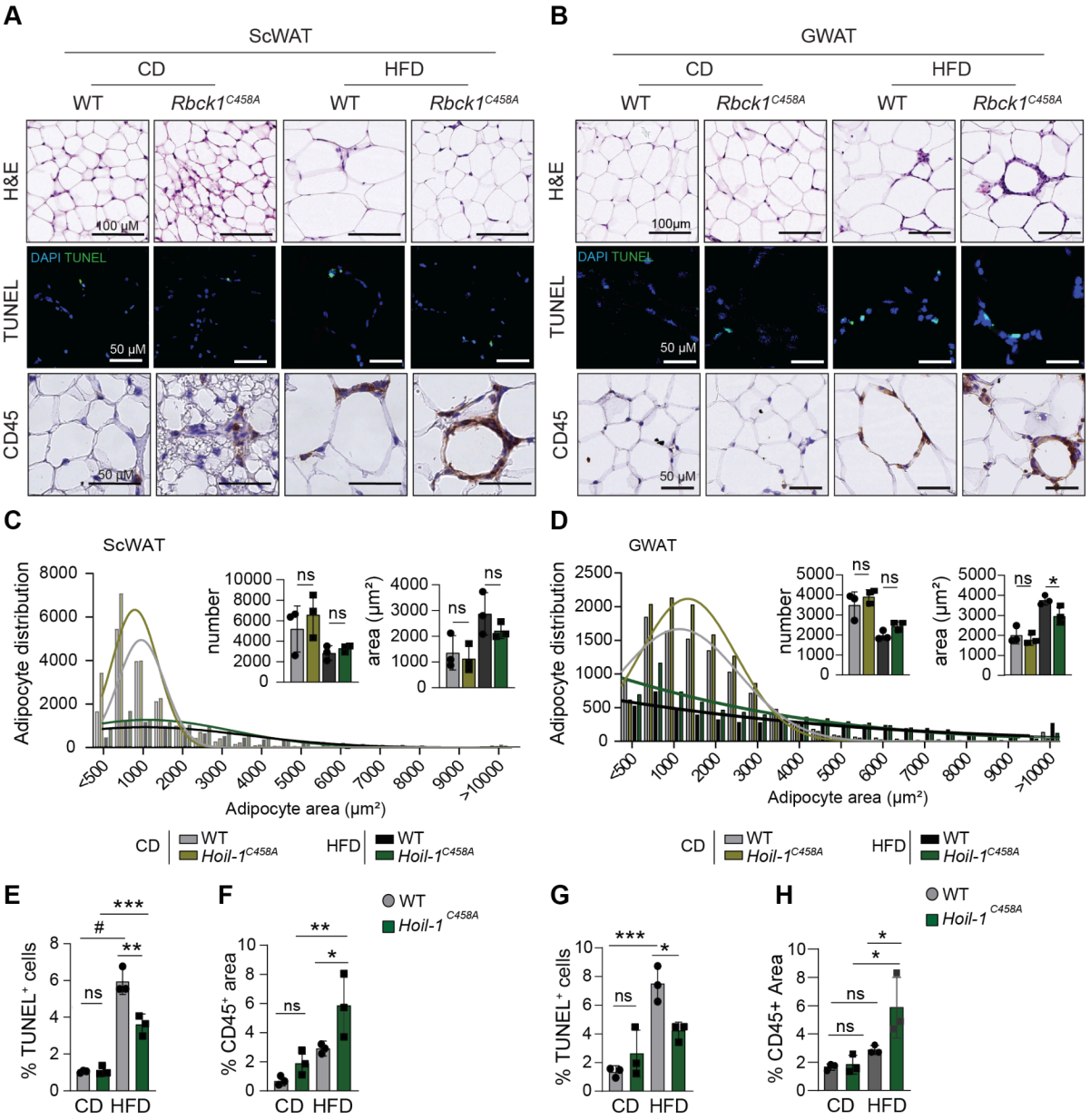

Figure 3.4.6 Increased linear ubiquitination protects against HFD-induced hypertrophy and cell death.

Representative pictures of H&E, TUNEL immunofluorescence and CD45 immunohistochemistry of A- ScWAT (n=3). B- GWAT (n=3). Adipocyte size distribution after 16 weeks of diet including mean area and number of adipocytes (n=3) of C- ScWAT, D-GWAT E- Percentage of TUNEL positive nuclei on ScWAT. F- Percentage of CD45 positive area in ScWAT. G- Percentage of TUNEL positive nuclei on GWAT. H- Percentage of CD45 positive area in ScWAT. Statistical test: 2-way ANOVA grouped by diet applying Bonferroni correction for múltiple comparisons. p-values: (#) p-<0,0001, (***) p-<0,0002, (**) p-<0,0021, (*) p-<0,033, (ns) not significant.

Given the observed protection against BAT whitening under HFD, reduced ScWAT expansion upon HFD and the preliminary H&Es suggesting increased browning in ScWAT of mutant mice (Figure 3.4.2), we hypothesized the increase LinUb was promoting thermogenesis. To assess this, anti-UCP-1 staining was conducted on both BAT and ScWAT tissues.

These analyses showed higher basal UCP-1 levels in ScWAT from mutant mice in CD, yet, the increase in UCP-1 positive areas within ScWAT was not uniform throughout the tissue (Figure 3.4.7 A) and did not translated in increased RER or caloric expenditure during CD (Figure 3.4.7 B). In addition, a strong brown adipocyte content preservation in *Hoil-1*^{C458A} animals against HFD-induced whitening was confirmed by UCP-1 density (Figure 3.4.7 C). Unfortunately, a proper quantification of UCP-1 content was not feasible due to issues with cell shape and limitations of the analysis software. Despite this conserved UCP-1 content in BAT, RER or energy expenditure in HFD did not reveal significant differences (Figure 3.4.7 D). Last, since immune cells can influence brown adipocyte differentiation, we also investigated whether enhanced Hoil-1 activity led to increased immune infiltration. While there was a trend toward greater CD45 positivity in mutant mice, quantification identified no significant differences among the groups (Figure 3.4.7 E).

Of note, whole-body oxygen consumption and RER are subject to factors beyond BAT and ScWAT activity, while the mere presence of UCP1 does not guarantee higher thermogenic output, as its activity must be triggered by other mechanisms, thus localised increased energy expenditure remains underscored in our model. However overall, our findings indicate that mitochondrial content and UCP-1 presence may be supported by LinUb.

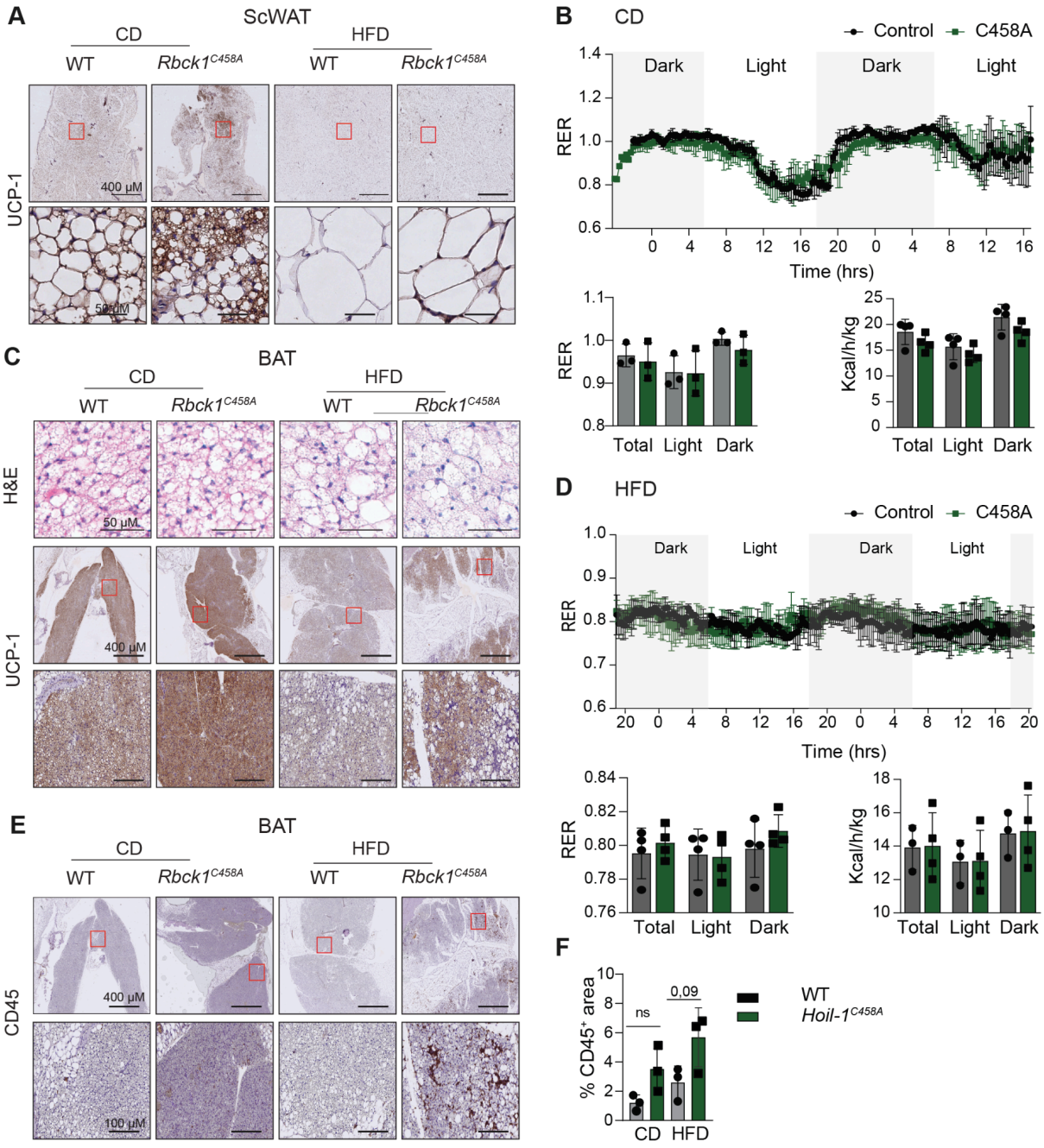

Figure 3.4.7 Increase linear chains seems to increase thermogenesis.

A. Immunohistochemistry staining of UCP-1 in ScWAT after 16 weeks of diet (n = 3). B. Metabolic cage measurements of males after 16 weeks of control diet (n = 3–4), including average 72-hour measurements of respiratory exchange ratio (RER) and calorie expenditure during light and dark cycles. C. Immunohistochemistry staining of UCP-1 in BAT after 16 weeks of diet (n = 3). D. Metabolic cage measurements of males after 16 weeks of HFD (n = 3–4), including average 72-hour measurements of respiratory exchange ratio (RER) and calorie expenditure during light and dark cycles. E. CD45 immunostaining of BAT after 16 weeks of diet. F. Quantification of CD45-positive area in (E). Statistical test: Two-way ANOVA grouped by diet, with Bonferroni correction for multiple comparisons. p-values: (#) $p < 0.0001$; () $p < 0.0002$; () $p < 0.0021$; () $p < 0.033$; (ns) not significant.

3.4.2 Increase linear ubiquitination protects against cell death.

Several studies suggest that LUBAC's primary role in TNF-dependent tissue homeostasis is the suppression of programmed cell death rather than solely activation of NF-κB signaling(K. Sasaki & Iwai, 2023). Consistent with this, our *Hoil-1*^{C458A} mutant mice, harbor a mutation protected against DIO-AT cell death (Figure 3.3.6). Interestingly, despite reducing cell death, increase in LiUb also led to increased CD45 positive cell infiltration. This suggests that while LUBAC-mediated suppression of cell death limits adipocyte loss, it does not completely prevent the inflammatory response associated with obesity (or, even promotes it by increasing NF-κB).

Given that TNF is a key inflammatory cytokine elevated during obesity and is associated with inflammation, adipocyte cell death and CLS formation (all also linked to metabolic syndrome) we sought to dissect how LUBAC influences TNF-induced cell death in distinct AT cell populations.

To address this, we employed ex-vivo models using primary preadipocytes, bone marrow-derived macrophages (BMDMs), and AT explants isolated from *Hoil-1*^{C458A} mice. These cells and tissues were subjected to apoptotic (TNF+BV6) and necroptotic (TNF+BV6+Zvad) stimuli through TNF in combination with sensitizers to mimic inflammatory cell death conditions (Figure 3.4.8 A). This approach allows us to dissect the cell type-specific effects of LUBAC hyperactivation on TNF-mediated cell death pathways within the adipose tissue microenvironment, providing insight into the molecular mechanisms by which LUBAC protects against obesity-associated AT dysfunction.

Experiments with primary preadipocytes isolated from ScWAT demonstrated that an increase in linear ubiquitin chains conferred protection against both apoptosis and necroptosis stimuli (TNF+BV6 and TNF+Zvad, respectively) (Figure 3.4.8 B). Notably, this protective effect diminished when K63 ubiquitination mediated by cIAPs (which facilitate the attachment of upstream M1 chains) was inhibited by BV6 (Figure 3.4.8 B). These results suggest that the antiapoptotic effect is likely due to upregulation of pro-survival NF-κB (Figure 3.4.8 A), which is basally active in mutant mice as we corroborated by WB (Figure 3.4.8 C).

Continuing with this hypothesis, we incubated GWAT explants with different TNF-dependent cell death treatments for 24 hours and assessed cell death levels by TUNEL staining (Figure 3.4.8 D). Mutant explants exhibited clear protection against TNF-induced apoptosis (TNF+BV6) compared to WT controls. In line with results from our *Hoip*$^{A\text{-}KO}$*;Casp8*$^{A\text{-}KO}$ model,

WT explants also showed reduced cell death when treated with TNF+BV6+Zvad, suggesting that inhibition of caspase activity partially rescues cIAP-depletion-induced apoptosis. Taken together with observations in HFD-challenged *Casp8*$^{A\text{-}KO}$ mice, these findings suggest that there is a decreased tendency toward necroptosis in AT/adipocytes, even in the presence of pan-caspase inhibition.

Unexpectedly, and consistent with previous publications (Weinelt et al., 2024), explants from mutant mice exhibited a pronounced sensitization to necroptosis under TNF+BV6+Zvad treatment. Notably, since TUNEL staining does not distinguish which cell populations are undergoing TNF-induced cell death in these conditions, we cannot rule out that the mutation differentially affects immune cells and adipocytes. Based on our results, it seems that LinUb promotes the execution of necroptosis machinery in mutant mice. However, considering that Casp8 deletion in adipocytes alone does not lead to aberrant necroptosis, and given the cellular heterogeneity within the tissue, the heightened sensitization to necroptosis may primarily occur in macrophages or other resident immune cells rather than in adipocytes themselves.

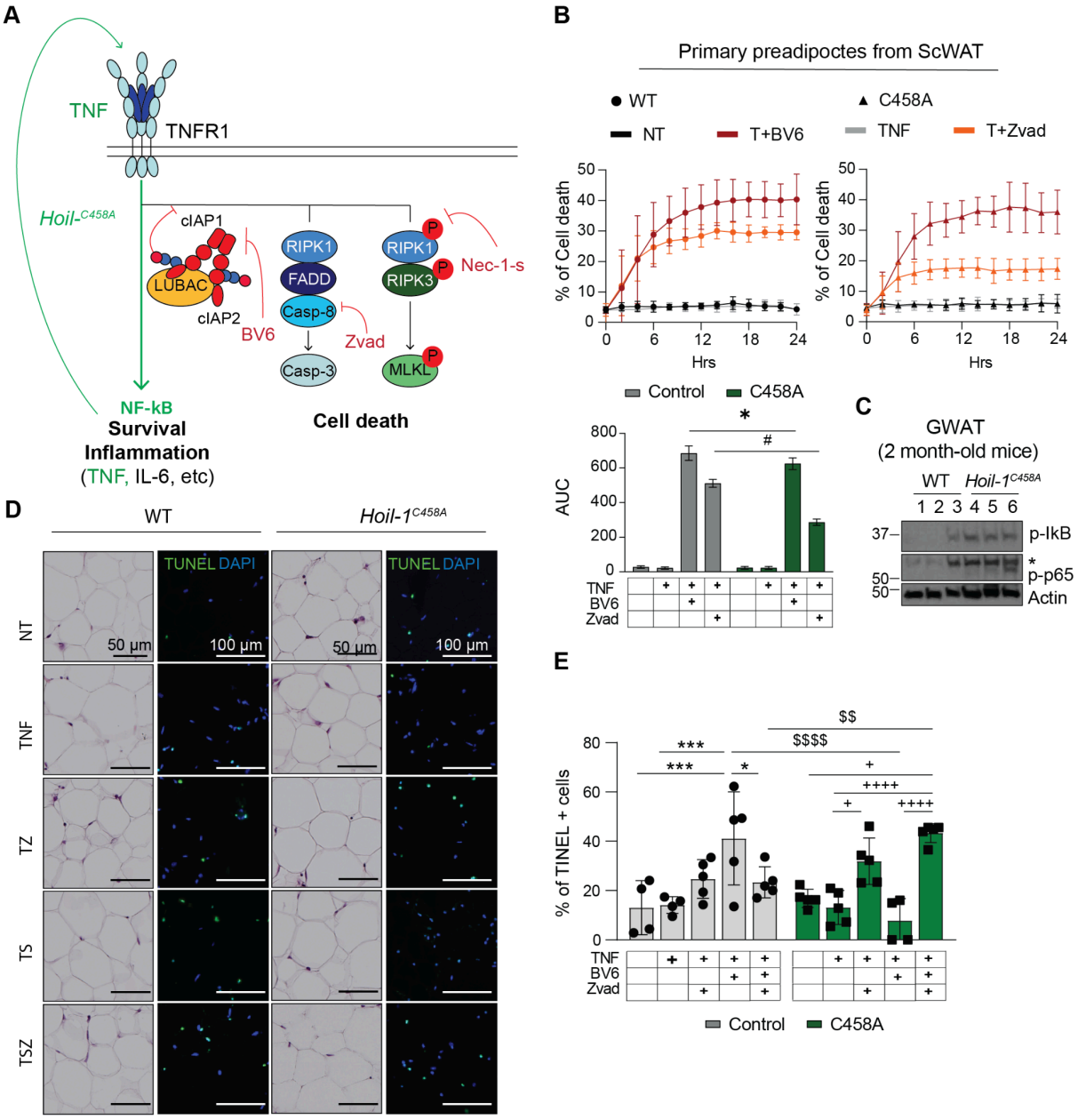

Figure 3.4.8 Hoil-1 catalytically inactive-derived preadipocytes are protected against TNF-induced cell death.

A-Diagram indicating where different drugs used in in vitro assays can induce or block TNF-dependent cell death, and how the Hoil-1^C458A mutation contributes to the TNF autocrine loop. B-Percentage of cell death of mouse derived ScWAT preadipocytes from 8 weeks old males measured by Incuctcyte (n=3) and AUC of the different treatments for comparison. C- Immunobloating of 2 months of tissue lysates form GWAT of male mice. D- TUNEL staining of GWAT explant of 4 month old male mice after 24 hs of the indicated treatment. E- Quantification of TUNEL positive cells of GWAT explants after 24 hs of treatment. Statistical analysis: 1-way ANOVA applying Bonferroni correction for multiple comparisons. For B only, p-values GP: (#) p-<0,0001, (***), p-<0,0002;(**) p-<0,0021; (*) p-<0,0332; (ns) p->0,0333. For D, symbols for comparison are (*) wt vs wt (treatment effect), ($) wt vs C458A within the same treatment (genotype effect) and (+) C458As C458A (treatment effect).

To further investigate how the mutation affects the main resident immune cells in AT, we evaluated the impact of increased LinUb on BMDMs subjected to TNF-induced cell death treatment.

In WT cells, addition of BV6 reduced viability of the BMDMs from basal conditions (Figure 3.4.9 A and B), probably due to autocrine TNF secretion or high dependence on cIAPs for survival. However, none of the evaluated cells were sensitive to caspase inhibition alone (Zvad) or its combination with TNF (Figure 3.4.9 B). Surprisingly, mutant cells were able to reduce cell death in apoptotic conditions (TNF+BV6). In contrast, were extremely sensitive to necroptotic stimuli in combination with cIAPs depletion, showing a 70% viability reduction already from basal conditions (Figure 3.4.9 B, dark green) (Figure 3.4.9 C). Overall, increased linear ubiquitination in BMDMs protected cells against all TNF-induced apoptosis stimuli but sensitized cells to the necroptotic cocktail (BV6+Zvad). In the presence of this cocktail, cells were almost entirely depleted, even in the absence of exogenous TNF addition (Figure 3.4.9 D). This heightened sensitivity could be attributed to either higher autocrine TNF secretion due to increased basal levels of NF-κB or to increased ripoptosome stabilization independently of TNF upon cIAP depletion, as previously reported (Tenev et al., 2011). These findings highlighted the complex role of linear ubiquitination in modulating cell death pathways, with differential effects observed between apoptosis and necroptosis in BMDMs.

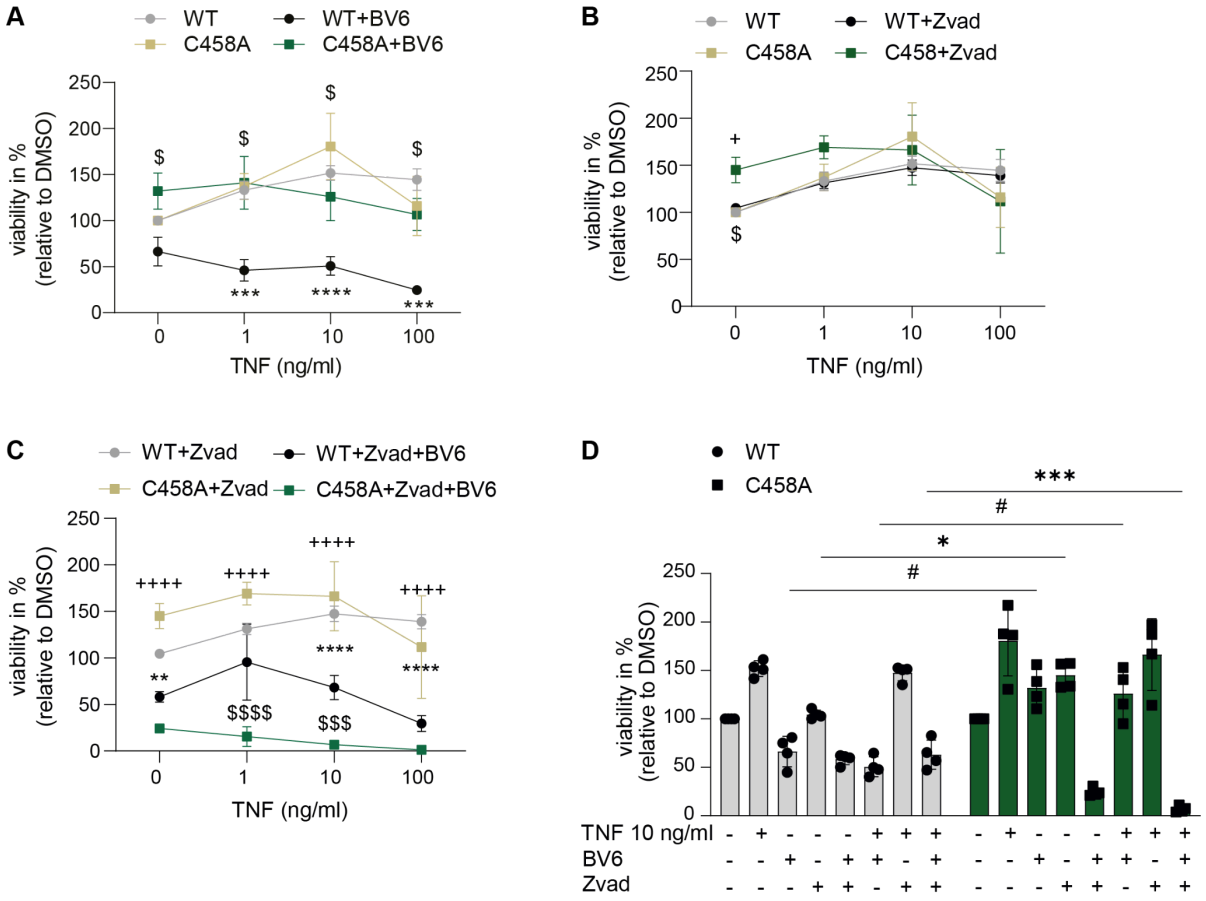

Figure 3.4.9 Hoil-1 catalytically inactive-derived BMDMs are protected against TNF-induced cell death.

A, B and C- Percentage of viability after 24 hs treatment with increasing doses of TNF (n=4). Symbols for comparisons using 2-way ANOVA grouped by TNF concentration: A: (*) WT vs WT+BV6, ($) WT+BV6 vs C458A+BV6. B: (+) C458A vs C458A+Zvad, ($) WT+ZVad vs C458A+Zvad. C: (*) WT+Zvad vs WT+Zvad+BV6, ($) WT+Zvad+BV6 vs C458A+Zvad+BV6, (+) C458A+Zvad vs C458A+Zvad+BV6. D- Percentage of BMDMs after treatment 24 hs treatment (n=4). Statistical analysis: 2-way ANOVA group by treatment applying Bonferroni correction for multiple comparisons. p-values GP: (#) p-<0,0001, (***), p-<0,0002;(**) p-<0,0021; () p-<0,0332; (ns) p->0,0333.

Continuing with our evaluation we challenged BMDMs to different TNF-dependent cell death treatment and measure over a 24 hrs time course. The observed increase in linear chains protected BMDMs against both apoptotic (Figure 3.4.10 A) and necroptotic stimuli (Figure 3.4.10 B) in early time points (Figure 3.4.10 C). However, this effect was only a delay in cell death execution since at 24 hs necroptotic stimuli killed BMDMs at a similar percentage (Figure 3.4.10 B and C), while TNF and TB cell death was reduced in mutant cells. Moreover, the addition of Nec1-s (TBN and TZN) fully rescued both types of cell death induction in WT and mutant cells at the same level (Figure 3.4.10 C), suggesting that in both cases RIPK-1 dependent cell death execution was triggered independently of linear chains levels.

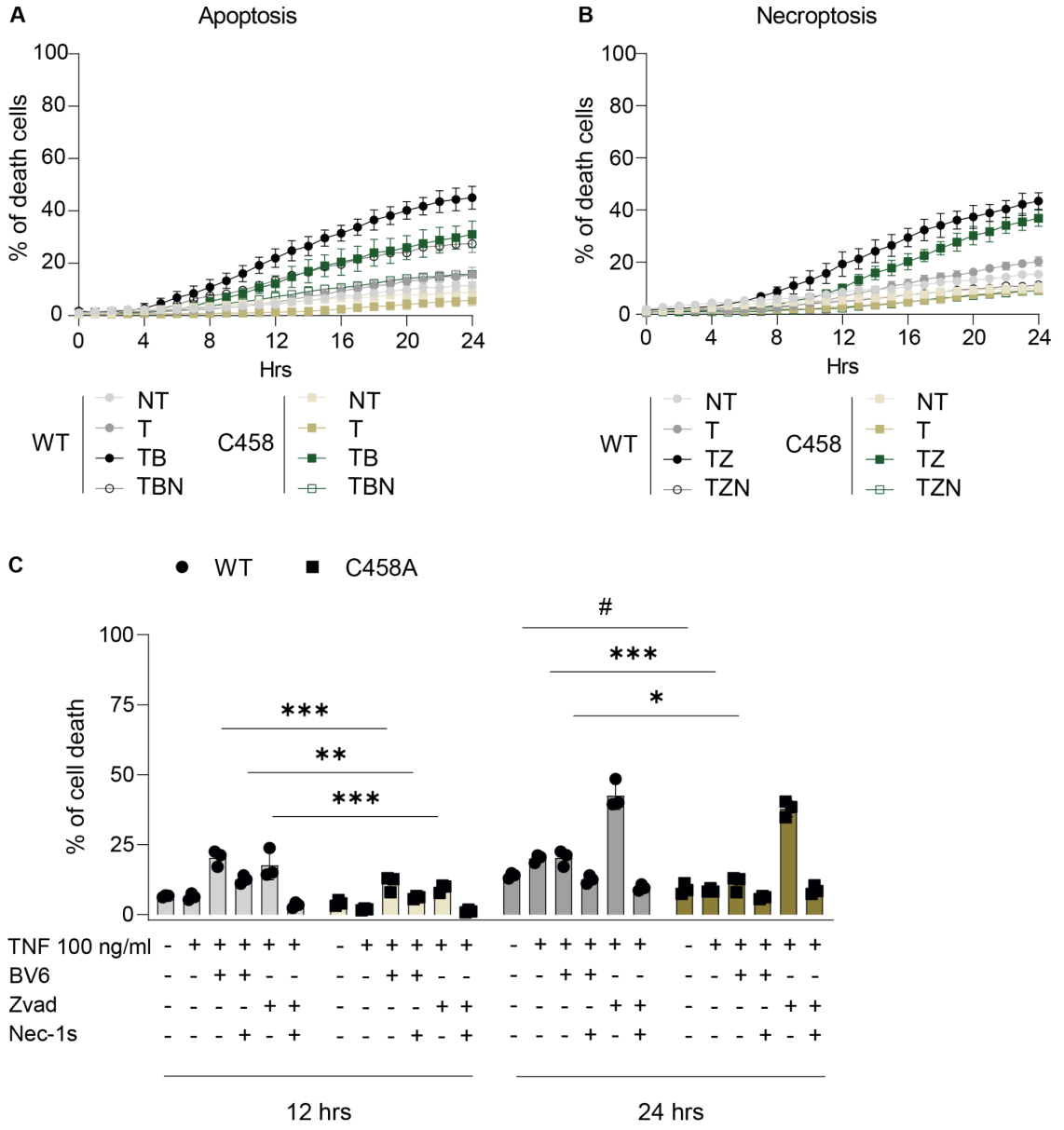

Figure 3.4.10 Hoil-1 catalytically inactive-derived BMDMs are protected against TNF-induced cell death.

A and B - Cell death percentage normalized to time 0 measured by PI incorporation after indicated treatments (n=3). C-Cell death percentages at 12 and 24 have been extracted from A and B for quantification. Statistical analysis: 2-way ANOVA WT vs C458A mean per treatment, grouped by timepoint applying Bonferroni correction for multiple comparisons. p-values GP: (#) p-<0,0001, (***), p-<0,0002;(**) p-<0,0021; (*) p-<0,0332; (ns) p->0,0333.(T) TNF 100 ng/ml, (B) BV6, (Z) Zvad, (N) Nec-1s.

To further sensitize cells to death, a combination of cIAP and caspase inhibition with TNF (TNF+BV6+ZVad or TBZ) was employed (Figure 3.4.11 A). The findings revealed that although increased linear chains ameliorated cell death rates at the initial time point (4 hours), they did not protect mutant BMDMs against complete necroptotic stimuli (Figure

2.4.11 B). However, upon Nec-1s addition, mutant cells showed further rescue, demonstrating an additive effect between RIPK1 inhibition and increased linear ubiquitination when both caspases and cIAPs are inactive (Figure 2.4.11 B)

Last, to determine the dependence on NF-κB activation in the protection against cell death conferred by increased LUBAC activity, we combined the aforementioned treatments with the IKK inhibitor, 2-[(aminocarbonyl)amino]-5-(4-fluorophenyl)-3-thiophenecarboxamide (TPCA-1) (Podolin et al., 2005) (Figure 3.4.11 C). When IKKs were inhibited, increased linear chains slightly delayed apoptotic and necroptotic cocktails (Figure 3.4.11 D). However, at 8 hours, significant protection was only observed in the single combination of TNF+TPCA (Figure 3.4.11 D). This result suggested that the protection against TNF-induced apoptosis (TNF+BV6) and necroptotic (TNF+BV6+Zvad) stimuli, conferred by increased linear chains, was NF-κB dependent. Most likely due to an increased pool of NF-κB pro-survival-related proteins, which have relatively short half-lives: e.g. cFLIP, which has a half-life of 34 to 120 minutes for its short form and 120 minutes for its long form (Golks et al., 2005), MCL-1 presents a half-life of 30 min upon translation inhibition (Adams et, al. 2007). Similarly, cIAP1 has a half-life of about 8 hours under basal conditions, which is reduced to 4 hours during apoptosis induction (Kenneth W. Adams, 2007; Stewart et al., 2017). These short half-lives could explain the time-dependent loss of protection observed in the experiment and suggest that the NF-κB-dependent pro-survival factors could be higher in the mutant cells, counteracting the effect of the inhibitors (BV6 and Zvad).

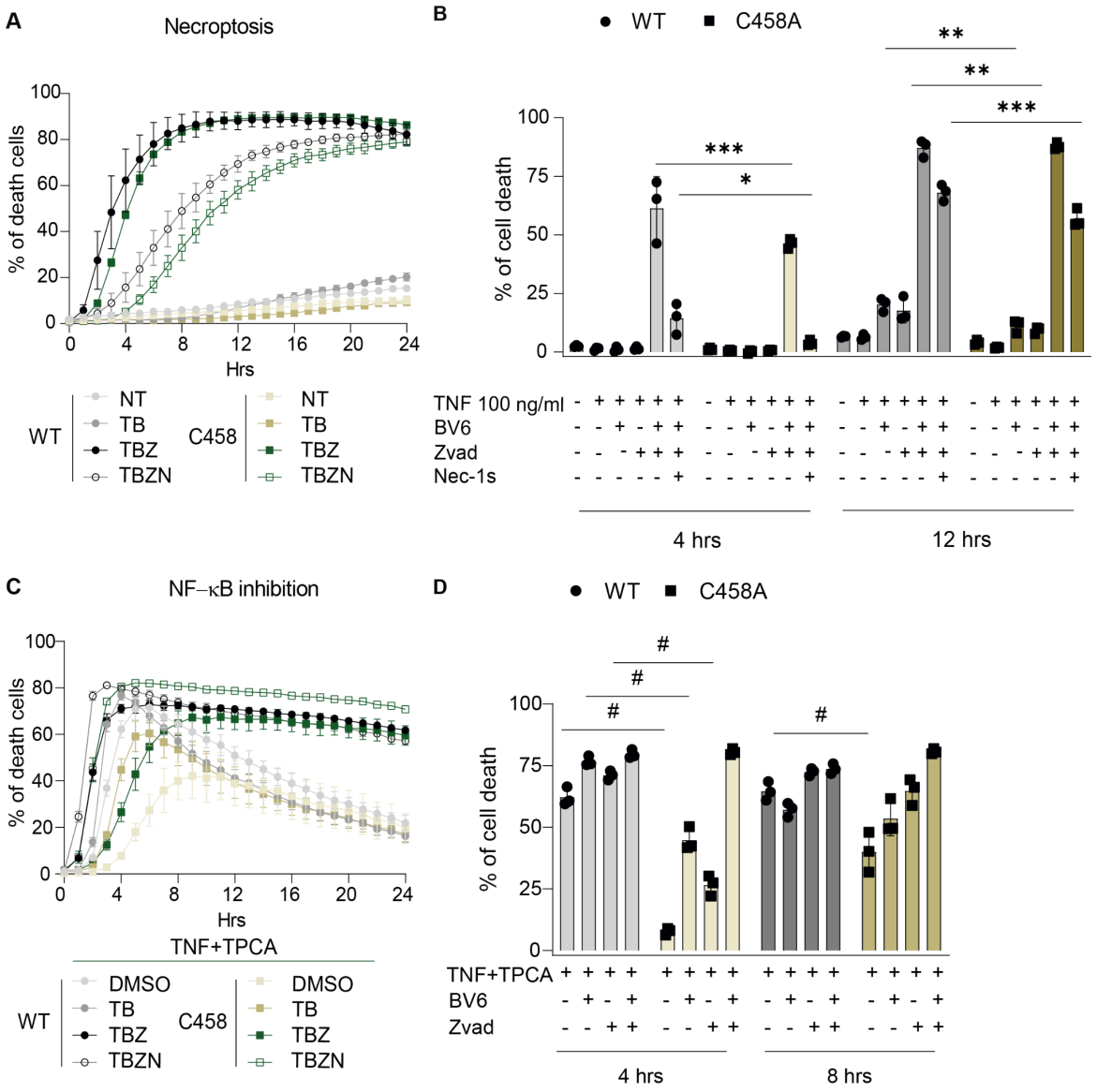

Figure 3.4.11 Hoil-1 catalytically inactive-derived BMDMs are protected against TNF-induced cell death in a NF-κB dependent way.

A- Cell death percentage normalized to time 0 measured by PI incorporation after indicated treatments (n=3). B-Cell death percentage at 4 and 12 hours extracted from A for quantification. C-Cell death percentage normalized to time 0 measured by PI incorporation after indicated treatments (n=3). D-Cell death percentage at 4 and 8 hours extracted from C for quantification.Statistical analysis: 2-way ANOVA WT vs C458A mean e\per treatment, grouped by time point applying Bonferroni correction for multiple comparisons. p-values GP: (#) p-<0,0001, (***), p-<0,0002;(**) p-<0,0021; (*) p-<0,0332; (ns) p->0,0333.(T) TNF 100 ng/ml, (B) BV6, (Z) Zvad, (N) Nec-1s

Results highlight the complex interplay between LinUb, NF-κB signaling, and cell death pathways in adipose tissue. LUBAC hyperactivation had differential effects on cell types, generally protecting adipocytes from apoptosis while sensitizing macrophages to necroptosis. This pro-survival effect of increased linear ubiquitination appears to depend on

NF-κB activation, likely through the production of short-lived, anti-apoptotic proteins downstream. Consequently, LUBAC finely balances cell survival and death within adipose tissue, potentially limiting adipocyte loss during obesity while modulating inflammation via distinct, cell-type-specific mechanisms. This tight regulation underscores LUBAC's critical role in obesity-associated adipose tissue dysfunction and inflammation.

3.4.3 Summary section 3.4

Results in section 3.4 showed that increased linear ubiquitination in *Hoil-1*^{C458A} led to an altered adipose tissue distribution and composition along with potential protection against some aspects of diet-induced metabolic dysfunction and complex changes in liver pathology in response to HFD.

Interestingly, despite no significant impact on weight gain or glucose metabolism, general lipid content in the liver, specially diet derived triglycerides, was reduced. In addition, ScWAT adipocytes were smaller, while fat deposition induced by the diet was impaired in this compartment. Furthermore, stainings revealed higher basal levels of UCP-1 in ScWAT and BAT of mutant mice, along with pronounced protection in BAT against HFD-induced whitening. Despite these changes, no significant differences in mean RER or caloric expenditure were observed among the groups, which contradicts the initial hypothesis that increased energy expenditure was responsible for subcutaneous mass reduction in mutant mice. Moreover, HFD-fed mutant groups showed a significant reduction in nearly all blood cholesterol species measured.

Regarding cell death regulation, increase of linear ubiquitination conferred protection against both TNF and diet-induced cell death. TUNEL staining in adipose tissue revealed less cell death in both GWAT and ScWAT upon obesity challenge, despite increased immune infiltration. On the other hand, experiments with primary preadipocytes isolated from ScWAT demonstrated that increased LinUb protects against both apoptosis and necroptosis stimuli. Moreover, increased LinUb in mutant BMDMs protected cells against all TNF-induced apoptosis, possibly due to basal higher levels of NF-κB anti-apoptotic proteins, since NF-κB inhibition delayed this effect. Despite this, mutant cells were sensitised to the necroptotic cocktail, even in the absence of exogenous TNF suggesting an mainly antiapoptotic role of linear chains in BMDMs. Despite this, upon Nec-1s addition, mutant cells showed further rescue that the wt counterparts, suggesting an additive effect between RIPK1 inhibition and increased linear ubiquitination when both caspases and cIAPs are inactive

These findings highlight LinUb protective role reducing cell death rates in AT during DIO, and suggest LUBAC activity as a protective mechanism against steatosis and blood cholesterol during obesity.

3.4.4 Author contribution section 3.4

Armel Hyoubi from Peltzer lab performed the following histological stainings: F480, CD45, UCP-1 and TUNEL. Öykü Kaya also contributed to establishing UCP-1 staining. Julian Rodefel and Phillipp Antczak performed the liver RNAseq. Ali Abdalla Phillipp Antczak performed the ScWAT and GWAT RNAseq. Julian Rodefel also optimized adipocyte distribution protocol and performed all the corresponding quantifications. Liand Gardeweg assisted in AT explant generation and performed and analysed TUNEL staining in these tissues. Yuan Wang assisted in mouse work and performed mice genotyping. Liane Gardeweg, Jutta Schillings, Pegi Koci, assisted in mouse work, tissue´s H&E scanning and data curation. Francesca Bonechi and Lucas Valdez Capuccino, assisted in mouse work. Micheal Singer and Tom Luedde assisted in the delivery of liver samples to perform the steatosis score, Dr. Aslihan Yavas, performed all the steatosis scores in this thesis. Lipidomics was performed by the CECAD facility. Most of the data analysis, interpretation, visualization and curation were performed by the author of this thesis.

4. Materials and Methods

4.1 In-vivo experiments

4.1.1 Animal care

All animal experiments were approved by the Federal Ministry for Nature, Environment and Consumers' Protection of the state of North Rhine-Westphalia and were performed by the respective national, federal and institutional regulations. At the end of the feeding protocol, mice were euthanized using Ketamine/Xylazine Cocktail (100 mg/kg Ketamine and 20 mg/kg Xylazine) with a dose of 5 µl/gr. Followed by heart puncture, cervical dislocation and tissue harvesting.

4.1.2 Generation of mutant lines

Hoip$^{A\text{-}KO}$ and *Casp8*$^{A\text{-}KO}$ mice were generated by crossing *Hoip*$^{fl/fl}$ (Taraborrelli et al., 2018) and *Casp*$^{fl/fl}$ *(Kang et al., 2018)* with AdipoQ.cre Strain #:010803 from The Jackson Laboratories (Eguchi et al., 2011). *MLKL*^{KO} (Peltzer et al., 2018) and *Rbck1*^{C458A} mice were generated and donated by Henning Walczak. For all the experiments Cre- littermates or *Rbck1*^{wt} were used as control.

4.1.3 Diet induced obesity

Control Diet (CD) LS- 13% fat, 11% sucrose (Ssniff, E15748-04) and High-fat diet (HFD) DIO- 60 kJ% fat (Lard) (Ssniff, E15742-347) cohorts breedings and diet feeding were performed simultaneously using the same parental line. In all experiments, 6-7-week-old male mice were fed with a CD or HFD as indicated for 16 weeks. 3 to 5 mice were placed per cage and weight body gain was measured weekly. Normal-fed blood glucose was taken every 3 weeks with Aida Glucometer and strips (Aida, 781783). Animals with no indication in the figures were fed with CHOW diet.

DIO – 60 kJ% fat (Lard)

ssniff

HF diet for rodents with lard (& soybean oil) ¦ corresponds to D12492

Description

This purified diet of the DIO series is characterized by very high fat contents (lard). It is therefore used to induce obesity and metabolic syndrome / diabetes (NIDDM) in mice. The diet is also available with beef tallow as fat source (more saturated FA).

The diet is intended for ad libitum feeding. The animals should have free access to fresh water.

Gross Energy (GE)	**25.0**	**MJ/kg**
Metabolizable Energy (ME) [1)]	**21.6**	**MJ/kg**

[1)] *= Physiological fuel value (Atwater); correspond to 5,150 kcal/kg*

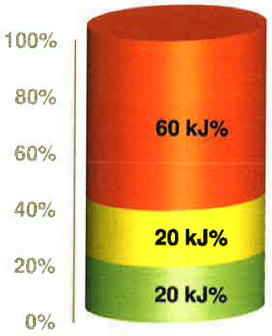

Crude Nutrients	**[%]**
Crude protein (N x 6.25)	24.4
Crude fat	34.6
Crude fibre	6.0
Crude ash	5.3
Starch	0.1
Sugar	9.4
N free extracts	26.3

Minerals	**[%]**
Calcium	0.92
Phosphorus	0.64
Ca / P	1.44
Sodium	0.20
Magnesium	0.23
Potassium	0.97

Fatty acids	**[%]**
C 12:0	0.07
C 14:0	0.44
C 16:0	7.93
C 18:0	4.37
C 20:0	0.11
C 16:1	0.94
C 18:1	13.97
C 18:2	4.64
C 18:3	0.49

Amino acids	**[%]**
Lysine	2.02
Methionine	0.86
Cystine	0.45
Met+Cys	1.31
Threonine	1.07
Tryptophan	0.33
Arginine	0.95
Histidine	0.74
Valine	1.70
Isoleucine	1.38
Leucine	2.42
Phenylalanine	1.27
Phe+Tyr	2.56
Glycine	0.52
Glutamic acid	5.50
Aspartic acid	1.82
Proline	2.80
Serine	1.46
Alanine	0.81

Vitamins	**per kg**	
Vitamin A	15,000	IU
Vitamin D_3	1,500	IU
Vitamin E	150	mg
Vitamin K (as MNB)	20	mg
Thiamine (B_1)	25	mg
Riboflavin (B_2)	16	mg
Pyridoxine (B_6)	16	mg
Cobalamin (B_{12})	30	µg
Nicotinic acid	47	mg
Pantothenic acid	55	mg
Folic acid	16	mg
Biotin	300	µg
Choline	1,140	mg

Trace elements	**per kg**	
Iron	168	mg
Manganese	95	mg
Zinc	65	mg
Copper	13	mg
Iodine	1.2	mg
Selenium	0.2	mg

Figure 4.1: High fat diet composition

4.1.4 In vivo metabolic studies

4.1.4.1 Insulin Tolerance Test

Insulin tolerance tests were performed on animals fasted for 6 h, using insulin lispro (Lilly) injected intraperitoneally. The dose was 0.75 U per kg body weight for HFD-fed mice and 0,5 U/Kilo for mice fed with the control diet. Measurements of blood glucose were taken at 0,

15,30, 45, 60 and 120 min after the injection and measured with Aida Glucometer and strips (Aida 781783).

4.1.4.2 Glucose Tolerance Test

Glucose tolerance tests were performed on 6 h fasted animals, using glucose 2 g/kg body weight supplied by oral gavage.Measurements of blood glucose were taken at 0, 15,30, 45, 60 and 120 min after the injection and measured with Aida Glucometer and strips (Aida 781783).

4.1.4.3 Metabolic cages

For energy expenditure, food, water and oxygen consumption measurements, mice were individually housed in metabolic cages (TSE PhenoMaster V7.7.3 (2021-4898)) with free access to food and water after 7 days of training at 22°C and 50% humidity. Data was collected during 72 hs and the average was expressed by consumption per day and relativized to initial body weight as indicated. Metabolic rate (kcal per day) was calculated using the formula = 1.44 × (3.94 × VO2 + 1.11 × VCO2) the average of the three days was taken as an individual value per mouse. Respiratory Exchange Ratios (RER) were calculated as VCO2/V02 at every single point (every 20 min) during 72 hs. The average in the different phases (Total, light and dark) of each mouse was expressed as a single RER value.

4.1.4.4 Serum and blood evaluations

Full blood (plus EDTA) was used to determine HbA1c values (Uniklinik Koeln chemical lab service) , for the rest blood was collected in Microvette® 100 Serum (Sarstedt, 20.1344) centrifuge at 10.000 rcf for 5 minutes at RT. Serum was stored at -80 C for future evaluation. ALT, AST, LDH, Urea and Albumin were determined by the UniKlinik chemical lab service. Serum values were determined following manufacturer instructions with the following kits: Free Fatty acids (Abnova, KA1667), cholesterol (Promega, J3190) and Triglycerides (Promega, J3160). Insulin levels were measured by a mouse insulin ELISA kit (CrystalChem, Inc.). Serum adipokines were measured by Luminex technology in a custom-made multiplex plate and Adiponectin Luminex Discovery Assay (R&D, LXSASM-01).

4.1.4.5 Echocardiography:

Transthoracic echocardiography was performed in isoflurane-anaesthetized mice (Isofluran-Piramal®, Piramal Critical Care, Voorschoten, The Netherlands; 5 % vol/vol for induction and 2 % vol/vol for maintenance of anaesthesia). Parasternal long-axis (PSLAX) and parasternal short-axis (PSAX) of the heart were imaged in B-Mode, M-Mode, and electrocardiogram-triggered kilohertz visualisation (EKV) using a Vevo 3100 ultrasound system (FUJIFILM VisualSonics, Toronto, ON, Canada) equipped with a MX550D transducer (25-55 MHz, centre transmit: 40 MHz, axial resolution: 40 µm) by a blinded examiner. Measurements were analysed using Vevo Lab v5 (VisualSonics, Fujifilm, Tokio, Japan) by two blinded investigators. Left ventricular ejection fraction (LV-EF) and cardiac output (CO) were determined by planimetry of end-systolic (LVESV) and end-diastolic (LVEDV left ventricular volumes in the B-mode/EKV PSLAX view.

4.1.5 Histological analysis

At the indicated endpoints, ScWAT, GWAT, BAT, Liver, Spleen, Pancreas, and Skin were harvested and fixed overnight in a 10% neutral buffered formalin solution (Sigma HT501128-4L) at 4°C, preserved at 4°C in PBS or EtOH 70% (only skin) until paraffin-embed. Tissue sections (4 µm) were processed as described in supplemental material. Colon and small intestine were isolated from the mouse, longitudinally cut and washed with PBS to remove faeces. Intestinal tissues were rolled up from proximal to distal and fixed in 4% PFA overnight at 4°C. Afterwards, sections were paraffin-embedded and cut to 4 µm thickness.

4.1.5.1 Haematoxylin & Eosin staining

Paraffin sections were stained with haematoxylin and eosin by the histology facility and acquired in the Slide Scanner (Hamamatsu S360) at 20X.

4.1.5.2 Adipocyte distribution:

Representative pictures of 3 mice per group were selected from 20X H&E scanned sections of GWAT or SWAT. The dimensions of the image were 4992x2640 for mice with 16 weeks of diet and 9984x5280 pixels for 12-week-old CHOW diet mice. The images were analysed with a modified version of the Adiposoft plugin (FIJI v1.54). Contrast enhancement was removed in this modified version. Instead of the global thresholding using the percentile

method, auto-local thresholding was performed in a 15-pixel radius using the mean pixel value. The prominence of local maxima in the distance map for water shedding was set to 7. Particles were identified as valid adipocytes if their diameter fell into the range between 10-200 µm and their circularity was between 0.27-1.00. The whole data obtained was used to generate distribution plots. Individual averages of adipocyte numbers and area were used to generate bar plots.

4.1.5.3 Liver steatosis score:

H&E stainings of 16-weeks diet and 18-month-old mice livers were evaluated by an experienced clinical pathologist who was blinded for mouse ID, age, genotype or diet. Standardised scores for non-alcoholic fatty liver disease (NAFLD) were performed according to the NAS score system: Steatosis (0-3), lobular inflammation (0-2), hepatocellular ballooning (0-2), and fibrosis (0-4) (Kleiner et al., 2005).

4.1.5.4 Intestinal histological evaluation:

The scoring system used is described in (Schwarzer et al., 2020). In brief, histopathology scores comprise four parameters: epithelial hyperplasia, epithelial injury, tissue inflammation and epithelial cell death. Histological sub-scores for each parameter: 0, absent; 1, mild; 2, moderate; 3, severe. An “area factor” for the fraction of affected tissue was assigned and multiplied with the respective parameter score (1=0-25%; 2=25-50%; 3=50-75%; 4=75-100%). Each area was scored individually and multiplied with the correlating area factor. Total histology score was calculated as a sum of all parameter scores multiplied by their area factors. The maximum score was 48. The evaluation was performed in a blinded fashion.

4.1.5.5 Oil Red O Staining

Cells were washed once with PBS prior to incubation with 4% paraformaldehyde (PFA) at room temperature. After 10 minutes, PFA was renewed. Samples were stored at 4°C until further analysis. For staining with Oil Red O, cells were washed with 60% isopropanol prior to addition of Oil Red O staining solution (6 parts of Oil Red O stock solution (3.5g Oil Red O in 1l isopropanol) were mixed with 4 parts of distilled water). After incubation at room temperature for 10 minutes, the staining solution was removed and cells were washed 3x with distilled H2O. Pictures were taken with the OLYMPUS CK40 microscope.

4.1.6 Immunofluorescence (IF)

4.1.6.1 D163, Mac2 and perilipin:

Samples were deparaffinized using xylene every 5 minutes, and alcohol series every 3 minutes. Citrate Ph6 was used for Antigen Retrievers. Samples were washed 5 times 5 min in PBS 0.3% Triton. Samples were blocked using 1% BSA in 0.3% Triton- PBS for 1 h. Samples were incubated overnight with primary Ab (see list). Afterwards, samples were washed 5 for 5 min 0.3% Triton- PBS (the last two times in cuvette) and incubated for 1h at RT with secondary Ab (see list). Followed by 4 washes of 5 min 0.3% Triton- PBS in cuvette, DAPI staining was performed for 10 min RT. TrueBlack (1:20 diluted in ethanol) was added for 15 sec, followed by 2 washes of 5 min in PBS and 2 washes of distilled water in a cuvette. DAKO Immunofluorescence Mounting Medium was used to seal the samples. Primary antibodies were dilated in Ab in 1% BSA and 0.3% Triton- PBS; in the followed concentrations: anti-Mac2 (rat), Cedarlane (CL8942AP), 1:1000; anti-CD163 (rabbit) Abcam, (ab182422) 1:100; anti-PerilipinA (goat) Abcam (ab61682), 1:200. Secondary Antibodies: donkey anti-rat AF488, Invitrogen, 1:200; donkey-anti-rabbit Cy3, Jackson, 1:200 ; donkey-anti-goat AF647 Invitrogen, 1:200; DAPI, Hoechst, 1:10.000.

4.1.6.2 Cleaved Caspase 3:

The slides were then incubated in 1X citrate buffer (pH 6.0; 10X stock, Cat: C999) for 10 minutes before heat-induced antigen retrieval. Slides were simmered in a microwave for 7 min. Afterward, they were cooled to room temperature. Tissue sections were permeabilized by incubating them in 0.2% Triton X-100 (Sigma-Aldrich, Cat: T8787), prepared in Animal-Free Blocker (Cat: SP-5035-100), for 10 minutes and slides were washed with 1X TBS for 5 min, then with 1X TBS-T for 5 min. Next, the slides were incubated with blocking solution (Cat: VEC-SP-6000) for 10 minutes, then with Animal-Free Blocker for 1 hour. After blocking, tissues were incubated overnight at 4 °C with Cleaved-Caspase-3 (Asp175) Antibody (Cat: 9661S; 1:50 dilution in Animal-Free Blocker). The following day, the slides were washed three times for 10 minutes each with 1X TBS-T, then incubated for 1 hour with Goat anti-Rabbit IgG (H+L) Cross-Adsorbed Secondary Antibody, Alexa Fluor™ 568 (Cat: A11011; 1:300 dilution in 1X TBS-T). Slides were then washed six times for 10 minutes each with 1X TBS-T. Finally, the slides were incubated with DAPI (1:1000) for 10 minutes, rinsed in 1X TBS-T, and mounted using Molecular Probes ProLong Gold Antifade Mountant (Cat: P10144). EVOS scanner at 20 X and quantified using positive cell detection tool on QuPhat

5.0 with a DAPI threshold of 25 and a cell expansion mask of 25 µm. Positive threshold was determined by negative control without primary Ab. The number of positive nuclei was normalised to the total nuclei and total tissue area of each corresponding section; visible blood vessel areas were excluded from the analysis due to autofluorescence.

4.1.6.3 TUNEL:

Perigonadal adipose tissue (GWAT) sections were used for TUNEL staining (Promega, G3250) according to manufacturer specifications and DAPI to identify the nucleus structure. Images were taken with the Confocal microscope Leica STELLARIS or EVOS scanner at 20 X and quantified using cell detection tools on QuPhat 5.0 threshold 25. Negative controls were used to determine the threshold for TUNEL positive nuclei. The number of positive nuclei was normalised to total the area of each corresponding section; visible blood vessels areas were excluded from the analysis due to autofluorescence of red cells.

Intestine histological score: Formalin-fixed and paraffin-embedded intestinal Swiss-rolls were sectioned (3µm) and stained with H&E. Histological evaluation was performed using the scoring system as described in (Schwarzer et al., 2020). In brief, histopathology scores are composed of four parameters: epithelial hyperplasia, epithelial injury, tissue inflammation and epithelial cell death. Histological sub-scores for each parameter: 0, absent; 1, mild; 2, moderate; 3, severe. An “area factor” for the fraction of affected tissue was assigned and multiplied with the respective parameter score (1=0-25%; 2=25-50%; 3=50-75%; 4=75-100%). Each area was scored individually and multiplied with the correlating area factor. Total histology score was calculated as a sum of all parameter scores multiplied with their area factors. The maximum score was 48. Evaluation was performed in a blinded fashion.

4.1.7 Immunohistochemistry

4.1.7.1 Pancreatic Insulin,CD45, F480, and UCP-1

Insulin (1:6400 diluted in Animal-Free Blocker, Cell signalling C27C9), CD45 (1:100, Thermofischer, 14-0451-82) , F4/80 (1:100 ref: MCA497R, BIO RAD) and UCP-1 (1:100 Abcam (ab10983)IHC, antigen retrieval was done by using citrate buffer, pH 6 (Sigma-Aldrich, C9999) in pancreas or GWAT sections (5 µM) by maintaining sub-boiling conditions in microwave for 5, 10, 10 and 7 mins respectively. The sections were incubated

with BLOXALL Endogenous Blocking Solution (VEC-SP-6000, Vector Laboratories) to block endogenous peroxidases. This is followed by 30 mins incubation with Animal-Free Blocker (VEC-SP-5035, Vector Laboratories). Following overnight incubation at 4^{o}C, with primary antibodies, sections were washed with TBS-T (pH 7.6, 0.5 % Tween) 3 times for 10 mins. Sections were incubated with immPRESS® HRP Goat Anti-Rabbit IgG Polymer Detection Kit, Peroxidase (MP-7451, Vector Laboratories) for 30 mins. Following 3 times 10 mins washes, the colour was developed by using HIGHDEF® DAB Chromogen/Substrate Set (ENZ-ACC105-0200, Enzo). The slides were scanned by slidescanner (Hamamatsu S360). The positive area was calculated by using QuPath0.4.0.

4.2 Molecular Biology

4.2.1 Isolation of genomic DNA from ear biopsies

DNA was extracted using the Accustart extraction kit kit (VWR, 733-2236) following the manufacturer's protocol. Samples from ears were submerged completely in 50 µl of extraction reagent, while tail samples were submerged in 100 µl. The samples were then incubated at 95 °C for 30 minutes. After incubation, 50 µl (for ears) or 100 µl (for tails) of stabilization buffer was added. Extracted samples were stored at 4 °C if they were to be used within a few weeks or at -20 °C for longer storage periods of several months.

4.2.2 Genotyping PCRs

Routine mouse genotyping was performed by polymerase chain reaction (PCR) on genomic DNA isolated from ear biopsies. Using AccuStart™ II GelTrack PCR SuperMix (Quantabio, QUNT95136-100) is a 2X concentrated, ready-to-use reaction cocktail for routine PCR amplification of DNA fragments up to 4 kb followed by analysis on agarose gels. Point mutations were screened with enzymatic digestion with enzyme Ehe1 (Thermo Fisher, ER0441) after amplification, since the presence or absence of a restriction enzyme site on the PCR fragment was the readout. To detect floxed alleles and transgenes, allele-specific genomic regions were amplified to determine genotypes via size of the resulting PCR product. PCR mixes were prepared following manufacturers instructions, using specific primers (Table 4.1). PCR programs consisted of a five step program comprising an initial denaturation (step 1), followed by denaturation (step 2), primer annealing (step 3), extension

(step 4) and a final extension (step5) (Table 4.1). PCR products were run in 2% agarose gels and visualised using UV light.

Gene	Primer name/code	Primer sequence	Company	WT band (size)	Mutant band (size)	PCR program
Mlkl KO	2266: (fw)	CATCAAGTTAGGCCA GCTCA	Merk	204 bp	173 bp	3 min 94°C 30 sec 94°C 30 sec 58°C (rep 35X) 30 sec 72°C Inf 4°C
	2267: (rev)	TCTGCTGGTTAGCCT CCTTC	Merk			
Casp8 fl/fl	985	ATAATTCCCCCAAATC CTCGCATC	Merk	200 bp	300 bp	3 min 95°C 30 sec 94°C 30 sec 62°C (rep 30X) 30 sec 72°C Inf 4°C
	986	GGC TCA CTC CCA GGG CTT CCT	Merk			
Cre	PDX1	TTG CCC CTG TTT CAC TAT CCA G	Merk	no amplification	400 bp	5 min 95°C 30 sec 95°C 30 sec 57°C (rep 33X) 1 min 72°C Inf 4°C
	PDX2	TGC TGT TTC ACT GGT TAT GCG G	Merk			
	366	CTA GGC CAC AGA ATT GAA AGA TCT	Merk			
	367	GTA GGT GGA AAT TCT AGC ATC ATC C	Merk			
Rbck1 C458A	mHOIL1_KI_tac_FW (name MGS081)	CGGCAGACGACAGA GATGC	Eurofins	After cleavage: 350 bp + 159 bp	No cleavage: 509	5 min 95°C 30 sec 95°C 30 sec 60°C (rep 35X) 1 min sec 72°C Inf 4°C
	mHOIL1_KI_tac_REV (name MGS082)	GGCTGGACTGAGTTC ATGGC	Eurofins			
Rnf31 fl/fl	RNF31 WT F (262)	CTCATTTGAATTCTAT GATGC	Eurofins	507	334	5 min 95°C 30 sec 95°C 30 sec 54°C (rep 33X) 1 min 72°C Inf 4°C
	RNF31 WT exon R (267)	GAAACAGGGACCAG GAGT	Eurofins			

Table 4.1 Genotyping PCR primers and programs

4.2.3 3’ mRNA isolation and qRT-PCR

4.2.3.1 Human adipocytes:

RNA was isolated with the Quick-RNA™ Miniprep Kit (Zymo) according to the manufacturer’s instructions. cDNA was synthesised using SuperScript II Reverse Transcriptase (Thermo Fisher Scientific) with random primers (Thermo Fisher Scientific). qRT-PCR was performed using SsoAdvanced Universal SYBR Green Supermix (Bio-Rad) on a Bio-Rad CFX Connect Real-Time PCR Detection System with the following protocol: 95°C for 30 seconds, then 40 cycles of 95 °C for 5 seconds followed by 60°C for 30 seconds.

4.2.3.2 Mouse adipose tissue:

100 mg of fat tissue was in 1 ml of QIAzol Lysis buffer (RLT Plus + DX) and a 5 mm bead to be homogenised in TissueLyser II in two rounds for 2 minutes at 30 1/s. Samples were processed according to manufacturer instructions using the RNAeasy Lipid Mini Kit (74804, Qiagen). A DNase digest kit was employed, involving the addition of 350 µl of Buffer RW1 to the RNeasy Mini spin column, followed by the addition of DNase I. The resulting RNA was evaluated for purity and concentration using a Nanodrop spectrophotometer from TECAN Reader (model).

4.2.3.3 Mouse Livers:

Total RNA purified from 200 mg snap-frozen liver tissue using RNeasy Midi Kit (Qiagen, #75144) in combination with tissue lyser II (Qiagen) according to the manufacturer’s instructions. Extraction quality and purity was determined spectroscopically using a nanodrop (TECAN). cDNA was synthesised using Transcriptor cDNALunaScript RT SuperMix Kit (New England Biolabs, #E3010) according to the manufacturer’s specifications. qRT-PCR was performed using 25ng of cDNA were used per single reaction using Luna Universal Probe qPCR Mastermix, (New England Biolabs, #M3004L) on CFX Opus 96 Real-Time PCR System (BioRad, #12011319) in a 96 well format with a final volume of 20 ul with the following protocol: 95°C for 30 seconds, then 40 cycles of 95 °C for 15 seconds followed by 60°C for 30 seconds (plus plate read). All real-time PCR reactions were performed in duplicates. Data was generated and analysed using (insert software).All values were normalised to the Gapdh mRNA mean value of wt control littermates (5 per

group) of each diet using the ΔΔ CT method. Data is expressed displaying the fold change values and Múltiple unpaired t-test was used to evaluate each gene. The expression of the genes tested using the primers as follows: Gck (ID:103988) Fw: CCCTGAGTGGCTTACAGTTC Rv: ACGGATGTGAGTGTTGAAGC ; Pfkl (ID: 18641) Fw: GGGTCATGTACAGCGAGGA Rv: GGCCTCCATACCCATCTTG; Pfkfb2 (ID: 18640) Fw: CGAGAGCGAGTTCAACCTTTTGG Rv: CTTCAACTGGCTCGTCCACACT; Pklr (ID: 18770) Fw: CGAAAAGCCAGTGATGTGGTGG Rv: GATGCCATCGCTCACTTCTAGG; G6pc1 (ID: 14377) Fw: ATGAACATTCTCCATGACTTTGGG Rv: GACAGGGAACTGCTTTATTATAGG; Pck1 (ID: 18534) Fw:CATAACGGTCTGGACTTCTCTGC Rv: GAATGGGATGACATACATGGTGCG ; Acly (ID: 104112) Fw: AGGAAGTGCCACCTCCAACAGT Rv: CGCTCATCACAGATGCTGGTCA; Acaca (ID: 107476) Fw: GTTCTGTTGGACAACGCCTTCAC Rv: GGAGTCACAGAAGCAGCCCATT; Fasn (ID: 14104) Fw: GCTGCGGAAACTTCAGGAAAT Rv: AGAGACGTGTCACTCCTGGACTT; Scd1 (ID: 20249) Fw: ACGATGGCTCATCTCTCAAGGC Rv: TGTGGTGCAACTGAGGCTTCGT; Elovl6 (ID: 170439) Fw: CGGCATCTGATGAACAAGCGAG Rv: GTACAGCATGTAAGCACCAGTTC; Srebf1 (ID: 20787) Fw: GGAGCCATGGATTGCACATT Rv: GGCCCGGGAAGTCACTGT .

4.2.4 Human RNAseq analysis

4.2.4.1 Correlation of Metabolic syndrome parameters vs LUBAC component expression in VAT

The human data were obtained from the Leipzig Obesity Biobank (LOBB, https://www.helmholtz-munich.de/en/hi-mag/cohort/leipzig-obesity-bio-bank-lobb), which includes samples of omental VAT of a cross-sectional cohort (CSC). This cohort included 1,479 participants, comprising individuals who were either normal weight or overweight (n = 31; 52% women; age: 55.8 ± 13.4 years; BMI: 25.7 ± 2.7 kg/m²) and those classified as obese (n = 1,448; 71% women; age: 46.9 ± 11.7 years; BMI: 49.2 ± 8.3 kg/m²). The study received approval from the Ethics Committee of the University of Leipzig (approval no: 159-12-21052012) and was conducted in compliance with the Declaration of Helsinki principles. All participants provided written informed consent prior to their inclusion in the study. VAT samples were obtained during elective laparoscopic abdominal surgeries, following established protocols (Langhardt et al., 2018; Mardinoglu et al., 2015). Body composition and metabolic parameters were assessed using standardised techniques as previously described (Blüher, 2020; Klöting et al., 2010). Participants were excluded based on several criteria: being under 18 years old, having a history of chronic substance or

alcohol abuse, smoking within the year leading up to surgery, suffering from acute inflammatory conditions, concurrently using glitazones, having advanced-stage cancers, experiencing a weight loss exceeding 3% in the three months prior to surgery, having uncontrolled thyroid disorders, or being diagnosed with Cushing's disease. The study was approved by the Ethics Committee of the University of Leipzig (approval number: 159-12-21052012) and was conducted in accordance with the principles outlined in the Declaration of Helsinki. All participants provided written informed consent before being included in the study. We conducted RNA sequencing on ribosomal RNA-depleted samples following the SMARTseq protoco l (Y. Song et al., 2018). The sequencing was performed as single-end reads using a Novaseq 6000 (Illumina, San Diego, CA, USA) at the Functional Genomics Center in Zurich, Switzerland. The preprocessing of the data adhered to previously established methods (Hagemann et al., 2023). In brief, we aligned adapter and quality-trimmed reads to the human reference genome (assembly GRCh38.p13, GENCODE release 32) and quantified gene-level expression with Kallisto version 0.48 (N. L. Bray et al., 2016). For samples that had read counts greater than 20 million, we utilised the R package ezRun version 3.14.1 (https://github.com/uzh/ezRun, accessed on April 27, 2023) to downsample them to a maximum of 20 million reads. Normalisation of the data was achieved through a weighted trimmed mean (TMM) of the log expression ratios, with adjustments made for age, transcript integrity numbers (TINs), and gender—except when analysing male and female samples separately. All analyses were carried out using R version 4.3.1 (www.R-project.org).

4.2.4.2 Hoip expression in VAT and ScWAT during ageing

The median TPM data for subcutaneous and visceral adipose tissue was obtained from the GTEx Portal v8 in October 2022. Levels of expression of genes of interest were evaluated in adipose tissue (both visceral and subcutaneous) of non-diseased individuals clustered by age.

4.2.5 RNA-seq from mouse GWAT

For RNA sequencing, we used 2 µg of total RNA per sample concentration range 50-200 ng/µL, at least 10µL volume, checking the quality by RIN > 7, OD260/280 = 1,8-2,1 and OD260/230 >1,5. mRNA libraries were prepared by mRNA Seq (Poly A+ selection) using ERCC RNA Spike-In controls. Libraries were prepared using the Illumina® Stranded TruSeq® RNA sample preparation kit. ERCC RNA Spike-In Mix (Thermo Fischer) was added to the samples before library preparation. Library preparation started with 1000 ng

total RNA. After poly-A selection (using poly-T oligo-attached magnetic beads), mRNA was purified and fragmented using divalent cations under elevated temperature. The RNA fragments underwent reverse transcription using random primers. This was followed by second strand cDNA synthesis with DNA Polymerase I and RNase H. After end repair and A-tailing, indexing adapters were ligated. The products were then purified and amplified (15 cycles) to create the final cDNA libraries. After library validation and quantification (Agilent Tape Station), equimolar amounts of the library were pooled. The pool was quantified by using the Peqlab KAPA Library Quantification Kit and the Applied Biosystems 7900HT Sequence Detection System. The pool was sequenced on an Illumina NovaSeq6000 sequencing instrument with a PE100 protocol aiming for 40 million clusters per sample.

The RNA-seq dataset was processed on the CHEOPS HPC cluster at the University of Cologne using the nf-core(P. A. Ewels et al., 2020) RNA-seq pipeline (v3.7)(Kurtzer et al., 2017) within a Singularity environment(*Rnaseq: Introduction*, n.d.) and managed by Nextflow (v21.10.6) (Di Tommaso et al., 2017). Quality control, including adapter trimming and sequence filtering, was performed with Trim Galore (v0.6.7)(*Babraham Bioinformatics - Trim Galore!*, n.d.), ensuring high-quality reads. Read quality was assessed via MultiQC (v1.11)(P. Ewels et al., 2016), aggregating FastQC(*Babraham Bioinformatics - FastQC A Quality Control Tool for High Throughput Sequence Data*, n.d.), Picard(*Picard*, n.d.), and Preseq(Daley & Smith, 2013) reports. No issues were detected. Reads were aligned to the GRCh38 reference genome with STAR (v2.7.10a)(Patro et al., 2017), and gene quantification was done using Salmon (v1.5.2)(Patro et al., 2017). Differential expression analysis was performed in DESeq2 (v1.38.1)(Love et al., 2014), with multiple testing corrections applied using the Benjamini-Hochberg method. Gene Ontology (GO) analysis, focusing on genes with an absolute log2FoldChange >1 and adjusted p-value <0.05, was carried out using gprofiler2 (v0.2.1)(Raudvere et al., 2019). Positively and negatively enriched pathways were identified separately using default parameters, including g_SCS correction. Pearson correlation tests were initially performed on the log2 fold changes of all genes between the Ctrl (HFD vs CD) and CD ($Hoip^{A\text{-}KO}$ vs Ctrl) comparisons. Genes were then grouped by significance in either or both comparisons, and correlation analyses were repeated for each group. All tests showed strong to very strong correlations (0.77 to 0.94), with statistically significant results. Cell-type deconvolution was performed using the deconvolute function from Granulator (v1.6.0) and the dtangle method(Hunt et al., 2019). As input we used Salmon's TPM values generated by the nf-core pipeline and perigonadal samples from the single-nuclei dataset GSE176171. The preprocessed Seurat object

(mouse_all.rds) was sourced from https://gitlab.com/rosen-lab/white-adipose-atlas and restricted to male perigonadal tissue.

4.2.6 Liver Lipidomics :

Glycerophospholipid (PC, PE, PI, PS; PG, PA), diacylglycerol (DAG), triacylglycerol (TAG), and cholesteryl ester (CE) species in mouse liver were analysed by Nano-Electrospray Ionization Tandem Mass Spectrometry (Nano-ESI-MS/MS) with direct infusion of the lipid extract (Shotgun Lipidomics) using a TriVersa NanoMate infusion system operated by the ChipSoft 8.3.1 software (Advion) and a QTRAP 6500 mass spectrometer operated by the Analyst 1.7.2 software (SCIEX).

Samples of mouse liver tissue were homogenized in Milli-Q water (1 mg / 10 µl) using the Precellys 24 Homogenisator (Peqlab) at 6.500 rpm for 30 sec. The protein content of the homogenate was routinely determined using bicinchoninic acid. For the analysis of GPL species, 15 µl of the homogenate were used for lipid extraction, whereas 20 µl were used for the analysis of DAG and 5 µl for TAG and CE species. The homogenate aliquots were brought to a volume of 500 µl with Milli-Q water. For the extraction of GPL species, 1.875 ml of methanol/chloroform 2:1 (v/v) and internal standards from Avanti Polar Lipids (122 pmol PC 17:0-20:4 (LM1002), 138 pmol PE 17:0-20:4 (LM1102) , 111 pmol PI 17:0-20:4 (LM1502), 118 pmol PS 17:0-20:4 (LM1302), 60 pmol PG 17:0-20:4 (LM1202), 72 pmol PA 17:0-20:4 (LM1402)) were added. DAG, TAG and CE species were extracted with 1.875 ml of chloroform/methanol/37 % hydrochloric acid 5:10:0.15 (v/v/v) and 20 µl each of 4 µM d5-DAG Internal Standard Mixtures I and II (LM6001 and LM6004, Avanti Polar Lipids) or 30 µl of 4 µM d5-TAG Internal Standard Mixture I (LM6000, Avanti Polar Lipids) and 2.28 nmol cholesteryl ester 19:0 (LM4000, Avanti Polar Lipids). Lipid extraction Nano-ESI-MS/MS analysis were performed as previously described (Kumar et al., 2015; Özbalci et al., 2013; Turpin-Nolan et al., 2019). Mass spectra were processed by the LipidView 1.2 software (SCIEX) for identification and quantification of lipids. Endogenous lipid species were quantified by referring their peak areas to those of the respective internal standard. The calculated lipid amounts were normalized to the protein content of the tissue homogenate.

4.3 In-vitro cell and tissue culture

4.3.1 SGBS cell culture (human preadipocytes)

SGBS cells were derived from the stromal vascular fraction of the subcutaneous adipose tissue from a patient with Simpson-Golabi-Behmel syndrome (SGBS) (Wabitsch et al, 2001). SGBS cells are maintained in DMEM/F12 containing 33 µM biotin (Sigma-Aldrich), 17 µM pantotenat (Sigma-Aldrich), and 10% FCS (Gibco, Thermo Fisher Scientific) in a humidified incubator at 37°C with 5% CO2.

4.3.2 Generation of SGBS empty vector and HOIP KO cells (human preadipocytes)

Knockout SGBS preadipocytes were generated using a CRISPR/Cas9 system. sgRNA duplexes for HOIP (sgRNA1: AACCGCGACATCGAGTCAGT, sgRNA2: GGTGGCACGACGCTTTCTGT) were designed using CRISPick (Broad Institute) and inserted into the pMuLE ENTR U6 stuffer sgRNA scaffold L1-R5, kindly provided by Ian Frew (Addgene #62127; http://n2t.net/addgene:62127; RRID:Addgene_62127) (Albers et al, 2015). Sanger sequencing was employed to verify the correct insertion. Using LR Clonase II Plus (ThermoFisher Scientific), the specific pMuLE ENTR U6-sgRNA and pMuLE ENTR CMV-hCas9 L5-L2 plasmids were recombined with SleepingBeauty transposon plasmid pMuSE eGFP-P2A-PuroR-DEST (Tews et al, 2019). SGBS preadipocytes were co-transfected with the resulting pMuSE U6-sgRNA+CMV-hCas9+RPBSA-eGFP-P2A-PuroR plasmids and the SleepingBeauty-expressing pCMV(CAT)T7-SB100 plasmid pCMV(CAT)T7-SB100, kindly provided by Zsuzsanna Izsvak (Addgene #34879; http://n2t.net/addgene:34879; RRID:Addgene_34879) (Mates et al, 2009) at a mass ratio of 19:1 using a Neon Transfection System (Thermo Fisher Scientific) with 3x10 ms pulses of 1400 V. Stable bulk cultures were obtained by puromycin selection at 0.5 µg/ml.

4.3.3 Cell viability assay (human and mouse pre/ and adipocytes):

Cell viability was determined using CellTiter-Glo® assay (G7572, Promega) according to the manufacturer’s instructions.

4.3.4 Mouse adipocyte and preadipocytes cell death assays:

cells were treated with pan caspase inhibitor 20 µM Z-VAD-fmk (Abcam , ab120382), BV6 (5 µM, Adooq Bioscience, Canada, A14231) , RIPK1 inhibitor Nec-1 (50 µM, Calbiochem, USA 1--5-2263) and co-stimulated with home made 125 ng/ml xFlag-2xStrep-TNF (Haas et al., 2009) for the indicated times.

To detect dead adipocytes, cells were stained with fixable viability dye eFluor ™ 660 eBioscience™ (Thermo Scientific 65-0864-14) 1:1000 in PBS for 10 min , fixed with Fix and per kit Foxp3 / transcription factor staining (eBioscience, 00-5523-00) for 20 min, filtered in 100 µm strainers and acquired in FACS Symphony III BD using FACSDiva software (BD) and analysed in FloJo.v10.8.1. For representative pictures cells were stained with Lipid droplet stain (Linaria, BOT-70065-T) and Sytox Green (Thermo Fisher, S7020) and images were acquired with S3 Incucyte® Live-Cell Analysis (Sartorius).

To detect dead 3T3-L1 preadipocytes, cells were stained with Sytox Green (Thermo Fisher, S7020) and acquired in S3 Incucyte® and analysed for count and classification of adherent cell populations with Cell-by-Cell Analysis Software Module v2019A.

4.3.5 Adipogenic differentiation

4.3.5.1 Human adipocytes:

Adipogenic differentiation of SGBS cells was induced when cells reached 90% confluency. On day 0, cells were carefully washed twice with DPBS (Gibco). Culture medium was replaced by Adipogenic Medium I containing DMEM/F12 medium (Gibco) supplemented with 33µM biotin (SA), 17µM pantothenate (SA), 10µg/ml transferrin, 20nM insulin, 100nM cortisol, 0.2nM triiodothyronine (T3), 25nM dexamethasone, 250µM 3-isobutyl-1-methylxanthine (IBMX) and 2µM rosiglitazone. On day 4 of adipogenic differentiation, Adipogenic Medium I was replaced by Adipogenic Medium II consisting of DMEM/F12 medium supplemented with 33µM biotin, 17µM pantothenate, 10µg/ml transferrin, 20nM insulin, 100nM cortisol, and 0.2nM T3. SGBS cells are fully differentiated on day 14 of adipogenic differentiation.

4.3.5.2 Mouse adipocytes:

Adipogenic differentiation of 3T3-L1 ATCC cells was induced when cells reached 100% confluency. On day 0, culture medium was replaced by Adipogenic Medium I containing DMEM high glucose 10% FBS, 1% Pen/strep, 1µg/ml Insulin (I-9278-10mg/ml), Sigam), Dexamethasone 0,25 µM (D-2915-100mg, Sigma) , 3-isobutyl-1-methylxanthine (IBMX, I-7018-250mg, Sigma) 500 µM and rosiglitazone 2µM (R2408-10mg, Sigma). On day 3 of adipogenic differentiation, Adipogenic Medium I was replaced by Adipogenic Medium II consisting of DMEM high glucose 10% FBS 1% P/S and 1µg/ml Insulin, and change every 2 days, cells were fully differentiated on day 10 of adipogenic differentiation.

4.3.6 Bone marrow-derived macrophages (BMDMs)

For the differentiation of bone marrow-derived macrophages (BMDMs) from bone marrow, tibia and femur from mice were collected and kept in PBS on ice. Under the sterile hood, excess muscle and fibre was removed and bones were flushed with ice-cold PBS to isolate the bone marrow using a 23G needle. Following protocol was used as guidance (Ying et al., 2013).

4.3.7 Adipose tissue explant culture

GWAT was harvested and placed in DMEM/F12 medium supplemented with Pen/Strep. Under sterile conditions, tissue was cut into small 25-60 mg and weighed. Two explants were placed per well in 24-well plates containing 350 µL of DMEM/F12 + 0.2% BSA (0.2 µm filtered). Explants were fully submerged and incubated at 37°C with 5% CO_2 for 1–2 h to allow stabilization. Cell death-inducing treatments were initiated simultaneously across conditions at defined time point (24 h) and included 20 µM z-VAD-FMK (Catalog#S8102, Selleck), 2 µM BV6, and 100 ng/ml of TNF (Prepotech 315-01A). Treatments were stopped at defined endpoints, followed immediately by tissue fixation. At each time point, the culture medium was aspirated, and 500 µL of either 10% formalin was added to each well for 1 hour at room temperature. Fixed tissues were then transferred to histology cassettes and stored in PBS at 4 °C. Subsequently, paraffin embedded tissue sections were processed for TUNEL staining.

4.4 Biochemistry

4.4.1 Preparation of protein extracts from tissue

100 mg of fat tissue was in 500 ul of RIPA buffer (Tris-HCL (pH 8) 50 mM, NaCl 150 mM) without detergents and a 5 mm bead to be homogenised in TissueLyser II in two rounds for 2 minutes at 30 1/s. After tissue disruption detergents (NP-40 0.5%, 0.5% Sodium Deoxycholate) were added together with EDTA-free protease inhibitor cocktail (Roche) and 1× phosphatase-inhibitor cocktail 2 (Sigma) and deubiquitinase inhibitor (S7130, Selleck Chemicals) sampler were incubated at 4 °C for 30 min on agitation. Lysates were denatured with a reduced sample buffer and b-mercaptoethanol at 95 °C for 10 min.

4.4.2 Protein lysate preparation from cells

4.5.2.1 Human adipocytes:

Cells were lysed in lysis buffer (30 mM Tris-HCl, pH 7.4, 150 mM NaCl, 2 mM EDTA, 2 mM KCl, 10% Glycerol) supplemented with 1% Triton X-100, 1x complete EDTA-free protease-inhibitor mix (Roche), and 1x phosphatase-inhibitor cocktail 2 (SA). Lysates were denatured in reducing sample buffer before separation by SDS-PAGE (BoltTM 4-12% Bis-Tris). Membranes were incubated with primary antibodies at 4°C overnight or for 1 hour at room temperature (RT). Washing of membranes was performed in 1xPBS containing 0.1% Tween-20 (SA) for 3 × 10 min prior to incubation with the HRP-conjugated or StarBright Blue 700 fluorescent secondary antibody for 1 hour at RT. Membranes were subsequently imaged on a ChemiDoc Imaging System.

4.4.2.2 Mouse differentiated adipocytes:

Minute™ Total Protein Extraction Kit for Adipose Tissues/Cultured Adipocytes (AT-022) was used according to the manufacturer's instructions.

4.4.3 Western blot analysis

Proteins were separated by precasted 4-15% polyacrylamide gels (5678085, Bio Rad) at 150 Volts for 50 minutes, transfer in Bio Render Transfer Blot mix programme (1704159, Bio-Rad) cat number) and analysed by western blotting with antibodies. Membranes were incubated with primary antibodies at 4°C overnight). Washing of membranes was performed in 1xTBS containing 0.1% Tween-20 (SA) for 3 × 5 min prior to incubation with the HRP-conjugated for 1 hour at RT. Membranes were subsequently incubated with ECL (BioRad 1705060) and films (11820, Radiolix).

4.4.3.1 Western Blot antibodies

4.4.3.1.1 Human adipocytes:

PPARg (rabbit polyclonal, R&D Systems, 2443, dilution 1:1000), Adiponectin (rabbit polyclonal, GeneTex, GTX112777, dilution 1:1000), GAPDH (Bio-Rad, AbD22549, dilution 1:5000), ERK (rabbit, Cell signalling Technology (CST), 9102, dilution 1:2000), phospho-IkBa (IgG1, CST, 9246, dilution 1:1000), IkBa (rabbit, CST, 9242, dilution 1:1000), phospho ERK (rabbit, CST, 9101, dilution 1:2000), Tubulin (Bio-Rad, AbD22584, dilution 1:5000), FLAG (IgG1, Sigma Aldrich (SA), F3165, dilution 1:1000), HOIP (sheep, Ubiquigent, 68-0013-100, dilution 1:1000), SHARPIN (rabbit, Proteintech, 14626-1-AP, dilution 1:2000), HOIL-1 (IgG1,

SA, clone 2E2, dilution 1:1000). Antibody detecting linear ubiquitin (rabbit) was generated using amino acid sequences as described previously (dilution 1:1000) (Matsumoto et al, 2012).

4.4.3.1.1 Mouse adipocytes and tissues:

(all primary antibodies were used at a 1/1000 dilution), actin (A1978, Sigma), tubulin (T9026, Sigma), RIPK1 (610459, BD), cleaved caspase-8 (9429, Cell signalling), MLKL (MABC604, Millipore), phosphorylated IκBα (9246, Cell signalling), IκBα (9242, Cell signalling) and: p-ripk1 (31122S, Cell Signalling) p-mlkl (37333, Cell Signalling) hoip (68-0013-100, Ubiquigent,). M1 chains (custom made), cleaved casp 3 Asp175 (9661s, Cell signalling), perilipin(ab3526, abcam), p-p65 (3033, cell signalling),

4.4.3.2 M1 TUBE

Anti-M1 TUBE (FLAG, UM606, Life Sensors) was performed according to the manufacturer's instructions.

4.5 Statistical analysis

Data was analysed using GraphPad Prism software (version 8.4.1) (San Diego, CA). Area under the curve (AUC) and Area over the curve (AOC) were calculated according to (Virtue & Vidal-Puig, 2021) instructions. Statistical tests were used as described in the Figure legends. All data are presented as Mean ± SD and was analysed by analysis of variance (ANOVA) with Bonferroni's post hoc multiple comparison test, in all cases test were applied to each group control (cells to not treated, mice to WT littermate control with the same diet) except for experiments with only two groups in which Unpaired individual parametric Student's t-test was performed assuming same SD between populations. Correlations were assessed by non-parametric Spearman's test. Statistical significance was indicated as follows: # P-value <0.0001 *** P-value <0.001; ** P-value <0.01; * P-value <0.05; ns not significant. In the serum analyses, some results from different longitudinally followed groups of mice were combined. Animals with same sex and same age were employed to minimise physiological variability and to reduce SD from the mean. In case of death or sickness, the animal was excluded from analysis. Tissue samples were excluded in cases of failure in extraction of RNA or protein of suitable quality and quantity.

4.6 AI tools

In the preparation of this thesis, the Perplexity.ai website was used as an AI writing assistant to improve coherence, enhance writing structure by suggesting and pre-formulated sentences, and to check for grammar and spelling mistakes. The author retains full responsibility for the quality, accuracy, and originality of the text. The core intellectual contributions, including critical thinking, development of original arguments, data interpretation, and drawing conclusions, were solely performed by the author. All AI-assisted sections were reviewed and revised to maintain the scholarly integrity of this thesis.

5. Discussion

5.1 Linear ubiquitination regulates NF-κB, the balance between cell death and survival

The balance between cell death, proliferation and inflammation is fundamental for maintaining tissue homeostasis and preventing disease. Cells are constantly exposed to both intrinsic and extrinsic signals that can trigger programmed cell death, yet a complex network of checkpoints is in place to tightly regulate this process and ensure that unwanted cell loss does not occur. Among the various cell death pathways, those triggered by extrinsic signals, especially through death receptors, are the most well-characterized during inflammatory diseases.

TNFR1, in particular, stands out due to its dual functionality: it can activate NF-κB/MAPK signaling, promoting cell survival and inflammation, but can also induce cell death, depending on the cellular context and the signaling thresholds involved. This dual functionality is particularly significant in AT, where both processes seem to contribute to local inflammation and metabolic dysfunction during obesity (Hildebrandt et al., 2022; Ju et al., 2019), underscoring the need to elucidate the mechanisms that regulate this balance in this setting.

For several years LUBAC has been placed as a crucial regulator downstream of TNFR1 activation (Haas et al., 2009; Peltzer et al., 2014, 2018; Rickard et al., 2014; Taraborrelli et al., 2018). Its activity plays a pivotal role in determining cellular fate, typically favoring pro-survival outcomes (Y.-G. Chen et al., 2024; Niu et al., 2011). In fact, several authors have shown that cancer cells upregulate LUBAC activity to enhance their survival capabilities, highlighting its importance in disease progression (J. Cheng et al., 2024; Y. Guo et al., 2022; Ruiz et al., 2019; Z. Song et al., 2020).

The formation and disassembly of linear ubiquitin chains are highly specific processes, with HOIP being the only E3 ubiquitin ligase generating linear ubiquitin chains and OTULIN the only deubiquitinase exclusively hydrolyzing them. This specificity allows for unique study opportunities in contrast to other types of ubiquitination.

Our study revealed a significant increase in LinUb chains within adipose tissue during obesity, suggesting a novel adaptive mechanism employed by adipocytes. This upregulation of linear chains formation likely serves as a protective response against the cellular stress induced by overnutrition, enhancing adipocyte survival through LUBAC activation. This

finding not only exemplifies the complex interplay between cellular stress responses and metabolic regulation but also underscores the potential tissue-specific roles of LinUb.

5.1.1 Linear ubiquitin chains prevent adipocyte cell death: metabolic implications

Preventing adipocyte apoptosis during HFD has been shown to reduce metabolic inflammation and protect against metabolic syndrome (e.g., adipocyte-specific ablation of Bid (Alkhouri et al., 2010) and Casp8 (Luk et al., 2023)), conversely, acute induction of caspase-8–mediated apoptosis in adipocytes (FAT-ATTAC model) leads to severe lipodystrophy and metabolic syndrome during diet-induced and genetic obesity (Pajvani et al., 2005). This FAT-ATTAC model provided as a proof of concept, that increased adipocyte apoptosis directly causes metabolic syndrome upon obesity. Similar pathological phenotypes are observed with adipocyte-specific deletion of IKKβ, which causes lipodystrophy-like features and insulin resistance (Kwon et al., 2014; S.-H. Park et al., 2016; Yuan et al., 2001), which was attributed to lower pro-survival signalling, (although IKKβ can regulate cell death independently of NF-κB (Dondelinger et al., 2015)). Diverging from prior publications, our study was specifically focused on the interplay between adipocyte cell death and NF-κB-driven inflammation in adipose tissue during obesity-associated inflammation. In this context, LUBAC constitutes a unique platform, linking gene activation of these dual pathways. Our experimental setup establishes an elegant 'metabolic switch' system, enabling direct comparison of linear ubiquitin chain depletion against increased LUBAC activity.

On one hand, HOIP deficiency in adipocytes leads to early-onset lipodystrophy-like syndrome, increased GWAT hypertrophy, and predisposition to metabolic syndrome, even under chow diet conditions. This phenotype is associated with reduced secretion of key adipokines such as adiponectin and leptin, likely contributing to hepatic lipid metabolism disturbances and the development of MASLD (Mantovani et al., 2022). Moreover, RNA sequencing of HOIP-deficient mice revealed an obesogenic and ageing-related pre-diabetic transcriptional profile, even in the absence of dietary challenge, emphasizing the importance of LUBAC in maintaining adipose tissue health during ageing.

Furthermore, cell-type deconvolution analyses indicated that much of the altered transcriptional signature in HOIP-deficient adipose tissue originates from macrophages, with early increases in F4/80-positive cells and CLS in GWAT. This supports the model in which adipocyte death precedes and drives macrophage activation, contributing to local inflammation and systemic metabolic dysfunction, as previously suggested in acute

apoptosis models (Fischer-Posovszky et al., 2011; Murano et al., 2013), (Pajvani et al., 2005; Trujillo et al., 2005). However, unlike acute models, HOIP-deficient mice provide a physiological platform to study chronic adipocyte cell death and its metabolic consequences over time and under various dietary conditions.

Mechanistically, our data demonstrate that caspase-8 is the primary driver of cell death in HOIP-deficient adipocytes. Caspase-8 deletion was sufficient to prevent the lipodystrophy and metabolic syndrome caused by HOIP loss, positioning LUBAC as a key checkpoint restraining caspase-8–dependent cell death. Notably, while mouse adipocytes can execute necroptosis in-vitro, caspase-8 deletion did not unleash aberrant necroptosis in-vivo, even when HOIP was absent. This contrasts with keratinocytes where HOIP and caspase-8 deletion still triggers necroptosis (Peltzer et al., 2018; Taraborrelli et al., 2018). Of note, the deletion of caspase-8 alone did not result in spontaneous increases in cell death rates, unlike in other tissues such as intestinal epithelial cells (Günther et al., 2011; Luk et al., 2023), endothelial cells (Bader et al., 2023; Kang et al., 2004), keratinocytes (Andrew Kovalenko, Jin-Chul Kim, Tae-Bong Kang, Akhil Rajput, Konstantin Bogdanov, Oliver Dittrich-Breiholz, Michael Kracht, Ori Brenner, David Wallach, 2009) or bone marrow progenitors (Kang et al., 2004). This finding suggests a yet undescribed mechanism regulating the prevention of acute necroptosis in adipocytes. However, although some studies report improved glucose tolerance and protection from insulin resistance in *Casp8*$^{A\text{-}KO}$ mice under HFD (Luk et al., 2023), we did not observe such protection in our models, suggesting that additional factors such as diet composition and housing conditions can be affecting the outcome of this measurements.

Adipocytes are not the first time in which caspase-8 deletion does not result in aberrant necroptosis rates. In pancreatic β-cells, caspase-8 has been shown to protect against both type 1 and type 2 diabetes challenges (Liadis et al., 2007), while in the liver, several models demonstrate its protective role, such as limiting spontaneous apoptosis following NEMO deletion (Liedtke et al., 2011), preventing diet-induced steatosis (Hao et al., 2017), preventing cytotoxicity on anti-Fas Abs injection (Kang et al., 2004) and accelerating liver regeneration through increased basal NF-κB activity (Freimuth et al., 2013). Although it is true that in these tissues, the lack of necroptosis is generally attributed to low RIPK3 expression, in the case of β-cell-specific-Casp8-knockout-model, loss of β-cells during ageing led to their gradual depletion, suggesting a possible sub-lethal necroptotic process that leads to β-cell demise in the long run. Supporting this, a recent study in hepatocellular carcinoma described a sub-lethal necroptosis state that promotes tumorigenesis via the release of inflammatory cytokines in an NF-κB–dependent manner (Vucur et al., 2023).

While this mechanism could potentially explain the ageing-related β-cell loss, it remains a hypothesis requiring further investigation.

Unfortunately, to the date, the contribution of necroptosis to obesity and metabolic disorders remains controversial. Some studies report increased levels of RIPK1, RIPK3, and MLKL in adipose tissue during obesity (Gautheron et al., 2016; Karunakaran et al., 2020; H. Xu et al., 2019), despite this, the role of MLKL in different HFD models remains inconsistent (Miyata et al., 2021; Ohene-Marfo et al., 2024; Saeed et al., 2019; H. Xu et al., 2019). The lack of standardised procedures regarding diet composition and housing conditions in the different models, interferes with our data interpretation, while, in addition, several authors highlight non-canonical roles of MLKL in lipid metabolism that may influence adipose tissue biology and inflammation independently of cell death execution (Ohene-Marfo et al., 2024; Tye et al., 2025).

Comparing our data in differentiated adipocytes to our in-vivo models (*Hoip*$^{A\text{-}KO}$ and *Hoip*$^{A\text{-}KO}$*;Casp8*$^{A\text{-}KO}$), absence of necroptosis in adipocytes may reflect tissue-specific regulation or limitations of in-vitro models to recapitulate in vivo complexity. However, although this could be linked to the tissue specific implication of Lin-Ub, it also supports the notion than, in some contexts LUBAC might be a necessary actor for final necroptosis execution (Weinelt et al., 2024), in fact, in our *Hoil-1*^{C458A} derived BMDMs, increase linear chains led to further sensitization towards necroptotic stimuli.

Our results indicate that necroptosis does not play a major role in adipocyte death in vivo under HOIP and caspase-8 deficiency. However, although caspase-8 loss effectively prevents cell death in HOIP-deficient adipocytes, as shown by TUNEL staining, we still observed increased inflammation in obese *Hoip*$^{A\text{-}KO}$*;Casp8*$^{A\text{-}KO}$ mice. This raises the possibility that sub-lethal necroptotic signaling, rather than overt cell death execution may contribute to adipose tissue dysfunction and GWAT hypertrophy in this context. Thus, while lethal necroptosis appears to be absent in adipocytes lacking caspase-8, we cannot rule out the involvement of non-canonical, sub-lethal necroptotic pathways in driving inflammatory and metabolic changes.

Cell death prevention is key to maintain AT function and limit liver lipid accumulation. Several studies have also highlighted the importance of NF-κB activation for adipocyte survival and macrophage activation during obesity (Hildebrandt et al., 2022). Still, the correct balance between pro-survival and detrimental pro-inflammatory implications of NF-κB is still ill defined (Catrysse & van Loo, 2017; Hildebrandt et al., 2022). In fact, while some

publications show that reducing NF-κB–mediated inflammation (TNF- or TNFR1-deficient mice) protects against HFD-induced obesity (Romanatto et al., 2009; S.-Y. Yu et al., 2020), other authors claim that increased NF-κB in adipocytes showed beneficial outcomes regarding metabolic health (Jiao et al., 2012).

In our increased LinUb model, *Hoil-1*^{C458A} AT revealed protection against cell death in obese mutants, similarly to other cell models with the same mutation (J. Guo et al., 2023; J. Yu et al., 2024). However, since TUNEL staining detects cell death across all cell populations, we cannot attribute the protection only to adipocytes. In addition, we found that HFD-fed *Hoil-1*^{C458A} mice exhibited diminished ScWAT expansion, reduced adipocyte size, and significant increase in immune infiltration (most likely due to increased NF-κB activation). TNF (and other NF-κB–related genes such as IL-1 and IL-6) can also suppress lipid storage and promote fatty acid release through various pathways (Kolb, 2022). Thus, it is plausible that increased LinUb supports adipocyte survival also by preventing hypertrophy, thereby limiting tissue expansion, although this did not translate into lower weight gain or improved glucose metabolism under HFD challenge (unlike other models with increased NF-κB activation in adipocytes (Jiao et al., 2012; T. Tang et al., 2010) and macrophages (Catrysse et al., 2021)) .

Of note, one of the most pronounced effects in our obese mice was the improved liver pathology. Specifically, *Hoil-1*^{C458A} mice showed reduced hepatic lipid deposition (although the overall steatotic score remained unchanged) during the HFD challenge. This reduction in hepatic steatosis was consistent across all lipid species measured in our lipidomic analysis. In line with these findings, mutant mice also exhibited lower cholesterol levels in their bloodstream, further supporting the notion of preserved liver function. Despite these improvements, and in contrast to what is seen in NF-κB overactive models, no amelioration in insulin sensitivity, except for reduced serum insulin levels in mutant mice at the endpoint, was observed. Conversely, we identified gene-regulation abnormalities in lipid uptake pathways and reduced long-chain fatty acid metabolism in the liver of mutant mice, including impaired lipogenesis and mitochondrial oxidation, pointing to broader metabolic dysregulation. Whether this is the cause or consequence of lower lipid content in hepatocytes still remains inconclusive.

Protection against apoptosis has been shown to prevent liver damage (Catrysse et al., 2016). On the other hand, increased NF-κB activation is generally considered detrimental in liver-specific models (Heida et al., 2021). In the liver, *Hoil-1*^{C458A} mutation may exert contradictory effects, and although we observed protection against diet-induced steatosis in

the livers of mutant mice, the elevated gene signature associated with NASH, alongside increased inflammatory markers and IFN response, does not facilitate our interpretation. Our observed protection remains paradoxical, as activation of innate immune cells (e.g., macrophages, neutrophils) in the liver is strongly linked to the progression from hepatic steatosis to NASH (Nati et al., 2022) and NF-κB, has also been strongly associated with MASLD pathogenesis (D. Cai et al., 2005). In this train of thought, it is expected that the increased NF-κB and IFN signature perpetuates inflammation in a vicious cycle of liver damage.

Notably, *Hoil-1*^{C458S} mutant mice have been reported to exhibit a systemically hyperactive immune phenotype, with both macrophages and cytotoxic T cells showing heightened inflammatory and interferon responses even under basal conditions (Fuseya et al., 2024; Petrova et al., 2021). And although other liver cell types may contribute to this gene signature, it is likely that the IFN response originates mainly from immune cells.

Moreover, liver RNAseq data from mutant mice also revealed elevated anti-apoptotic cFLIP levels, which could potentially contribute to protection against liver damage, while simultaneously showing upregulation of pyroptotic signature genes. Noteworthy, LUBAC is fundamental for NLRP3 activation in macrophages (Rodgers et al., 2014), a pathway highly linked to liver inflammation and NASH in acute liver injury models (Mridha et al., 2017; L. Yu et al., 2022), especially in myeloid cells (Kaufmann et al., 2022). Taken together with our results, it highlights the possibility that differential NF-κB activity impacts on cell populations. Most likely, increased LinUb pushes towards pyroptosis sensitization in immune cells, while simultaneously providing anti-apoptotic protection to hepatocytes. Elucidating these mechanisms in detail would require single-cell sequencing or tissue-specific mutant models.

Collectively, these results argue against attributing liver protection solely to the prevention of hepatocyte or adipocyte apoptosis. Instead, they highlight a complex interplay between LinUb-mediated cell survival, NF-κB-driven inflammation, and metabolic adaptation across tissues.

Another possibility to explain reduced liver steatosis is an increase in basal beta oxidation. The enhanced browning of ScWAT in unchallenged mice, the protection of BAT whitening during HFD, and previous reports of increased energy expenditure in enhanced NF-κB models (Catrysse et al., 2016; Jiao et al., 2012; T. Tang et al., 2010), could in principle reduce the lower liver steatosis to a consequential hallmark rather than a tissue specific protection. In fact, unchallenged *Hoil-1*^{C458A} mice also exhibited elevated UCP-1 content in

both BAT and ScWAT, without apparent changes in RER. This finding remains controversial as studies suggest that NF-κB activation (Romanatto et al., 2009) or its proinflammatory related molecules TNF, IL-1β (Goto et al., 2016), and LPS can inhibit brown adipocyte differentiation or UCP-1 expression, thereby impairing thermogenic activity. In line with our observations, other studies suggest a supportive role of NF-κB during browning. For instance, NF-κB activity has been shown to increase during brown adipocyte differentiation through the elevation of p65 (RelA) and is transcriptionally upregulated during cold stimulation (Peng et al., 2022), while it has been reported that preventing brown adipocyte apoptosis increases cell number and enhances the metabolic capacity of brown adipose tissue (Nedergaard et al., 2019). Yet, since NF-κB–mediated inflammatory gene activation and cell death regulation are highly interlinked processes, their respective contributions to inflammation during metabolic dysfunction remain unknown.

On the other hand, recent work has shown that LUBAC can mediate stress responses, with HOIP stabilizing complexes at the mitochondrial membrane to amplify NF-κB upon TNF activation (Z. Wu et al., 2022), and although adipocyte mitochondria are relatively low in abundance compared to other tissues, they play essential roles in differentiation, lipogenesis, adipokine secretion, and the browning process (Honecker et al., 2021; Keuper et al., 2014; Koh et al., 2007). Increased LUBAC activity may protect mitochondria from diet-induced cell death, which could explain the observed protection against whitening in BAT of mutant mice. Further studies in primary isolated cells need to be conducted to further corroborate mitochondria stability in LUBAC mutant cells.

This knowledge gap, together with the suggested tissue-specific functions of NF-κB during metabolic syndrome (Catrysse & van Loo, 2017) leads to controversies on the reported importance of NF-κB signalling in metabolic homeostasis (Hildebrandt et al., 2022). Additionally, plasma IL-6 (an NF-κB target gene) has been shown to play a crucial role in thermogenic adaptation. IL-6 is essential for increasing ScWAT UCP1 mRNA and protein expression during exercise training and cold exposure(Knudsen et al., 2014) and appears fundamental for beige adipocyte differentiation(Carrière et al., 2014). This suggests that increased linear chains might be supporting both BAT brown adipocyte survival and ScWAT browning by upregulating NF-κB. Moreover, these processes might occur simultaneously and explain the prevention of BAT whitening during HFD.

It remains unclear whether the browning phenotype is driven by adipocyte-specific protection, as previously observed with the constitutive activation of IKKβ in adipocytes (Jiao et al., 2012), or by intrinsic macrophage reprogramming, as seen in the A20 KO model in

myeloid cells, which exhibited elevated energy expenditure due to enhanced ATM metabolism (Catrysse et al., 2021). Our results suggest both mechanisms may be contributing to our phenotype.

The contrasting findings in *Hoil-1*^{C458A} mice suggest that increased LinUb potentially preserves thermogenic function in BAT and ScWAT despite an inflammatory environment. However based on literature we cannot rule out that an increased lipid metabolism in myeloid cells on these tissue (or the liver itself) might also be the reason why we see reduced lipid accumulation, further experiments regarding lipid metabolism in these cells need to be conducted to further elucidate this mechanism. In sum, our results underscores the need for further investigation into the interplay between inflammation, LinUb signaling, and thermogenesis in adipose tissue.

5.1.1.1 The central role of adipocyte cell death and NF-κB in MASLD progression

In contrast to our findings with the *Hoil-1*^{C458A} model, the cell-death-driven MASLD model (*Hoip*$^{A\text{-}KO}$) exhibited a pronounced exacerbation of metabolic disturbances during obesity challenge, with hepatic steatosis and hepatomegaly evident from the early stages of disease. Notably, in double knockout (*Hoip*$^{A\text{-}KO}$*;Casp8*$^{A\text{-}KO}$) mice, despite preventing adipocytes apoptosis, there was no improvement in liver steatosis compared to littermate controls; in fact, some results indicated even higher cholesterol secretion and increased insulin levels in both *Casp8*$^{A\text{-}KO}$ and *Hoip*$^{A\text{-}KO}$*;Casp8*$^{A\text{-}KO}$ mice. This is in stark contrast to the *Hoil-1*^{C458A} mice, which display lower cholesterol and insulin levels, and are resistant to ectopic lipid deposition. Examining GWAT architecture, we found that while cell death was prevented in both models (*Hoip*$^{A\text{-}KO}$*;Casp8*$^{A\text{-}KO}$ and *Hoil-1*^{C458A}), however, pronounced and thick CLS and hypertrophic adipocytes persisted in *Hoip*$^{A\text{-}KO}$*;Casp8*$^{A\text{-}KO}$ mice. In contrast, *Hoil-1*^{C458A} HFD mice, despite increased immune cell infiltration (CD45+ cells). These findings underscore adipocyte cell death-driven inflammation as a primary contributor to MASLD exacerbation in *Hoip*$^{A\text{-}KO}$ mice, while also suggest that a certain level of NF-κB activation in adipocytes may be necessary to adipocyte hypertrophy in response to HFD.

Indeed, adipocyte metabolic inflexibility alone is sufficient to trigger steatosis and hepatic IR (E. Lee et al., 2023). IL-6 produced by VAT for example has been highlighted as a necessary response for fat mobilization, and interestingly, IL-6-deficient mice display paradoxical IR along with steatosis and inflammation, even on a standard diet (Matthews et al., 2010). Which, in principle, goes in line with our observation in human data and Hoil-1 levels in obese patients and the reduced lipid deposition in the *Hoil-1*^{C458A} mice. Moreover, beyond

adipokine secretion, AT is also a key source of circulating exosomal miRNAs that regulate specific transcriptional events in the liver (Korf & van der Merwe, 2017; E. Lee et al., 2023). Further studies need to be conducted to understand which metabolic routes might be interrupted in these mice to fully elucidate the implications of LUBAC activity in adipose tissue-liver cross talk.

Another intriguing finding is the absence of dyslipidemia in *Hoip*$^{A\text{-}KO}$ mice. Our results suggest a disrupted crosstalk between the liver and WAT, where lipids were synthesized at similar rates across all groups but were not secreted into the bloodstream (at least not in higher amounts than in WT littermate controls) leading to their accumulation at the site of origin. Early hepatic insulin resistance in *Hoip*$^{A\text{-}KO}$ mice was clearly evidenced by impaired ITT response, hyperglycemia, and hepatomegaly after just 8 weeks of diet. Interestingly, HFD-fed *Hoil-1*^{C458A} mice showed lower insulin resistance in the ITT at 8 weeks, although this effect disappeared at later time points. Although this remains speculative, it is important to note that we are comparing a full-body mutant to a tissue-specific deletion. It is possible that in the early stages of obesity, when adipose tissue is the first to bear the metabolic burden, increased LinUb in this compartment may offer a slight delay in the onset of IR in the overall phenotype. Yet, as the disease unfolds and liver inflammation intensifies—likely exacerbated in the mutant models, as previously discussed—this early protection is gradually eclipsed, ultimately giving way to IR levels to become comparable to those of their littermate controls.

Taken together, these findings highlight a possible critical role of LUBAC regulation in adipocyte-derived TNF/NF-κB-dependent cytokine release, adipokines, and/or the adipocyte apoptotic secretome in driving liver steatosis during obesity challenges. Paradoxically, it might be that TNF activates LUBAC to protect stressed adipocytes from TNF-induced cell death while maintaining homeostatic NF-κB activation.

5.1.1.2 Linear ubiquitination in the crosstalk between adipocytes and macrophages

Our lipodystrophy model allowed us to elucidate the inflammatory consequences on macrophages due to impaired NF-κB signaling and excessive cell death in adipocytes. The marked increase in immune cell infiltration in *Hoip*$^{A\text{-}KO}$ GWAT was particularly associated with M1-like macrophages, which are known to exacerbate metabolic dysfunction (Lindhorst et al., 2021; Yao et al., 2022).

Interestingly, systemic inflammation in *Hoip*$^{A\text{-}KO}$ mice was only mildly elevated, suggesting that the primary impact of HOIP deletion occurs within the local AT environment rather than spreading to other tissues. From the inflammatory panel that we evaluated, the only altered

cytokine detected in the bloodstream *of Hoip*$^{A\text{-}KO}$ mice in CD conditions was G-CSF. Notably, this cytokine (gene name: CSF3), a member of IL-6 superfamily, was negatively correlated with LUBAC expression in our dataset from human adipose tissue, and is strongly associated with inflammation and insulin resistance (Ordelheide et al., 2016). This observation implies that myeloid/granulocyte recruitment and subsequent local reprogramming may be necessary for the development of MASLD, although we cannot rule out the possibility that this cytokine could also be secreted by the liver (R. S. Khan et al., 2023).

Moreover, our in-vitro experiments showed that increased LinUb protects against both apoptosis and necroptosis stimuli in preadipocytes, likely due to enhanced pro-survival NF-κB activation. However it had a differential effect in BMDMs. Primary macrophages with increased linear ubiquitin chains were protected from apoptosis but became more sensitive to necroptotic stimuli, indicating a mainly anti-apoptotic role for linear chains in BMDMs. This cell-type–specific effect, possibly due to LUBAC's differential regulation of NF-κB-dependent IL-1β responses (Boisson et al., 2012), was further supported by enhanced rescue with RIPK1 inhibition and delayed cell death with NF-κB inhibition, suggesting additive protection and a basal anti-apoptotic state in mutant BMDMs.

From a myeloid-specific perspective, adipocyte-A20-deficient mice (despite an inflammatory environment in metabolic tissues), presented increased mitochondrial respiratory function, promoting fat utilization and resulting in a leaner phenotype upon HFD (Catrysse et al., 2021). However, like in the liver (Catrysse et al., 2016), myeloid cells were more susceptible to cell death due to A20 deletion. This highlights the importance of our murine model, in which NF-κB signaling is not only upregulated but also cell-death-driven inflammation is suppressed. This approach enables us to investigate the precise role of NF-κB signaling during DIO without depleting the cell population of interest.

Notably, our model exhibits a reduced steatotic phenotype despite the presence of DIO and NF-κB-driven inflammation in both immune and liver cells. Thus, our findings underscore the potentially underestimated impact of cell-death-driven inflammation during HFD models (except acute liver injury models, in which cell death contribution is remarkably described) on the development of MASLD.

On the other hand, it is also known that tissue-resident macrophages in BAT contribute to thermogenesis and energy homeostasis (Daemen & Schilling, 2019; Wolf et al., 2017). During obesity rewiring of cellular metabolism plays a critical role in regulating macrophage

function. In fact, ATMs from obese mice exhibit distinct metabolic profiles characterized by elevated glycolysis and oxidative phosphorylation compared to those from lean mice.

Furthermore, pro-inflammatory functions of ATMs are highly dependent on glycolytic metabolism (Wculek et al., 2022). Proteins and enzymes involved in glucose uptake and catabolism, such as GLUT1 and hexokinase 2, are also induced in BAT during cold exposure (H. P. Nguyen, Yi, Lin, et al., 2020; Winther et al., 2018). In fact, aerobic glycolysis not only supports BAT thermogenesis but also contributes to the browning of WAT through lactate signaling and metabolic reprogramming. Interestingly, overexpression of HOIL-1, a component of LUBAC, markedly increased GLUT1 expression in Hep3B cells, thereby enhancing glycolysis (Z. Xu et al., 2022). In addition, increased activation of HIF-1α in ATMs from obese visceral adipose tissue has been shown to induce IL-1β expression and upregulate genes involved in glycolysis (M. Sharma et al., 2020), while LUBAC has also been proposed to stabilize HIF-1α in cancer models supporting tumorigenesis.

Although these interactions require further corroboration, our findings suggest that the increased UCP1 content in ScWAT and protection against HFD-induced BAT whitening might be linked to LUBAC-dependent priming of metabolic reprogramming. LUBAC-mediated NF-κB activation may support macrophage survival and cytokine production, while HIF-1α stabilization could enhance glycolytic flux and metabolic adaptation. Together, these mechanisms could sustain macrophage function within thermogenic niches.

In light of our results, it seems that besides preventing cell death, LUBAC might also be playing a role in the regulation of macrophage recruitment and/or activation in response through adipocyte secretion. However, whether TNF is the sole trigger or is primarily secreted by ATMs or adipocytes remains an open question.

5.2 Clinical relevance of this study

LUBAC-deficient patients present with a paradoxical combination of hyperinflammation and immunodeficiency, which may be explained by cell type-specific responses to Lin-Ub dysregulation (Boisson et al., 2012; Jahan et al., 2021). These patients often exhibit severe autoinflammation and recurrent infections, with TNF inhibition providing partial symptom relief in some cases.

Treatment responses vary among LinUb-deficient patients. Those with HOIL-1 deficiency generally respond well to corticosteroids, while TNF blockade has limited efficacy and has even exacerbated inflammation in one case (Boisson et al., 2012). In contrast, ORAS patients typically respond well to anti-TNF therapy.

The metabolic implications of Lin-Ub deficiency remain underestimated. So far, it is reported that patients with HOIL-1 deficiency accumulate polyglucosan bodies in various organs, particularly skeletal and cardiac muscle, leading to myopathy and cardiomyopathy with heart failure (Boisson et al., 2015). In addition, these patients also presented liver fibrosis with hepatocyte vacuoles resembling glycogenosis and hepatosplenomegaly (Boisson et al., 2015). Moreover, one patient with impaired HOIP expression presented high triglycerides concentrations and fatty diarrhea, along with diffuse muscular atrophy and fatty infiltration of certain muscle groups (Boisson et al., 2015). Interestingly, patients with biallelic homozygous mutant variants in OTULIN, resulting in ORAS, present with progressive lipodystrophy, panniculitis, and spontaneous steatotic liver disease, mirroring some features observed in our mouse model (Damgaard et al., 2020; Dou et al., 2024; Zhou, Yu, et al., 2016). Despite this observation, the metabolic complications of linear ubiquitination in these patients remained largely unexplored.

In addition, our collaborators identified LUBAC and OTULIN as physiological regulators of AMP-activated protein kinase (AMPK), a key metabolic regulator (Elbæk et al., 2024). LUBAC promotes AMPK activation, while OTULIN restricts it. During starvation, LUBAC deficiency impairs autophagy induction and hinders the shift from oxidative phosphorylation to glycolysis. Strikingly, our collaborators also find that LUBAC-deficient Drosophila have a strongly reduced survival rate after starvation(Elbæk et al., 2024).

Our cross-sectional cohort study revealed that expression of LUBAC components in adipose tissue was associated with improved metabolic fitness in obese patients. This finding, combined with our model results, suggests that increased linear ubiquitination in adipose tissue may prevent caspase-8-dependent cell death during obesity, ameliorating metabolic

inflammation. Additionally, HOIL-1 activity appears to be involved in lipogenesis during weight loss in morbidly obese patients after bariatric surgery, possibly due to IL-6 production from visceral adipose tissue .

In our analysis of human-derived expression levels of LUBAC components in adipose tissue during aging, we found that HOIP expression was upregulated in both ScWAT and VAT of elderly males, along with a concurrent increase in *Casp8* expression in ScWAT. This suggests a potential role for HOIP in maintaining adipose tissue homeostasis and possibly regulating apoptotic programs in aging males. Additionally, RNA levels of HOIL-1 and SHARPIN were elevated in ScWAT during male aging, while these changes were not observed in females. In females, the only notable change was an increase in HOIL-1 expression in ScWAT with no alterations in *Casp8* levels, underscoring potential sex-specific differences in LUBAC expression across adipose tissue depots with age. These findings suggest that LUBAC may play a role in adipose tissue remodeling and metabolic adaptation throughout the lifespan, although further studies are needed to fully understand its contribution to age-related metabolic health.

In sum, our human data analysis indicates that LUBAC expression could serve as a protective mechanism for adipocyte survival during obesity and ageing.

5.2.1 *Hoip*$^{A\text{-}KO}$ a possible model for autoimmune lipodystrophies

Hoip$^{A\text{-}KO}$ mice is an intrinsic mature adipocyte cell death murine model that features some aspects of autoimmune lipodystrophies. Despite not directly replicating the autoimmune mechanisms, this model mimics a gradual fat loss through apoptosis that varies in sensitivity of the different adipose tissue depots. This could effectively replicate the pattern of fat loss observed in partial lipodystrophies, such as Barraquer-Simons syndrome (Oliveira et al., 2016), providing insights into the factors that influence regional fat distribution in these conditions.

As our model develops complete lipodystrophy over time, it exhibits features of metabolic syndrome, mirroring the clinical presentation of lipodystrophy patients. This progression could allow the study of the relationship between adipose tissue loss and the development of metabolic complications, a critical aspect of lipodystrophy pathophysiology. Furthermore, our model could offer a platform for investigating the impact of adipocyte death on surrounding tissues and systemic metabolism, like the severe lipodystrophies and panniculitis observed in ORAS patients (Damgaard et al., 2020; Dou et al., 2024; Zhou, Yu, et al., 2016).

In addition, in familial partial lipodystrophy (FPLD), women tend to experience more severe metabolic complications related to insulin resistance compared to men, including higher prevalence of diabetes (Araújo-Vilar et al., 2003; Garg, 2000), a feature also observed in our model by increase the observed liver steatosis.

Moreover, while *Hoip*$^{A\text{-}KO}$ mice are not a perfect representation of autoimmune lipodystrophies, it could be particularly useful for testing interventions aimed to preserve adipocyte function or mitigate the metabolic consequences of fat loss. In essence, this intrinsic cell death model could serve as a complement to existing research approaches and could still provide valuable insights into the downstream effects of adipocyte loss, regardless of the initial trigger.

5.2.2 Sex and species-specific implication in adipocyte cell death mechanisms regulated by LUBAC

LUBAC-deficient mouse models demonstrated susceptibility to both TNF-induced apoptotic and necroptotic cell death, being both Casp8 and RIPK3/MLKL depletion necessary to rescue its aberrant cell death rates (Peltzer et al., 2014, 2018; Peltzer & Annibaldi, 2022; Rickard et al., 2014; Taraborrelli et al., 2018). However, our experiments revealed notable species-specific differences in TNF-induced cell death mechanisms between murine and human adipocytes. In murine models, both 3T3-L1 preadipocytes and differentiated adipocytes underwent TNF-induced apoptosis and necroptosis, with mature adipocytes showing a stronger and faster tendency toward necroptosis. In contrast, human adipocytes exhibited a predominantly caspase-dependent response, requiring additional sensitization with cycloheximide (CHX) or BV6 alongside TNF to induce cell death, consistent with findings by Oda et al (Oda et al., 2022).

On the other hand, our findings also reveal that LUBAC activity regulates metabolic processes in a sex- and depot-specific manner, with distinct phenotypic consequences in adipose tissue. In our murine model, male GWAT was the most affected depot upon LUBAC depletion, displaying detrimental expansion from an early age, which persisted over time. In contrast, ScWAT and BAT in males were only affected later in life, at 18 months of age. However, females showed a different pattern, with young females appearing less sensitive to LUBAC loss, as changes in adipose tissue depots were primarily observed at older ages. These observations suggest a gender-specific penetrance of the phenotype across adipose tissue compartments.

Interestingly, despite both sexes exhibiting increased IR at 18 months of age, females developed pronounced steatosis during aging, while males showed only minor signs of kidney damage and colon inflammation. This indicates that LUBAC activity may influence systemic metabolic outcomes differently in males and females. Furthermore, females presented enhanced splenomegaly along with enlarged thymus and lymph nodes near ScWAT and mesenteric adipose tissues, suggesting sex-specific differences in the immune response to inflammation resulting from adipose tissue loss.

Together, these findings underscore the complex interplay between LUBAC, inflammation, and metabolism across species and adipose tissue depots, and highlight the critical need for research approaches that carefully consider both species-specific and sex-specific factors in the execution of cell death modalities.

5.3 Closing remarks

Our comprehensive analysis of human databases and experimental findings revealed complex relationships between LUBAC expression, adipocyte survival, and cell death mechanisms in obesity. LUBAC expression in human adipose tissue correlates with improved metabolic syndrome biomarkers in obese patients, suggesting a protective role. This protection likely stems from LUBAC's enhancement of NF-κB's pro-survival activity and possible promotion of thermogenesis (or at least UCP-1 content), which may help reduce adipocyte hypertrophy and promote healthy adipose tissue expansion during obesity.

Adipose tissue dysfunction during obesity disrupts circulating levels of FFAs, adipokines, exosomes, and pro-inflammatory cytokines, all of which contribute to hepatic triglyceride accumulation and the progression of MASLD. This underscores the importance of early interventions targeting obesity-induced adipose tissue dysfunction as promising therapeutic strategies for MASLD. Approaches such as promoting healthy adipose tissue expansion or enhancing oxidative capacity through BAT activation or WAT browning could redirect lipids away from the liver, preventing excessive triglyceride accumulation. These strategies have the potential to prevent or reverse MASLD before it triggers an uncontrollable inflammatory cascade that exceeds the reach of current therapeutic options.

It is clear that Lin-Ub plays a critical role in preventing adipocyte cell death while preserving adipokine secretion and maintaining NF-κB activation at homeostatic levels. By stabilizing adipose tissue function, Lin-Ub alleviates obesity-induced adipose tissue dysfunction, supporting healthy adipose tissue expansion and brown fat activation. Consequently, Lin-Ub may prevent lipid accumulation in the liver and the subsequent development of MASLD. This model highlights the central role of LUBAC in regulating adipose tissue-liver crosstalk during obesity, offering a potential therapeutic target for mitigating metabolic complications associated with obesity

We propose a model in which cytokines, such as TNF, trigger the activation of LUBAC to protect stressed adipocytes from cell death while maintaining sufficient levels of NF-κB activation. Under obesity conditions, adipocyte death activates inflammatory macrophage infiltration, amplifying the inflammatory response and leading to metabolic syndrome. This cell death is exacerbated when Lin-Ub is low or absent, further boosting inflammation and metabolic dysfunction.

The interplay between LUBAC activity and cell death mechanisms underscores its function as a protective shield against adipocyte death, defending against metabolic syndrome and potentially other conditions like lipodystrophies. By preventing ectopic lipid deposition, LUBAC may serve as a key metabolic safeguard mechanism against obesity-associated disorders in humans, particularly MASLD.

Notably, LUBAC may also be important for the homeostatic response to other stress factors in adipose tissue during obesity, such as hypoxia. Indeed, LUBAC has been reported to be crucial in protecting cells against hypoxia-mediated cell death, further highlighting its role in maintaining adipose tissue health under various stress conditions (Aalto et al., 2022; Jin et al., 2024; Yin & Liu, 2021)..

Last, our analysis revealed compartment tissue-specific features of linear ubiquitination between ScWAT and GWAT in a gender-specific effect, possibly contributing to the different outcomes of metabolic syndromes between male and female mice, highlighting the need for further gender specific analysis regarding cell death regulation.

These novel insights into linear ubiquitination's role in adipose tissue biology and metabolic regulation have potential implications for understanding and treating obesity-related disorders. Future research should focus on elucidating the consequences of programmed cell death in metabolic phenotypes with gender perspective, particularly during the crosstalk between adipose tissue secretome and liver metabolism.

6.Publications

6.1 First Author publications

6.1.1 Hildebrandt et. al, Science Advances (2025)

"Linear ubiquitination maintains adipose tissue integrity and prevents cell death-driven metabolic syndrome"

Ximena Hildebrandt, Önay Veli, Armel Hyoubi, Julia Zinngrebe, Anne Hoffmann, Ali Abdallah, Julian Rodefeld, Öykü Kaya, Elena Wagner, Andreas Lindhorst, Matea Poggenberg, Yuan Wang, Liane Gardenweg, Joëlle Dimmler, Jutta Schillings, Pegi Koci, Francesca Bonechi, Lucas Valdez Capuccino, Adhideb Ghosh, Falko Noé, Christian Wolfrum, Micheal Singer, Tom Luedde, Aslihan Yavas, Martin Gericke, Holger Winkels, Matthias Blüher, Henning Walczak, Alessandro Annibaldi, Pamela Fischer-Posovszky, Nieves Peltzer

DOI: 10.1126/sciadv.adw2539

Abstract

Adipocyte hypertrophy during obesity triggers chronic inflammation, leading to metabolic disorders. However, the role of adipocyte-specific inflammatory signalling in metabolic syndrome remains unclear. The linear ubiquitin chain assembly complex, LUBAC, is an E3-ligase that generates non-degradative linear ubiquitination (Lin-Ub). LUBAC regulates NF-κB/MAPK-driven inflammation and prevents cell death triggered by immune receptors like TNF-receptor-1. Here we show that mice lacking HOIP, LUBAC's catalytic subunit, in adipocytes (*Hoip*$^{A\text{-}KO}$) display lipodystrophy and heightened susceptibility to obesity-induced metabolic syndrome, particularly Metabolic Dysfunction-Associated Steatotic Liver Disease (MASLD). Mechanistically, loss of HOIP attenuates TNF-induced NF-κB activation and promotes cell death in human adipocytes. Inhibiting caspase-8-mediated cell death is sufficient to prevent lipodystrophy and MASLD in *Hoip*$^{A\text{-}KO}$ obese mice. Importantly, HOIP expression in adipose tissue positively correlates with metabolic fitness in obese individuals. Overall, our findings reveal a critical role for Lin-Ub in protecting against obesity-related metabolic syndrome by mitigating cell death-driven adipose tissue inflammation.

Contributions:

Study design, data generation of most of the experiment, data curation, data analysis and visualisation, manuscript writing and editing.

6.1.2 Review: Hildebrandt et. al, 2022, Cell Death and Differentiation.

Cell death and inflammation during obesity: "Know my methods, WAT(son)"

Ximena Hildebrandt , Mohamed Ibrahim, Nieves Peltzer

Cell Death and Differentiation. 2023 Feb;30(2):279-292. DOI: 10.1038/s41418-022-01062-4. Epub 2022 Sep 29. DOI: 10.1038/s41418-022-01062-4

Abstract

Obesity is a state of low-grade chronic inflammation that causes multiple metabolic diseases. During obesity, signalling via cytokines of the TNF family mediates cell death and inflammation within the adipose tissue, eventually resulting in lipid spill-over, glucotoxicity and insulin resistance. These events ultimately lead to ectopic lipid deposition, glucose intolerance and other metabolic complications with life-threatening consequences. Here we review the literature on how inflammatory responses affect metabolic processes such as energy homeostasis and insulin signalling. This review mainly focuses on the role of cell death in the adipose tissue as a key player in metabolic inflammation.

Contributions:

Literature research, figure design, manuscript editing.

6.2 Published manuscripts under collaboration:

Contribution of the author to collaborative publications are listed below:

6.2.1 Kaul et. al, Nature Metabolism, 2025

"2-hydroxyglutarate mediates whitening of brown adipocytes coupled to nuclear softening upon mitochondrial dysfunction"

Harshita Kaul, Lea Isermann, Katharina Senft, Milica Popovic, Theodoros Georgomanolis, Linda Baumann, Pujyanathan Sivanesan, Andromachi, Pouikli, Hendrik Nolte, Bojana Lucic, **Ximena Hildebrandt,** Katrin Seidel, Thorsten Gnad, Felix Gaedke, Ulrike Göbel, Franziska Peters, Maksym Cherevatenko, Joo Hyun Park, Astrid Schauss, Nieves Peltzer, Jens Claus Brüning, Jan-Wilhelm Kornfeld, Alexander Pfeifer, Thomas Langer, Marina Lusic, Sara A. Wickström, Christian Frezza, Aleksandra Trifunovic.

DOI: https://doi.org/10.1038/s42255-025-01332-8

Contributions: Brown Adipose Tissue and Bone Marrow FACS analysis. Performance of the experiment, analysis, data curation and visualisation.

6.2.2 Veli.et al., Molecular Metabolism, 2024

"RIPK1 is dispensable for cell death regulation in β-cells during hyperglycemia"

Önay Veli Öykü Kaya, Ana Beatriz Varanda, **Ximena Hildebrandt,** Peng Xiao, Yann Estornes, Matea Poggenberg, Yuan Wang, Manolis Pasparakis, Mathieu J.M. Bertrand, Henning Walczak, Alessandro Annibaldi, Alessandra K. Cardozo, Nieves Peltzer https://doi.org/10.1016/j.molmet.2024.101988

Contributions: Data generation, mouse work assistance, methodology and manuscript editing.

6.2.3 Martinez-Lagunas et.al, Science Advances, 2023

"Cleavage of cFLIP restrains cell death during viral infection and tissue injury and favours tissue repair"

Kristel Martinez Lagunas, Deniz Pinar Savcigil, Matea Zrilic Carlos Carvajal Fraile, Andrew Craxton, Emily Self, Iratxe Uranga-Murillo, Diego De Miguel, Maykel Arias, Sebastian

Willenborg, Michael Piekarek, Marie Christine Albert, Kalvin Nugraha, Ina Lisewski, Erika Janakova, Natalia Igual, Wulf Tonnus, **Ximena Hildebrandt**, Mohammed Ibrahim, Marlies Ballegeer, Xavier Saelens, Andrew Kueh, Pascal Meier, Andreas Linkermann, Julian Pardo, Sabine Eming, Henning Walczak, Marion Macfarlane, Nieves Peltzer and Alessandro Annibaldi.

Sci. Adv.9 ,eadg2829 (2023). DOI:10.1126/sciadv.adg2829

Contributions: Data generation, data analysis.

6.2.4 Schorn et. al, EMBO Journal, 2023

"cIAPs control RIPK1 kinase activity-dependent and -independent cell death and tissue inflammation"

Fabian Schorn, J Paul Werthenbach, Mattes Hoffmann, Mila Daoud, Johanna Stachelscheid, Lars M Schiffmann, **Ximena Hildebrandt** X, Su Ir Lyu, Nieves Peltzer, Alexander Quaas, Domagoj Vucic, John Silke,, Manolis Pasparakis and Hamid Kashkar,

EMBO J (2023) 42: e113614. https://doi.org/10.15252/embj.2023113614

Contributions: Data generation, data analysis.

6.3 Other manuscripts under collaboration:

7.3.1 Elbæk et al (in revision)

"M1-linked Ubiquitination by LUBAC Regulates AMPK Signalling, Bioenergetic Metabolism, and Organismal Survival"

Camilla R. Elbæk, Akhee S. Jahan, Joyceline Cuenco, Anna Aalto, Anna Dahlström, John Rizk, Simon A. Hawley, Sarah N. J. Franks, Michael Stumpe, Srinivasa Prasad Kolapalli, **Ximena Hildebrandt,** Alexander Erwin Früh, Klara Nielsen, Dominik Priesmann, Julian Koch, Mathilde Deichmann, Josef Gullmets, Lien Verboom, Geert van Loo, Nieves Peltzer, Lisa B. Frankl, Mads Gyrd-Hansen, Jörn Dengjel, Brent J. Ryan, D. Grahame Hardie, Annika Meinander, Kei Sakamoto, and Rune Busk Damgaard.

Contributions: Adipose tissue sample donation, data visualisation and manuscript editing.

6.3.2 Rivera-Hernández et al (in preparation)

"Pluronic® F127-PP123-Hyaluronic Acid based injectable hydrogels for localized cervical cancer therapy"

Gabriela Rivera-Hernández, **Ximena Hildebrandt,** Patricia Martínez-Morales, Marilena Antunes-Ricardo, Francisco J. Sierra-Valdez, Marcela Arango-Ospina, Nieves Peltzer, Aldo R. Boccaccini, Mirna L. Sánchez

Contributions: Cell death assays, data visualisation and manuscript editing.

6.3.3 Smith et.al, (in preparation)

"Single muscle fiber proteomics of pre-diabetic mice revealed increased mitochondrial fission in type IIa fibers"

Luisa Schmidt, Katharina Neuser, Christiana Zollo, Peter Zentis, **Ximena Hildebrandt**, Michael Saynisch, Philipp Antczak, Bianca Collins, Ana Garcia, Nieves Peltzer, Marcus Krüger.

Luisa Smith PhD Thesis including these results is available at the Cologne University Library. In addition code script regarding this study can be found in: https://doi.org/10.5281/zenodo.12737398 and https://doi.org/10.5281/zenodo.12731434.

Contributions: Adipose tissue sample donation, data visualisation and manuscript editing.

7. References

Aalto, A., Martínez-Chacón, G., Kietz, C., Tsyganova, N., Kreutzer, J., Kallio, P., Broemer, M., & Meinander, A. (2022). M1-linked ubiquitination facilitates NF-κB activation and survival during sterile inflammation. *The FEBS Journal*, *289*(17), 5180–5197.

Abbasi, F., Brown, B. W., Jr, Lamendola, C., McLaughlin, T., & Reaven, G. M. (2002). Relationship between obesity, insulin resistance, and coronary heart disease risk. *Journal of the American College of Cardiology*, *40*(5), 937–943.

Afonso, M. B., Islam, T., Magusto, J., Amorim, R., Lenoir, V., Simões, R. F., Teixeira, J., Silva, L. C., Wendum, D., Jéru, I., Vigouroux, C., Castro, R. E., Oliveira, P. J., Prip-Buus, C., Ratziu, V., Gautheron, J., & Rodrigues, C. M. P. (2023). RIPK3 dampens mitochondrial bioenergetics and lipid droplet dynamics in metabolic liver disease. *Hepatology* , *77*(4), 1319–1334.

AlAnzi, T., Al Harbi, F., AlGhamdi, A., & Mohamed, S. (2022). A novel variant of RBCK1 gene causes mild polyglucosan myopathy. *Neurosciences* , *27*(1), 45–49.

Alcalá, M., Calderon-Dominguez, M., Serra, D., Herrero, L., & Viana, M. (2019). Mechanisms of impaired brown adipose tissue recruitment in obesity. *Frontiers in Physiology*, *10*, 94.

Alfadda, A. A., Sallam, R. M., Chishti, M. A., Moustafa, A. S., Fatma, S., Alomaim, W. S., Al-Naami, M. Y., Bassas, A. F., Chrousos, G. P., & Jo, H. (2012). Differential patterns of serum concentration and adipose tissue expression of chemerin in obesity: adipose depot specificity and gender dimorphism. *Molecules and Cells*, *33*(6), 591–596.

Al-Hamad, D., & Raman, V. (2017). Metabolic syndrome in children and adolescents. *Translational Pediatrics*, *6*(4), 397–407.

Alkhouri, N., Gornicka, A., Berk, M. P., Thapaliya, S., Dixon, L. J., Kashyap, S., Schauer, P. R., & Feldstein, A. E. (2010). Adipocyte apoptosis, a link between obesity, insulin resistance, and hepatic steatosis. *The Journal of Biological Chemistry*, *285*(5), 3428–3438.

Altshuler-Keylin, S., Shinoda, K., Hasegawa, Y., Ikeda, K., Hong, H., Kang, Q., Yang, Y., Perera, R. M., Debnath, J., & Kajimura, S. (2016). Beige Adipocyte Maintenance Is Regulated by Autophagy-Induced Mitochondrial Clearance. *Cell Metabolism*, *24*(3), 402–419.

Andrew Kovalenko, Jin-Chul Kim, Tae-Bong Kang, Akhil Rajput, Konstantin Bogdanov, Oliver Dittrich-Breiholz, Michael Kracht, Ori Brenner, David Wallach. (2009). Caspase-8 deficiency in epidermal keratinocytes triggers an inflammatory skin disease. *J Exp Med*, *206*(10), 2161–2177.

Annibaldi, A., & Walczak, H. (2020). Death receptors and their ligands in inflammatory disease and cancer. *Cold Spring Harbor Perspectives in Biology*, *12*(9), a036384.

Annibaldi, A., Wicky John, S., Vanden Berghe, T., Swatek, K. N., Ruan, J., Liccardi, G., Bianchi, K., Elliott, P. R., Choi, S. M., Van Coillie, S., Bertin, J., Wu, H., Komander, D., Vandenabeele, P., Silke, J., & Meier, P. (2018). Ubiquitin-Mediated Regulation of RIPK1 Kinase Activity Independent of IKK and MK2. *Molecular Cell*, *69*(4), 566–580.e5.

Araújo-Vilar, D., Loidi, L., Domínguez, F., & Cabezas-Cerrato, J. (2003). Phenotypic gender differences in subjects with familial partial lipodystrophy (Dunnigan variety) due to a nuclear lamin A/C R482W mutation. *Hormone and Metabolic Research = Hormon- Und Stoffwechselforschung = Hormones et Metabolisme*, *35*(1). https://doi.org/10.1055/s-2003-38388

Arkan, M. C., Hevener, A. L., Greten, F. R., Maeda, S., Li, Z.-W., Long, J. M., Wynshaw-Boris, A., Poli, G., Olefsky, J., & Karin, M. (2005). IKK-beta links inflammation to obesity-induced insulin resistance. *Nature Medicine*, *11*(2), 191–198.

Arner, P., Hellström, L., Wahrenberg, H., & Brönnegård, M. (1990). Beta-adrenoceptor expression in human fat cells from different regions. *The Journal of Clinical*

Investigation, *86*(5), 1595–1600.

Azzu, V., Vacca, M., Virtue, S., Allison, M., & Vidal-Puig, A. (2020). Adipose Tissue-Liver Cross Talk in the Control of Whole-Body Metabolism: Implications in Nonalcoholic Fatty Liver Disease. *Gastroenterology*, *158*(7), 1899–1912.

Babraham Bioinformatics - FastQC A Quality Control tool for High Throughput Sequence Data. (n.d.). Retrieved October 18, 2024, from http://www.bioinformatics.babraham.ac.uk/projects/fastqc

Babraham Bioinformatics - Trim Galore! (n.d.). Retrieved October 18, 2024, from https://www.bioinformatics.babraham.ac.uk/projects/trim_galore/

Bader, S. M., Preston, S. P., Saliba, K., Lipszyc, A., Grant, Z. L., Mackiewicz, L., Baldi, A., Hempel, A., Clark, M. P., Peiris, T., Clow, W., Bjelic, J., Stutz, M. D., Arandjelovic, P., Teale, J., Du, F., Coultas, L., Murphy, J. M., Allison, C. C., … Samson, A. L. (2023). Endothelial Caspase-8 prevents fatal necroptotic hemorrhage caused by commensal bacteria. *Cell Death and Differentiation*, *30*(1), 27–36.

Bae, J., Ricciardi, C. J., Esposito, D., Komarnytsky, S., Hu, P., Curry, B. J., Brown, P. L., Gao, Z., Biggerstaff, J. P., Chen, J., & Zhao, L. (2014). Activation of pattern recognition receptors in brown adipocytes induces inflammation and suppresses uncoupling protein 1 expression and mitochondrial respiration. *American Journal of Physiology. Cell Physiology*, *306*(10), C918–C930.

Baker, R. G., Hayden, M. S., & Ghosh, S. (2011). NF-κB, inflammation, and metabolic disease. *Cell Metabolism*, *13*(1), 11–22.

Bender, L. M., Morgan, M. J., Thomas, L. R., Liu, Z.-G., & Thorburn, A. (2005). The adaptor protein TRADD activates distinct mechanisms of apoptosis from the nucleus and the cytoplasm. *Cell Death and Differentiation*, *12*(5), 473–481.

Ben, J., Jiang, B., Wang, D., Liu, Q., Zhang, Y., Qi, Y., Tong, X., Chen, L., Liu, X., Zhang, Y., Zhu, X., Li, X., Zhang, H., Bai, H., Yang, Q., Ma, J., Wiemer, E. A. C., Xu, Y., & Chen, Q. (2019). Major vault protein suppresses obesity and atherosclerosis through inhibiting IKK-NF-κB signaling mediated inflammation. *Nature Communications*, *10*(1), 1801.

Benrick, A., Wallenius, V., & Asterholm, I. W. (2012). Interleukin-6 mediates exercise-induced increase in insulin sensitivity in mice. *Experimental Physiology*, *97*(11), 1224–1235.

Berger, S. B., Kasparcova, V., Hoffman, S., Swift, B., Dare, L., Schaeffer, M., Capriotti, C., Cook, M., Finger, J., Hughes-Earle, A., Harris, P. A., Kaiser, W. J., Mocarski, E. S., Bertin, J., & Gough, P. J. (2014). Cutting Edge: RIP1 kinase activity is dispensable for normal development but is a key regulator of inflammation in SHARPIN-deficient mice. *Journal of Immunology* , *192*(12), 5476–5480.

Bertrand, M. J. M., Milutinovic, S., Dickson, K. M., Ho, W. C., Boudreault, A., Durkin, J., Gillard, J. W., Jaquith, J. B., Morris, S. J., & Barker, P. A. (2008). cIAP1 and cIAP2 facilitate cancer cell survival by functioning as E3 ligases that promote RIP1 ubiquitination. *Molecular Cell*, *30*(6), 689–700.

Bhagavathula, A. S., Clark, C. C. T., Rahmani, J., & Chattu, V. K. (2021). Impact of Body Mass Index on the Development of Inflammatory Bowel Disease: A Systematic Review and Dose-Response Analysis of 15.6 Million Participants. *Healthcare (Basel, Switzerland)*, *9*(1). https://doi.org/10.3390/healthcare9010035

Billon, N., Iannarelli, P., Monteiro, M. C., Glavieux-Pardanaud, C., Richardson, W. D., Kessaris, N., Dani, C., & Dupin, E. (2007). The generation of adipocytes by the neural crest. *Development* , *134*(12), 2283–2292.

Blüher, M. (2020). Metabolically Healthy Obesity. *Endocrine Reviews*, *41*(3). https://doi.org/10.1210/endrev/bnaa004

Boisson, B., Laplantine, E., Dobbs, K., Cobat, A., Tarantino, N., Hazen, M., Lidov, H. G. W., Hopkins, G., Du, L., Belkadi, A., Chrabieh, M., Itan, Y., Picard, C., Fournet, J.-C., Eibel,

H., Tsitsikov, E., Pai, S.-Y., Abel, L., Al-Herz, W., … Notarangelo, L. D. (2015). Human HOIP and LUBAC deficiency underlies autoinflammation, immunodeficiency, amylopectinosis, and lymphangiectasia. *The Journal of Experimental Medicine*, *212*(6), 939–951.

Boisson, B., Laplantine, E., Prando, C., Giliani, S., Israelsson, E., Xu, Z., Abhyankar, A., Israël, L., Trevejo-Nunez, G., Bogunovic, D., Cepika, A.-M., MacDuff, D., Chrabieh, M., Hubeau, M., Bajolle, F., Debré, M., Mazzolari, E., Vairo, D., Agou, F., … Picard, C. (2012). Immunodeficiency, autoinflammation and amylopectinosis in humans with inherited HOIL-1 and LUBAC deficiency. *Nature Immunology*, *13*(12), 1178–1186.

Boone, D. L., Turer, E. E., Lee, E. G., Ahmad, R.-C., Wheeler, M. T., Tsui, C., Hurley, P., Chien, M., Chai, S., Hitotsumatsu, O., McNally, E., Pickart, C., & Ma, A. (2004). The ubiquitin-modifying enzyme A20 is required for termination of Toll-like receptor responses. *Nature Immunology*, *5*(10), 1052–1060.

Boronat-Toscano, A., Monfort-Ferré, D., Menacho, M., Caro, A., Bosch, R., Espina, B., Algaba-Chueca, F., Saera-Vila, A., Moliné, A., Marti, M., Espin, E., Millan, M., & Serena, C. (2022). Anti-TNF Therapies Suppress Adipose Tissue Inflammation in Crohn's Disease. *International Journal of Molecular Sciences*, *23*(19). https://doi.org/10.3390/ijms231911170

Bo, T., Gao, L., Yao, Z., Shao, S., Wang, X., Proud, C. G., & Zhao, J. (2024). Hepatic selective insulin resistance at the intersection of insulin signaling and metabolic dysfunction-associated steatotic liver disease. *Cell Metabolism*, *36*(5), 947–968.

Boutens, L., & Stienstra, R. (2016). Adipose tissue macrophages: going off track during obesity. *Diabetologia*, *59*(5), 879–894.

Boutros, M., & Maron, D. (2011). Inflammatory bowel disease in the obese patient. *Clinics in Colon and Rectal Surgery*, *24*(4), 244–252.

Bouzakri, K., Roques, M., Gual, P., Espinosa, S., Guebre-Egziabher, F., Riou, J.-P., Laville, M., Le Marchand-Brustel, Y., Tanti, J.-F., & Vidal, H. (2003). Reduced activation of phosphatidylinositol-3 kinase and increased serine 636 phosphorylation of insulin receptor substrate-1 in primary culture of skeletal muscle cells from patients with type 2 diabetes. *Diabetes*, *52*(6), 1319–1325.

Bowker, N., Shah, R. L., Sharp, S. J., Luan, J. 'an, Stewart, I. D., Wheeler, E., Ferreira, M. A. R., Baras, A., Wareham, N. J., Langenberg, C., & Lotta, L. A. (2020). Meta-analysis investigating the role of interleukin-6 mediated inflammation in type 2 diabetes. *EBioMedicine*, *61*, 103062.

Bray, G. A., Kim, K. K., Wilding, J. P. H., & World Obesity Federation. (2017). Obesity: a chronic relapsing progressive disease process. A position statement of the World Obesity Federation. *Obesity Reviews: An Official Journal of the International Association for the Study of Obesity*, *18*(7), 715–723.

Bray, N. L., Pimentel, H., Melsted, P., & Pachter, L. (2016). Near-optimal probabilistic RNA-seq quantification. *Nature Biotechnology*, *34*(5), 525–527.

Bukowiecki, L., Collet, A. J., Follea, N., Guay, G., & Jahjah, L. (1982). Brown adipose tissue hyperplasia: a fundamental mechanism of adaptation to cold and hyperphagia. *The American Journal of Physiology*, *242*(6), E353–E359.

Caër, C., Rouault, C., Le Roy, T., Poitou, C., Aron-Wisnewsky, J., Torcivia, A., Bichet, J.-C., Clément, K., Guerre-Millo, M., & André, S. (2017). Immune cell-derived cytokines contribute to obesity-related inflammation, fibrogenesis and metabolic deregulation in human adipose tissue. *Scientific Reports*, *7*(1), 3000.

Cai, D., Yuan, M., Frantz, D. F., Melendez, P. A., Hansen, L., Lee, J., & Shoelson, S. E. (2005). Local and systemic insulin resistance resulting from hepatic activation of IKK-beta and NF-kappaB. *Nature Medicine*, *11*(2), 183–190.

Cai, Z., Jitkaew, S., Zhao, J., Chiang, H.-C., Choksi, S., Liu, J., Ward, Y., Wu, L.-G., & Liu,

Z.-G. (2014). Plasma membrane translocation of trimerized MLKL protein is required for TNF-induced necroptosis. *Nature Cell Biology*, *16*(1), 55–65.

Cannon, B., & Nedergaard, J. (2004). Brown adipose tissue: function and physiological significance. *Physiological Reviews*, *84*(1), 277–359.

Cao, E., Watt, M. J., Nowell, C. J., Quach, T., Simpson, J. S., De Melo Ferreira, V., Agarwal, S., Chu, H., Srivastava, A., Anderson, D., Gracia, G., Lam, A., Segal, G., Hong, J., Hu, L., Phang, K. L., Escott, A. B. J., Windsor, J. A., Phillips, A. R. J., … Trevaskis, N. L. (2021). Mesenteric lymphatic dysfunction promotes insulin resistance and represents a potential treatment target in obesity. *Nature Metabolism*, *3*(9), 1175–1188.

Carrière, A., Jeanson, Y., Berger-Müller, S., André, M., Chenouard, V., Arnaud, E., Barreau, C., Walther, R., Galinier, A., Wdziekonski, B., Villageois, P., Louche, K., Collas, P., Moro, C., Dani, C., Villarroya, F., & Casteilla, L. (2014). Browning of white adipose cells by intermediate metabolites: an adaptive mechanism to alleviate redox pressure. *Diabetes*, *63*(10), 3253–3265.

Cartier, A., Lemieux, I., Alméras, N., Tremblay, A., Bergeron, J., & Després, J.-P. (2008). Visceral obesity and plasma glucose-insulin homeostasis: contributions of interleukin-6 and tumor necrosis factor-alpha in men. *The Journal of Clinical Endocrinology and Metabolism*, *93*(5), 1931–1938.

Cartwright, M. J., Tchkonia, T., & Kirkland, J. L. (2007). Aging in adipocytes: potential impact of inherent, depot-specific mechanisms. *Experimental Gerontology*, *42*(6), 463–471.

Catharina, A. S., Modolo, R., Ritter, A. M. V., Sabbatini, A. R., Lopes, H. F., Moreno Junior, H., & Faria, A. P. de. (2018). Metabolic Syndrome-Related Features in Controlled and Resistant Hypertensive Subjects. *Arquivos Brasileiros de Cardiologia*, *110*(6), 514–521.

Catrysse, L., Farhang Ghahremani, M., Vereecke, L., Youssef, S. A., Mc Guire, C., Sze, M., Weber, A., Heikenwalder, M., de Bruin, A., Beyaert, R., & van Loo, G. (2016). A20 prevents chronic liver inflammation and cancer by protecting hepatocytes from death. *Cell Death & Disease*, *7*(6), e2250.

Catrysse, L., Maes, B., Mehrotra, P., Martens, A., Hoste, E., Martens, L., Maueröder, C., Remmerie, A., Bujko, A., Slowicka, K., Sze, M., Vikkula, H., Ghesquière, B., Scott, C. L., Saeys, Y., van de Sluis, B., Ravichandran, K., Janssens, S., & van Loo, G. (2021). A20 deficiency in myeloid cells protects mice from diet-induced obesity and insulin resistance due to increased fatty acid metabolism. *Cell Reports*, *36*(12), 109748.

Catrysse, L., & van Loo, G. (2017). Inflammation and the Metabolic Syndrome: The Tissue-Specific Functions of NF-κB. *Trends in Cell Biology*, *27*(6), 417–429.

Cenacchi, G., Papa, V., Costa, R., Pegoraro, V., Marozzo, R., Fanin, M., & Angelini, C. (2019). Update on polyglucosan storage diseases. *Virchows Archiv: An International Journal of Pathology*, *475*(6), 671–686.

Cereijo, R., Giralt, M., & Villarroya, F. (2015). Thermogenic brown and beige/brite adipogenesis in humans. *Annals of Medicine*, *47*(2), 169–177.

Cerf, M. E. (2013). Beta cell dysfunction and insulin resistance. *Frontiers in Endocrinology*, *4*, 37.

Cero, C., Lea, H. J., Zhu, K. Y., Shamsi, F., Tseng, Y.-H., & Cypess, A. M. (2021). β3-Adrenergic receptors regulate human brown/beige adipocyte lipolysis and thermogenesis. *JCI Insight*, *6*(11). https://doi.org/10.1172/jci.insight.139160

Chait, A., & den Hartigh, L. J. (2020). Adipose Tissue Distribution, Inflammation and Its Metabolic Consequences, Including Diabetes and Cardiovascular Disease. *Frontiers in Cardiovascular Medicine*, *7*, 22.

Cheng, J., Xu, L., Xuan, Y., Zhou, F., Huang, A., Zeng, S., Wang, H., Wang, Y., Zhan, Y., Yan, X., Luo, S., Liu, Y., & Cheng, M. (2024). Linear polyubiquitylation of Gli protein regulates its protein stability and facilitates tumor growth in colorectal cancer. *Cell Death Discovery*, *10*(1), 369.

Cheng, L., Wang, J., Dai, H., Duan, Y., An, Y., Shi, L., Lv, Y., Li, H., Wang, C., Ma, Q., Li, Y., Li, P., Du, H., & Zhao, B. (2021). Brown and beige adipose tissue: a novel therapeutic strategy for obesity and type 2 diabetes mellitus. *Adipocyte*, *10*(1), 48–65.

Chen, J., & Chen, Z. J. (2013). Regulation of NF-κB by ubiquitination. *Current Opinion in Immunology*, *25*(1), 4–12.

Chen, L., Wang, N., Hu, W., Yu, X., Yang, R., Han, Y., Yan, Y., Nian, N., & Sha, C. (2021). Polyglucosan body myopathy 1 may cause cognitive impairment: a case report from China. *BMC Musculoskeletal Disorders*, *22*(1), 35.

Chen, X., Liu, Z., Liu, W., Wang, S., Jiang, R., Hu, K., Sheng, L., Xu, G., Kou, X., & Song, Y. (2023). NF-κB-Inducing Kinase Provokes Insulin Resistance in Skeletal Muscle of Obese Mice. *Inflammation*, *46*(4), 1445–1457.

Chen, Y.-G., Rieser, E., Bhamra, A., Surinova, S., Kreuzaler, P., Ho, M.-H., Tsai, W.-C., Peltzer, N., de Miguel, D., & Walczak, H. (2024). LUBAC enables tumor-promoting LTβ receptor signaling by activating canonical NF-κB. *Cell Death and Differentiation*, *31*(10), 1267–1284.

Chen, Z. H., Mousavi, S., Mandhane, P. J., Simons, E., Turvey, S. E., Moraes, T. J., Subbarao, P., & Miliku, K. (2025). Ultraprocessed food consumption and obesity development in Canadian children. *JAMA Network Open*, *8*(1), e2457341.

Chiang, S.-H., Bazuine, M., Lumeng, C. N., Geletka, L. M., Mowers, J., White, N. M., Ma, J.-T., Zhou, J., Qi, N., Westcott, D., Delproposto, J. B., Blackwell, T. S., Yull, F. E., & Saltiel, A. R. (2009). The protein kinase IKKepsilon regulates energy balance in obese mice. *Cell*, *138*(5), 961–975.

Chiazza, F., Couturier-Maillard, A., Benetti, E., Mastrocola, R., Nigro, D., Cutrin, J. C., Serpe, L., Aragno, M., Fantozzi, R., Ryffel, B., Thiemermann, C., & Collino, M. (2016). Targeting the NLRP3 Inflammasome to Reduce Diet-Induced Metabolic Abnormalities in Mice. *Molecular Medicine* , *21*(1), 1025–1037.

Choudhary, S., Sinha, S., Zhao, Y., Banerjee, S., Sathyanarayana, P., Shahani, S., Sherman, V., Tilton, R. G., & Bajaj, M. (2011). NF-kappaB-inducing kinase (NIK) mediates skeletal muscle insulin resistance: blockade by adiponectin. *Endocrinology*, *152*(10), 3622–3627.

Chu, Y., Kang, Y., Yan, C., Yang, C., Zhang, T., Huo, H., & Liu, Y. (2021). LUBAC and OTULIN regulate autophagy initiation and maturation by mediating the linear ubiquitination and the stabilization of ATG13. *Autophagy*, *17*(7), 1684–1699.

Cinti, S., Mitchell, G., Barbatelli, G., Murano, I., Ceresi, E., Faloia, E., Wang, S., Fortier, M., Greenberg, A. S., & Obin, M. S. (2005). Adipocyte death defines macrophage localization and function in adipose tissue of obese mice and humans. *Journal of Lipid Research*, *46*(11), 2347–2355.

ClinicalTrials.Gov. (n.d.). Retrieved May 24, 2024, from https://clinicaltrials.gov/study/NCT00303394

Cohen, P., Kelsall, I. R., Nanda, S. K., & Zhang, J. (2020). HOIL-1, an atypical E3 ligase that controls MyD88 signalling by forming ester bonds between ubiquitin and components of the Myddosome. *Advances in Biological Regulation*, *75*, 100666.

Conus, F., Rabasa-Lhoret, R., & Péronnet, F. (2007). Characteristics of metabolically obese normal-weight (MONW) subjects. *Applied Physiology, Nutrition, and Metabolism = Physiologie Appliquee, Nutrition et Metabolisme*, *32*(1), 4–12.

Coppack, S. W. (2001). Pro-inflammatory cytokines and adipose tissue. *The Proceedings of the Nutrition Society*, *60*(3), 349–356.

Costa, C. S., Rauber, F., Leffa, P. S., Sangalli, C. N., Campagnolo, P. D. B., & Vitolo, M. R. (2019). Ultra-processed food consumption and its effects on anthropometric and glucose profile: A longitudinal study during childhood. *Nutrition, Metabolism, and Cardiovascular Diseases: NMCD*, *29*(2), 177–184.

Cozzone, D., Fröjdö, S., Disse, E., Debard, C., Laville, M., Pirola, L., & Vidal, H. (2008). Isoform-specific defects of insulin stimulation of Akt/protein kinase B (PKB) in skeletal muscle cells from type 2 diabetic patients. *Diabetologia*, *51*(3), 512–521.

Daemen, S., & Schilling, J. D. (2019). The interplay between tissue niche and macrophage cellular metabolism in obesity. *Frontiers in Immunology*, *10*, 3133.

Daley, T., & Smith, A. D. (2013). Predicting the molecular complexity of sequencing libraries. *Nature Methods*, *10*(4), 325–327.

Damgaard, R. B., Elliott, P. R., Swatek, K. N., Maher, E. R., Stepensky, P., Elpeleg, O., Komander, D., & Berkun, Y. (2019). OTULIN deficiency in ORAS causes cell type-specific LUBAC degradation, dysregulated TNF signalling and cell death. *EMBO Molecular Medicine*, *11*(3), e9324.

Damgaard, R. B., Jolin, H. E., Allison, M. E. D., Davies, S. E., Titheradge, H. L., McKenzie, A. N. J., & Komander, D. (2020). OTULIN protects the liver against cell death, inflammation, fibrosis, and cancer. *Cell Death and Differentiation*, *27*(5), 1457–1474.

Damgaard, R. B., Walker, J. A., Marco-Casanova, P., Morgan, N. V., Titheradge, H. L., Elliott, P. R., McHale, D., Maher, E. R., McKenzie, A. N. J., & Komander, D. (2016). The Deubiquitinase OTULIN Is an Essential Negative Regulator of Inflammation and Autoimmunity. *Cell*, *166*(5), 1215–1230.e20.

Dannappel, M., Vlantis, K., Kumari, S., Polykratis, A., Kim, C., Wachsmuth, L., Eftychi, C., Lin, J., Corona, T., Hermance, N., Zelic, M., Kirsch, P., Basic, M., Bleich, A., Kelliher, M., & Pasparakis, M. (2014). RIPK1 maintains epithelial homeostasis by inhibiting apoptosis and necroptosis. *Nature*, *513*(7516), 90–94.

da Silva Rosa, S. C., Nayak, N., Caymo, A. M., & Gordon, J. W. (2020). Mechanisms of muscle insulin resistance and the cross-talk with liver and adipose tissue. *Physiological Reports*, *8*(19), e14607.

Day, A. J., & Milner, C. M. (2019). TSG-6: A multifunctional protein with anti-inflammatory and tissue-protective properties. *Matrix Biology : Journal of the International Society for Matrix Biology*, *78-79*. https://doi.org/10.1016/j.matbio.2018.01.011

Deng, T., Tang, C., Zhang, G., & Wan, X. (2021). DAMPs released by pyroptotic cells as major contributors and therapeutic targets for CAR-T-related toxicities. *Cell Death & Disease*, *12*(1), 129.

Deng, Y., & Scherer, P. E. (2010). Adipokines as novel biomarkers and regulators of the metabolic syndrome. *Annals of the New York Academy of Sciences*, *1212*, E1–E19.

Després, J.-P., & Lemieux, I. (2006). Abdominal obesity and metabolic syndrome. *Nature*, *444*(7121), 881–887.

Diabetes. (n.d.). Retrieved May 1, 2024, from https://www.who.int/news-room/fact-sheets/detail/diabetes

Dikic, I., Wakatsuki, S., & Walters, K. J. (2009). Ubiquitin-binding domains - from structures to functions. *Nature Reviews. Molecular Cell Biology*, *10*(10), 659–671.

Dimova, R., & Tankova, T. (2015). The role of vaspin in the development of metabolic and glucose tolerance disorders and atherosclerosis. *BioMed Research International*, *2015*, 823481.

Di Tommaso, P., Chatzou, M., Floden, E. W., Barja, P. P., Palumbo, E., & Notredame, C. (2017). Nextflow enables reproducible computational workflows. *Nature Biotechnology*, *35*(4), 316–319.

Dondelinger, Y., Jouan-Lanhouet, S., Divert, T., Theatre, E., Bertin, J., Gough, P. J., Giansanti, P., Heck, A. J. R., Dejardin, E., Vandenabeele, P., & Bertrand, M. J. M. (2015). NF-κB-independent role of IKKα/IKKβ in preventing RIPK1 kinase-dependent apoptotic and necroptotic cell death during TNF signaling. *Molecular Cell*, *60*(1), 63–76.

Dou, B., Jiang, G., Peng, W., & Liu, C. (2024). OTULIN deficiency: focus on innate immune system impairment. *Frontiers in Immunology*, *15*, 1371564.

Draber, P., Kupka, S., Reichert, M., Draberova, H., Lafont, E., de Miguel, D., Spilgies, L., Surinova, S., Taraborrelli, L., Hartwig, T., Rieser, E., Martino, L., Rittinger, K., & Walczak, H. (2015). LUBAC-Recruited CYLD and A20 Regulate Gene Activation and Cell Death by Exerting Opposing Effects on Linear Ubiquitin in Signaling Complexes. *Cell Reports*, *13*(10), 2258–2272.

Dusserre, E., Moulin, P., & Vidal, H. (2000). Differences in mRNA expression of the proteins secreted by the adipocytes in human subcutaneous and visceral adipose tissues. *Biochimica et Biophysica Acta*, *1500*(1), 88–96.

Dynek, J. N., Goncharov, T., Dueber, E. C., Fedorova, A. V., Izrael-Tomasevic, A., Phu, L., Helgason, E., Fairbrother, W. J., Deshayes, K., Kirkpatrick, D. S., & Vucic, D. (2010). c-IAP1 and UbcH5 promote K11-linked polyubiquitination of RIP1 in TNF signalling. *The EMBO Journal*, *29*(24), 4198–4209.

Eckel, R. H., Kahn, S. E., Ferrannini, E., Goldfine, A. B., Nathan, D. M., Schwartz, M. W., Smith, R. J., Smith, S. R., Endocrine Society, American Diabetes Association, & European Association for the Study of Diabetes. (2011). Obesity and type 2 diabetes: what can be unified and what needs to be individualized? *Diabetes Care*, *34*(6), 1424–1430.

Eguchi, J., Wang, X., Yu, S., Kershaw, E. E., Chiu, P. C., Dushay, J., Estall, J. L., Klein, U., Maratos-Flier, E., & Rosen, E. D. (2011). Transcriptional control of adipose lipid handling by IRF4. *Cell Metabolism*, *13*(3), 249–259.

Ehrlund, A., Anthonisen, E. H., Gustafsson, N., Venteclef, N., Robertson Remen, K., Damdimopoulos, A. E., Galeeva, A., Pelto-Huikko, M., Lalli, E., Steffensen, K. R., Gustafsson, J.-A., & Treuter, E. (2009). E3 ubiquitin ligase RNF31 cooperates with DAX-1 in transcriptional repression of steroidogenesis. *Molecular and Cellular Biology*, *29*(8), 2230–2242.

Ehrlund, A., Jonsson, P., Vedin, L.-L., Williams, C., Gustafsson, J.-Å., & Treuter, E. (2012). Knockdown of SF-1 and RNF31 affects components of steroidogenesis, TGFβ, and Wnt/β-catenin signaling in adrenocortical carcinoma cells. *PloS One*, *7*(3), e32080.

Elbæk, C. R., Jahan, A. S., Cuenco, J., Dahlström, A. M., Aalto, A. L., Rizk, J., Hawley, S. A., Franks, S. N. J., Stumpe, M., Kolapalli, S. P., Hildebrandt, X., Früh, A. E., Nielsen, K., Priesmann, D., Koch, J., Deichmann, M., Gullmets, J., Verboom, L., van Loo, G., … Damgaard, R. B. (2024). M1-linked ubiquitination by LUBAC regulates AMPK activity and the response to energetic stress. In *bioRxiv* (p. 2024.11.08.622598). https://doi.org/10.1101/2024.11.08.622598

Emmerich, C. H., Ordureau, A., Strickson, S., Arthur, J. S. C., Pedrioli, P. G. A., Komander, D., & Cohen, P. (2013). Activation of the canonical IKK complex by K63/M1-linked hybrid ubiquitin chains. *Proceedings of the National Academy of Sciences of the United States of America*, *110*(38), 15247–15252.

Engin, A. (2017). The Definition and Prevalence of Obesity and Metabolic Syndrome. *Advances in Experimental Medicine and Biology*, *960*, 1–17.

Enzi, G., Gasparo, M., Biondetti, P. R., Fiore, D., Semisa, M., & Zurlo, F. (1986). Subcutaneous and visceral fat distribution according to sex, age, and overweight, evaluated by computed tomography. *The American Journal of Clinical Nutrition*, *44*(6), 739–746.

Ewels, P. A., Peltzer, A., Fillinger, S., Patel, H., Alneberg, J., Wilm, A., Garcia, M. U., Di Tommaso, P., & Nahnsen, S. (2020). The nf-core framework for community-curated bioinformatics pipelines. *Nature Biotechnology*, *38*(3), 276–278.

Ewels, P., Magnusson, M., Lundin, S., & Käller, M. (2016). MultiQC: summarize analysis results for multiple tools and samples in a single report. *Bioinformatics* , *32*(19), 3047–3048.

Fearon, K., Arends, J., & Baracos, V. (2013). Understanding the mechanisms and treatment options in cancer cachexia. *Nature Reviews. Clinical Oncology*, *10*(2), 90–99.

Featured JAX Mice Models of Type 2 Diabetes & Obesity. (n.d.). The Jackson Laboratory. Retrieved March 4, 2024, from https://www.jax.org/jax-mice-and-services/solutions-by-therapeutic-area/metabolic-diseases/featured-mice-for-type-2-and-obesity

Fiil, B. K., & Gyrd-Hansen, M. (2021). The Met1-linked ubiquitin machinery in inflammation and infection. *Cell Death and Differentiation*, *28*(2), 557–569.

Fischer-Posovszky, P., Wang, Q. A., Asterholm, I. W., Rutkowski, J. M., & Scherer, P. E. (2011). Targeted deletion of adipocytes by apoptosis leads to adipose tissue recruitment of alternatively activated M2 macrophages. *Endocrinology*, *152*(8), 3074–3081.

Florance, I., & Ramasubbu, S. (2022). Current Understanding on the Role of Lipids in Macrophages and Associated Diseases. *International Journal of Molecular Sciences*, *24*(1). https://doi.org/10.3390/ijms24010589

Fontana, L., Eagon, J. C., Trujillo, M. E., Scherer, P. E., & Klein, S. (2007). Visceral fat adipokine secretion is associated with systemic inflammation in obese humans. *Diabetes*, *56*(4), 1010–1013.

Freeman, A. M., Acevedo, L. A., & Pennings, N. (2023). *Insulin Resistance*. StatPearls Publishing.

Freimuth, J., Bangen, J. M., Lambertz, D., Hu, W., Nevzorova, Y. A., Sonntag, R., Gassler, N., Riethmacher, D., Trautwein, C., & Liedtke, C. (2013). Loss of caspase-8 in hepatocytes accelerates the onset of liver regeneration in mice through premature nuclear factor kappa B activation. *Hepatology (Baltimore, Md.)*, *58*(5). https://doi.org/10.1002/hep.26538

Frontini, A., & Cinti, S. (2010). Distribution and development of brown adipocytes in the murine and human adipose organ. *Cell Metabolism*, *11*(4), 253–256.

Fujita, H., Tokunaga, A., Shimizu, S., Whiting, A. L., Aguilar-Alonso, F., Takagi, K., Walinda, E., Sasaki, Y., Shimokawa, T., Mizushima, T., Ohki, I., Ariyoshi, M., Tochio, H., Bernal, F., Shirakawa, M., & Iwai, K. (2018). Cooperative Domain Formation by Homologous Motifs in HOIL-1L and SHARPIN Plays A Crucial Role in LUBAC Stabilization. *Cell Reports*, *23*(4), 1192–1204.

Fukaya, M., Brorsson, C. A., Meyerovich, K., Catrysse, L., Delaroche, D., Vanzela, E. C., Ortis, F., Beyaert, R., Nielsen, L. B., Andersen, M. L., Mortensen, H. B., Pociot, F., van Loo, G., Størling, J., & Cardozo, A. K. (2016). A20 Inhibits β-Cell Apoptosis by Multiple Mechanisms and Predicts Residual β-Cell Function in Type 1 Diabetes. *Molecular Endocrinology* , *30*(1), 48–61.

Fuseya, Y., Fujita, H., Kim, M., Ohtake, F., Nishide, A., Sasaki, K., Saeki, Y., Tanaka, K., Takahashi, R., & Iwai, K. (2020). The HOIL-1L ligase modulates immune signalling and cell death via monoubiquitination of LUBAC. *Nature Cell Biology*, *22*(6), 663–673.

Fuseya, Y., Kadoba, K., Liu, X., Suetsugu, H., Iwasaki, T., Ohmura, K., Sumida, T., Kochi, Y., Morinobu, A., Terao, C., & Iwai, K. (2024). Attenuation of HOIL-1L ligase activity promotes systemic autoimmune disorders by augmenting linear ubiquitin signaling. *JCI Insight*, *9*(3). https://doi.org/10.1172/jci.insight.171108

Fu, Y., Li, L., Zhang, X., Deng, Z., Wu, Y., Chen, W., Liu, Y., He, S., Wang, J., Xie, Y., Tu, Z., Lyu, Y., Wei, Y., Wang, S., Cui, C.-P., Liu, C. H., & Zhang, L. (2024). Systematic HOIP interactome profiling reveals critical roles of linear ubiquitination in tissue homeostasis. *Nature Communications*, *15*(1), 2974.

Galassi, A., Reynolds, K., & He, J. (2006). Metabolic syndrome and risk of cardiovascular disease: a meta-analysis. *The American Journal of Medicine*, *119*(10), 812–819.

Galic, S., Oakhill, J. S., & Steinberg, G. R. (2010). Adipose tissue as an endocrine organ. *Molecular and Cellular Endocrinology*, *316*(2), 129–139.

Galluzzi, L., Kepp, O., Trojel-Hansen, C., & Kroemer, G. (2012). Non-apoptotic functions of apoptosis-regulatory proteins. *EMBO Reports*, *13*(4), 322–330.

Gao, L., Zhang, W., Shi, X. H., Chang, X., Han, Y., Liu, C., Jiang, Z., & Yang, X. (2023). The mechanism of linear ubiquitination in regulating cell death and correlative diseases. *Cell Death & Disease*, *14*(10), 659.

Gao, T., Liu, T., Ko, C.-J., Zhang, L., Joo, D., Xie, X., Zhu, L., Li, Y., Cheng, X., & Sun, S.-C. (2022). Myeloid cell TBK1 restricts inflammatory responses. *Proceedings of the National Academy of Sciences of the United States of America*, *119*(4). https://doi.org/10.1073/pnas.2107742119

Gao, Z., Zhang, J., Henagan, T. M., Lee, J. H., Ye, X., Wang, H., & Ye, J. (2015). P65 inactivation in adipocytes and macrophages attenuates adipose inflammatory response in lean but not in obese mice. *American Journal of Physiology. Endocrinology and Metabolism*, *308*(6), E496–E505.

Garg, A. (2000). Gender differences in the prevalence of metabolic complications in familial partial lipodystrophy (Dunnigan variety). *The Journal of Clinical Endocrinology and Metabolism*, *85*(5). https://doi.org/10.1210/jcem.85.5.6605

Gautheron, J., Vucur, M., Reisinger, F., Cardenas, D. V., Roderburg, C., Koppe, C., Kreggenwinkel, K., Schneider, A. T., Bartneck, M., Neumann, U. P., Canbay, A., Reeves, H. L., Luedde, M., Tacke, F., Trautwein, C., Heikenwalder, M., & Luedde, T. (2014). A positive feedback loop between RIP3 and JNK controls non-alcoholic steatohepatitis. *EMBO Molecular Medicine*, *6*(8), 1062–1074.

Gautheron, J., Vucur, M., Schneider, A. T., Severi, I., Roderburg, C., Roy, S., Bartneck, M., Schrammen, P., Diaz, M. B., Ehling, J., Gremse, F., Heymann, F., Koppe, C., Lammers, T., Kiessling, F., Van Best, N., Pabst, O., Courtois, G., Linkermann, A., … Luedde, T. (2016). The necroptosis-inducing kinase RIPK3 dampens adipose tissue inflammation and glucose intolerance. *Nature Communications*, *7*, 11869.

GBD Results. (n.d.). Institute for Health Metrics and Evaluation. Retrieved May 1, 2024, from https://vizhub.healthdata.org/gbd-results/

Gerlach, B., Cordier, S. M., Schmukle, A. C., Emmerich, C. H., Rieser, E., Haas, T. L., Webb, A. I., Rickard, J. A., Anderton, H., Wong, W. W.-L., Nachbur, U., Gangoda, L., Warnken, U., Purcell, A. W., Silke, J., & Walczak, H. (2011). Linear ubiquitination prevents inflammation and regulates immune signalling. *Nature*, *471*(7340), 591–596.

Ghaben, A. L., & Scherer, P. E. (2019). Adipogenesis and metabolic health. *Nature Reviews. Molecular Cell Biology*, *20*(4), 242–258.

Ghesmati, Z., Rashid, M., Fayezi, S., Gieseler, F., Alizadeh, E., & Darabi, M. (2024). An update on the secretory functions of brown, white, and beige adipose tissue: Towards therapeutic applications. *Reviews in Endocrine & Metabolic Disorders*, *25*(2), 279–308.

Ghorbani, M., Claus, T. H., & Himms-Hagen, J. (1997). Hypertrophy of brown adipocytes in brown and white adipose tissues and reversal of diet-induced obesity in rats treated with a beta3-adrenoceptor agonist. *Biochemical Pharmacology*, *54*(1), 121–131.

Ginting, R. P., Lee, J.-M., & Lee, M.-W. (2023). The Influence of Ambient Temperature on Adipose Tissue Homeostasis, Metabolic Diseases and Cancers. *Cells* , *12*(6). https://doi.org/10.3390/cells12060881

Giralt, M., & Villarroya, F. (2013). White, brown, beige/brite: different adipose cells for different functions? *Endocrinology*, *154*(9), 2992–3000.

Gire, D., Inamdar, S., Acharya, J., Sadawarte, S., Kulkarni, A., & Ghaskadbi, S. (2024). Dynamic changes in the gene expression during adipogenesis in hMSCs. *Gene Reports*, *34*, 101860.

Golks, A., Brenner, D., Fritsch, C., Krammer, P. H., & Lavrik, I. N. (2005). c-FLIPR, a new regulator of death receptor-induced apoptosis. *The Journal of Biological Chemistry*, *280*(15). https://doi.org/10.1074/jbc.M414425200

Gomez-Diaz, C., Jonsson, G., Schodl, K., Deszcz, L., Bestehorn, A., Eislmayr, K., Almagro, J., Kavirayani, A., Seida, M., Fennell, L. M., Hagelkruys, A., Kovarik, P., Penninger, J.

M., & Ikeda, F. (2021). The ubiquitin ligase HOIL-1L regulates immune responses by interacting with linear ubiquitin chains. *iScience*, *24*(11), 103241.

Goto, T., Naknukool, S., Yoshitake, R., Hanafusa, Y., Tokiwa, S., Li, Y., Sakamoto, T., Nitta, T., Kim, M., Takahashi, N., Yu, R., Daiyasu, H., Seno, S., Matsuda, H., & Kawada, T. (2016). Proinflammatory cytokine interleukin-1β suppresses cold-induced thermogenesis in adipocytes. *Cytokine*, *77*, 107–114.

Green, D. R., Galluzzi, L., & Kroemer, G. (2014). Cell biology. Metabolic control of cell death. *Science*, *345*(6203), 1250256.

Griffin, M. J. (2022). On the Immunometabolic Role of NF-κB in Adipocytes. *Immunometabolism*, *4*(1). https://doi.org/10.20900/immunometab20220003

Guicciardi, M. E., & Gores, G. J. (2009). Life and death by death receptors. *FASEB Journal: Official Publication of the Federation of American Societies for Experimental Biology*, *23*(6), 1625–1637.

Günther, C., Martini, E., Wittkopf, N., Amann, K., Weigmann, B., Neumann, H., Waldner, M. J., Hedrick, S. M., Tenzer, S., Neurath, M. F., & Becker, C. (2011). Caspase-8 regulates TNF-α-induced epithelial necroptosis and terminal ileitis. *Nature*, *477*(7364), 335–339.

Guo, J., Sun, D., Zhang, J., Guo, J., Wu, Z., Chen, Y., Xu, Y., Zhou, D., Cui, Y., Mo, Q., Li, Y., Zhao, T., & You, Q. (2023). The E3 ubiquitin ligase RBCK1: Implications in the tumor immune microenvironment and antiangiogenic therapy of glioma. *Computational and Structural Biotechnology Journal*, *21*, 5212–5227.

Guo, Q., Jin, Y., Chen, X., Ye, X., Shen, X., Lin, M., Zeng, C., Zhou, T., & Zhang, J. (2024). NF-κB in biology and targeted therapy: new insights and translational implications. *Signal Transduction and Targeted Therapy*, *9*(1), 53.

Guo, R., Wang, H., Cui, N., Perez, F., Ruera, C., Miculan, E., Chirdo, F., Vasudevan, S. O., Russo, A., Kumari, P., Rathinam, V. A., Planes, R., Santoni, K., Salimata, B., Meunier, E., Magnani, L., Colantuoni, M., & Mortellaro, A. (n.d.). *Canonical and noncanonical pyroptosis pathways. The canonical*. ResearchGate. Retrieved May 30, 2024, from https://www.researchgate.net/figure/Canonical-and-noncanonical-pyroptosis-pathways-The-canonical-pyroptosis-pathway-requires_fig1_352755367

Guo, Y., He, J., Zhang, H., Chen, R., Li, L., Liu, X., Huang, C., Qiang, Z., Zhou, Z., Wang, Y., Huang, J., Zhao, X., Zheng, J., Chen, G.-Q., & Yu, J. (2022). Linear ubiquitination of PTEN impairs its function to promote prostate cancer progression. *Oncogene*, *41*(44), 4877–4892.

Haas, T. L., Emmerich, C. H., Gerlach, B., Schmukle, A. C., Cordier, S. M., Rieser, E., Feltham, R., Vince, J., Warnken, U., Wenger, T., Koschny, R., Komander, D., Silke, J., & Walczak, H. (2009). Recruitment of the linear ubiquitin chain assembly complex stabilizes the TNF-R1 signaling complex and is required for TNF-mediated gene induction. *Molecular Cell*, *36*(5), 831–844.

Hagberg, C. E., & Spalding, K. L. (2024). White adipocyte dysfunction and obesity-associated pathologies in humans. *Nature Reviews. Molecular Cell Biology*, *25*(4), 270–289.

Hagemann, T., Czechowski, P., Ghosh, A., Sun, W., Dong, H., Noé, F., Wolfrum, C., Blüher, M., & Hoffmann, A. (2023). Laminin α4 expression in human adipose tissue depots and its association with obesity and obesity related traits. *Biomedicines*, *11*(10), 2806.

Halberg, N., Khan, T., Trujillo, M. E., Wernstedt-Asterholm, I., Attie, A. D., Sherwani, S., Wang, Z. V., Landskroner-Eiger, S., Dineen, S., Magalang, U. J., Brekken, R. A., & Scherer, P. E. (2009). Hypoxia-inducible factor 1alpha induces fibrosis and insulin resistance in white adipose tissue. *Molecular and Cellular Biology*, *29*(16), 4467–4483.

Handakas, E., Chang, K., Khandpur, N., Vamos, E. P., Millett, C., Sassi, F., Vineis, P., & Robinson, O. (2022). Metabolic profiles of ultra-processed food consumption and their role in obesity risk in British children. *Clinical Nutrition (Edinburgh, Scotland)*, *41*(11),

2537–2548.

Han, H.-S., Kang, G., Kim, J. S., Choi, B. H., & Koo, S.-H. (2016). Regulation of glucose metabolism from a liver-centric perspective. *Experimental & Molecular Medicine*, *48*(3), e218.

Hao, F., Cubero, F. J., Ramadori, P., Liao, L., Haas, U., Lambertz, D., Sonntag, R., Bangen, J.-M., Gassler, N., Hoss, M., Streetz, K. L., Reissing, J., Zimmermann, H. W., Trautwein, C., Liedtke, C., & Nevzorova, Y. A. (2017). Inhibition of Caspase-8 does not protect from alcohol-induced liver apoptosis but alleviates alcoholic hepatic steatosis in mice. *Cell Death & Disease*, *8*(10), e3152–e3152.

Haque, W. A., Shimomura, I., Matsuzawa, Y., & Garg, A. (2002). Serum adiponectin and leptin levels in patients with lipodystrophies. *The Journal of Clinical Endocrinology and Metabolism*, *87*(5), 2395.

Harman-Boehm, I., Blüher, M., Redel, H., Sion-Vardy, N., Ovadia, S., Avinoach, E., Shai, I., Klöting, N., Stumvoll, M., Bashan, N., & Rudich, A. (2007). Macrophage infiltration into omental versus subcutaneous fat across different populations: effect of regional adiposity and the comorbidities of obesity. *The Journal of Clinical Endocrinology and Metabolism*, *92*(6), 2240–2247.

Hayden, M. S., & Ghosh, S. (2014). Regulation of NF-κB by TNF family cytokines. *Seminars in Immunology*, *26*(3), 253–266.

Heeren, J., & Scheja, L. (2021). Metabolic-associated fatty liver disease and lipoprotein metabolism. *Molecular Metabolism*, *50*, 101238.

Heger, K., Wickliffe, K. E., Ndoja, A., Zhang, J., Murthy, A., Dugger, D. L., Maltzman, A., de Sousa E Melo, F., Hung, J., Zeng, Y., Verschueren, E., Kirkpatrick, D. S., Vucic, D., Lee, W. P., Roose-Girma, M., Newman, R. J., Warming, S., Hsiao, Y.-C., Kőműves, L. G., … Dixit, V. M. (2018). OTULIN limits cell death and inflammation by deubiquitinating LUBAC. *Nature*, *559*(7712), 120–124.

Heida, A., Gruben, N., Catrysse, L., Koehorst, M., Koster, M., Kloosterhuis, N. J., Gerding, A., Havinga, R., Bloks, V. W., Bongiovanni, L., Wolters, J. C., van Dijk, T., van Loo, G., de Bruin, A., Kuipers, F., Koonen, D. P. Y., & van de Sluis, B. (2021). The hepatocyte IKK:NF-κB axis promotes liver steatosis by stimulating de novo lipogenesis and cholesterol synthesis. *Molecular Metabolism*, *54*(101349), 101349.

Hellmér, J., Marcus, C., Sonnenfeld, T., & Arner, P. (1992). Mechanisms for differences in lipolysis between human subcutaneous and omental fat cells. *The Journal of Clinical Endocrinology and Metabolism*, *75*(1), 15–20.

Herz, C. T., & Kiefer, F. W. (2019). Adipose tissue browning in mice and humans. *The Journal of Endocrinology*, *241*(3), R97–R109.

He, S., Wang, L., Miao, L., Wang, T., Du, F., Zhao, L., & Wang, X. (2009). Receptor interacting protein kinase-3 determines cellular necrotic response to TNF-alpha. *Cell*, *137*(6), 1100–1111.

Hida, K., Wada, J., Eguchi, J., Zhang, H., Baba, M., Seida, A., Hashimoto, I., Okada, T., Yasuhara, A., Nakatsuka, A., Shikata, K., Hourai, S., Futami, J., Watanabe, E., Matsuki, Y., Hiramatsu, R., Akagi, S., Makino, H., & Kanwar, Y. S. (2005). Visceral adipose tissue-derived serine protease inhibitor: a unique insulin-sensitizing adipocytokine in obesity. *Proceedings of the National Academy of Sciences of the United States of America*, *102*(30), 10610–10615.

Hildebrand, J. M., Tanzer, M. C., Lucet, I. S., Young, S. N., Spall, S. K., Sharma, P., Pierotti, C., Garnier, J.-M., Dobson, R. C. J., Webb, A. I., Tripaydonis, A., Babon, J. J., Mulcair, M. D., Scanlon, M. J., Alexander, W. S., Wilks, A. F., Czabotar, P. E., Lessene, G., Murphy, J. M., & Silke, J. (2014). Activation of the pseudokinase MLKL unleashes the four-helix bundle domain to induce membrane localization and necroptotic cell death. *Proceedings of the National Academy of Sciences of the United States of America*, *111*(42), 15072–15077.

Hildebrandt, X., Ibrahim, M., & Peltzer, N. (2022). Cell death and inflammation during obesity: “Know my methods, WAT(son).” *Cell Death and Differentiation*, *30*(2), 279–292.

Hildreth, A. D., Ma, F., Wong, Y. Y., Sun, R., Pellegrini, M., & O’Sullivan, T. E. (2021). Single-cell sequencing of human white adipose tissue identifies new cell states in health and obesity. *Nature Immunology*, *22*(5), 639–653.

Hill, A. A., Anderson-Baucum, E. K., Kennedy, A. J., Webb, C. D., Yull, F. E., & Hasty, A. H. (2015). Activation of NF-κB drives the enhanced survival of adipose tissue macrophages in an obesogenic environment. *Molecular Metabolism*, *4*(10), 665–677.

Hillert-Richter, L. K., König, C., Ivanisenko, N. V., Reinhold, D., & Lavrik, I. N. (2024). Targeting caspase-8/c-FLIPL heterodimer in complex II promotes DL-mediated cell death. *Frontiers in Cell and Developmental Biology*, *12*, 1471216.

Hitotsumatsu, O., Ahmad, R.-C., Tavares, R., Wang, M., Philpott, D., Turer, E. E., Lee, B. L., Shiffin, N., Advincula, R., Malynn, B. A., Werts, C., & Ma, A. (2008). The ubiquitin-editing enzyme A20 restricts nucleotide-binding oligomerization domain containing 2-triggered signals. *Immunity*, *28*(3), 381–390.

Hochberg, I., Tran, Q. T., Barkan, A. L., Saltiel, A. R., Chandler, W. F., & Bridges, D. (2015). Gene Expression Signature in Adipose Tissue of Acromegaly Patients. *PloS One*, *10*(6), e0129359.

Hoesel, B., & Schmid, J. A. (2013). The complexity of NF-κB signaling in inflammation and cancer. *Molecular Cancer*, *12*, 86.

HogenEsch, H., Gijbels, M. J., Offerman, E., van Hooft, J., van Bekkum, D. W., & Zurcher, C. (1993). A spontaneous mutation characterized by chronic proliferative dermatitis in C57BL mice. *The American Journal of Pathology*, *143*(3), 972–982.

HogenEsch, H., Torregrosa, S. E., Boggess, D., Sundberg, B. A., Carroll, J., & Sundberg, J. P. (2001). Increased expression of type 2 cytokines in chronic proliferative dermatitis (cpdm) mutant mice and resolution of inflammation following treatment with IL-12. *European Journal of Immunology*, *31*(3), 734–742.

Honecker, J., Weidlich, D., Heisz, S., Lindgren, C. M., Karampinos, D. C., Claussnitzer, M., & Hauner, H. (2021). A distribution-centered approach for analyzing human adipocyte size estimates and their association with obesity-related traits and mitochondrial function. *International Journal of Obesity (2005)* , *45*(9), 2108–2117.

Hong, S., Song, W., Zushin, P.-J. H., Liu, B., Jedrychowski, M. P., Mina, A. I., Deng, Z., Cabarkapa, D., Hall, J. A., Palmer, C. J., Aliakbarian, H., Szpyt, J., Gygi, S. P., Tavakkoli, A., Lynch, L., Perrimon, N., & Banks, A. S. (2018). Phosphorylation of Beta-3 adrenergic receptor at serine 247 by ERK MAP kinase drives lipolysis in obese adipocytes. *Molecular Metabolism*, *12*, 25–38.

Hoover, S. E., Il’yasova, D., Fontaine, K. R., Spasojevic, I., Gower, B. A., & Goss, A. M. (2021). A Pilot Study of Associations Between Visceral Fat, IL-6, and Urinary F2-Isoprostanes in Older Adults Exposed to a Diet Intervention. *Current Developments in Nutrition*, *5*(6), nzab082.

Ho, P.-C., Chuang, Y.-S., Hung, C.-H., & Wei, L.-N. (2011). Cytoplasmic receptor-interacting protein 140 (RIP140) interacts with perilipin to regulate lipolysis. *Cellular Signalling*, *23*(8), 1396–1403.

Hotamisligil, G. S. (2017). Inflammation, metaflammation and immunometabolic disorders. *Nature*, *542*(7640), 177–185.

Hrdinka, M., & Gyrd-Hansen, M. (2017). The Met1-Linked Ubiquitin Machinery: Emerging Themes of (De)regulation. *Molecular Cell*, *68*(2), 265–280.

Hsu, H., Shu, H. B., Pan, M. G., & Goeddel, D. V. (1996). TRADD-TRAF2 and TRADD-FADD interactions define two distinct TNF receptor 1 signal transduction pathways. *Cell*, *84*(2), 299–308.

Huang, B., DePaolo, J., Judy, R. L., Shakt, G., Witschey, W. R., Levin, M. G., & Gershuni, V.

M. (2023). Relationships between body fat distribution and metabolic syndrome traits and outcomes: A mendelian randomization study. *PloS One*, *18*(10), e0293017.

Hughes, M. A., Powley, I. R., Jukes-Jones, R., Horn, S., Feoktistova, M., Fairall, L., Schwabe, J. W. R., Leverkus, M., Cain, K., & MacFarlane, M. (2016). Co-operative and hierarchical binding of c-FLIP and caspase-8: A unified model defines how c-FLIP isoforms differentially control cell fate. *Molecular Cell*, *61*(6), 834–849.

Hunt, G. J., Freytag, S., Bahlo, M., & Gagnon-Bartsch, J. A. (2019). Dtangle: Accurate and robust cell type deconvolution. *Bioinformatics* , *35*(12), 2093–2099.

Huo, M., Ye, J., Zhang, Y., Wang, M., Zhang, J., Feng, S.-T., Cai, H., Zhong, B., & Dong, Z. (2024). Quantitative assessment of brown adipose tissue whitening in a high-fat-diet murine model using synthetic magnetic resonance imaging. *Heliyon*, *10*(6), e27314.

Husnjak, K., & Dikic, I. (2012). Ubiquitin-binding proteins: decoders of ubiquitin-mediated cellular functions. *Annual Review of Biochemistry*, *81*, 291–322.

Huttlin, E. L., Jedrychowski, M. P., Elias, J. E., Goswami, T., Rad, R., Beausoleil, S. A., Villén, J., Haas, W., Sowa, M. E., & Gygi, S. P. (2010). A tissue-specific atlas of mouse protein phosphorylation and expression. *Cell*, *143*(7), 1174–1189.

Ikeda, F., Deribe, Y. L., Skånland, S. S., Stieglitz, B., Grabbe, C., Franz-Wachtel, M., van Wijk, S. J. L., Goswami, P., Nagy, V., Terzic, J., Tokunaga, F., Androulidaki, A., Nakagawa, T., Pasparakis, M., Iwai, K., Sundberg, J. P., Schaefer, L., Rittinger, K., Macek, B., & Dikic, I. (2011). SHARPIN forms a linear ubiquitin ligase complex regulating NF-κB activity and apoptosis. *Nature*, *471*(7340), 637–641.

Inagaki, T., Sakai, J., & Kajimura, S. (2016). Transcriptional and epigenetic control of brown and beige adipose cell fate and function. *Nature Reviews. Molecular Cell Biology*, *17*(8), 480–495.

Islam, T., Afonso, M. B., & Rodrigues, C. M. P. (2022). The role of RIPK3 in liver mitochondria bioenergetics and function. *European Journal of Clinical Investigation*, *52*(3), e13648.

Israël, A. (2010). The IKK complex, a central regulator of NF-kappaB activation. *Cold Spring Harbor Perspectives in Biology*, *2*(3), a000158.

Item, F., & Konrad, D. (2012). Visceral fat and metabolic inflammation: the portal theory revisited. *Obesity Reviews: An Official Journal of the International Association for the Study of Obesity*, *13 Suppl 2*, 30–39.

Jahan, A. S., Elbæk, C. R., & Damgaard, R. B. (2021). Met1-linked ubiquitin signalling in health and disease: inflammation, immunity, cancer, and beyond. *Cell Death and Differentiation*, *28*(2), 473–492.

Jais, A., Solas, M., Backes, H., Chaurasia, B., Kleinridders, A., Theurich, S., Mauer, J., Steculorum, S. M., Hampel, B., Goldau, J., Alber, J., Förster, C. Y., Eming, S. A., Schwaninger, M., Ferrara, N., Karsenty, G., & Brüning, J. C. (2016). Myeloid-Cell-Derived VEGF Maintains Brain Glucose Uptake and Limits Cognitive Impairment in Obesity. *Cell*, *165*(4), 882–895.

James, D. E., Stöckli, J., & Birnbaum, M. J. (2021). The aetiology and molecular landscape of insulin resistance. *Nature Reviews. Molecular Cell Biology*, *22*(11), 751–771.

Jiao, P., Feng, B., Ma, J., Nie, Y., Paul, E., Li, Y., & Xu, H. (2012). Constitutive activation of IKKβ in adipose tissue prevents diet-induced obesity in mice. *Endocrinology*, *153*(1), 154–165.

Jin, Y., Peng, Y., Xu, J., Yuan, Y., Yang, N., Zhang, Z., Xu, L., Li, L., Xiong, Y., Sun, D., Pan, Y., Wu, R., & Fu, J. (2024). LUBAC promotes angiogenesis and lung tumorigenesis by ubiquitinating and antagonizing autophagic degradation of HIF1α. *Oncogenesis*, *13*(1), 6.

Ji, P., Drackley, J. K., Khan, M. J., & Loor, J. J. (2014). Inflammation- and lipid metabolism-related gene network expression in visceral and subcutaneous adipose

depots of Holstein cows. *Journal of Dairy Science*, *97*(6), 3441–3448.

Johnson, A. M. F., & Olefsky, J. M. (2013). The origins and drivers of insulin resistance. *Cell*, *152*(4), 673–684.

Johnson, J. A., Fried, S. K., Pi-Sunyer, F. X., & Albu, J. B. (2001). Impaired insulin action in subcutaneous adipocytes from women with visceral obesity. *American Journal of Physiology. Endocrinology and Metabolism*, *280*(1), E40–E49.

Ju, L., Han, J., Zhang, X., Deng, Y., Yan, H., Wang, C., Li, X., Chen, S., Alimujiang, M., Li, X., Fang, Q., Yang, Y., & Jia, W. (2019). Obesity-associated inflammation triggers an autophagy-lysosomal response in adipocytes and causes degradation of perilipin 1. *Cell Death & Disease*, *10*(2), 121.

Jun, H., Ma, Y., Chen, Y., Gong, J., Liu, S., Wang, J., Knights, A. J., Qiao, X., Emont, M. P., Xu, X. Z. S., Kajimura, S., & Wu, J. (2020). Adrenergic-Independent Signaling via CHRNA2 Regulates Beige Fat Activation. *Developmental Cell*, *54*(1), 106–116.e5.

Kahn, C. R. (1994). Banting Lecture. Insulin action, diabetogenes, and the cause of type II diabetes. *Diabetes*, *43*(8), 1066–1084.

Kahn, C. R., Wang, G., & Lee, K. Y. (2019). Altered adipose tissue and adipocyte function in the pathogenesis of metabolic syndrome. *The Journal of Clinical Investigation*, *129*(10), 3990–4000.

Kajimura, S., Spiegelman, B. M., & Seale, P. (2015). Brown and beige fat: Physiological roles beyond heat generation. *Cell Metabolism*, *22*(4), 546–559.

Kang, T.-B., Ben-Moshe, T., Varfolomeev, E. E., Pewzner-Jung, Y., Yogev, N., Jurewicz, A., Waisman, A., Brenner, O., Haffner, R., Gustafsson, E., Ramakrishnan, P., Lapidot, T., & Wallach, D. (2004). Caspase-8 Serves Both Apoptotic and Nonapoptotic Roles. *J Immunol*, *173*(5), 2976–2984.

Kang, T.-B., Jeong, J.-S., Yang, S.-H., Kovalenko, A., & Wallach, D. (2018). Caspase-8 deficiency in mouse embryos triggers chronic RIPK1-dependent activation of inflammatory genes, independently of RIPK3. *Cell Death and Differentiation*, *25*(6), 1107–1117.

Kantari, C., & Walczak, H. (2011). Caspase-8 and bid: caught in the act between death receptors and mitochondria. *Biochimica et Biophysica Acta*, *1813*(4), 558–563.

Karin, M. (2006). Nuclear factor-kappaB in cancer development and progression. *Nature*, *441*(7092), 431–436.

Karri, U., Harasimowicz, M., Carpio Tumba, M., & Schwartz, D. M. (2024). The complexity of being A20: From biological functions to genetic associations. *Journal of Clinical Immunology*, *44*(3), 76.

Karunakaran, D., Turner, A. W., Duchez, A.-C., Soubeyrand, S., Rasheed, A., Smyth, D., Cook, D. P., Nikpay, M., Kandiah, J. W., Pan, C., Geoffrion, M., Lee, R., Boytard, L., Wyatt, H., Nguyen, M.-A., Lau, P., Laakso, M., Ramkhelawon, B., Alvarez, M., … Rayner, K. J. (2020). RIPK1 gene variants associate with obesity in humans and can be therapeutically silenced to reduce obesity in mice. *Nature Metabolism*, *2*(10), 1113–1125.

Kaufmann, B., Kui, L., Reca, A., Leszczynska, A., Kim, A. D., Booshehri, L. M., Wree, A., Friess, H., Hartmann, D., Broderick, L., Hoffman, H. M., & Feldstein, A. E. (2022). Cell-specific deletion of NLRP3 inflammasome identifies myeloid cells as key drivers of liver inflammation and fibrosis in Murine steatohepatitis. *Cellular and Molecular Gastroenterology and Hepatology*, *14*(4), 751–767.

Kearney, C. J., & Martin, S. J. (2017). An Inflammatory Perspective on Necroptosis. *Molecular Cell*, *65*(6), 965–973.

Kelley, N., Jeltema, D., Duan, Y., & He, Y. (2019). The NLRP3 Inflammasome: An Overview of Mechanisms of Activation and Regulation. *International Journal of Molecular Sciences*, *20*(13). https://doi.org/10.3390/ijms20133328

Kelsall, I. R., McCrory, E. H., Xu, Y., Scudamore, C. L., Nanda, S. K., Mancebo-Gamella, P., Wood, N. T., Knebel, A., Matthews, S. J., & Cohen, P. (2022). HOIL-1 ubiquitin ligase activity targets unbranched glucosaccharides and is required to prevent polyglucosan accumulation. *The EMBO Journal*, *41*(8), e109700.

Kelsall, I. R., Zhang, J., Knebel, A., Arthur, J. S. C., & Cohen, P. (2019). The E3 ligase HOIL-1 catalyses ester bond formation between ubiquitin and components of the Myddosome in mammalian cells. *Proceedings of the National Academy of Sciences of the United States of America*, *116*(27), 13293–13298.

Kennedy, C., McPhie, K., & Rittinger, K. (2022). Targeting the ubiquitin system by fragment-based drug discovery. *Frontiers in Molecular Biosciences*, *9*, 1019636.

Kenneth W. Adams, G. M. C. (2007). Rapid Turnover of Mcl-1 Couples Translation to Cell Survival and Apoptosis. *Journal of Biological Chemistry*, *282*(9), 6192–6200.

Keuper, M., Jastroch, M., Yi, C.-X., Fischer-Posovszky, P., Wabitsch, M., Tschöp, M. H., & Hofmann, S. M. (2014). Spare mitochondrial respiratory capacity permits human adipocytes to maintain ATP homeostasis under hypoglycemic conditions. *FASEB Journal: Official Publication of the Federation of American Societies for Experimental Biology*, *28*(2), 761–770.

Khan, A. S., Subramaniam, S., Dramane, G., Khelifi, D., & Khan, N. A. (2017). ERK1 and ERK2 activation modulates diet-induced obesity in mice. *Biochimie*, *137*, 78–87.

Khan, R. S., Lalor, P. F., Thursz, M., & Newsome, P. N. (2023). The role of neutrophils in alcohol-related hepatitis. *Journal of Hepatology*, *79*(4), 1037–1048.

Kim, B., Lee, B., Kim, M.-K., Gong, S. P., Park, N. H., Chung, H. H., Kim, H. S., No, J. H., Park, W. Y., Park, A. K., Lim, J. M., & Song, Y. S. (2016). Gene expression profiles of human subcutaneous and visceral adipose-derived stem cells. *Cell Biochemistry and Function*, *34*(8), 563–571.

Kirisako, T., Kamei, K., Murata, S., Kato, M., Fukumoto, H., Kanie, M., Sano, S., Tokunaga, F., Tanaka, K., & Iwai, K. (2006). A ubiquitin ligase complex assembles linear polyubiquitin chains. *The EMBO Journal*, *25*(20), 4877–4887.

Kirkland, J. L., Tchkonia, T., Pirtskhalava, T., Han, J., & Karagiannides, I. (2002). Adipogenesis and aging: does aging make fat go MAD? *Experimental Gerontology*, *37*(6), 757–767.

Kleiner, D. E., Brunt, E. M., Van Natta, M., Behling, C., Contos, M. J., Cummings, O. W., Ferrell, L. D., Liu, Y.-C., Torbenson, M. S., Unalp-Arida, A., Yeh, M., McCullough, A. J., Sanyal, A. J., & Nonalcoholic Steatohepatitis Clinical Research Network. (2005). Design and validation of a histological scoring system for nonalcoholic fatty liver disease. *Hepatology* , *41*(6), 1313–1321.

Klemm, D. J., Leitner, J. W., Watson, P., Nesterova, A., Reusch, J. E., Goalstone, M. L., & Draznin, B. (2001). Insulin-induced adipocyte differentiation. Activation of CREB rescues adipogenesis from the arrest caused by inhibition of prenylation. *The Journal of Biological Chemistry*, *276*(30), 28430–28435.

Klöting, N., Fasshauer, M., Dietrich, A., Kovacs, P., Schön, M. R., Kern, M., Stumvoll, M., & Blüher, M. (2010). Insulin-sensitive obesity. *American Journal of Physiology. Endocrinology and Metabolism*, *299*(3), E506–E515.

Knudsen, J. G., Murholm, M., Carey, A. L., Biensø, R. S., Basse, A. L., Allen, T. L., Hidalgo, J., Kingwell, B. A., Febbraio, M. A., Hansen, J. B., & Pilegaard, H. (2014). Role of IL-6 in exercise training- and cold-induced UCP1 expression in subcutaneous white adipose tissue. *PloS One*, *9*(1), e84910.

Koenen, T. B., Stienstra, R., van Tits, L. J., Joosten, L. A. B., van Velzen, J. F., Hijmans, A., Pol, J. A., van der Vliet, J. A., Netea, M. G., Tack, C. J., Stalenhoef, A. F. H., & de Graaf, J. (2011). The inflammasome and caspase-1 activation: a new mechanism underlying increased inflammatory activity in human visceral adipose tissue. *Endocrinology*,

152(10), 3769–3778.

Koh, E. H., Park, J.-Y., Park, H.-S., Jeon, M. J., Ryu, J. W., Kim, M., Kim, S. Y., Kim, M.-S., Kim, S.-W., Park, I. S., Youn, J. H., & Lee, K.-U. (2007). Essential role of mitochondrial function in adiponectin synthesis in adipocytes. *Diabetes*, *56*(12), 2973–2981.

Kolb, H. (2022). Obese visceral fat tissue inflammation: from protective to detrimental? *BMC Medicine*, *20*(1), 494.

Komander, D., & Barford, D. (2008). Structure of the A20 OTU domain and mechanistic insights into deubiquitination. *Biochemical Journal*, *409*(1), 77–85.

Komander, D., & Rape, M. (2012). The ubiquitin code. *Annual Review of Biochemistry*, *81*, 203–229.

Komander, D., Reyes-Turcu, F., Licchesi, J. D. F., Odenwaelder, P., Wilkinson, K. D., & Barford, D. (2009). Molecular discrimination of structurally equivalent Lys 63-linked and linear polyubiquitin chains. *EMBO Reports*, *10*(5), 466–473.

Korf, H., & van der Merwe, S. (2017). Adipose-derived exosomal MicroRNAs orchestrate gene regulation in the liver: Is this the missing link in nonalcoholic fatty liver disease? *Hepatology (Baltimore, Md.)*, *66*(5), 1689–1691.

Kos, K., Wong, S., Tan, B. K., Kerrigan, D., Randeva, H. S., Pinkney, J. H., & Wilding, J. P. H. (2011). Human RBP4 adipose tissue expression is gender specific and influenced by leptin: Adipose tissue derived RBP4, gender and leptin. *Clinical Endocrinology*, *74*(2), 197–205.

Kotzbeck, P., Giordano, A., Mondini, E., Murano, I., Severi, I., Venema, W., Cecchini, M. P., Kershaw, E. E., Barbatelli, G., Haemmerle, G., Zechner, R., & Cinti, S. (2018). Brown adipose tissue whitening leads to brown adipocyte death and adipose tissue inflammation. *Journal of Lipid Research*, *59*(5), 784–794.

Kovacova, Z., Tencerova, M., Roussel, B., Wedellova, Z., Rossmeislova, L., Langin, D., Polak, J., & Stich, V. (2012). The impact of obesity on secretion of adiponectin multimeric isoforms differs in visceral and subcutaneous adipose tissue. *International Journal of Obesity (2005)* , *36*(10), 1360–1365.

Krenn, M., Salzer, E., Simonitsch-Klupp, I., Rath, J., Wagner, M., Haack, T. B., Strom, T. M., Schänzer, A., Kilimann, M. W., Schmidt, R. L. J., Schmetterer, K. G., Zimprich, A., Boztug, K., Hahn, A., & Zimprich, F. (2018). Mutations outside the N-terminal part of RBCK1 may cause polyglucosan body myopathy with immunological dysfunction: expanding the genotype-phenotype spectrum. *Journal of Neurology*, *265*(2), 394–401.

Kulathu, Y., & Komander, D. (2012). Atypical ubiquitylation - the unexplored world of polyubiquitin beyond Lys48 and Lys63 linkages. *Nature Reviews. Molecular Cell Biology*, *13*(8), 508–523.

Kumari, S., Redouane, Y., Lopez-Mosqueda, J., Shiraishi, R., Romanowska, M., Lutzmayer, S., Kuiper, J., Martinez, C., Dikic, I., Pasparakis, M., & Ikeda, F. (2014). Sharpin prevents skin inflammation by inhibiting TNFR1-induced keratinocyte apoptosis. *eLife*, *3*. https://doi.org/10.7554/eLife.03422

Kumar, V., Bouameur, J.-E., Bär, J., Rice, R. H., Hornig-Do, H.-T., Roop, D. R., Schwarz, N., Brodesser, S., Thiering, S., Leube, R. E., Wiesner, R. J., Vijayaraj, P., Brazel, C. B., Heller, S., Binder, H., Löffler-Wirth, H., Seibel, P., & Magin, T. M. (2015). A keratin scaffold regulates epidermal barrier formation, mitochondrial lipid composition, and activity. *The Journal of Cell Biology*, *211*(5), 1057–1075.

Kurtzer, G. M., Sochat, V., & Bauer, M. W. (2017). Singularity: Scientific containers for mobility of compute. *PloS One*, *12*(5), e0177459.

Kuwana, T., Smith, J. J., Muzio, M., Dixit, V., Newmeyer, D. D., & Kornbluth, S. (1998). Apoptosis induction by caspase-8 is amplified through the mitochondrial release of cytochrome c. *The Journal of Biological Chemistry*, *273*(26), 16589–16594.

Kwon, H., Laurent, S., Tang, Y., Zong, H., Vemulapalli, P., & Pessin, J. E. (2014).

Adipocyte-specific IKKβ signaling suppresses adipose tissue inflammation through an IL-13-dependent paracrine feedback pathway. *Cell Reports*, *9*(5), 1574–1583.

Lambertucci, F., Arboatti, A., Sedlmeier, M. G., Motiño, O., Alvarez, M. de L., Ceballos, M. P., Villar, S. R., Roggero, E., Monti, J. A., Pisani, G., Quiroga, A. D., Martín-Sanz, P., Carnovale, C. E., Francés, D. E., & Ronco, M. T. (2018). Disruption of tumor necrosis factor alpha receptor 1 signaling accelerates NAFLD progression in mice upon a high-fat diet. *The Journal of Nutritional Biochemistry*, *58*, 17–27.

Langhardt, J., Flehmig, G., Klöting, N., Lehmann, S., Ebert, T., Kern, M., Schön, M. R., Gärtner, D., Lohmann, T., Dressler, M., Fasshauer, M., Kovacs, P., Stumvoll, M., Dietrich, A., & Blüher, M. (2018). Effects of weight loss on glutathione peroxidase 3 serum concentrations and adipose tissue expression in human obesity. *Obesity Facts*, *11*(6), 475–490.

Larsen, C. M., Faulenbach, M., Vaag, A., Vølund, A., Ehses, J. A., Seifert, B., Mandrup-Poulsen, T., & Donath, M. Y. (2007). Interleukin-1-receptor antagonist in type 2 diabetes mellitus. *The New England Journal of Medicine*, *356*(15), 1517–1526.

Lee, D.-F., Kuo, H.-P., Chen, C.-T., Wei, Y., Chou, C.-K., Hung, J.-Y., Yen, C.-J., & Hung, M.-C. (2008). IKKbeta suppression of TSC1 function links the mTOR pathway with insulin resistance. *International Journal of Molecular Medicine*, *22*(5), 633–638.

Lee, E. G., Boone, D. L., Chai, S., Libby, S. L., Chien, M., Lodolce, J. P., & Ma, A. (2000). Failure to regulate TNF-induced NF-kappaB and cell death responses in A20-deficient mice. *Science*, *289*(5488), 2350–2354.

Lee, E., Korf, H., & Vidal-Puig, A. (2023). An adipocentric perspective on the development and progression of non-alcoholic fatty liver disease. *Journal of Hepatology*, *78*(5), 1048–1062.

Lee, J.-E., Schmidt, H., Lai, B., & Ge, K. (2019). Transcriptional and epigenomic regulation of adipogenesis. *Molecular and Cellular Biology*, *39*(11), 1–20.

Lee, Y.-H., Petkova, A. P., Mottillo, E. P., & Granneman, J. G. (2012). In vivo identification of bipotential adipocyte progenitors recruited by β3-adrenoceptor activation and high-fat feeding. *Cell Metabolism*, *15*(4), 480–491.

Lefebvre, A. M., Laville, M., Vega, N., Riou, J. P., van Gaal, L., Auwerx, J., & Vidal, H. (1998). Depot-specific differences in adipose tissue gene expression in lean and obese subjects. *Diabetes*, *47*(1), 98–103.

Liadis, N., Salmena, L., Kwan, E., Tajmir, P., Schroer, S. A., Radziszewska, A., Li, X., Sheu, L., Eweida, M., Xu, S., Gaisano, H. Y., Hakem, R., & Woo, M. (2007). Distinct In Vivo Roles of Caspase-8 in β-Cells in Physiological and Diabetes Models. *Diabetes*, *56*(9), 2302–2311.

Li, C., Qin, D., Hu, J., Yang, Y., Hu, D., & Yu, B. (2022). Inflamed adipose tissue: A culprit underlying obesity and heart failure with preserved ejection fraction. *Frontiers in Immunology*, *13*, 947147.

Liedtke, C., Bangen, J. M., Freimuth, J., Beraza, N., Lambertz, D., Cubero, F. J., Hatting, M., Karlmark, K. R., Streetz, K. L., Krombach, G. A., Tacke, F., Gassler, N., Riethmacher, D., & Trautwein, C. (2011). Loss of caspase-8 protects mice against inflammation-related hepatocarcinogenesis but induces non-apoptotic liver injury. *Gastroenterology*, *141*(6). https://doi.org/10.1053/j.gastro.2011.08.037

Li, G.-M., Liu, H.-M., Guan, W.-Z., Xu, H., Wu, B.-B., & Sun, L. (2019). Expanding the spectrum of A20 haploinsufficiency in two Chinese families: cases report. *BMC Medical Genetics*, *20*(1), 124.

Li, G., Xie, C., Lu, S., Nichols, R. G., Tian, Y., Li, L., Patel, D., Ma, Y., Brocker, C. N., Yan, T., Krausz, K. W., Xiang, R., Gavrilova, O., Patterson, A. D., & Gonzalez, F. J. (2017). Intermittent Fasting Promotes White Adipose Browning and Decreases Obesity by Shaping the Gut Microbiota. *Cell Metabolism*, *26*(4), 672–685.e4.

Li, M., Chi, X., Wang, Y., Setrerrahmane, S., Xie, W., & Xu, H. (2022). Trends in insulin resistance: insights into mechanisms and therapeutic strategy. *Signal Transduction and Targeted Therapy*, *7*(1), 1–25.

Lindhorst, A., Raulien, N., Wieghofer, P., Eilers, J., Rossi, F. M. V., Bechmann, I., & Gericke, M. (2021). Adipocyte death triggers a pro-inflammatory response and induces metabolic activation of resident macrophages. *Cell Death & Disease*, *12*(6), 579.

Lindquist, J. M., & Rehnmark, S. (1998). Ambient temperature regulation of apoptosis in brown adipose tissue. Erk1/2 promotes norepinephrine-dependent cell survival. *The Journal of Biological Chemistry*, *273*(46), 30147–30156.

Lin, J., Li, H., Yang, M., Ren, J., Huang, Z., Han, F., Huang, J., Ma, J., Zhang, D., Zhang, Z., Wu, J., Huang, D., Qiao, M., Jin, G., Wu, Q., Huang, Y., Du, J., & Han, J. (2013). A role of RIP3-mediated macrophage necrosis in atherosclerosis development. *Cell Reports*, *3*(1), 200–210.

Linkermann, A., Bräsen, J. H., Darding, M., Jin, M. K., Sanz, A. B., Heller, J.-O., De Zen, F., Weinlich, R., Ortiz, A., Walczak, H., Weinberg, J. M., Green, D. R., Kunzendorf, U., & Krautwald, S. (2013). Two independent pathways of regulated necrosis mediate ischemia-reperfusion injury. *Proceedings of the National Academy of Sciences of the United States of America*, *110*(29), 12024–12029.

Lin, S.-C., Chung, J. Y., Lamothe, B., Rajashankar, K., Lu, M., Lo, Y.-C., Lam, A. Y., Darnay, B. G., & Wu, H. (2008). Molecular basis for the unique deubiquitinating activity of the NF-kappaB inhibitor A20. *Journal of Molecular Biology*, *376*(2), 526–540.

Li, Q., Hagberg, C. E., Silva Cascales, H., Lang, S., Hyvönen, M. T., Salehzadeh, F., Chen, P., Alexandersson, I., Terezaki, E., Harms, M. J., Kutschke, M., Arifen, N., Krämer, N., Aouadi, M., Knibbe, C., Boucher, J., Thorell, A., & Spalding, K. L. (2021). Obesity and hyperinsulinemia drive adipocytes to activate a cell cycle program and senesce. *Nature Medicine*, *27*(11), 1941–1953.

Liu, R., & Nikolajczyk, B. S. (2019). Tissue Immune Cells Fuel Obesity-Associated Inflammation in Adipose Tissue and Beyond. *Frontiers in Immunology*, *10*, 1587.

Liu, R., Pulliam, D. A., Liu, Y., & Salmon, A. B. (2015). Dynamic differences in oxidative stress and the regulation of metabolism with age in visceral versus subcutaneous adipose. *Redox Biology*, *6*, 401–408.

Liu, T., Zhang, L., Joo, D., & Sun, S.-C. (2017). NF-κB signaling in inflammation. *Signal Transduction and Targeted Therapy*, *2*, 17023 – .

Liu, Y., Liang, J., Liu, Z., Tian, X., & Sun, C. (2024). Dihydrolipoyl dehydrogenase promotes white adipocytes browning by activating the RAS/ERK pathway and undergoing crotonylation modification. *International Journal of Biological Macromolecules*, *265*(Pt 1), 130816.

Li, W., Bengtson, M. H., Ulbrich, A., Matsuda, A., Reddy, V. A., Orth, A., Chanda, S. K., Batalov, S., & Joazeiro, C. A. P. (2008). Genome-wide and functional annotation of human E3 ubiquitin ligases identifies MULAN, a mitochondrial E3 that regulates the organelle's dynamics and signaling. *PloS One*, *3*(1), e1487.

Louzada, M. L. da C., Baraldi, L. G., Steele, E. M., Martins, A. P. B., Canella, D. S., Moubarac, J.-C., Levy, R. B., Cannon, G., Afshin, A., Imamura, F., Mozaffarian, D., & Monteiro, C. A. (2015). Consumption of ultra-processed foods and obesity in Brazilian adolescents and adults. *Preventive Medicine*, *81*, 9–15.

Love, M. I., Huber, W., & Anders, S. (2014). Moderated estimation of fold change and dispersion for RNA-seq data with DESeq2. *Genome Biology*, *15*(12), 550.

Luedde, M., Lutz, M., Carter, N., Sosna, J., Jacoby, C., Vucur, M., Gautheron, J., Roderburg, C., Borg, N., Reisinger, F., Hippe, H.-J., Linkermann, A., Wolf, M. J., Rose-John, S., Lüllmann-Rauch, R., Adam, D., Flögel, U., Heikenwalder, M., Luedde, T., & Frey, N. (2014). RIP3, a kinase promoting necroptotic cell death, mediates adverse remodelling

after myocardial infarction. *Cardiovascular Research*, *103*(2), 206–216.

Lu, J., Zhao, J., Meng, H., & Zhang, X. (2019). Adipose Tissue-Resident Immune Cells in Obesity and Type 2 Diabetes. *Frontiers in Immunology*, *10*, 1173.

Luk, C. T., Chan, C. K., Chiu, F., Shi, S. Y., Misra, P. S., Li, Y. Z., Pollock-Tahiri, E., Schroer, S. A., Desai, H. R., Sivasubramaniyam, T., Cai, E. P., Krishnamurthy, M., Han, D. J., Chowdhury, A., Aslam, R., Yuen, D. A., Hakem, A., Hakem, R., & Woo, M. (2023). Dual Role of Caspase 8 in Adipocyte Apoptosis and Metabolic Inflammation. *Diabetes*, *72*(12), 1751–1765.

Lumeng, C. N., Bodzin, J. L., & Saltiel, A. R. (2007). Obesity induces a phenotypic switch in adipose tissue macrophage polarization. *The Journal of Clinical Investigation*, *117*(1), 175–184.

Luo, J.-L., Kamata, H., & Karin, M. (2005). IKK/NF-kappaB signaling: balancing life and death--a new approach to cancer therapy. *The Journal of Clinical Investigation*, *115*(10), 2625–2632.

Lu, Y., Fujioka, H., Joshi, D., Li, Q., Sangwung, P., Hsieh, P., Zhu, J., Torio, J., Sweet, D., Wang, L., Chiu, S. Y., Croniger, C., Liao, X., & Jain, M. K. (2018). Mitophagy is required for brown adipose tissue mitochondrial homeostasis during cold challenge. *Scientific Reports*, *8*(1), 8251.

Macotela, Y., Emanuelli, B., Mori, M. A., Gesta, S., Schulz, T. J., Tseng, Y.-H., & Kahn, C. R. (2012). Intrinsic differences in adipocyte precursor cells from different white fat depots. *Diabetes*, *61*(7), 1691–1699.

Madani, R., Karastergiou, K., Ogston, N. C., Miheisi, N., Bhome, R., Haloob, N., Tan, G. D., Karpe, F., Malone-Lee, J., Hashemi, M., Jahangiri, M., & Mohamed-Ali, V. (2009). RANTES release by human adipose tissue in vivo and evidence for depot-specific differences. *American Journal of Physiology. Endocrinology and Metabolism*, *296*(6), E1262–E1268.

Ma, E. B., Javaid, H. M. A., Jung, D.-H., Park, J.-H., & Huh, J. Y. (2022). Gasdermin D deficiency does not protect mice from high-fat diet-induced glucose intolerance and adipose tissue inflammation. *Mediators of Inflammation*, *2022*, 7853482.

Magusto, J., Beaupère, C., Afonso, M. B., Auclair, M., Delaunay, J.-L., Soret, P.-A., Courtois, G., Aït-Slimane, T., Housset, C., Jéru, I., Fève, B., Ratziu, V., Rodrigues, C. M. P., & Gautheron, J. (2022). The necroptosis-inducing pseudokinase mixed lineage kinase domain-like regulates the adipogenic differentiation of pre-adipocytes. *iScience*, *25*(10), 105166.

Manning, B. D., & Cantley, L. C. (2007). AKT/PKB signaling: navigating downstream. *Cell*, *129*(7), 1261–1274.

Mann, J. P., & Savage, D. B. (2019). What lipodystrophies teach us about the metabolic syndrome. *The Journal of Clinical Investigation*, *129*(10), 4009–4021.

Mantovani, A., Zusi, C., Csermely, A., Salvagno, G. L., Colecchia, A., Lippi, G., Maffeis, C., & Targher, G. (2022). Association between lower plasma adiponectin levels and higher liver stiffness in type 2 diabetic individuals with nonalcoholic fatty liver disease: an observational cross-sectional study. *Hormones*, *21*(3), 477–486.

Mardinoglu, A., Heiker, J. T., Gärtner, D., Björnson, E., Schön, M. R., Flehmig, G., Klöting, N., Krohn, K., Fasshauer, M., Stumvoll, M., Nielsen, J., & Blüher, M. (2015). Extensive weight loss reveals distinct gene expression changes in human subcutaneous and visceral adipose tissue. *Scientific Reports*, *5*(1), 14841.

Marvyn, P. M., Bradley, R. M., Mardian, E. B., Marks, K. A., & Duncan, R. E. (2016). Data on oxygen consumption rate, respiratory exchange ratio, and movement in C57BL/6J female mice on the third day of consuming a high-fat diet. *Data in Brief*, *7*, 472–475.

Matacchione, G., Perugini, J., Di Mercurio, E., Sabbatinelli, J., Prattichizzo, F., Senzacqua, M., Storci, G., Dani, C., Lezoche, G., Guerrieri, M., Giordano, A., Bonafè, M., & Olivieri,

F. (2022). Senescent macrophages in the human adipose tissue as a source of inflammaging. *GeroScience*, *44*(4), 1941–1960.

Matsuo, F. S., Cavalcanti de Araújo, P. H., Mota, R. F., Carvalho, A. J. R., Santos de Queiroz, M., Baldo de Almeida, B., Ferreira, K. C. de O. S., Metzner, R. J. M., Ferrari, G. D., Alberici, L. C., & Osako, M. K. (2020). RANKL induces beige adipocyte differentiation in preadipocytes. *American Journal of Physiology. Endocrinology and Metabolism*, *318*(6), E866–E877.

Matthews, V. B., Allen, T. L., Risis, S., Chan, M. H. S., Henstridge, D. C., Watson, N., Zaffino, L. A., Babb, J. R., Boon, J., Meikle, P. J., Jowett, J. B., Watt, M. J., Jansson, J.-O., Bruce, C. R., & Febbraio, M. A. (2010). Interleukin-6-deficient mice develop hepatic inflammation and systemic insulin resistance. *Diabetologia*, *53*(11), 2431–2441.

McLaughlin, T., Lamendola, C., Liu, A., & Abbasi, F. (2011). Preferential fat deposition in subcutaneous versus visceral depots is associated with insulin sensitivity. *The Journal of Clinical Endocrinology and Metabolism*, *96*(11), E1756–E1760.

Mevissen, T. E. T., Hospenthal, M. K., Geurink, P. P., Elliott, P. R., Akutsu, M., Arnaudo, N., Ekkebus, R., Kulathu, Y., Wauer, T., El Oualid, F., Freund, S. M. V., Ovaa, H., & Komander, D. (2013). OTU deubiquitinases reveal mechanisms of linkage specificity and enable ubiquitin chain restriction analysis. *Cell*, *154*(1), 169–184.

Micheau, O., & Tschopp, J. (2003). Induction of TNF receptor I-mediated apoptosis via two sequential signaling complexes. *Cell*, *114*(2), 181–190.

Miller, N. E., Michel, C. C., Nanjee, M. N., Olszewski, W. L., Miller, I. P., Hazell, M., Olivecrona, G., Sutton, P., Humphreys, S. M., & Frayn, K. N. (2011). Secretion of adipokines by human adipose tissue in vivo: partitioning between capillary and lymphatic transport. *American Journal of Physiology. Endocrinology and Metabolism*, *301*(4), E659–E667.

Mittal, B. (2019). Subcutaneous adipose tissue & visceral adipose tissue. *The Indian Journal of Medical Research*, *149*(5), 571–573.

Miyata, T., Wu, X., Fan, X., Huang, E., Sanz-Garcia, C., Ross, C. K. C.-D., Roychowdhury, S., Bellar, A., McMullen, M. R., Dasarathy, J., Allende, D. S., Caballeria, J., Sancho-Bru, P., McClain, C. J., Mitchell, M., McCullough, A. J., Radaeva, S., Barton, B., Szabo, G., … Nagy, L. E. (2021). Differential role of MLKL in alcohol-associated and non-alcohol-associated fatty liver diseases in mice and humans. *JCI Insight*, *6*(4). https://doi.org/10.1172/jci.insight.140180

Moller, D. E. (2000). Potential Role of TNF-α in the Pathogenesis of Insulin Resistance and Type 2 Diabetes. *Trends in Endocrinology and Metabolism: TEM*, *11*(6), 212–217.

Möller, M., Wasel, J., Schmetzer, J., Weiß, U., Meissner, M., Schiffmann, S., Weigert, A., Möser, C. V., & Niederberger, E. (2020). The Specific IKKε/TBK1 Inhibitor Amlexanox Suppresses Human Melanoma by the Inhibition of Autophagy, NF-κB and MAP Kinase Pathways. *International Journal of Molecular Sciences*, *21*(13). https://doi.org/10.3390/ijms21134721

Monteiro, C. A., Moubarac, J.-C., Cannon, G., Ng, S. W., & Popkin, B. (2013). Ultra-processed products are becoming dominant in the global food system: Ultra-processed products: global dominance. *Obesity Reviews: An Official Journal of the International Association for the Study of Obesity*, *14 Suppl 2*(S2), 21–28.

Moreno-Navarrete, J. M., & Fernandez-Real, J. M. (2019). The gut microbiota modulates both browning of white adipose tissue and the activity of brown adipose tissue. *Reviews in Endocrine & Metabolic Disorders*, *20*(4), 387–397.

Morrison, M. C., Mulder, P., Salic, K., Verheij, J., Liang, W., van Duyvenvoorde, W., Menke, A., Kooistra, T., Kleemann, R., & Wielinga, P. Y. (2016). Intervention with a caspase-1 inhibitor reduces obesity-associated hyperinsulinemia, non-alcoholic steatohepatitis and hepatic fibrosis in LDLR-/-.Leiden mice. *International Journal of Obesity* , *40*(9), 1416–1423.

Mowers, J., Uhm, M., Reilly, S. M., Simon, J., Leto, D., Chiang, S.-H., Chang, L., & Saltiel, A. R. (2013). Inflammation produces catecholamine resistance in obesity via activation of PDE3B by the protein kinases IKKε and TBK1. *eLife*, *2*, e01119.

Mridha, A. R., Wree, A., Robertson, A. A. B., Yeh, M. M., Johnson, C. D., Van Rooyen, D. M., Haczeyni, F., Teoh, N. C.-H., Savard, C., Ioannou, G. N., Masters, S. L., Schroder, K., Cooper, M. A., Feldstein, A. E., & Farrell, G. C. (2017). NLRP3 inflammasome blockade reduces liver inflammation and fibrosis in experimental NASH in mice. *Journal of Hepatology*, *66*(5), 1037–1046.

Murano, I., Barbatelli, G., Parisani, V., Latini, C., Muzzonigro, G., Castellucci, M., & Cinti, S. (2008). Dead adipocytes, detected as crown-like structures, are prevalent in visceral fat depots of genetically obese mice. *Journal of Lipid Research*, *49*(7), 1562–1568.

Murano, I., Rutkowski, J. M., Wang, Q. A., Cho, Y.-R., Scherer, P. E., & Cinti, S. (2013). Time course of histomorphological changes in adipose tissue upon acute lipoatrophy. *Nutrition, Metabolism, and Cardiovascular Diseases: NMCD*, *23*(8), 723–731.

Murphy, J. M., Lucet, I. S., Hildebrand, J. M., Tanzer, M. C., Young, S. N., Sharma, P., Lessene, G., Alexander, W. S., Babon, J. J., Silke, J., & Czabotar, P. E. (2014). Insights into the evolution of divergent nucleotide-binding mechanisms among pseudokinases revealed by crystal structures of human and mouse MLKL. *The Biochemical Journal*, *457*(3), 369–377.

Musone, S. L., Taylor, K. E., Lu, T. T., Nititham, J., Ferreira, R. C., Ortmann, W., Shifrin, N., Petri, M. A., Kamboh, M. I., Manzi, S., Seldin, M. F., Gregersen, P. K., Behrens, T. W., Ma, A., Kwok, P.-Y., & Criswell, L. A. (2008). Multiple polymorphisms in the TNFAIP3 region are independently associated with systemic lupus erythematosus. *Nature Genetics*, *40*(9), 1062–1064.

Nabavi, M., Shahrooei, M., Rokni-Zadeh, H., Vrancken, J., Changi-Ashtiani, M., Darabi, K., Manian, M., Seif, F., Meyts, I., Voet, A., Moens, L., & Bossuyt, X. (2019). Auto-inflammation in a patient with a novel homozygous OTULIN mutation. *Journal of Clinical Immunology*, *39*(2), 138–141.

Narazaki, M., Tanaka, T., & Kishimoto, T. (2017). The role and therapeutic targeting of IL-6 in rheumatoid arthritis. *Expert Review of Clinical Immunology*, *13*(6), 535–551.

Nati, M., Chung, K.-J., & Chavakis, T. (2022). The role of innate immune cells in nonalcoholic fatty liver disease. *Journal of Innate Immunity*, *14*(1), 31–41.

Nedergaard, J., Wang, Y., & Cannon, B. (2019). Cell proliferation and apoptosis inhibition: essential processes for recruitment of the full thermogenic capacity of brown adipose tissue. *Biochimica et Biophysica Acta, Molecular and Cell Biology of Lipids*, *1864*(1), 51–58.

Newton, K., Strasser, A., Kayagaki, N., & Dixit, V. M. (2024). Cell death. *Cell*, *187*(2), 235–256.

Nguyen, H. P., Yi, D., Lin, F., Viscarra, J. A., Tabuchi, C., Ngo, K., Shin, G., Lee, A. Y.-F., Wang, Y., & Sul, H. S. (2020). Aifm2, a NADH oxidase, supports robust glycolysis and is required for cold- and diet-induced thermogenesis. *Molecular Cell*, *77*(3), 600–617.e4.

Nguyen, H. P., Yi, D., & Sul, H. S. (2020). Adipose tissue development and metabolic regulation. In *Lipid Signaling and Metabolism* (pp. 521–534). Elsevier.

Nguyen, K. D., Qiu, Y., Cui, X., Goh, Y. P. S., Mwangi, J., David, T., Mukundan, L., Brombacher, F., Locksley, R. M., & Chawla, A. (2011). Alternatively activated macrophages produce catecholamines to sustain adaptive thermogenesis. *Nature*, *480*(7375), 104–108.

Nilsson, J., Schoser, B., Laforet, P., Kalev, O., Lindberg, C., Romero, N. B., Dávila López, M., Akman, H. O., Wahbi, K., Iglseder, S., Eggers, C., Engel, A. G., Dimauro, S., & Oldfors, A. (2013). Polyglucosan body myopathy caused by defective ubiquitin ligase RBCK1. *Annals of Neurology*, *74*(6), 914–919.

Nitschke, S., Sullivan, M. A., Mitra, S., Marchioni, C. R., Lee, J. P. Y., Smith, B. H., Ahonen, S., Wu, J., Chown, E. E., Wang, P., Petković, S., Zhao, X., DiGiovanni, L. F., Perri, A. M., Israelian, L., Grossman, T. R., Kordasiewicz, H., Vilaplana, F., Iwai, K., … Minassian, B. A. (2022). Glycogen synthase downregulation rescues the amylopectinosis of murine RBCK1 deficiency. *Brain: A Journal of Neurology*, *145*(7), 2361–2377.

Niu, J., Shi, Y., Iwai, K., & Wu, Z.-H. (2011). LUBAC regulates NF-κB activation upon genotoxic stress by promoting linear ubiquitination of NEMO: NEMO linear ubiquitination upon genotoxic stress. *The EMBO Journal*, *30*(18), 3741–3753.

Noubiap, J. J., Nansseu, J. R., Lontchi-Yimagou, E., Nkeck, J. R., Nyaga, U. F., Ngouo, A. T., Tounouga, D. N., Tianyi, F. L., Foka, A. J., Ndoadoumgue, A. L., & Bigna, J. J. (2022). Global, regional, and country estimates of metabolic syndrome burden in children and adolescents in 2020: a systematic review and modelling analysis. *The Lancet. Child & Adolescent Health*, *6*(3), 158–170.

Obesity and overweight. (n.d.). Retrieved May 1, 2024, from https://www.who.int/news-room/fact-sheets/detail/obesity-and-overweight

Oda, H., Beck, D. B., Kuehn, H. S., Sampaio Moura, N., Hoffmann, P., Ibarra, M., Stoddard, J., Tsai, W. L., Gutierrez-Cruz, G., Gadina, M., Rosenzweig, S. D., Kastner, D. L., Notarangelo, L. D., & Aksentijevich, I. (2019). Second Case of HOIP Deficiency Expands Clinical Features and Defines Inflammatory Transcriptome Regulated by LUBAC. *Frontiers in Immunology*, *10*, 479.

Oda, H., Manthiram, K., Chavan, P. P., Nakabo, S., Kuehn, H. S., Beck, D. B., Chae, J. J., Nehrebecky, M., Ombrello, A. K., Romeo, T., Deuitch, N., Matthíasardóttir, B., Mullikin, J., Stoddard, J., Niemela, J., Anderton, H., Lawlor, K. E., Yoshitomi, H., Yang, D., … Kastner, D. L. (2022). Human LUBAC deficiency leads to autoinflammation and immunodeficiency by dysregulation in TNF-mediated cell death. In *medRxiv* (p. 2022.11.09.22281431). https://doi.org/10.1101/2022.11.09.22281431

Oda, H., Manthiram, K., Chavan, P. P., Rieser, E., Veli, Ö., Kaya, Ö., Rauch, C., Nakabo, S., Kuehn, H. S., Swart, M., Wang, Y., Çelik, N. I., Molitor, A., Ziaee, V., Movahedi, N., Shahrooei, M., Parvaneh, N., Alipour-Olyei, N., Carapito, R., … Kastner, D. L. (2024). Biallelic human SHARPIN loss of function induces autoinflammation and immunodeficiency. *Nature Immunology*, *25*(5), 764–777.

Oeckinghaus, A., & Ghosh, S. (2009). The NF-kappaB family of transcription factors and its regulation. *Cold Spring Harbor Perspectives in Biology*, *1*(4), a000034.

Ohene-Marfo, P., Nguyen, H. V. M., Mohammed, S., Thadathil, N., Tran, A., Nicklas, E. H., Wang, D., Selvarani, R., Farriester, J. W., Varshney, R., Kinter, M., Richardson, A., Rudolph, M. C., & Deepa, S. S. (2024). Non-Necroptotic Roles of MLKL in Diet-Induced Obesity, Liver Pathology, and Insulin Sensitivity: Insights from a High-Fat, High-Fructose, High-Cholesterol Diet Mouse Model. *International Journal of Molecular Sciences*, *25*(5). https://doi.org/10.3390/ijms25052813

Okamura, K., Kitamura, A., Sasaki, Y., Chung, D. H., Kagami, S., Iwai, K., & Yasutomo, K. (2016). Survival of mature T cells depends on signaling through HOIP. *Scientific Reports*, *6*, 36135.

Okunogbe, A., Nugent, R., Spencer, G., Powis, J., Ralston, J., & Wilding, J. (2022). Economic impacts of overweight and obesity: current and future estimates for 161 countries. *BMJ Global Health*, *7*(9). https://doi.org/10.1136/bmjgh-2022-009773

Oliveira, J., Freitas, P., Lau, E., & Carvalho, D. (2016). Barraquer–Simons syndrome: a rare form of acquired lipodystrophy. *BMC Research Notes*, *9*, 175.

Ordelheide, A.-M., Gommer, N., Böhm, A., Hermann, C., Thielker, I., Machicao, F., Fritsche, A., Stefan, N., Häring, H.-U., & Staiger, H. (2016). Granulocyte colony-stimulating factor (G-CSF): A saturated fatty acid-induced myokine with insulin-desensitizing properties in humans. *Molecular Metabolism*, *5*(4), 305.

Osborn, O., Brownell, S. E., Sanchez-Alavez, M., Salomon, D., Gram, H., & Bartfai, T.

(2008). Treatment with an Interleukin 1 beta antibody improves glycemic control in diet-induced obesity. *Cytokine*, *44*(1), 141–148.

Özbalci, C., Sachsenheimer, T., & Brügger, B. (2013). Quantitative analysis of cellular lipids by nano-electrospray ionization mass spectrometry. *Methods in Molecular Biology* , *1033*, 3–20.

Pajvani, U. B., Trujillo, M. E., Combs, T. P., Iyengar, P., Jelicks, L., Roth, K. A., Kitsis, R. N., & Scherer, P. E. (2005). Fat apoptosis through targeted activation of caspase 8: a new mouse model of inducible and reversible lipoatrophy. *Nature Medicine*, *11*(7), 797–803.

Palmer, A. K., Xu, M., Zhu, Y., Pirtskhalava, T., Weivoda, M. M., Hachfeld, C. M., Prata, L. G., van Dijk, T. H., Verkade, E., Casaclang-Verzosa, G., Johnson, K. O., Cubro, H., Doornebal, E. J., Ogrodnik, M., Jurk, D., Jensen, M. D., Chini, E. N., Miller, J. D., Matveyenko, A., … Kirkland, J. L. (2019). Targeting senescent cells alleviates obesity-induced metabolic dysfunction. *Aging Cell*, *18*(3), e12950.

Pal, M., Febbraio, M. A., & Whitham, M. (2014). From cytokine to myokine: the emerging role of interleukin-6 in metabolic regulation. *Immunology and Cell Biology*, *92*(4), 331–339.

Park, E., Wong, V., Guan, X., Oprescu, A. I., & Giacca, A. (2007). Salicylate prevents hepatic insulin resistance caused by short-term elevation of free fatty acids in vivo. *The Journal of Endocrinology*, *195*(2), 323–331.

Park, S.-H., Liu, Z., Sui, Y., Helsley, R. N., Zhu, B., Powell, D. K., Kern, P. A., & Zhou, C. (2016). IKKβ Is Essential for Adipocyte Survival and Adaptive Adipose Remodeling in Obesity. *Diabetes*, *65*(6), 1616–1629.

Parsons, J. K., Sarma, A. V., McVary, K., & Wei, J. T. (2013). Obesity and benign prostatic hyperplasia: clinical connections, emerging etiological paradigms and future directions. *The Journal of Urology*, *189*(1 Suppl), S102–S106.

Patel, P., & Abate, N. (2013). Body fat distribution and insulin resistance. *Nutrients*, *5*(6), 2019–2027.

Patro, R., Duggal, G., Love, M. I., Irizarry, R. A., & Kingsford, C. (2017). Salmon provides fast and bias-aware quantification of transcript expression. *Nature Methods*, *14*(4), 417–419.

Patti, M.-E., & Corvera, S. (2010). The role of mitochondria in the pathogenesis of type 2 diabetes. *Endocrine Reviews*, *31*(3), 364–395.

Pękalski, J., Zuk, P. J., Kochańczyk, M., Junkin, M., Kellogg, R., Tay, S., & Lipniacki, T. (2013). Spontaneous NF-κB activation by autocrine TNFα signaling: a computational analysis. *PloS One*, *8*(11), e78887.

Pellegrinelli, V., Carobbio, S., & Vidal-Puig, A. (2016). Adipose tissue plasticity: how fat depots respond differently to pathophysiological cues. *Diabetologia*, *59*(6), 1075–1088.

Peltzer, N., & Annibaldi, A. (2022). Cell death-related ubiquitin modifications in inflammatory syndromes: From mice to men. *Biomedicines*, *10*(6), 1436.

Peltzer, N., Darding, M., Montinaro, A., Draber, P., Draberova, H., Kupka, S., Rieser, E., Fisher, A., Hutchinson, C., Taraborrelli, L., Hartwig, T., Lafont, E., Haas, T. L., Shimizu, Y., Böiers, C., Sarr, A., Rickard, J., Alvarez-Diaz, S., Ashworth, M. T., … Walczak, H. (2018). LUBAC is essential for embryogenesis by preventing cell death and enabling haematopoiesis. *Nature*, *557*(7703), 112–117.

Peltzer, N., Rieser, E., Taraborrelli, L., Draber, P., Darding, M., Pernaute, B., Shimizu, Y., Sarr, A., Draberova, H., Montinaro, A., Martinez-Barbera, J. P., Silke, J., Rodriguez, T. A., & Walczak, H. (2014). HOIP deficiency causes embryonic lethality by aberrant TNFR1-mediated endothelial cell death. *Cell Reports*, *9*(1), 153–165.

Peng, S., Zhang, X., Yu, L., Xu, Y., Zhou, Y., Qian, S., Cao, X., Ye, X., Yang, J., Jia, W., & Ye, J. (2022). NF-κB regulates brown adipocyte function through suppression of ANT2. *Acta Pharmaceutica Sinica. B*, *12*(3), 1186–1197.

Perrini, S., Laviola, L., Cignarelli, A., Melchiorre, M., De Stefano, F., Caccioppoli, C., Natalicchio, A., Orlando, M. R., Garruti, G., De Fazio, M., Catalano, G., Memeo, V., Giorgino, R., & Giorgino, F. (2008). Fat depot-related differences in gene expression, adiponectin secretion, and insulin action and signalling in human adipocytes differentiated in vitro from precursor stromal cells. *Diabetologia*, *51*(1), 155–164.

Peter, A., Stefan, N., Cegan, A., Walenta, M., Wagner, S., Königsrainer, A., Königsrainer, I., Machicao, F., Schick, F., Häring, H.-U., & Schleicher, E. (2011). Hepatic glucokinase expression is associated with lipogenesis and fatty liver in humans. *The Journal of Clinical Endocrinology and Metabolism*, *96*(7), E1126–E1130.

Petersen, S. L., Wang, L., Yalcin-Chin, A., Li, L., Peyton, M., Minna, J., Harran, P., & Wang, X. (2007). Autocrine TNFalpha signaling renders human cancer cells susceptible to Smac-mimetic-induced apoptosis. *Cancer Cell*, *12*(5), 445–456.

Peters, R. T., Liao, S. M., & Maniatis, T. (2000). IKKepsilon is part of a novel PMA-inducible IkappaB kinase complex. *Molecular Cell*, *5*(3), 513–522.

Petrova, T., Zhang, J., Nanda, S. K., Figueras-Vadillo, C., & Cohen, P. (2021). HOIL-1-catalysed, ester-linked ubiquitylation restricts IL-18 signaling in cytotoxic T cells but promotes TLR signalling in macrophages. *The FEBS Journal*, *288*(20), 5909–5924.

Phadke, R., Hedberg-Oldfors, C., Scalco, R. S., Lowe, D. M., Ashworth, M., Novelli, M., Vara, R., Merwick, A., Amer, H., Sofat, R., Sugarman, M., Jovanovic, A., Roberts, M., Nakou, V., King, A., Bodi, I., Jungbluth, H., Oldfors, A., & Murphy, E. (2020). RBCK1-related disease: A rare multisystem disorder with polyglucosan storage, auto-inflammation, recurrent infections, skeletal, and cardiac myopathy-Four additional patients and a review of the current literature. *Journal of Inherited Metabolic Disease*, *43*(5), 1002–1013.

Picard. (n.d.). Retrieved October 18, 2024, from https://broadinstitute.github.io/picard/

Pilkington, A.-C., Paz, H. A., & Wankhade, U. D. (2021). Beige adipose tissue identification and marker specificity-overview. *Frontiers in Endocrinology*, *12*, 599134.

Plenge, R. M., Cotsapas, C., Davies, L., Price, A. L., de Bakker, P. I. W., Maller, J., Pe'er, I., Burtt, N. P., Blumenstiel, B., DeFelice, M., Parkin, M., Barry, R., Winslow, W., Healy, C., Graham, R. R., Neale, B. M., Izmailova, E., Roubenoff, R., Parker, A. N., … Altshuler, D. (2007). Two independent alleles at 6q23 associated with risk of rheumatoid arthritis. *Nature Genetics*, *39*(12), 1477–1482.

Podolin, P. L., Callahan, J. F., Bolognese, B. J., Li, Y. H., Carlson, K., Davis, T. G., Mellor, G. W., Evans, C., & Roshak, A. K. (2005). Attenuation of murine collagen-induced arthritis by a novel, potent, selective small molecule inhibitor of IkappaB Kinase 2, TPCA-1 (2-[(aminocarbonyl)amino]-5-(4-fluorophenyl)-3-thiophenecarboxamide), occurs via reduction of proinflammatory cytokines and antigen-induced T cell Proliferation. *The Journal of Pharmacology and Experimental Therapeutics*, *312*(1). https://doi.org/10.1124/jpet.104.074484

Pomerantz, J. L., & Baltimore, D. (1999). NF-kappaB activation by a signaling complex containing TRAF2, TANK and TBK1, a novel IKK-related kinase. *The EMBO Journal*, *18*(23), 6694–6704.

Pou, K. M., Massaro, J. M., Hoffmann, U., Vasan, R. S., Maurovich-Horvat, P., Larson, M. G., Keaney, J. F., Jr, Meigs, J. B., Lipinska, I., Kathiresan, S., Murabito, J. M., O'Donnell, C. J., Benjamin, E. J., & Fox, C. S. (2007). Visceral and subcutaneous adipose tissue volumes are cross-sectionally related to markers of inflammation and oxidative stress: the Framingham Heart Study. *Circulation*, *116*(11), 1234–1241.

Priem, D., Devos, M., Druwé, S., Martens, A., Slowicka, K., Ting, A. T., Pasparakis, M., Declercq, W., Vandenabeele, P., van Loo, G., & Bertrand, M. J. M. (2019). A20 protects cells from TNF-induced apoptosis through linear ubiquitin-dependent and -independent mechanisms. *Cell Death & Disease*, *10*(10), 692.

Qiu, W., Hu, Y., Andersen, T. E., Jafari, A., Li, N., Chen, W., & Kassem, M. (2010). Tumor

necrosis factor receptor superfamily member 19 (TNFRSF19) regulates differentiation fate of human mesenchymal (stromal) stem cells through canonical Wnt signaling and C/EBP. *The Journal of Biological Chemistry*, *285*(19). https://doi.org/10.1074/jbc.M109.052001

Rabe, K., Lehrke, M., Parhofer, K. G., & Broedl, U. C. (2008). Adipokines and insulin resistance. *Molecular Medicine* , *14*(11-12), 741–751.

Rangel-Azevedo, C., Santana-Oliveira, D. A., Miranda, C. S., Martins, F. F., Mandarim-de-Lacerda, C. A., & Souza-Mello, V. (2022). Progressive brown adipocyte dysfunction: Whitening and impaired nonshivering thermogenesis as long-term obesity complications. *The Journal of Nutritional Biochemistry*, *105*, 109002.

Rao, R. R., Long, J. Z., White, J. P., Svensson, K. J., Lou, J., Lokurkar, I., Jedrychowski, M. P., Ruas, J. L., Wrann, C. D., Lo, J. C., Camera, D. M., Lachey, J., Gygi, S., Seehra, J., Hawley, J. A., & Spiegelman, B. M. (2014). Meteorin-like is a hormone that regulates immune-adipose interactions to increase beige fat thermogenesis. *Cell*, *157*(6), 1279–1291.

Rasheed, A., Robichaud, S., Nguyen, M.-A., Geoffrion, M., Wyatt, H., Cottee, M. L., Dennison, T., Pietrangelo, A., Lee, R., Lagace, T. A., Ouimet, M., & Rayner, K. J. (2020). Loss of MLKL (mixed lineage kinase domain-like protein) decreases necrotic core but increases macrophage lipid accumulation in atherosclerosis. *Arteriosclerosis, Thrombosis, and Vascular Biology*, *40*(5), 1155–1167.

Rask-Madsen, C., & Kahn, C. R. (2012). Tissue-specific insulin signaling, metabolic syndrome, and cardiovascular disease. *Arteriosclerosis, Thrombosis, and Vascular Biology*, *32*(9), 2052–2059.

Rauber, F., Campagnolo, P. D. B., Hoffman, D. J., & Vitolo, M. R. (2015). Consumption of ultra-processed food products and its effects on children's lipid profiles: a longitudinal study. *Nutrition, Metabolism, and Cardiovascular Diseases: NMCD*, *25*(1), 116–122.

Raudvere, U., Kolberg, L., Kuzmin, I., Arak, T., Adler, P., Peterson, H., & Vilo, J. (2019). g:Profiler: a web server for functional enrichment analysis and conversions of gene lists (2019 update). *Nucleic Acids Research*, *47*(W1), W191–W198.

Reddy, P., Lent-Schochet, D., Ramakrishnan, N., McLaughlin, M., & Jialal, I. (2019). Metabolic syndrome is an inflammatory disorder: A conspiracy between adipose tissue and phagocytes. *Clinica Chimica Acta; International Journal of Clinical Chemistry*, *496*, 35–44.

Redecke, V., Chaturvedi, V., Kuriakose, J., & Häcker, H. (2016). SHARPIN controls the development of regulatory T cells. *Immunology*, *148*(2), 216–226.

Reilly, S. M., Chiang, S.-H., Decker, S. J., Chang, L., Uhm, M., Larsen, M. J., Rubin, J. R., Mowers, J., White, N. M., Hochberg, I., Downes, M., Yu, R. T., Liddle, C., Evans, R. M., Oh, D., Li, P., Olefsky, J. M., & Saltiel, A. R. (2013). An inhibitor of the protein kinases TBK1 and IKK-ε improves obesity-related metabolic dysfunctions in mice. *Nature Medicine*, *19*(3), 313–321.

Rena, G., & Sakamoto, K. (2014). Salicylic acid: old and new implications for the treatment of type 2 diabetes? *Diabetology International*, *5*(4), 212–218.

Reyes-Turcu, F. E., Ventii, K. H., & Wilkinson, K. D. (2009). Regulation and cellular roles of ubiquitin-specific deubiquitinating enzymes. *Annual Review of Biochemistry*, *78*, 363–397.

Rickard, J. A., Anderton, H., Etemadi, N., Nachbur, U., Darding, M., Peltzer, N., Lalaoui, N., Lawlor, K. E., Vanyai, H., Hall, C., Bankovacki, A., Gangoda, L., Wong, W. W.-L., Corbin, J., Huang, C., Mocarski, E. S., Murphy, J. M., Alexander, W. S., Voss, A. K., … Silke, J. (2014). TNFR1-dependent cell death drives inflammation in Sharpin-deficient mice. *eLife*, *3*. https://doi.org/10.7554/eLife.03464

Rittinger, K., & Ikeda, F. (2017). Linear ubiquitin chains: enzymes, mechanisms and biology.

Open Biology, *7*(4). https://doi.org/10.1098/rsob.170026

Rivkin, E., Almeida, S. M., Ceccarelli, D. F., Juang, Y.-C., MacLean, T. A., Srikumar, T., Huang, H., Dunham, W. H., Fukumura, R., Xie, G., Gondo, Y., Raught, B., Gingras, A.-C., Sicheri, F., & Cordes, S. P. (2013). The linear ubiquitin-specific deubiquitinase gumby regulates angiogenesis. *Nature*, *498*(7454), 318–324.

rnaseq: Introduction. (n.d.). Retrieved October 18, 2024, from https://nf-co.re/rnaseq

Rock, K. L., & Kono, H. (2008). The inflammatory response to cell death. *Annual Review of Pathology*, *3*(1), 99–126.

Rodgers, M. A., Bowman, J. W., Fujita, H., Orazio, N., Shi, M., Liang, Q., Amatya, R., Kelly, T. J., Iwai, K., Ting, J., & Jung, J. U. (2014). The linear ubiquitin assembly complex (LUBAC) is essential for NLRP3 inflammasome activation. *The Journal of Experimental Medicine*, *211*(7), 1333–1347.

Rodriguez Carvajal, A., Grishkovskaya, I., Gomez Diaz, C., Vogel, A., Sonn-Segev, A., Kushwah, M. S., Schodl, K., Deszcz, L., Orban-Nemeth, Z., Sakamoto, S., Mechtler, K., Kukura, P., Clausen, T., Haselbach, D., & Ikeda, F. (2021). The linear ubiquitin chain assembly complex (LUBAC) generates heterotypic ubiquitin chains. *eLife*, *10*. https://doi.org/10.7554/eLife.60660

Rogers, C., Erkes, D. A., Nardone, A., Aplin, A. E., Fernandes-Alnemri, T., & Alnemri, E. S. (2019). Gasdermin pores permeabilize mitochondria to augment caspase-3 activation during apoptosis and inflammasome activation. *Nature Communications*, *10*(1), 1689.

Rogers, C., Fernandes-Alnemri, T., Mayes, L., Alnemri, D., Cingolani, G., & Alnemri, E. S. (2017). Cleavage of DFNA5 by caspase-3 during apoptosis mediates progression to secondary necrotic/pyroptotic cell death. *Nature Communications*, *8*, 14128.

Roh, H. C., Tsai, L. T. Y., Shao, M., Tenen, D., Shen, Y., Kumari, M., Lyubetskaya, A., Jacobs, C., Dawes, B., Gupta, R. K., & Rosen, E. D. (2018). Warming Induces Significant Reprogramming of Beige, but Not Brown, Adipocyte Cellular Identity. *Cell Metabolism*, *27*(5), 1121–1137.e5.

Romanatto, T., Roman, E. A., Arruda, A. P., Denis, R. G., Solon, C., Milanski, M., Moraes, J. C., Bonfleur, M. L., Degasperi, G. R., Picardi, P. K., Hirabara, S., Boschero, A. C., Curi, R., & Velloso, L. A. (2009). Deletion of tumor necrosis factor-alpha receptor 1 (TNFR1) protects against diet-induced obesity by means of increased thermogenesis. *The Journal of Biological Chemistry*, *284*(52), 36213–36222.

Rönn, T., & Ling, C. (2015). DNA methylation as a diagnostic and therapeutic target in the battle against Type 2 diabetes. *Epigenomics*, *7*(3), 451–460.

Ronquillo, M. D., Mellnyk, A., Cárdenas-Rodríguez, N., Martínez, E., Comoto, D. A., Carmona-Aparicio, L., Herrera, N. E., Lara, E., Pereyra, A., & Floriano-Sánchez, E. (2019). Different gene expression profiles in subcutaneous & visceral adipose tissues from Mexican patients with obesity. *The Indian Journal of Medical Research*, *149*(5), 616–626.

Rosell, M., Kaforou, M., Frontini, A., Okolo, A., Chan, Y.-W., Nikolopoulou, E., Millership, S., Fenech, M. E., MacIntyre, D., Turner, J. O., Moore, J. D., Blackburn, E., Gullick, W. J., Cinti, S., Montana, G., Parker, M. G., & Christian, M. (2014). Brown and white adipose tissues: intrinsic differences in gene expression and response to cold exposure in mice. *American Journal of Physiology. Endocrinology and Metabolism*, *306*(8), E945–E964.

Ros Pérez, M., & Medina-Gómez, G. (2011). [Obesity, adipogenesis and insulin resistance]. *Endocrinologia y nutricion: organo de la Sociedad Espanola de Endocrinologia y Nutricion*, *58*(7), 360–369.

Röszer, T. (2021). Adipose Tissue Immunometabolism and Apoptotic Cell Clearance. *Cells* , *10*(9). https://doi.org/10.3390/cells10092288

Rothe, J., Lesslauer, W., Lötscher, H., Lang, Y., Koebel, P., Köntgen, F., Althage, A., Zinkernagel, R., Steinmetz, M., & Bluethmann, H. (1993). Mice lacking the tumour

necrosis factor receptor 1 are resistant to TNF-mediated toxicity but highly susceptible to infection by Listeria monocytogenes. *Nature*, *364*(6440), 798–802.

Roychowdhury, S., McMullen, M. R., Pisano, S. G., Liu, X., & Nagy, L. E. (2013). Absence of receptor interacting protein kinase 3 prevents ethanol-induced liver injury. *Hepatology* , *57*(5), 1773–1783.

Ruiz, E. J., Diefenbacher, M. E., Nelson, J. K., Sancho, R., Pucci, F., Chakraborty, A., Moreno, P., Annibaldi, A., Liccardi, G., Encheva, V., Mitter, R., Rosenfeldt, M., Snijders, A. P., Meier, P., Calzado, M. A., & Behrens, A. (2019). LUBAC determines chemotherapy resistance in squamous cell lung cancer. *The Journal of Experimental Medicine*, *216*(2), 450–465.

Saeed, W. K., Jun, D. W., Jang, K., Oh, J. H., Chae, Y. J., Lee, J. S., Koh, D. H., & Kang, H. T. (2019). Decrease in fat de novo synthesis and chemokine ligand expression in non-alcoholic fatty liver disease caused by inhibition of mixed lineage kinase domain-like pseudokinase. *Journal of Gastroenterology and Hepatology*, *34*(12), 2206–2218.

Sakamoto, Y., Sasaki, K., Omatsu, M., Hamada, K., Nakanishi, Y., Itatani, Y., Kawada, K., Obama, K., Seno, H., & Iwai, K. (2023). Differential involvement of LUBAC-mediated linear ubiquitination in intestinal epithelial cells and macrophages during intestinal inflammation. *The Journal of Pathology*, *259*(3), 304–317.

Salles, J., Tardif, N., Landrier, J.-F., Mothe-Satney, I., Guillet, C., Boue-Vaysse, C., Combaret, L., Giraudet, C., Patrac, V., Bertrand-Michel, J., Denis, P., Chardigny, J.-M., Boirie, Y., & Walrand, S. (2012). TNFα gene knockout differentially affects lipid deposition in liver and skeletal muscle of high-fat-diet mice. *The Journal of Nutritional Biochemistry*, *23*(12), 1685–1693.

Saltiel, A. R., & Pessin, J. E. (2002). Insulin signaling pathways in time and space. *Trends in Cell Biology*, *12*(2), 65–71.

Samuel, V. T., & Shulman, G. I. (2012). Mechanisms for insulin resistance: common threads and missing links. *Cell*, *148*(5), 852–871.

Sarbassov, D. D., Guertin, D. A., Ali, S. M., & Sabatini, D. M. (2005). Phosphorylation and regulation of Akt/PKB by the rictor-mTOR complex. *Science (New York, N.Y.)*, *307*(5712), 1098–1101.

Sarwar, R., Pierce, N., & Koppe, S. (2018). Obesity and nonalcoholic fatty liver disease: current perspectives. *Diabetes, Metabolic Syndrome and Obesity: Targets and Therapy*, *11*, 533–542.

Sasaki, K., & Iwai, K. (2023). Role of linear ubiquitination in inflammatory responses and tissue homeostasis. *International Immunology*, *35*(1), 19–25.

Sasaki, Y., Sano, S., Nakahara, M., Murata, S., Kometani, K., Aiba, Y., Sakamoto, S., Watanabe, Y., Tanaka, K., Kurosaki, T., & Iwai, K. (2013). Defective immune responses in mice lacking LUBAC-mediated linear ubiquitination in B cells. *The EMBO Journal*, *32*(18), 2463–2476.

Sauter, N. S., Schulthess, F. T., Galasso, R., Castellani, L. W., & Maedler, K. (2008). The antiinflammatory cytokine interleukin-1 receptor antagonist protects from high-fat diet-induced hyperglycemia. *Endocrinology*, *149*(5), 2208–2218.

Schlein, C., Fischer, A. W., Sass, F., Worthmann, A., Tödter, K., Jaeckstein, M. Y., Behrens, J., Lynes, M. D., Kiebish, M. A., Narain, N. R., Bussberg, V., Darkwah, A., Jespersen, N. Z., Nielsen, S., Scheele, C., Schweizer, M., Braren, I., Bartelt, A., Tseng, Y.-H., … Scheja, L. (2021). Endogenous Fatty Acid Synthesis Drives Brown Adipose Tissue Involution. *Cell Reports*, *34*(2), 108624.

Schulman, B. A., & Harper, J. W. (2009). Ubiquitin-like protein activation by E1 enzymes: the apex for downstream signalling pathways. *Nature Reviews. Molecular Cell Biology*, *10*(5), 319–331.

Schwarzer, R., Jiao, H., Wachsmuth, L., Tresch, A., & Pasparakis, M. (2020). FADD and caspase-8 regulate gut homeostasis and inflammation by controlling MLKL- and GSDMD-mediated death of intestinal epithelial cells. *Immunity*, *52*(6), 978–993.e6.

Seale, P., Bjork, B., Yang, W., Kajimura, S., Chin, S., Kuang, S., Scimè, A., Devarakonda, S., Conroe, H. M., Erdjument-Bromage, H., Tempst, P., Rudnicki, M. A., Beier, D. R., & Spiegelman, B. M. (2008). PRDM16 controls a brown fat/skeletal muscle switch. *Nature*, *454*(7207), 961–967.

Seriolo, B., Ferrone, C., & Cutolo, M. (2008). Longterm anti-tumor necrosis factor-alpha treatment in patients with refractory rheumatoid arthritis: relationship between insulin resistance and disease activity. *The Journal of Rheumatology*, *35*(2), 355–357.

Sethi, J. K., & Hotamisligil, G. S. (2021). Metabolic Messengers: tumour necrosis factor. *Nature Metabolism*, *3*(10), 1302–1312.

Seymour, R. E., Hasham, M. G., Cox, G. A., Shultz, L. D., Hogenesch, H., Roopenian, D. C., & Sundberg, J. P. (2007). Spontaneous mutations in the mouse Sharpin gene result in multiorgan inflammation, immune system dysregulation and dermatitis. *Genes and Immunity*, *8*(5), 416–421.

Sharma, M., Boytard, L., Hadi, T., Koelwyn, G., Simon, R., Ouimet, M., Seifert, L., Spiro, W., Yan, B., Hutchison, S., Fisher, E. A., Ramasamy, R., Ramkhelawon, B., & Moore, K. J. (2020). Enhanced glycolysis and HIF-1α activation in adipose tissue macrophages sustains local and systemic interleukin-1β production in obesity. *Scientific Reports*, *10*(1), 5555.

Sharma, N. K., Sajuthi, S. P., Chou, J. W., Calles-Escandon, J., Demons, J., Rogers, S., Ma, L., Palmer, N. D., McWilliams, D. R., Beal, J., Comeau, M. E., Cherry, K., Hawkins, G. A., Menon, L., Kouba, E., Davis, D., Burris, M., Byerly, S. J., Easter, L., … Das, S. K. (2016). Tissue-Specific and Genetic Regulation of Insulin Sensitivity-Associated Transcripts in African Americans. *The Journal of Clinical Endocrinology and Metabolism*, *101*(4), 1455–1468.

Sheng, L., Zhou, Y., Chen, Z., Ren, D., Cho, K. W., Jiang, L., Shen, H., Sasaki, Y., & Rui, L. (2012). NF-κB–inducing kinase (NIK) promotes hyperglycemia and glucose intolerance in obesity by augmenting glucagon action. *Nature Medicine*, *18*(6), 943–949.

Shimada, T., Kawai, T., Takeda, K., Matsumoto, M., Inoue, J., Tatsumi, Y., Kanamaru, A., & Akira, S. (1999). IKK-i, a novel lipopolysaccharide-inducible kinase that is related to IkappaB kinases. *International Immunology*, *11*(8), 1357–1362.

Shimizu, S., Fujita, H., Sasaki, Y., Tsuruyama, T., Fukuda, K., & Iwai, K. (2016). Differential Involvement of the Npl4 Zinc Finger Domains of SHARPIN and HOIL-1L in Linear Ubiquitin Chain Assembly Complex-Mediated Cell Death Protection. *Molecular and Cellular Biology*, *36*(10), 1569–1583.

Shimizu, Y., Peltzer, N., Sevko, A., Lafont, E., Sarr, A., Draberova, H., & Walczak, H. (2017). The Linear ubiquitin chain assembly complex acts as a liver tumor suppressor and inhibits hepatocyte apoptosis and hepatitis. *Hepatology* , *65*(6), 1963–1978.

Shin, C. H., & Choi, D.-S. (2019). Essential Roles for the Non-Canonical IκB Kinases in Linking Inflammation to Cancer, Obesity, and Diabetes. *Cells* , *8*(2). https://doi.org/10.3390/cells8020178

Shoelson, S. E., Lee, J., & Goldfine, A. B. (2006). Inflammation and insulin resistance. *The Journal of Clinical Investigation*, *116*(7), 1793–1801.

Shunkina Skuratovskaia, D., Komar, A., Vulf, M., Quang, H. V., Shunkin, E., Kirienkova, E., Dakchnevich, A., Malkov, D., Zatolokin, P., & Litvinova, L. (2021). Tumor Necrosis Receptor Superfamily Interact with Fusion and Fission of Mitochondria of Adipose Tissue in Obese Patients without Type 2 Diabetes. *Biomedicines*, *9*(9). https://doi.org/10.3390/biomedicines9091260

Sidossis, L., & Kajimura, S. (2015). Brown and beige fat in humans: thermogenic adipocytes

that control energy and glucose homeostasis. *The Journal of Clinical Investigation*, *125*(2), 478–486.

Silva, G. da N., & Amato, A. A. (2022). Thermogenic adipose tissue aging: Mechanisms and implications. *Frontiers in Cell and Developmental Biology*, *10*, 955612.

Silva, M. T., do Vale, A., & dos Santos, N. M. N. (2008). Secondary necrosis in multicellular animals: an outcome of apoptosis with pathogenic implications. *Apoptosis: An International Journal on Programmed Cell Death*, *13*(4), 463–482.

Sisto, M., Lisi, S., Lofrumento, D. D., Ingravallo, G., Maiorano, E., & D'Amore, M. (2011). A failure of TNFAIP3 negative regulation maintains sustained NF-κB activation in Sjögren's syndrome. *Histochemistry and Cell Biology*, *135*(6), 615–625.

Smith, U., & Kahn, B. B. (2016). Adipose tissue regulates insulin sensitivity: role of adipogenesis, de novo lipogenesis and novel lipids. *Journal of Internal Medicine*, *280*(5), 465–475.

Song, K., & Li, S. (2021). The Role of Ubiquitination in NF-κB Signaling during Virus Infection. *Viruses*, *13*(2). https://doi.org/10.3390/v13020145

Song, Y., Milon, B., Ott, S., Zhao, X., Sadzewicz, L., Shetty, A., Boger, E. T., Tallon, L. J., Morell, R. J., Mahurkar, A., & Hertzano, R. (2018). A comparative analysis of library prep approaches for sequencing low input translatome samples. *BMC Genomics*, *19*(1), 696.

Song, Z., Wei, W., Xiao, W., Al-Saleem, E. D., Nejati, R., Chen, L., Yin, J., Fabrizio, J., Petrus, M. N., Waldmann, T. A., & Yang, Y. (2020). Essential role of the linear ubiquitin chain assembly complex and TAK1 kinase in A20 mutant Hodgkin lymphoma. *Proceedings of the National Academy of Sciences of the United States of America*, *117*(46), 28980–28991.

Spoto, B., Di Betta, E., Mattace-Raso, F., Sijbrands, E., Vilardi, A., Parlongo, R. M., Pizzini, P., Pisano, A., Vermi, W., Testa, A., Cutrupi, S., D'Arrigo, G., Lonardi, S., Tripepi, G., Cancarini, G., & Zoccali, C. (2014). Pro- and anti-inflammatory cytokine gene expression in subcutaneous and visceral fat in severe obesity. *Nutrition, Metabolism, and Cardiovascular Diseases: NMCD*, *24*(10), 1137–1143.

Stangl, A., Elliott, P. R., Pinto-Fernandez, A., Bonham, S., Harrison, L., Schaub, A., Kutzner, K., Keusekotten, K., Pfluger, P. T., El Oualid, F., Kessler, B. M., Komander, D., & Krappmann, D. (2019). Regulation of the endosomal SNX27-retromer by OTULIN. *Nature Communications*, *10*(1), 4320.

Stefan, N., Schick, F., & Häring, H.-U. (2017). Causes, Characteristics, and Consequences of Metabolically Unhealthy Normal Weight in Humans. *Cell Metabolism*, *26*(2), 292–300.

Stenkula, K. G., & Erlanson-Albertsson, C. (2018). Adipose cell size: importance in health and disease. *American Journal of Physiology. Regulatory, Integrative and Comparative Physiology*, *315*(2), R284–R295.

Stewart, K., Tang, Y. C., Shafer, M. E. R., Graham-Paquin, A.-L., & Bouchard, M. (2017). Modulation of apoptotic response by LAR family phosphatases–cIAP1 signaling during urinary tract morphogenesis. *Proceedings of the National Academy of Sciences of the United States of America*, *114*(43), E9016.

Stieglitz, B., Morris-Davies, A. C., Koliopoulos, M. G., Christodoulou, E., & Rittinger, K. (2012). LUBAC synthesizes linear ubiquitin chains via a thioester intermediate. *EMBO Reports*, *13*(9), 840–846.

Stieglitz, B., Rana, R. R., Koliopoulos, M. G., Morris-Davies, A. C., Schaeffer, V., Christodoulou, E., Howell, S., Brown, N. R., Dikic, I., & Rittinger, K. (2013). Structural basis for ligase-specific conjugation of linear ubiquitin chains by HOIP. *Nature*, *503*(7476), 422–426.

Stienstra, R., Joosten, L. A. B., Koenen, T., van Tits, B., van Diepen, J. A., van den Berg, S. A. A., Rensen, P. C. N., Voshol, P. J., Fantuzzi, G., Hijmans, A., Kersten, S., Müller, M., van den Berg, W. B., van Rooijen, N., Wabitsch, M., Kullberg, B.-J., van der Meer, J. W.

M., Kanneganti, T., Tack, C. J., & Netea, M. G. (2010). The inflammasome-mediated caspase-1 activation controls adipocyte differentiation and insulin sensitivity. *Cell Metabolism*, *12*(6), 593–605.

Strissel, K. J., Stancheva, Z., Miyoshi, H., Perfield, J. W., 2nd, DeFuria, J., Jick, Z., Greenberg, A. S., & Obin, M. S. (2007). Adipocyte death, adipose tissue remodeling, and obesity complications. *Diabetes*, *56*(12), 2910–2918.

Stutz, M. D., Allison, C. C., Ojaimi, S., Preston, S. P., Doerflinger, M., Arandjelovic, P., Whitehead, L., Bader, S. M., Batey, D., Asselin-Labat, M.-L., Herold, M. J., Strasser, A., West, N. P., & Pellegrini, M. (2021). Macrophage and neutrophil death programs differentially confer resistance to tuberculosis. *Immunity*, *54*(8), 1758–1771.e7.

Sun, L., Wang, H., Wang, Z., He, S., Chen, S., Liao, D., Wang, L., Yan, J., Liu, W., Lei, X., & Wang, X. (2012). Mixed lineage kinase domain-like protein mediates necrosis signaling downstream of RIP3 kinase. *Cell*, *148*(1-2), 213–227.

Swarup, S., Goyal, A., Grigorova, Y., & Zeltser, R. (2022). *Metabolic Syndrome*. StatPearls Publishing.

Swatek, K. N., & Komander, D. (2016). Ubiquitin modifications. *Cell Research*, *26*(4), 399–422.

Taabazuing, C. Y., Okondo, M. C., & Bachovchin, D. A. (2017). Pyroptosis and Apoptosis Pathways Engage in Bidirectional Crosstalk in Monocytes and Macrophages. *Cell Chemical Biology*, *24*(4), 507–514.e4.

Tack, C. J., Stienstra, R., Joosten, L. A. B., & Netea, M. G. (2012). Inflammation links excess fat to insulin resistance: the role of the interleukin-1 family. *Immunological Reviews*, *249*(1), 239–252.

Takeuchi, O., & Akira, S. (2010). Pattern recognition receptors and inflammation. *Cell*, *140*(6), 805–820.

Tang, G., Minemoto, Y., Dibling, B., Purcell, N. H., Li, Z., Karin, M., & Lin, A. (2001). Inhibition of JNK activation through NF-kappaB target genes. *Nature*, *414*(6861), 313–317.

Tang, T., Zhang, J., Yin, J., Staszkiewicz, J., Gawronska-Kozak, B., Jung, D. Y., Ko, H. J., Ong, H., Kim, J. K., Mynatt, R., Martin, R. J., Keenan, M., Gao, Z., & Ye, J. (2010). Uncoupling of inflammation and insulin resistance by NF-kappaB in transgenic mice through elevated energy expenditure. *The Journal of Biological Chemistry*, *285*(7), 4637–4644.

Tanzer, M. C., Frauenstein, A., Stafford, C. A., Phulphagar, K., Mann, M., & Meissner, F. (2020). Quantitative and dynamic catalogs of proteins released during apoptotic and necroptotic cell death. *Cell Reports*, *30*(4), 1260–1270.e5.

Taraborrelli, L., Peltzer, N., Montinaro, A., Kupka, S., Rieser, E., Hartwig, T., Sarr, A., Darding, M., Draber, P., Haas, T. L., Akarca, A., Marafioti, T., Pasparakis, M., Bertin, J., Gough, P. J., Bouillet, P., Strasser, A., Leverkus, M., Silke, J., & Walczak, H. (2018). LUBAC prevents lethal dermatitis by inhibiting cell death induced by TNF, TRAIL and CD95L. *Nature Communications*, *9*(1), 3910.

Targher, G., Byrne, C. D., & Tilg, H. (2024). MASLD: a systemic metabolic disorder with cardiovascular and malignant complications. *Gut*, *73*(4), 691–702.

Tatematsu, K., Yoshimoto, N., Okajima, T., Tanizawa, K., & Kuroda, S. 'ichi. (2008). Identification of ubiquitin ligase activity of RBCK1 and its inhibition by splice variant RBCK2 and protein kinase Cbeta. *The Journal of Biological Chemistry*, *283*(17), 11575–11585.

Tchernof, A., & Després, J.-P. (2013). Pathophysiology of human visceral obesity: an update. *Physiological Reviews*, *93*(1), 359–404.

Tchkonia, T., Thomou, T., Zhu, Y., Karagiannides, I., Pothoulakis, C., Jensen, M. D., & Kirkland, J. L. (2013). Mechanisms and metabolic implications of regional differences among fat depots. *Cell Metabolism*, *17*(5), 644–656.

Teh, C. E., Lalaoui, N., Jain, R., Policheni, A. N., Heinlein, M., Alvarez-Diaz, S., Sheridan, J. M., Rieser, E., Deuser, S., Darding, M., Koay, H.-F., Hu, Y., Kupresanin, F., O'Reilly, L. A., Godfrey, D. I., Smyth, G. K., Bouillet, P., Strasser, A., Walczak, H., … Gray, D. H. D. (2016). Linear ubiquitin chain assembly complex coordinates late thymic T-cell differentiation and regulatory T-cell homeostasis. *Nature Communications*, *7*, 13353.

Tejasvi, T., Stuart, P. E., Chandran, V., Voorhees, J. J., Gladman, D. D., Rahman, P., Elder, J. T., & Nair, R. P. (2012). TNFAIP3 gene polymorphisms are associated with response to TNF blockade in psoriasis. *The Journal of Investigative Dermatology*, *132*(3 Pt 1), 593–600.

Tenev, T., Bianchi, K., Darding, M., Broemer, M., Langlais, C., Wallberg, F., Zachariou, A., Lopez, J., MacFarlane, M., Cain, K., & Meier, P. (2011). The Ripoptosome, a signaling platform that assembles in response to genotoxic stress and loss of IAPs. *Molecular Cell*, *43*(3), 432–448.

Thapaliya, S., Wree, A., Povero, D., Inzaugarat, M. E., Berk, M., Dixon, L., Papouchado, B. G., & Feldstein, A. E. (2014). Caspase 3 inactivation protects against hepatic cell death and ameliorates fibrogenesis in a diet-induced NASH model. *Digestive Diseases and Sciences*, *59*(6), 1197–1206.

Ting, A. T., & Bertrand, M. J. M. (2016). More to life than NF-κB in TNFR1 signaling. *Trends in Immunology*, *37*(8), 535–545.

Tojima, Y., Fujimoto, A., Delhase, M., Chen, Y., Hatakeyama, S., Nakayama, K., Kaneko, Y., Nimura, Y., Motoyama, N., Ikeda, K., Karin, M., & Nakanishi, M. (2000). NAK is an IkappaB kinase-activating kinase. *Nature*, *404*(6779), 778–782.

Tokunaga, F., Nakagawa, T., Nakahara, M., Saeki, Y., Taniguchi, M., Sakata, S.-I., Tanaka, K., Nakano, H., & Iwai, K. (2011). SHARPIN is a component of the NF-κB-activating linear ubiquitin chain assembly complex. *Nature*, *471*(7340), 633–636.

Tokunaga, F., Sakata, S., Saeki, Y., Satomi, Y., Kirisako, T., Kamei, K., Nakagawa, T., Kato, M., Murata, S., Yamaoka, S., Yamamoto, M., Akira, S., Takao, T., Tanaka, K., & Iwai, K. (2009). Involvement of linear polyubiquitylation of NEMO in NF-kappaB activation. *Nature Cell Biology*, *11*(2). https://doi.org/10.1038/ncb1821

Trujillo, M. E., Pajvani, U. B., & Scherer, P. E. (2005). Apoptosis through targeted activation of caspase 8 ("ATTAC-mice"): novel mouse models of inducible and reversible tissue ablation. *Cell Cycle* , *4*(9), 1141–1145.

Turer, E. E., Tavares, R. M., Mortier, E., Hitotsumatsu, O., Advincula, R., Lee, B., Shifrin, N., Malynn, B. A., & Ma, A. (2008). Homeostatic MyD88-dependent signals cause lethal inflamMation in the absence of A20. *The Journal of Experimental Medicine*, *205*(2), 451–464.

Turpin-Nolan, S. M., Hammerschmidt, P., Chen, W., Jais, A., Timper, K., Awazawa, M., Brodesser, S., & Brüning, J. C. (2019). CerS1-Derived C18:0 Ceramide in Skeletal Muscle Promotes Obesity-Induced Insulin Resistance. *Cell Reports*, *26*(1), 1–10.e7.

Tye, H., Conos, S. A., Djajawi, T. M., Gottschalk, T. A., Abdoulkader, N., Kong, I. Y., Kammoun, H. L., Narayana, V. K., Kratina, T., Speir, M., Emery, J., Simpson, D. S., Hall, C., Vince, A. J., Russo, S., Crawley, R., Rashidi, M., Hildebrand, J. M., Murphy, J. M., … Lawlor, K. E. (2025). Divergent roles of RIPK3 and MLKL in high-fat diet-induced obesity and MAFLD in mice. *Life Science Alliance*, *8*(1), e202302446.

Tzenios, N., Tazanios, M. E., & Chahine, M. (2022). The impact of body mass index on prostate cancer: An updated systematic review and meta-analysis. *Medicine*, *101*(45), e30191.

Uldry, M., Yang, W., St-Pierre, J., Lin, J., Seale, P., & Spiegelman, B. M. (2006). Complementary action of the PGC-1 coactivators in mitochondrial biogenesis and brown fat differentiation. *Cell Metabolism*, *3*(5), 333–341.

Unamuno, X., Gómez-Ambrosi, J., Ramírez, B., Rodríguez, A., Becerril, S., Valentí, V.,

Moncada, R., Silva, C., Salvador, J., Frühbeck, G., & Catalán, V. (2021). NLRP3 inflammasome blockade reduces adipose tissue inflammation and extracellular matrix remodeling. *Cellular & Molecular Immunology*, *18*(4), 1045–1057.

Vallabhapurapu, S., Matsuzawa, A., Zhang, W., Tseng, P.-H., Keats, J. J., Wang, H., Vignali, D. A. A., Bergsagel, P. L., & Karin, M. (2008). Nonredundant and complementary functions of TRAF2 and TRAF3 in a ubiquitination cascade that activates NIK-dependent alternative NF-kappaB signaling. *Nature Immunology*, *9*(12), 1364–1370.

Vanden Berghe, T., Linkermann, A., Jouan-Lanhouet, S., Walczak, H., & Vandenabeele, P. (2014). Regulated necrosis: the expanding network of non-apoptotic cell death pathways. *Nature Reviews. Molecular Cell Biology*, *15*(2), 135–147.

van Hall, G., Steensberg, A., Sacchetti, M., Fischer, C., Keller, C., Schjerling, P., Hiscock, N., Møller, K., Saltin, B., Febbraio, M. A., & Pedersen, B. K. (2003). Interleukin-6 stimulates lipolysis and fat oxidation in humans. *The Journal of Clinical Endocrinology and Metabolism*, *88*(7), 3005–3010.

van Harmelen, V., Dicker, A., Rydén, M., Hauner, H., Lönnqvist, F., Näslund, E., & Arner, P. (2002). Increased lipolysis and decreased leptin production by human omental as compared with subcutaneous preadipocytes. *Diabetes*, *51*(7), 2029–2036.

van Harmelen, V., Elizalde, M., Ariapart, P., Bergstedt-Lindqvist, S., Reynisdottir, S., Hoffstedt, J., Lundkvist, I., Bringman, S., & Arner, P. (2000). The association of human adipose angiotensinogen gene expression with abdominal fat distribution in obesity. *International Journal of Obesity*, *24*(6), 673–678.

van Well, E. M., Bader, V., Patra, M., Sánchez-Vicente, A., Meschede, J., Furthmann, N., Schnack, C., Blusch, A., Longworth, J., Petrasch-Parwez, E., Mori, K., Arzberger, T., Trümbach, D., Angersbach, L., Showkat, C., Sehr, D. A., Berlemann, L. A., Goldmann, P., Clement, A. M., … Winklhofer, K. F. (2019). A protein quality control pathway regulated by linear ubiquitination. *The EMBO Journal*, *38*(9), e100730.

Veauthier, B., & Levy-Grau, B. (2024). Diabetic ketoacidosis: Evaluation and treatment. *American Family Physician*, *110*(5), 476–486.

Veilleux, A., Caron-Jobin, M., Noël, S., Laberge, P. Y., & Tchernof, A. (2011). Visceral adipocyte hypertrophy is associated with dyslipidemia independent of body composition and fat distribution in women. *Diabetes*, *60*(5), 1504–1511.

Velikova, T. V., Kabakchieva, P. P., Assyov, Y. S., & Georgiev, T. A. (2021). Targeting Inflammatory Cytokines to Improve Type 2 Diabetes Control. *BioMed Research International*, *2021*, 7297419.

Veli, Ö., Kaya, Ö., Varanda, A. B., Hildebrandt, X., Xiao, P., Estornes, Y., Poggenberg, M., Wang, Y., Pasparakis, M., Bertrand, M. J. M., Walczak, H., Annibaldi, A., Cardozo, A. K., & Peltzer, N. (2024). RIPK1 is dispensable for cell death regulation in β-cells during hyperglycemia. *Molecular Metabolism*, *87*, 101988.

Verboom, L., Martens, A., Priem, D., Hoste, E., Sze, M., Vikkula, H., Van Hove, L., Voet, S., Roels, J., Maelfait, J., Bongiovanni, L., de Bruin, A., Scott, C. L., Saeys, Y., Pasparakis, M., Bertrand, M. J. M., & van Loo, G. (2020). OTULIN prevents liver inflammation and hepatocellular carcinoma by inhibiting FADD- and RIPK1 kinase-mediated hepatocyte apoptosis. *Cell Reports*, *30*(7), 2237–2247.e6.

Verhelst, K., van Loo, G., & Beyaert, R. (2014). A20: attractive without showing cleavage. *EMBO Reports*, *15*(7), 734–735.

Vidal, H. (2001). Gene expression in visceral and subcutaneous adipose tissues. *Annals of Medicine*, *33*(8), 547–555.

Vince, J. E., Pantaki, D., Feltham, R., Mace, P. D., Cordier, S. M., Schmukle, A. C., Davidson, A. J., Callus, B. A., Wong, W. W.-L., Gentle, I. E., Carter, H., Lee, E. F., Walczak, H., Day, C. L., Vaux, D. L., & Silke, J. (2009). TRAF2 must bind to cellular

inhibitors of apoptosis for tumor necrosis factor (tnf) to efficiently activate nf-{kappa}b and to prevent tnf-induced apoptosis. *The Journal of Biological Chemistry*, *284*(51), 35906–35915.

Virtue, S., & Vidal-Puig, A. (2021). GTTs and ITTs in mice: simple tests, complex answers. *Nature Metabolism*, *3*(7), 883–886.

Vogel, A., Brunner, J. S., Hajto, A., Sharif, O., & Schabbauer, G. (2022). Lipid scavenging macrophages and inflammation. *Biochimica et Biophysica Acta, Molecular and Cell Biology of Lipids*, *1867*(1), 159066.

Vucur, M., Ghallab, A., Schneider, A. T., Adili, A., Cheng, M., Castoldi, M., Singer, M. T., Büttner, V., Keysberg, L. S., Küsgens, L., Kohlhepp, M., Görg, B., Gallage, S., Barragan Avila, J. E., Unger, K., Kordes, C., Leblond, A.-L., Albrecht, W., Loosen, S. H., … Luedde, T. (2023). Sublethal necroptosis signaling promotes inflammation and liver cancer. *Immunity*, *56*(7), 1578–1595.e8.

Wajant, H., Pfizenmaier, K., & Scheurich, P. (2003). Tumor necrosis factor signaling. *Cell Death and Differentiation*, *10*(1), 45–65.

Wajant, H., & Scheurich, P. (2001). Tumor necrosis factor receptor-associated factor (TRAF) 2 and its role in TNF signaling. *The International Journal of Biochemistry & Cell Biology*, *33*(1), 19–32.

Walczak, H. (2013). Death receptor-ligand systems in cancer, cell death, and inflammation. *Cold Spring Harbor Perspectives in Biology*, *5*(5), a008698.

Walczak, H., Iwai, K., & Dikic, I. (2012). Generation and physiological roles of linear ubiquitin chains. *BMC Biology*, *10*, 23.

Wallenius, V., Wallenius, K., Ahrén, B., Rudling, M., Carlsten, H., Dickson, S. L., Ohlsson, C., & Jansson, J.-O. (2002). Interleukin-6-deficient mice develop mature-onset obesity. *Nature Medicine*, *8*(1), 75–79.

Wang, C.-H., & Wei, Y.-H. (2021). Therapeutic perspectives of thermogenic adipocytes in obesity and related complications. *International Journal of Molecular Sciences*, *22*(13), 7177.

Wang, H., Capell, W., Yoon, J. H., Faubel, S., & Eckel, R. H. (2014). Obesity development in caspase-1-deficient mice. *International Journal of Obesity* , *38*(1), 152–155.

Wang, K., Kim, C., Bradfield, J., Guo, Y., Toskala, E., Otieno, F. G., Hou, C., Thomas, K., Cardinale, C., Lyon, G. J., Golhar, R., & Hakonarson, H. (2013). Whole-genome DNA/RNA sequencing identifies truncating mutations in RBCK1 in a novel Mendelian disease with neuromuscular and cardiac involvement. *Genome Medicine*, *5*(7), 67.

Wani, K., AlHarthi, H., Alghamdi, A., Sabico, S., & Al-Daghri, N. M. (2021). Role of NLRP3 Inflammasome Activation in Obesity-Mediated Metabolic Disorders. *International Journal of Environmental Research and Public Health*, *18*(2). https://doi.org/10.3390/ijerph18020511

Wculek, S. K., Dunphy, G., Heras-Murillo, I., Mastrangelo, A., & Sancho, D. (2022). Metabolism of tissue macrophages in homeostasis and pathology. *Cellular & Molecular Immunology*, *19*(3), 384–408.

Wedell-Neergaard, A.-S., Lang Lehrskov, L., Christensen, R. H., Legaard, G. E., Dorph, E., Larsen, M. K., Launbo, N., Fagerlind, S. R., Seide, S. K., Nymand, S., Ball, M., Vinum, N., Dahl, C. N., Henneberg, M., Ried-Larsen, M., Nybing, J. D., Christensen, R., Rosenmeier, J. B., Karstoft, K., … Krogh-Madsen, R. (2019). Exercise-Induced Changes in Visceral Adipose Tissue Mass Are Regulated by IL-6 Signaling: A Randomized Controlled Trial. *Cell Metabolism*, *29*(4), 844–855.e3.

Weidemann, A., Lovas, A., Rauch, A., Andreas, N., von Maltzahn, J., Riemann, M., & Weih, F. (2015). Classical and alternative NF-κB signaling cooperate in regulating adipocyte differentiation and function. *International Journal of Obesity*, *40*(3), 452–459.

Weinelt, N., Wächtershäuser, K. N., Celik, G., Jeiler, B., Gollin, I., Zein, L., Smith, S.,

Andrieux, G., Das, T., Roedig, J., Feist, L., Rotter, B., Boerries, M., Pampaloni, F., & van Wijk, S. J. L. (2024). LUBAC-mediated M1 Ub regulates necroptosis by segregating the cellular distribution of active MLKL. *Cell Death & Disease*, *15*(1), 77.

Weisberg, S. P., McCann, D., Desai, M., Rosenbaum, M., Leibel, R. L., & Ferrante, A. W., Jr. (2003). Obesity is associated with macrophage accumulation in adipose tissue. *The Journal of Clinical Investigation*, *112*(12), 1796–1808.

Wei, Y., Lan, B., Zheng, T., Yang, L., Zhang, X., Cheng, L., Tuerhongjiang, G., Yuan, Z., & Wu, Y. (2023). GSDME-mediated pyroptosis promotes the progression and associated inflammation of atherosclerosis. *Nature Communications*, *14*(1), 929.

Wei, Y., Wu, Y., Yuan, Z., Wang, J. 'an, & Yin, D. L. (2024). GSDME deficiency sensitizes mice to diet-induced obesity by suppressing lipolysis. *Endocrine Abstracts*, *99*. https://doi.org/10.1530/endoabs.99.oc4.6

Wellcome Trust Case Control Consortium. (2007). Genome-wide association study of 14,000 cases of seven common diseases and 3,000 shared controls. *Nature*, *447*(7145), 661–678.

Wenzel, D. M., Lissounov, A., Brzovic, P. S., & Klevit, R. E. (2011). UBCH7 reactivity profile reveals parkin and HHARI to be RING/HECT hybrids. *Nature*, *474*(7349), 105–108.

Wertz, I. E., O'Rourke, K. M., Zhou, H., Eby, M., Aravind, L., Seshagiri, S., Wu, P., Wiesmann, C., Baker, R., Boone, D. L., Ma, A., Koonin, E. V., & Dixit, V. M. (2004). De-ubiquitination and ubiquitin ligase domains of A20 downregulate NF-kappaB signalling. *Nature*, *430*(7000), 694–699.

Weyer, C., Foley, J. E., Bogardus, C., Tataranni, P. A., & Pratley, R. E. (2000). Enlarged subcutaneous abdominal adipocyte size, but not obesity itself, predicts type II diabetes independent of insulin resistance. *Diabetologia*, *43*(12), 1498–1506.

Wiest, R., Moleda, L., Farkas, S., Scherer, M., Kopp, A., Wönckhaus, U., Büchler, C., Schölmerich, J., & Schäffler, A. (2010). Splanchnic concentrations and postprandial release of visceral adipokines. *Metabolism: Clinical and Experimental*, *59*(5), 664–670.

Wilson, N. S., Dixit, V., & Ashkenazi, A. (2009). Death receptor signal transducers: nodes of coordination in immune signaling networks. *Nature Immunology*, *10*(4), 348–355.

Winther, S., Isidor, M. S., Basse, A. L., Skjoldborg, N., Cheung, A., Quistorff, B., & Hansen, J. B. (2018). Restricting glycolysis impairs brown adipocyte glucose and oxygen consumption. *American Journal of Physiology. Endocrinology and Metabolism*, *314*(3), E214–E223.

Wolf, Y., Boura-Halfon, S., Cortese, N., Haimon, Z., Sar Shalom, H., Kuperman, Y., Kalchenko, V., Brandis, A., David, E., Segal-Hayoun, Y., Chappell-Maor, L., Yaron, A., & Jung, S. (2017). Brown-adipose-tissue macrophages control tissue innervation and homeostatic energy expenditure. *Nature Immunology*, *18*(6), 665–674.

Wong, V. W.-S., Ekstedt, M., Wong, G. L.-H., & Hagström, H. (2023). Changing epidemiology, global trends and implications for outcomes of NAFLD. *Journal of Hepatology*, *79*(3), 842–852.

World obesity Atlas 2022. (n.d.). World Obesity Federation. Retrieved May 11, 2024, from https://www.worldobesity.org/resources/resource-library/world-obesity-atlas-2022

Wueest, S., & Konrad, D. (2018). The role of adipocyte-specific IL-6-type cytokine signaling in FFA and leptin release. *Adipocyte*, *7*(3), 226–228.

Wueest, S., & Konrad, D. (2020). The controversial role of IL-6 in adipose tissue on obesity-induced dysregulation of glucose metabolism. *American Journal of Physiology. Endocrinology and Metabolism*, *319*(3), E607–E613.

Wueest, S., Scaffidi, C., van Krieken, P. P., Konrad, N. K., Koch, C., Wiedemann, M. S. F., Goergen, A., Borsigova, M., Lempesis, I. G., Fullin, J., Manolopoulos, K. N., Böttcher, S., Goossens, G. H., Blüher, M., & Konrad, D. (2024). Fas (CD95) expression in adipocytes contributes to diet-induced obesity. *Obesity (Silver Spring, Md.)*, *32*(10).

https://doi.org/10.1002/oby.24092

Wu, J., Boström, P., Sparks, L. M., Ye, L., Choi, J. H., Giang, A.-H., Khandekar, M., Virtanen, K. A., Nuutila, P., Schaart, G., Huang, K., Tu, H., van Marken Lichtenbelt, W. D., Hoeks, J., Enerbäck, S., Schrauwen, P., & Spiegelman, B. M. (2012). Beige adipocytes are a distinct type of thermogenic fat cell in mouse and human. *Cell*, *150*(2), 366–376.

Wu, L., Zhang, X., Zheng, L., Zhao, H., Yan, G., Zhang, Q., Zhou, Y., Lei, J., Zhang, J., Wang, J., Xin, R., Jiang, L., Peng, J., Chen, Q., Lam, S. M., Shui, G., Miao, H., & Li, Y. (2020). RIPK3 Orchestrates Fatty Acid Metabolism in Tumor-Associated Macrophages and Hepatocarcinogenesis. *Cancer Immunology Research*, *8*(5), 710–721.

Wu, M., Chang, Y., Hu, H., Mu, R., Zhang, Y., Qin, X., Duan, X., Li, W., Tu, H., Zhang, W., Wang, G., Han, Q., Li, A., Zhou, T., Iwai, K., Zhang, X., & Li, H. (2019). LUBAC controls chromosome alignment by targeting CENP-E to attached kinetochores. *Nature Communications*, *10*(1), 273.

Wu, X., Poulsen, K. L., Sanz-Garcia, C., Huang, E., McMullen, M. R., Roychowdhury, S., Dasarathy, S., & Nagy, L. E. (2020). MLKL-dependent signaling regulates autophagic flux in a murine model of non-alcohol-associated fatty liver and steatohepatitis. *Journal of Hepatology*, *73*(3), 616–627.

Wu, Z., Berlemann, L. A., Bader, V., Sehr, D. A., Dawin, E., Covallero, A., Meschede, J., Angersbach, L., Showkat, C., Michaelis, J. B., Münch, C., Rieger, B., Namgaladze, D., Herrera, M. G., Fiesel, F. C., Springer, W., Mendes, M., Stepien, J., Barkovits, K., … Winklhofer, K. F. (2022). LUBAC assembles a ubiquitin signaling platform at mitochondria for signal amplification and transport of NF-κB to the nucleus. *The EMBO Journal*, *41*(24), e112006.

Xu, B., Jiang, M., Chu, Y., Wang, W., Chen, D., Li, X., Zhang, Z., Zhang, D., Fan, D., Nie, Y., Shao, F., Wu, K., & Liang, J. (2018). Gasdermin D plays a key role as a pyroptosis executor of non-alcoholic steatohepatitis in humans and mice. *Journal of Hepatology*, *68*(4), 773–782.

Xu, H., Du, X., Liu, G., Huang, S., Du, W., Zou, S., Tang, D., Fan, C., Xie, Y., Wei, Y., Tian, Y., & Fu, X. (2019). The pseudokinase MLKL regulates hepatic insulin sensitivity independently of inflammation. *Molecular Metabolism*, *23*, 14–23.

Xu, J., Jia, Y.-F., Tapadar, S., Weaver, J. D., Raji, I. O., Pithadia, D. J., Javeed, N., García, A. J., Choi, D.-S., Matveyenko, A. V., Oyelere, A. K., & Shin, C. H. (2018). Inhibition of TBK1/IKKε Promotes Regeneration of Pancreatic β-cells. *Scientific Reports*, *8*(1), 15587.

Xu, W., Wang, C., Liang, M., Chen, L., Fu, Q., Zhang, F., Wang, Y., Huang, D., & Huang, K. (2018). A20 prevents obesity-induced development of cardiac dysfunction. *Journal of Molecular Medicine* , *96*(2), 159–172.

Xu, X. J., Gauthier, M.-S., Hess, D. T., Apovian, C. M., Cacicedo, J. M., Gokce, N., Farb, M., Valentine, R. J., & Ruderman, N. B. (2012). Insulin sensitive and resistant obesity in humans: AMPK activity, oxidative stress, and depot-specific changes in gene expression in adipose tissue. *The Journal of Lipid Research*, *53*(4), 792–801.

Xu, Z., Shao, J., Zheng, C., Cai, J., Li, B., Peng, X., Chen, L., & Liu, T. (2022). The E3 ubiquitin ligase RBCK1 promotes the invasion and metastasis of hepatocellular carcinoma by destroying the PPARγ/PGC1α complex. *American Journal of Cancer Research*, *12*(3), 1372–1392.

Yamamotoya, T., Nakatsu, Y., Matsunaga, Y., Fukushima, T., Yamazaki, H., Kaneko, S., Fujishiro, M., Kikuchi, T., Kushiyama, A., Tokunaga, F., Asano, T., & Sakoda, H. (2017). Reduced SHARPIN and LUBAC Formation May Contribute to CCl_4- or Acetaminophen-Induced Liver Cirrhosis in Mice. *International Journal of Molecular Sciences*, *18*(2). https://doi.org/10.3390/ijms18020326

Yanai, H., Adachi, H., Hakoshima, M., Iida, S., & Katsuyama, H. (2023). Metabolic-Dysfunction-Associated Steatotic Liver Disease-Its Pathophysiology,

Association with Atherosclerosis and Cardiovascular Disease, and Treatments. *International Journal of Molecular Sciences*, *24*(20). https://doi.org/10.3390/ijms242015473

Yang, R.-Z., Lee, M.-J., Hu, H., Pray, J., Wu, H.-B., Hansen, B. C., Shuldiner, A. R., Fried, S. K., McLenithan, J. C., & Gong, D.-W. (2006). Identification of omentin as a novel depot-specific adipokine in human adipose tissue: possible role in modulating insulin action. *American Journal of Physiology. Endocrinology and Metabolism*, *290*(6), E1253–E1261.

Yao, J., Wu, D., & Qiu, Y. (2022). Adipose tissue macrophage in obesity-associated metabolic diseases. *Frontiers in Immunology*, *13*, 977485.

Yeh, T.-Y. J., Beiswenger, K. K., Li, P., Bolin, K. E., Lee, R. M., Tsao, T.-S., Murphy, A. N., Hevener, A. L., & Chi, N.-W. (2009). Hypermetabolism, hyperphagia, and reduced adiposity in tankyrase-deficient mice. *Diabetes*, *58*(11), 2476–2485.

Ye, J. (2011). Adipose tissue vascularization: its role in chronic inflammation. *Current Diabetes Reports*, *11*(3), 203–210.

Ye, Y., & Rape, M. (2009). Building ubiquitin chains: E2 enzymes at work. *Nature Reviews. Molecular Cell Biology*, *10*(11), 755–764.

Ying, W., Cheruku, P. S., Bazer, F. W., Safe, S. H., & Zhou, B. (2013). Investigation of macrophage polarization using bone marrow derived macrophages. *Journal of Visualized Experiments: JoVE*, *76*. https://doi.org/10.3791/50323

Yin, R., & Liu, S. (2021). SHARPIN regulates the development of clear cell renal cell carcinoma by promoting von Hippel-Lindau protein ubiquitination and degradation. *Cancer Science*, *112*(10), 4100–4111.

Younes, R., & Bugianesi, E. (2019). NASH in Lean Individuals. *Seminars in Liver Disease*, *39*(1), 86–95.

Younossi, Z., Anstee, Q. M., Marietti, M., Hardy, T., Henry, L., Eslam, M., George, J., & Bugianesi, E. (2018). Global burden of NAFLD and NASH: trends, predictions, risk factors and prevention. *Nature Reviews. Gastroenterology & Hepatology*, *15*(1), 11–20.

Yuan, M., Konstantopoulos, N., Lee, J., Hansen, L., Li, Z. W., Karin, M., & Shoelson, S. E. (2001). Reversal of obesity- and diet-induced insulin resistance with salicylates or targeted disruption of Ikkbeta. *Science*, *293*(5535), 1673–1677.

Yu, B., Wang, F., & Wang, Y. (2022). Advances in the Structural and Physiological Functions of SHARPIN. *Frontiers in Immunology*, *13*, 858505.

Yu, J., Liu, T., Liu, M., Jin, H., & Wei, Z. (2024). RBCK1 overexpression is associated with immune cell infiltration and poor prognosis in hepatocellular carcinoma. *Aging*, *16*(1), 538–549.

Yu, L., Hong, W., Lu, S., Li, Y., Guan, Y., Weng, X., & Feng, Z. (2022). The NLRP3 inflammasome in non-alcoholic fatty liver disease and steatohepatitis: Therapeutic targets and treatment. *Frontiers in Pharmacology*, *13*, 780496.

Yu, S.-Y., Li, J., Liu, Z., & Kim, Y.-C. (2020). Tumor necrosis factor alpha knockout promotes adipose fatty acid oxidation and attenuates insulin resistance and hepatic steatosis in high fat diet-fed mice. *Current Developments in Nutrition*, *4*(nzaa063_103), nzaa063_103.

Zarnegar, B. J., Wang, Y., Mahoney, D. J., Dempsey, P. W., Cheung, H. H., He, J., Shiba, T., Yang, X., Yeh, W.-C., Mak, T. W., Korneluk, R. G., & Cheng, G. (2008). Noncanonical NF-kappaB activation requires coordinated assembly of a regulatory complex of the adaptors cIAP1, cIAP2, TRAF2 and TRAF3 and the kinase NIK. *Nature Immunology*, *9*(12), 1371–1378.

Zeng, T., Zhou, J., He, L., Zheng, J., Chen, L., Wu, C., & Xia, W. (2016). Blocking Nuclear Factor-Kappa B Protects against Diet-Induced Hepatic Steatosis and Insulin Resistance in Mice. *PloS One*, *11*(3), e0149677.

Zhao, P., Wong, K. I., Sun, X., Reilly, S. M., Uhm, M., Liao, Z., Skorobogatko, Y., & Saltiel, A. R. (2018). TBK1 at the Crossroads of Inflammation and Energy Homeostasis in Adipose Tissue. *Cell*, *172*(4), 731–743.e12.

Zhou, Q., Wang, H., Schwartz, D. M., Stoffels, M., Park, Y. H., Zhang, Y., Yang, D., Demirkaya, E., Takeuchi, M., Tsai, W. L., Lyons, J. J., Yu, X., Ouyang, C., Chen, C., Chin, D. T., Zaal, K., Chandrasekharappa, S. C., Hanson, E. P., Yu, Z., … Aksentijevich, I. (2016). Loss-of-function mutations in TNFAIP3 leading to A20 haploinsufficiency cause an early-onset autoinflammatory disease. *Nature Genetics*, *48*(1), 67–73.

Zhou, Q., Yu, X., Demirkaya, E., Deuitch, N., Stone, D., Tsai, W. L., Kuehn, H. S., Wang, H., Yang, D., Park, Y. H., Ombrello, A. K., Blake, M., Romeo, T., Remmers, E. F., Chae, J. J., Mullikin, J. C., Güzel, F., Milner, J. D., Boehm, M., … Aksentijevich, I. (2016). Biallelic hypomorphic mutations in a linear deubiquitinase define otulipenia, an early-onset autoinflammatory disease. *Proceedings of the National Academy of Sciences*, *113*(36), 10127–10132.

Zhuang, H., Wang, X., Zha, D., Gan, Z., Cai, F., Du, P., Yang, Y., Yang, B., Zhang, X., Yao, C., Zhou, Y., Jiang, C., Guan, S., Zhang, X., Zhang, J., Jiang, W., Hu, Q., & Hua, Z.-C. (2016). FADD is a key regulator of lipid metabolism. *EMBO Molecular Medicine*, *8*(8), 895–918.

Zhu, M., Kohan, E., Bradley, J., Hedrick, M., Benhaim, P., & Zuk, P. (2009). The effect of age on osteogenic, adipogenic and proliferative potential of female adipose-derived stem cells. *Journal of Tissue Engineering and Regenerative Medicine*, *3*(4), 290–301.

Zilu, S., Qian, H., Haibin, W., Chenxu, G., Deshuai, L., Qiang, L., Linfeng, H., Jun, T., & Minxuan, X. (2019). Effects of XIAP on high fat diet-induced hepatic steatosis: a mechanism involving NLRP3 inflammasome and oxidative stress. *Aging*, *11*(24), 12177–12201.

Zinngrebe, J., Moepps, B., Monecke, T., Gierschik, P., Schlichtig, F., Barth, T. F. E., Strauß, G., Boldrin, E., Posovszky, C., Schulz, A., Beringer, O., Rieser, E., Jacobsen, E.-M., Lorenz, M. R., Schwarz, K., Pannicke, U., Walczak, H., Niessing, D., Schuetz, C., … Debatin, K.-M. (2022). Compound heterozygous variants in OTULIN are associated with fulminant atypical late-onset ORAS. *EMBO Molecular Medicine*, *14*(3), e14901.

Zinngrebe, J., Montinaro, A., Peltzer, N., & Walczak, H. (2014). Ubiquitin in the immune system. *EMBO Reports*, *15*(1), 28–45.

8. Erklärung zur Dissertation / Declaration on the dissertation

Ich versichere, dass ich die von mir vorgelegte Dissertation selbstständig angefertigt, die benutzten Quellen und Hilfsmittel vollständig angegeben und die Stellen der Arbeit -einschließlich Tabellen, Kar- ten und Abbildungen -, die anderen Werken im Wortlaut oder dem Sinn nach entnommen sind, in jedem Einzelfall als Entlehnung kenntlich gemacht habe; dass diese Dissertation noch keiner anderen Fakultät oder Universität zur Prüfung vorgelegen hat; dass sie - abgesehen von unten angegebenen Teilpublika- tionen - noch nicht veröffentlicht worden ist sowie, dass ich eine solche Veröffentlichung vor Abschluss des Promotionsverfahrens nicht vornehmen werde. Die Bestimmungen dieser Promotionsordnung sind mir bekannt. Die von mir vorgelegte Dissertation ist von Prof. Dr. Nieves Peltzer betreut worden.

Übersicht der Publikationen:

Hildebrandt et. al, 2025. “Linear ubiquitination prevents lipodystrophy and obesity-associated metabolic syndrome“, Science Advances. DOI: 10.1126/sciadv.adw2539

Hildebrandt et. al, 2022. Review: “Cell death and inflammation during obesity: "Know my methods, WAT(son)" “ , Cell Death and Differentiation. DOI: 10.1038/s41418-022-01062-4.

Ich versichere, dass ich alle Angaben wahrheitsgemäß nach bestem Wissen und Gewissen gemacht habe und verpflichte mich, jedmögliche, die obigen Angaben betreffenden Veränderungen, dem Promotionsausschuss unverzüglich mitzuteilen.

Ximena Hildebrandt, Köln, 08/01/2026